DEVELOPMENT AND ASSESSMENT OF SOLAR-ASSISTED GAS TURBINE COGENERATION SYSTEMS IN SAUDI ARABIA

BY

YOUSEF NAJI DABWAN AHMED

A Thesis Presented to the
DEANSHIP OF GRADUATE STUDIES

KING FAHD UNIVERSITY OF PETROLEUM & MINERALS

DHAHRAN, SAUDI ARABIA

In Partial Fulfillment of the
Requirements for the Degree of

MASTER OF SCIENCE

In

Mechanical engineering

May, 2013

KING FAHD UNIVERSITY OF PETROLEUM & MINERALS

DHAHRAN- 31261, SAUDI ARABIA

DEANSHIP OF GRADUATE STUDIES

This thesis, written by **Yousef Naji Dabwan Ahmed** under the direction of his thesis advisor and approved by his thesis committee, has been presented and accepted by the Dean of Graduate Studies, in partial fulfillment of the requirements for the degree of **MASTER OF SCIENCE IN MECHANICAL ENGINEERING.**

Dr. Zuhiar M. Gasem
Department Chairman

Dr. Esmail M. A. Mokheimer
(Advisor)

Dr. Salam A. Zummo
Dean of Graduate Studies

Dr. Mohamed A. Habib
(Member)

11/7/13
Date

Dr. Syed A. M. Said
(Member)

I dedicate this dissertation with all of my love to my father, to the memory of my late mother, my wife, my son, my daughter, my brothers and sisters.

ACKNOWLEDGMENTS

First of all, I thank Allah (SWT), the most Compassionate, the most Merciful, and the most Benevolent for his blessing throughout my life in general and in the course of this thesis in particular.

I would like to express my profound gratitude and appreciation to my advisor Dr. Esmail M. A. Mokheimer, for his consistent help, guidance, encouragement and the invaluable support that he devoted throughout the course of this work. His appreciation and words of encouragement gave a new life to my efforts in times of difficulty. I am also indebted to him for his valuable time, efforts and his continuous support and inspiration. I am also grateful to him for providing me with some of his authorized computer programs.

I would like also to express my deep appreciation to my committee members, Dr. Mohamed A. Habib and Dr. Syed A. M. Said, for their constant help and encouragement.

I would like to thank King Fahd University of Petroleum and Minerals for sponsoring me throughout my graduate studies. I also would like to thank Sana'a University for giving me the opportunity to complete my MSc degree at KFUPM.

Finally, I would like to thank my father, my wife, my son, my daughter, my brothers, and my sisters who always support me with their love, patience encouragement and constant prayers throughout my study.

TABLE OF CONTENTS

DEVELOPMENT AND ASSESSMENT OF SOLAR-ASSISTED GAS TURBINE COGENERATION SYSTEMS IN SAUDI ARABIA

BY

YOUSEF NAJI DABWAN AHMED

A Thesis Presented to the
DEANSHIP OF GRADUATE STUDIES

KING FAHD UNIVERSITY OF PETROLEUM & MINERALS

DHAHRAN, SAUDI ARABIA

In Partial Fulfillment of the
Requirements for the Degree of

MASTER OF SCIENCE

In

Mechanical engineering

May, 2013

LIST OF TABLES

LIST OF FIGURES

LIST OF ABBREVIATIONS

PTC	Parabolic Trough Collector.
LFR	Linear Fresnel Reflector.
ST	Solar Tower.
CSP	Concentrating Solar Power.
HRSG	Heat Recovery Steam Generation.
$\dot{\mathbf{m}}_{\mathbf{fuel}}$	Fuel mass flow rate.
$\boldsymbol{lHV}$	Lower heating value of fuel.
$\dot{\mathbf{m}}_{\mathbf{w}}$	Water flow rate through solar collector field.
$\mathbf{h}_{\mathbf{outlet,SF}}$	Enthalpy of water at output of solar collector field.
$\boldsymbol{h_{inlet,SF}}$	Enthalpy of water at input of solar collector field.
ISGCP	Integrated Solar Gas Turbine Cogeneration Power Plant.
$\boldsymbol{GCP}$	Gas Turbine Cogeneration Power Plant.
$\boldsymbol{Ref}.$	Reference cycle.
$\mathbf{P}_{\mathbf{gen,ISGCP}}$	Total power generated from integrated solar gas turbine cogeneration power.
$\boldsymbol{\eta}_{\mathbf{ref}}$	Net efficiency of the reference power plant.
$\boldsymbol{P_{fuel,}}_{\mathbf{ISGCP}}$	Power generated from fuel only of integrated solar gas turbine cogeneration.
$\boldsymbol{P_{th,solar}}$	Thermal power produced by solar field.
$\mathbf{CO_2}_{\boldsymbol{GCP,}\mathbf{Ref}}$	Annual emission of CO_2 from a gas turbine cogeneration power plant.
$\mathbf{CO_2}_{\mathbf{ISGCP}}$	Annual emission of CO_2 from an integrated solar gas turbine cogeneration power plant.
LEC	Levelized Energy Cost.

SLEC	Solar Levelized Energy Cost.
$\boldsymbol{I_{tot}}$	Total investment cost.
$\boldsymbol{fcr}$	Annuity factor.
$\boldsymbol{OM_{ann}}$	Annual Operation and Maintenance costs.
$\boldsymbol{F_{ann}}$	Annual fuel consumption cost.
$\boldsymbol{E_{ann}}$	Annual total generated power.
$\mathbf{Q_{abs}}$	Solar radiation absorbed by the receiver tubes.
$\boldsymbol{\eta_{opt}}$	Optical efficiency
ANI	Aperture Normal Irradiance.
$\boldsymbol{DNI}$	Direct Normal Irradiance.
Ɵ	Angle of incidence.
$\boldsymbol{\eta_{nominal}}$	Nominal optical efficiency.
IAM	Incidence Angle Modifier.
$\boldsymbol{f_{end\ loss}}$	Performance factor that accounts for losses from ends of heat collector element
$\boldsymbol{f_{clean}}$	Cleanliness factor
$\boldsymbol{f_{rowshadow}}$	Performance factor that accounts for mutual shading of parallel collector rows during early morning and late evening
$\boldsymbol{\rho_{cl}}$	Clean mirror reflectivity
$\boldsymbol{\tau}$	Transmittance of the glass envelope.
$\boldsymbol{\alpha_c}$	Absorptance of the absorber surface coating.
$(\boldsymbol{\tau\alpha_c})_{\boldsymbol{n}}$	The effective product of τ and α_c.
$\boldsymbol{\gamma}$	Intercept factor.

$\mathbf{n}$	The day number of the year.
$\mathbf{L}_{st}$	Standard meridian for the local time zone.
$\mathbf{L}_{loc}$	The longitude of the location of the collector site.
$\boldsymbol{E}$	Equation Time.
$\boldsymbol{\emptyset}$	Latitude location of the solar field.
$\boldsymbol{L_{space}}$	Distance between two parallel collectors.
$\boldsymbol{W_a}$	Aperture width.
Θ_z	Zenith angle.
$\boldsymbol{r}$	Local mirror radius
$\boldsymbol{L_{SCA}}$	Length of a single solar collector.
$\boldsymbol{f_n}$	Focal length of the collectors.
$\boldsymbol{\eta_{th,collector}}$	Thermal collector efficiency
$\mathbf{Qu}$	Net energy transferred to the fluid in receiver tubes
$\boldsymbol{ANI}$	Aperture normal irradiance
$\boldsymbol{A_a}$	Aperture area
$\boldsymbol{D_o}$	Outer diameter of absorber tube.
$\boldsymbol{D_i}$	Inner diameter of absorber tube.
$\mathbf{A}_r$	Receiver area.
$\boldsymbol{U_L}$	Collector over all heat losses.
$\boldsymbol{h_{fi}}$	Heat transfer coefficient inside tube.
$\boldsymbol{F'}$	Collector efficiency factor.
$\boldsymbol{F}^{"}$	Collector flow factor.

$\boldsymbol{F_R}$	Collector heat removal factor.
$\boldsymbol{C_p}$	Specific heat.
$\mathbf{T}_i$	Fluid inlet temperature.
$\mathbf{T}_a$	Ambient temperature.
$\boldsymbol{L}$	Collector length.
$\mathbf{h}_w$	Wind heat transfer coefficient
$\mathbf{T}_{co}$	Outer glass envelope temperature.
ε_c	Emittance for glass envelope
$\mathbf{T}_{sky}$	Sky temperature.
$\boldsymbol{\sigma}$	Stefan- Boltzman constant.
$\boldsymbol{T_{ci}}$	Inner temperature of glass envelope.
$\boldsymbol{T_{co}}$	Outer temperature of glass envelope.
$\boldsymbol{k_c}$	Thermal conductivity of the glass envelope.
$\boldsymbol{D_{co}}$	Outer diameter of glass envelope.
$\boldsymbol{D_{ci}}$	Inner diameter of glass envelope.
$\boldsymbol{V_f}$	Velocity of HTF inside the tube.
$\boldsymbol{\mu}$	Absolute viscosity for heat transfer fluid.
$\boldsymbol{\rho_f}$	Density for heat transfer fluid.
$\boldsymbol{A_{i,r}}$	Inside cross sectional area of the absorber tube.
$\mathbf{f_2}$	Friction factor for the inner surface of the absorber pipe.
$\mathbf{P_r}$	Prandtl number.
$\boldsymbol{T_{fm}}$	Main fluid temperature.

ABSTRACT

Full Name : Yousef Naji Dabwan Ahmed

Thesis Title : Development and Assessment of Solar-Assisted Gas Turbine Cogeneration Systems in Saudi Arabia

Major Field : Mechanical Engineering

Date of Degree : May / 2013

Saudi Arabia occupies a large portion of high insolation regions where solar energy conversion systems can produce the maximum amount of energy from a specific collector field size. Several solar technologies can convert solar resources into thermal energy; Parabolic Trough System, Fresnel Reflector System, and Solar Tower System are some of these techniques that have proven their ability and reliability when integrated with conventional thermal power plants. Integrating solar technologies with gas turbine cogeneration power plants can definitely reduce conventional fuel consumption, which will result in a considerable reduction in gas emissions. This integration is expected to play an important role in solving the global and environmental energy problems.

The present work provides an investigation of the technical and economic feasibility of integrating Concentrating Solar Power (CSP) technologies with cogeneration gas turbine systems that are progressively being installed in Saudi Arabia to produce electricity and steam. In this regard, different designs of hybrid solar/fossil fuel gas turbine cogeneration systems have been proposed. These proposed systems designs consider the possible integration of three main Concentrating Solar Power (CSP) technologies with conventional gas turbine cogeneration systems. These CSP technologies are namely,

Solar Tower (ST) systems, Parabolic Trough Collector (PTC) system, and Linear Fresnel Reflector (LFR) systems.

An integrated solar gas turbine cogeneration system that generates steam at a constant flow rate of 81.44 kg/s at P = 45.88 (bar) and temperature of T = 394°C throughout the year in addition to the generation of electricity has been simulated and assessed for different CSP technologies and different sizes of gas turbines. THERMOFLEX with PEACE simulation software has been used to assess the performance of each proposed integration design. Thermo-economical analysis was conducted on different designs to reach at the optimal operating design under Dhahran weather conditions.

Finally, the optimal integration configuration is found to be the solarization of the steam side in 50 MWe gas turbine cogeneration plant integrated with 0.8 solar multiple (90 hectare) of LFR system. The levelized electricity cost for this configuration is 5.1 US¢/kWh. Furthermore, the solarization steam side in 50 MWe gas turbine cogeneration plant integrated with 0.8 solar multiple (104 hectare) of PTC system is not too far compared to that for LFR. Obviously the PTC system has the big advantage of being experimentally and commercially validated whereas the figures for the Fresnel collector are only theoretical. Moreover, the results indicate that the proper location to apply optimal integration configuration is Jizan city.

ملخص الرسالة

الاسم الكامل: يوسف ناجي دبوان احمد

عنوان الرسالة: تطوير وتقييم دمج الطاقة الشمسية مع أنظمة الأنتاج المزدوج التى تستخدم تربينة غازية في المملكة العربية السعودية

التخصص: هندسة ميكانيكية

تاريخ الدرجة العلمية: جمادى الآخر/١٤٣٤هـ

تعتبر المملكه العربية السعودية من أكثر مناطق العالم تعرضاً للإشعاع الشمشي حيث يمكن إستخدام تقنيات تحويل الطاقة الشمشية الى طاقة حرارية و بكفائة تشغيل عالية. تتوفر العديد من تقنيات تحويل الطاقة السمشية الى طاقة حرارية التى اثبتت كفاءتها عند دمجها مع محطات توليد الكهرباء. من هذه التقنيات مركزات القطع المكافئ وعاكسات فرينيل بالإضافة الى ابراج الطاقة الشمسية. إن دمج تكنولوجيا الطاقة الشمسية مع محطات الإنتاج المزدوج سوف يؤدي الى خفض إستهلاك الوقود وبالتالي الى خفض الوقود المستهلك للمحطة الذي بدوره سوف يؤدي الى الحد من التلوث البيئي نتيجة إنبعاثات غاز ثاني أكسيد الكربون والغازات الأخرى والتي أدت إلى الانحباس الحراري وارتفاع درجات حرارة الجو وتساقط الأمطار الحامضية وذوبان الثلوج وإنغمار أراضي صالحة للزراعه وإنحباس الأمطار عن مناطق أخرى مما يؤدي إلى التصحر.

يقدم هذا العمل دراسة للجدوى الفنية والإقتصادية لدمج الطاقة الشمية فى محطات الإنتاج المزدوج في اللملكة العربية السعودية. ولهذا الغرض تم إقتراح تصاميم هجينة ما بين الوقود الاحفوري ومجمعات الطاقة الشمسية . هذه التصاميم أخذت بعين الإعتبار دمج ثلاثة انواع من مركزات الطاقة الشمسية وهي مركزات القطع المكافئ وعاكسات فريسنيل بالإضافة الى أبراج الطاقة.

لقد تم تصميم المحطات لتوليد بخار بمعدل تدفق ثابت (٨١,٤٤ كجم في الثانية) وبدرجة حرارة ثابتة (٣٩٤ درجة مئوية) عند ضغط ثابت (٤٥,٤٤ ضغط جوي) خلال العام بالإضافة الى إنتاج الكهرباء. أخذت بعين الاعتبار عند التصميم الثلاثة الأنواع من مركزات الطاقة الشمية المذكورا سابقاً بالإضافة الى أنه تم إستخدام أحجام مختلفة من

التوربينات الغازية. وقد استخدم برنامج ثيرموفليكس في عملية المحاكاه والتقييم لجميع التصاميم المقترحة. وقد اجريت عملية التحليل الحراري والإقتصادي لجميع التصاميم بهدف الوصول الى التصميم التشغيلي الأمثل لأجواء المملكه العربية السعودية.

وفي النهاية تم تحديد التصميم الأمثل وهو دمج عاكسات فرينيل بمساحة تقدر حوالى ٩٣ هكتار الى الجانب البخاري لمحطة الإنتاج المزدوج وكان سعر وحدة الطاقة المنتجة من هذه المحطة حوالى ٥,١ سنت امريكي لكل كيلووات ساعة. وفي هذه الدراسة تم التوصل الى انة يمكن دمج مركزات القطع المكافئ بمساحة تقدر حوالى ١٠٤ هكتار في الجانب البخاري أيضاً مع فارق بسيط جدا في سعر وحدة الطاقة المنتجة. مع الأخذ بعين الاعتبار ان مركزات القطع المكافئ تم تركيبها و التحقق من كفائتها في محطات مختلفة حول العالم وعلى العكس من ذلك فإن عاكسات فريسنيل ما زالت نظرية فقط. لذلك لابد أن يتم التحقق من الجدوى التشغلية والتجارية لعاكسات فرينيل تحت ظروف تشغلية حقيقية. إضافة الى ما سبق لقد تم محاكاة المحطة المثالية في مناطق مختلفة في المملكة العربية السعودية وتم التوصل الى ان أفضل منطقة لإنشاء هذه المحطة هي مدينة جزان الواقعة في حنوب اللملكة العربية السعودية.

CHAPTER 1

INTRODUCTION

1.1 Definition of Cogeneration

Cogeneration is the production of electrical power and heat simultaneously from the same fuel source. Probably the most widely used definition of cogeneration is the following:

> *"Cogeneration is the combined production of electrical (or mechanical) and useful thermal energy from the same primary energy source."* [1].

Cogeneration is the most efficient way of energy conversion. Its wider use has various positive impacts on the economy, the environment, the responsible use of resources and security of energy supply. Cogeneration is usually used for large towns, hotels, hospitals, universities, office buildings, swimming pools and leisure centres, enhanced oil recovery wells, oil refineries, the chemical industry, and many other industrial applications with substantial heating needs [1, 2]. Cogeneration is also adaptable for smaller projects or homes (called micro cogeneration).

A typical cogeneration system consists of a prime mover (heat engine) where fuel is converted to mechanical power and heat, a generator where the mechanical energy is used to produces electrical energy, a heat recovery steam generator that recovers waste

heat from the exhaust gas to produce hot water or steam, a heat rejection system, pumps and other electromechanical interconnections between the power blocks, and a control system. The prime movers for cogeneration systems include steam turbines, gas turbines, reciprocating engines, and diesel engines. Among these prime movers, the gas turbine will be considered to be the prime mover for this study.

Most cogeneration systems can be characterized either as a topping cycle cogeneration or as a bottoming cycle cogeneration. In topping cycle cogeneration; a fluid with a high temperature (exhaust gases, or steam, 600-1200°C) is used to drive an engine to produce electrical power, while low temperature fluid (200–600°C) is used for industrial processes or space heating. In bottoming cycle cogeneration, the high temperature heat (1000-1200°C) is first produced for industrial process (e.g. in a furnace of a glass-works or a metals-works) and after that the hot fluid from the industrial process (500–600°C) is used to drive a turbine to generate electrical power. Topping cycle cogeneration plants are the most common ones [1, 4].

1.2 Importance of Cogeneration

Because cogeneration is simply combined heat and power production, it is most cost-effective. Actually, cogeneration offers several economic benefits. The cogeneration plant reduces the waste heat from the power generation system that in turn lead to raise the plant efficiency when its compared with the efficiency of traditional power plants. As a result, energy cost is lower for cogeneration plants [1, 2].

For most applications, heating requirement determines the size of a cogeneration plant. This is because electricity is relatively easy to buy and sell to or from a local utility, and as a consequence, cogeneration units are usually sized to meet the heat demands of a site. As a result, in many cases, a cogeneration scheme will produce more electricity than it needs, and the operator can sell the excess electricity generated to the electricity market that leads to more opportunities for energy savings.

Studies have conclusively shown that cogeneration is more environmentally friendly than conventional power plants; also cogeneration is generally the most cost-effective way of reducing carbon emissions. It is highly fuel efficient, and ensures that maximum amount of energy production is achieved for the minimum level of emissions at minimum cost. The fact that cogeneration reduces demand for fuel means that it reduces the demand on natural resources, and it also reduces both the economic and environmental impacts of transporting and storing fuel.

1.3 Solar Thermal Description and Technology

1.3.1 Parabolic Trough Collector (PTC) System

A Parabolic Trough Collector (PTC) system consists of curved mirrors, a receiver, steel structure, and a tracking system as shown in Figure 1.1. The curved mirrors are reflecting and concentrating the solar radiation into an absorber tube (receiver) which is located in the focal line of the collector. The receiver consists of a special tube through which a heat transfer fluid is flowing heated up to about 400°C. Then the heat transfer fluid is used to boil water in a conventional steam generator to produce steam.

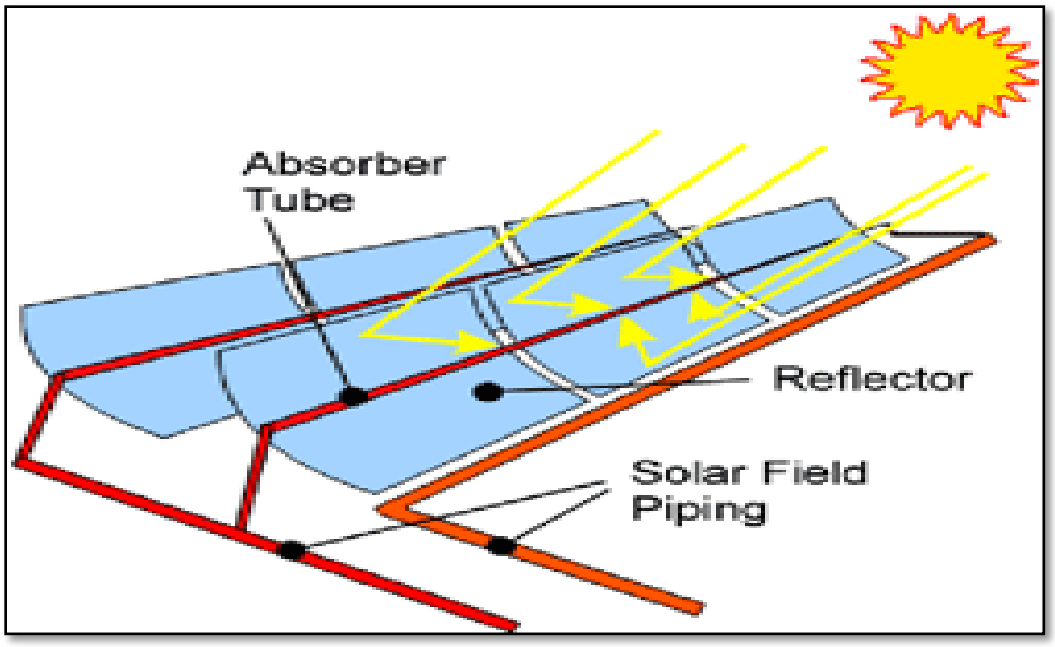

Figure 1.1: Component parts of a solar field for a parabolic trough system [6].

For direct steam generation collector, the heat transfer fluid is replaced by water which is boiled directly in the collector. During the day time, the parabolic mirrors follow the path of the sun in order to optimize the amount of radiation received.

1.3.1.1 Parabolic Reflector

The parabolic reflector consists of one surface with a reflecting layer or with several curved mirror segments. In commercial projects, the second variant is more usually applied. Reflectors are mounted on a steel structure and track the sun using a single axis system following the path of the sun. The mirrors typically utilize back-silvered white low iron glass with weather proof attributes to achieve high reflectivity over the mean value of 94%. This high reflectivity of the mirror segments can be maintained through regular cleaning of the solar collector [7].

1.3.1.2 Heat Absorber (Receiver)

The receiver tubes are installed on the focal line of the parabolic trough reflectors, as shown in figure 1.2, in order to minimize heat losses, steel absorber tubes with selective absorbing materials are enclosed in an evacuated glass tube. This vacuum design serves also to protect the selective coating.

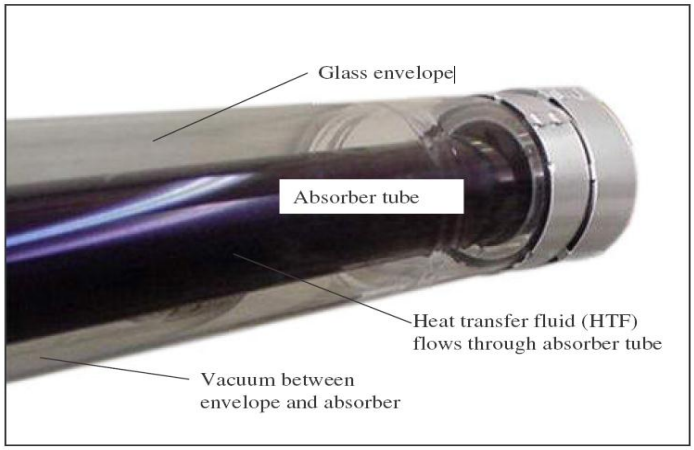

Figure 1.2: Receiver of a parabolic trough system [8]

Nowadays, the solar absorption of such selective coatings is above 95%, and at a temperature of 400°C emissivity is below 14 %. On the surface of the glass tubes, there is a layer of anti-reflective coating to collect maximum solar radiation [8].

1.3.2 Linear Fresnel Reflector (LFR) System

A Linear Fresnel Reflector (LFR) system consists of narrow mirror segments and a linear receiver above them. On top of the receiver, there is another long mirror to focus the radiation towards the receiver. In this system, several mirror segments share one linear receiver above them. Figure 1.3 shows a typical Linear Fresnel Reflector system.

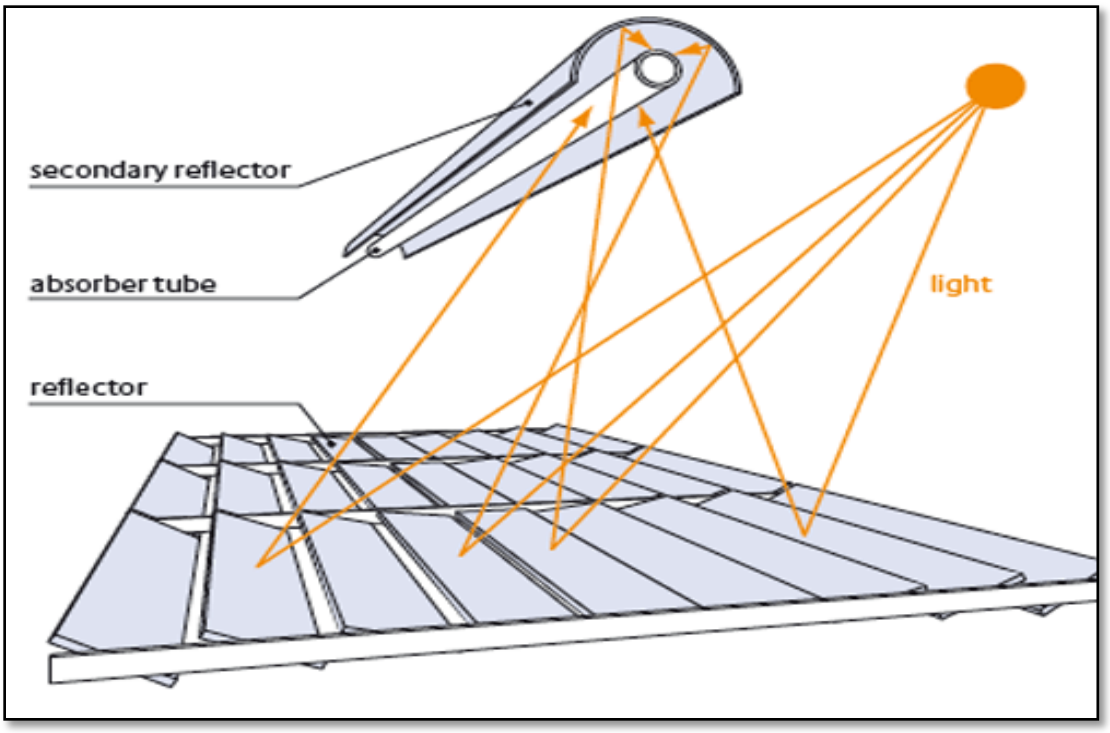

Figure 1.3: Component parts of a solar field for a linear Fresnel reflector system [6].

The LFR system is similar to the trough design in its use of one axis tracking system, but the structure of the LFR system is simpler than the trough design. This is because the narrow flat mirrors are used rather than parabolic formed ones. Also LFR mirrors do not support the receiver and the receiver is stationary. As a result, the cost of LFR is less and the lifetime is longer compared with a parabolic trough collector. Each mirror of the LFR is adjusted by a small motor and they can also reflect solar radiation to different receivers at different times of the day. This design provides the possibility of more mirrors installed on the available land area.

1.3.2.1 Fresnel Reflector

The Fresnel reflector is made of low-iron glass. The individual mirror segments are mounted on the steel frame at the same height and they can be rotated through 360° driven by a solar tracking system. During strong wind, the mirrors can turn upside down to avoid damage to the equipment. The lower width of the Fresnel reflectors can also reduce their wind loads. Figure 1.4 shows the reflector structure of the LFR system [9].

Due to their simpler structure, Fresnel reflectors have a lower concentrations and a lower optical efficiency than parabolic trough reflectors, though individually micro-adjustment of each reflector can compensate for such disadvantages. However, the sophisticated tracking system and the required large number of drive motors lead to high costs.

Figure 1.4: Fresnel reflectors of a linear Fresnel reflector system [9]

1.3.2.2 Fresnel Absorber

As shown in figure 1.5, the absorbers of the linear Fresnel systems are a group of tubes located in their wider focal line. These pipes are located inside a cavity and the bottom of the cavity is covered with a transparent cover, which is intended to reduce convective losses by trapping layers of hot air next to the hot heat transfer fluid pipes. This cover is commonly made from low-iron glass because the angled glass reduces reflective losses of solar radiation and low-iron glass has improved optical properties compared to standard grade window glass.

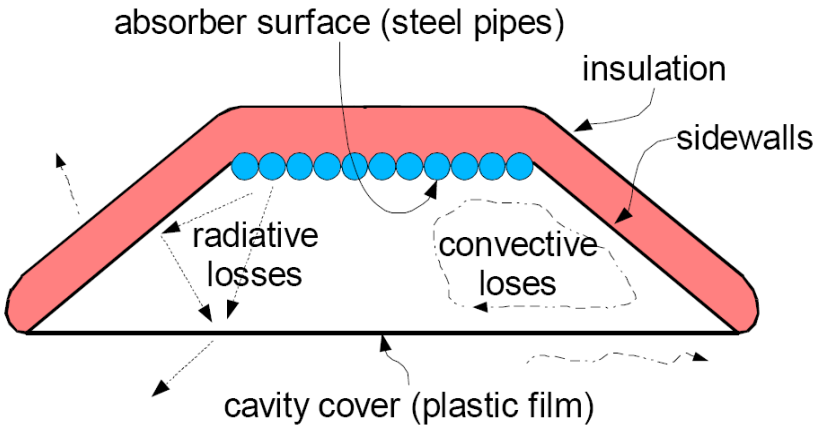

Figure 1.5: Receiver used in linear Fresnel reflector system [10]

1.3.3 Solar Tower (ST) System

In a Solar Tower (ST) system, the solar radiation is collected by mirrors called heliostats with a dual axis tracking system, and they are controlled so that they gather the incident solar radiation and reflect it on top of a tower, where the solar energy is absorbed by a receiver. The receiver absorbs the concentrated solar energy and then passes it to the heat transfer fluid which flows through the receiver. According to different types of heat

transfer fluid such as, water/ steam, molten salt, liquid sodium and air, the temperature of the receiver can range between 500°C to over 1000°C. The Figure below shows the basic layout of a solar power tower plant.

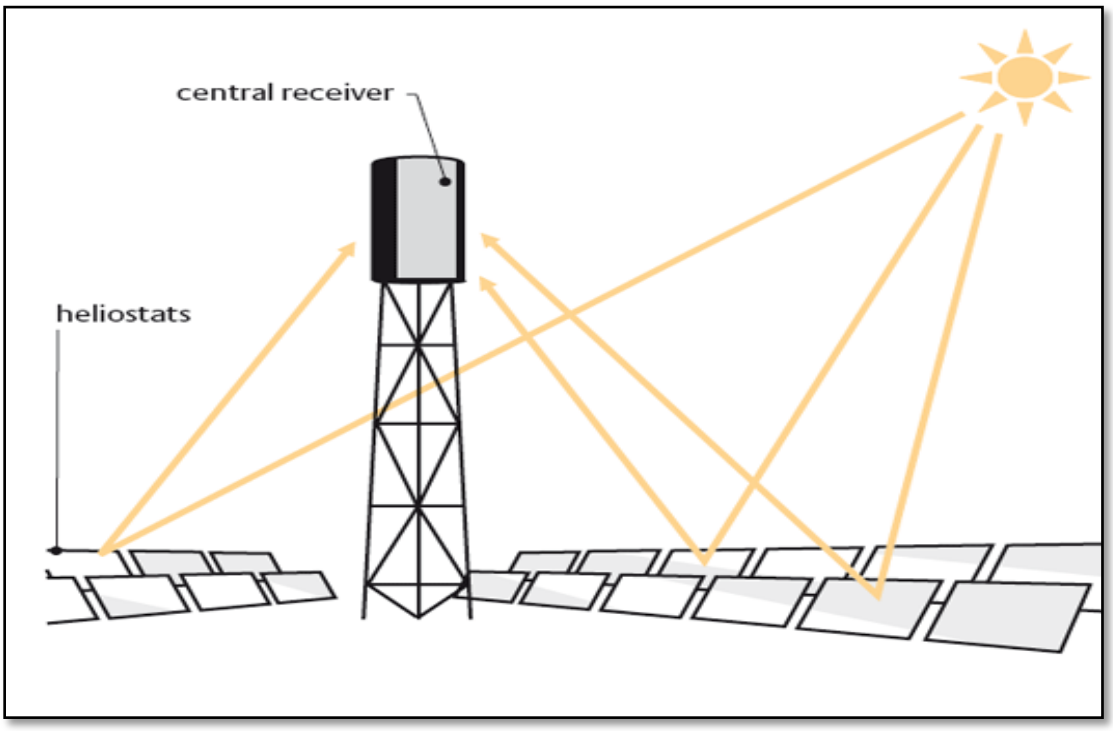

Figure 1.6: Component parts of the solar field for a solar tower system [6].

1.3.3.1 Solar Tower Reflector

The reflecting mirrors for a solar tower system are called heliostats. The heliostat's field consists of a large number of individual heliostats (from several hundreds to thousands). Heliostats are mirrors that are managed by a dual axis optical solar tracking system. The analog solar tracking circuit controls two mechanical actuators that move a mirror plane on two axes. The tracking system of the heliostats will keep the mirrors in position making them reflect the maximum possible incident solar radiation during the day to the

central receiver. The heliostat consists of a solar reflector, a tracking unit with a driving motor, the foundation, and an electronic control system [11]. The cost of the heliostats is a heavy weight of the total cost of solar tower power plant. As a result, the great effort is consumed on the development of heliostats to get a high optical quality and reliability with a long life and low area-specific costs. There are different types of heliostat mirrors such as faceted glass/metal heliostats, and membrane heliostats [11].

1.3.3.2 Tower and Receiver

The receiver of a central solar tower power plant is located on the top of the tower. As support of the receiver the tower is commonly with a height of 80 to 100 m and is made of concrete or steel structure. A higher tower is preferable for bigger and denser heliostats fields but it should avoid the shades or objects that block the sun. At the same time, the technical factors, e.g., tracking precision and the economic factors, e.g., tower costs should also be considered in determining the height of the tower. The receiver of solar tower power plant transforms the concentrated solar energy into the thermal energy of working fluid. This working fluid could be commonly water/steam or molten salts. In further research air is applied for use in high temperature power towers. Water/steam receivers are the most used receiver in solar tower power plants.

1.4 Database of the Cogeneration Plants in Saudi Arabia

The survey conducted at the beginning of this work revealed that the following plants that are installed and running in Saudi Arabia can be classified as cogeneration plants. These plants are briefly described in the following list.

Table1.1: Cogeneration plants in Saudi Arabia [61]

	Plant Organization	**Project Location**	**Production Capacity**
1	Rayet Al-Hijaz Trading Est.	Rabigh	Electricity: 5,000 MW Desalinated water: 150,000 m^3 /day
2	Rabigh International Power & Water Co.	Rabigh	Electricity: 1,200 MW Desalinated water: 450,000 m^3 /day
3	Misha'al Atiyah Al-Malki Est.	Rabigh	Electricity: 1,400 MW Desalinated water: 1,000,000 m^3 /day
4	Itlal Al-Ghad Group	Rabigh	Electricity: 1,000 MW Desalinated water: 100,000 m^3 /day Steam: 100,000 Tonne/hour
5	Arabian Paper Co.	Dammam	Electricity: 50 MW. Steam: 250 Tonne/hour
6	District Cooling Systems Co.	Taif	Electricity: 600 MW Desalinated water: Not determined yet. Steam: Not determined yet.
7	Mabaher Al-Jazeerah Strategic Power & Water	Rabigh	Electricity: 2060 MW Desalinated water:1,500 m^3 /day
8	Saline Water Conversion Corporation (SWCC)	Throughout the Kingdom	Electricity: 5,017.6 MW Desalinated water: 2,923,387 m^3 /day Steam: 28,692 Tonne/hour

9	Jubail Power Co.	Jubail Industrial City	Electricity: 250 MW Steam: 510 Tonne/hour
10	Tihama Power Generation Ltd. (Saudi Aramco Independent Projects)	Juaimah	Electricity; 308 MW Steam: 640 Tonne/hr
		Othmaniyah	Electricity; 308 MW Steam: 640 Tonne/hr
		Shadgum	Electricity; 308 MW Steam: 640 Tonne/hr
		Ras Tanura	Electricity; 150 MW Steam: 293 Tonne/hr
11	Shuaibah National Water & Electricity Co.	Shuaibah	Electricity: 1,191 MW Desalinated water: 888,000 m^3 /day Steam: 6,053 Tonne /hour
12	Shuqaiq Water & Electricity Co.	Shuqaiq	Electricity: 1,020 MW Desalinated water: 212,000 m^3 /day
13	Jubail Water & Electricity Co.	Jubail	Electricity: 2,875 MW Desalinated water: 805,464 m^3 /day
14	Rabigh Arabian Water & Electricity	Rabigh	Electricity: 120 MW Desalinated water: 12,000 m^3 /day Steam: 470 Tonne/hour
15	Saudi Aramco	Riyadh, Buqaiq, Qatif, Kharasaniyah, Barri, Yanbu	Electricity: 1,051 MW Desalinated water: 2,514 m^3 /day
16	Power and Water Utility Company for Jubail and Yanbu (Marafiq)	Yanbu	Electricity: 1,533 MW Desalinated water: 95,760 m^3 /day

CHAPTER 2

LITERATURE REVIEW

Gas turbine analysis covering material, energy, and entropy balances as well as detailed design equations can be found in Bathie [12]. In this book, compressors, turbines, and combustion chambers are examined first before proceeding to overall gas turbine modeling. Numerous problems were solved using both ideal gas and real gas models.

Cogeneration is a more efficient way to reduce fuel consumption; as a result, the efficiency of a cogeneration plant is high when it is compared to a conventional power plant. To increase efficiency of a cogeneration plant the design and operation of a Heat Recovery Steam Generator (HRSG) is the key. Much attention of research work has focused on this area [13, 14, 15, and 16]. Heat recovery steam generator modeling and simulation have been studied involving fired and unfired modes. Infect, selecting the temperature profiles in HRSG is one very important concept to study HRSG.

Combining gas turbines and heat recovery steam generator into a cogeneration system has been investigated by many researchers. Kim et al. [17] investigated the off-design performance of a gas turbine cogeneration facility. The performance of gas turbine was estimated using realistic compressor and turbine performance maps; also the performance of a Heat Recovery Steam Generator was modeled using heat transfer process.

Decreasing fuel consumption and electricity costs are very important for industries, especially energy intensive ones. Rosen [18] concluded that the substitution of cogeneration for separate electrical and heat generation processes leads to significant reduction in fuel energy consumption (24±61%), which in turn leads to approximately proportioning reductions in emissions.

Faqeeh et al. [19] studied the feasibility of cogeneration for Jeddah and Yanbu refinery plants in Saudi Arabia. A heat recovery boiler equipped with an auxiliary burner has been proposed. Thermo-economic analyses have been used to prove the feasibility of the proposed system. They concluded that the cogeneration option for these refinery plants is feasible and can lead to a considerable saving in fuel consumption.

Kanoglu and dincer [20] studied four different cogeneration systems: steam-turbine system, diesel-engine system, gas-turbine system, and a geothermal system. The energy and exergy efficiency were used to evaluate systems performance. Also, the same amount of thermal and electrical outputs was considered for all systems, except the diesel-engine system, to facilitate comparisons. Furthermore, the impacts of certain operating parameters (e.g., water temperature, steam pressure) on the energy and exergy efficiencies were investigated. The results showed that the diesel-engine and geothermal systems appear to be thermodynamically more attractive, in that they have higher exergy efficiencies, than steam-turbine and gas-turbine systems.

Combining the first or second law of thermodynamics with economics analysis (thermo-economics) provides a powerful tool for optimizing the complex power plants. Hamed et al. [21] evaluated different methods for cost application in cogeneration plants. They found that the exergy prorating cost allocation method is a suitable and rationalistic method for estimating the cost of unit electricity and water of a cogeneration plant. They also found that the fuel consumption and its costs are the most effective parameter on water and electrical power costs. Heans, the economic feasibility of power/water cogeneration plants can be significantly improved by selecting a cheap fuel source.

The design and performance of the Ghazlan power plant (Kingdom of Saudi Arabia) have been described by Habib et al. [22]. Their study was carried out based on first- and second-law of thermodynamic analyses; the main objective of their study was to identify the potential for improving the plant efficiency.

As a result of their improved energy performance, Cogeneration and trigeneration systems can also bring important advantages in terms of greenhouse gas emission reduction compared with a conventional power plant. Chicco and Mancarella [23] have presented and discussed a novel approach, based upon an original indicator called trigeneration CO_2 emission reduction (TCO_2ER), to assess the emission reduction of CO_2 and other greenhouse gases from combined heat and power (CHP) and combined cooling heat and power (CCHP) systems with respect to the separate production.

There are three methods, which have been employed to generate industrial process steam using line-focus solar collectors Kutscher et al. [24]: the steam-flash concept, in which pressurized water is heated in the collector field and then flashed to steam; the unfired-boiler concept, in which a nonfreezing, heat-transfer fluid is circulated through the collector field to generate steam through heat-exchange in an unfired boiler; and the direct steam generation concept, water is boiled in the collector and circulated through a steam process. The direct steam generation system was used in this study.

Parabolic trough collectors are preferred for steam generation in solar power plants, because high temperatures can be obtained without any serious degradation of the collector's efficiency. The development of a PTC system by universities and institutes for research purposes is well documented in the literature. For example, Kalogirou [25] described the design of a trough collector with an aperture area of 3.5 m², rim angle of 90° and a concentration ratio of 21.2. The performance of the collector was reported in terms of the recommended ASHRAE 93 procedure. Also Ibrahim [26] reported the performance of a multiple-trough collector, consisting of six connected parabolic troughs, each 1.14 m in length and 0.12 m wide giving a total aperture area of 0.82 m². Furthermore, Almanza et al. [27] successfully produced steam in the absorber tubes of an existing 29 m long parabolic trough collector with an aperture width 2.5 m and an absorber diameter of 25.4 mm. Moreover, Bakos et al. [28] described the construction of a trough with approximately 12 m² of aperture area and the capacity to track the sun about two axes.

A detailed thermodynamic analysis of thermal gains and losses through the heat collection element (HCE) has been completed by Forristall [29]. This model has been validated with several sets of performance data from the collectors and used to study the influence of different absorber tube materials, annulus gases, selective surface coatings, and glass envelope diameters on HCE performance.

A direct steam generation collector has been investigated by Cohen and Kearney [30] as a future development of the steam generation trough collector in order to eliminate the cost of heat transfer fluid and oil steam heat exchanger. Three concepts for a direct steam generation collector system have been proposed by Dagan et al. [31] as well as Lippke [32]: the once-through concept to generate superheated steam in one pass; the recirculation process concept to generate wet steam; and the injected water system to control steam quality and flow instability along the absorber tube.

Cogeneration assisted with solar system is one of the best energy production techniques that can be used to preserve the quality and accessibility in energy production while reducing fuel consumption, thereby, representing conservation of energy and more efficient way to use the energy resources. Alrobaei [33] identified and investigated the effectiveness and thermodynamic performance of concentrating solar cogeneration power plants. His results have shown that the integrated gas turbine solar cogeneration power plant is the most effective technology in terms of thermo-economy and environmental sustainability.

Dersch et al. [34] studied performance and economic analysis for three different power plants in different places (California and Spain). Those plants are conventional combined cycle, integrated solar combined cycle systems, and solar electric generating systems. Their results have shown that the integrated solar combined cycle systems provide a better solution than others.

The performance of the first integrated solar combined cycle system in Algeria has been presented by Behar et al. [35]. The simulated results showed that the capacity of the power plant increased by 17% by using an integrated solar combined cycle system without burning any extra fossil fuel in the heat recovery steam generator even in the gas turbines; also its efficiency increased by 9.5 %.

Montes, et al. [36] analyzed the annual operation of an integrated solar combined cycle system, in comparison to a conventional combined cycle gas turbine system. Their study was carried out at two locations: Almeria (Spain), and Las Vegas (USA). Their results showed that, whereas the conventional combined cycle gas turbine power plant worked badly in Las Vegas, an integrated solar combined cycle system operated better in Las Vegas than in Almeria, because solar hybridization is especially well coupled to the conventional combined cycle gas turbine power plant in the frequent days with great solar radiation and high temperatures in Las Vegas.

An integrated solar combined cycle system was technically and economically studied in Egypt by Horn, et al. [37]. Both, a parabolic trough collector system and a volumetric air

receiver tower system were considered as solar systems in their study. Also a fossil fired combined cycle power plant was assumed as a reference cycle to follow the same daily load profiles. Their results showed that, the total levelised electricity cost is equal for both integrated solar combined cycle system variants, but the solar levelised electricity cost is a quite different, whereas the levelised electricity cost for the reference cycle is less. But the integrated solar combined cycle system still provides an environmentally beneficial and economically attractive option for renewable power generation in Egypt.

A combined Rankine/Kalina cycle power plant was investigated for concentrating solar thermal power plants by Mittelman and Epstein [38]. That combination allows production of power during low insolation periods, and it also leads reduction the installation cost by using smaller condensing system requirements when they used parabolic trough technology for their combination plant with a capacity 50 MW. Their result showed that a 4–11% savings of electrical costs power could be achieved.

Baghernejad and Yaghoubi [39] applied the thermo-economic concept using a genetic algorithm to optimize an integrated solar combined cycle system that produces 400 MW of electricity in Iran. Their results showed that the objective function for the optimum operation was reduced by about 11%. Also the cost of electricity produced by steam turbine and gas turbine in the optimum design of the integrated solar combined cycle system are about 7.1% and 1.17% lower with respect to the base case. These objectives were achieved with a 13.3% increase in capital investment.

Eter [40] investigated the feasibility of integrating concentrated solar power (CSP) technology with the conventional combined cycle technology for electric generation in Saudi Arabia. The optimal integration configuration has been investigated further to achieve the optimal design of the solar field that gives the optimal solar share. He found that the optimal integration configuration is solarization steam side in a conventional combined cycle with solar multiple 0.38 which needs 29 hectare and LEC of Hybrid Solar Combined Cycle (HYCS) was 63.17 $/MWh under Dhahran weather conditions.

Mokheimer et al. [41] have presented a simulation of Integrated Solar Cogeneration Gas Turbine Systems (ISCGS), in which they presented and discussed the technical and economical feasibility of integrating parabolic trough solar technology with gas turbine cogeneration plants that are progressively installed in Saudi Arabia to produce steam and replace industrial boilers

CHAPTER 3

OBJECTIVES

The main objectives of the proposed work are to develop a solar assisted gas turbine cogeneration system and assess its thermodynamic, its economical, and environmental impact under Saudi Arabia's weather conditions. In this regard, different designs of hybrid solar/fossil fuel gas turbine cogeneration systems have been proposed. The proposed designs will consider the possible integration of three main Concentrating Solar Power (CSP) technologies with conventional gas turbine cogeneration systems. These CSP technologies are namely, Solar Tower (ST) Systems, Parabolic Trough Collector (PTC) Systems, and Linear Fresnel Reflector (LFR) Systems. THERMOFLEX + PEACE simulation software is used to assess the performance of each proposed integration design. Thermo-economical analysis is conducted for different designs under Dhahran weather conditions in KSA.

The specific objectives of the proposed work are:

1. To develop a simulation code for evaluating optical and thermal efficiencies of Parabolic Trough Collector (PTC) under Dhahran's weather conditions

2. To simulate and analyze the different sizes of the gas turbine and the duct burner of a conventional cogeneration plant for a fixed thermal load (reference cycle).

3. To integrate and simulate a Parabolic Trough Collector (PTC) system with the steam generation side in gas turbine cogeneration plant and investigate its operation.

4. To integrate and simulate a Linear Fresnel Reflector (LFR) system with the steam generation side in gas turbine cogeneration plant and investigate its operation.

5. To integrate and simulate a Solar Tower (ST) system with the gas side of a gas turbine cogeneration plant and investigate its operation.

6. To compare the optimal integrated configuration according to thermo-economic analysis.

CHAPTER 4

PROBLEM STATEMENT AND APPROACH OF SOLUTION

4.1 Problem Statement

The incident solar radiation is hourly and seasonally fluctuating, and as a result the outlet energy from a solar field will also change over time. If there is a need for a stable power outlet from solar thermal power, many strategies may be used. Integrating a gas turbine cogeneration plant the solar system to provide a compensation effect is one of them.

The cogeneration plant of Ras Tanura with 150 MWe and 81.44 kg/s steam production [43] has been the aim of simulation and design modification in the present work. The steam temperature is 394°C, whereas in this study the steam pressure is 45.88 bars. Figure 4.1 shows a schematic diagram for the conventional gas turbine cogeneration plant. As can be seen in the Figure 4.1, the plant has one gas turbine, one duct burner, one superheater, an evaporator, one economizer, and a pump. The gas turbine was connected to heat recovery steam generation through a supplementary duct burner. In order to explain the plant's working in the clearest way it is essential to remember that this plant works with two different working fluids: air/gas and steam/water.

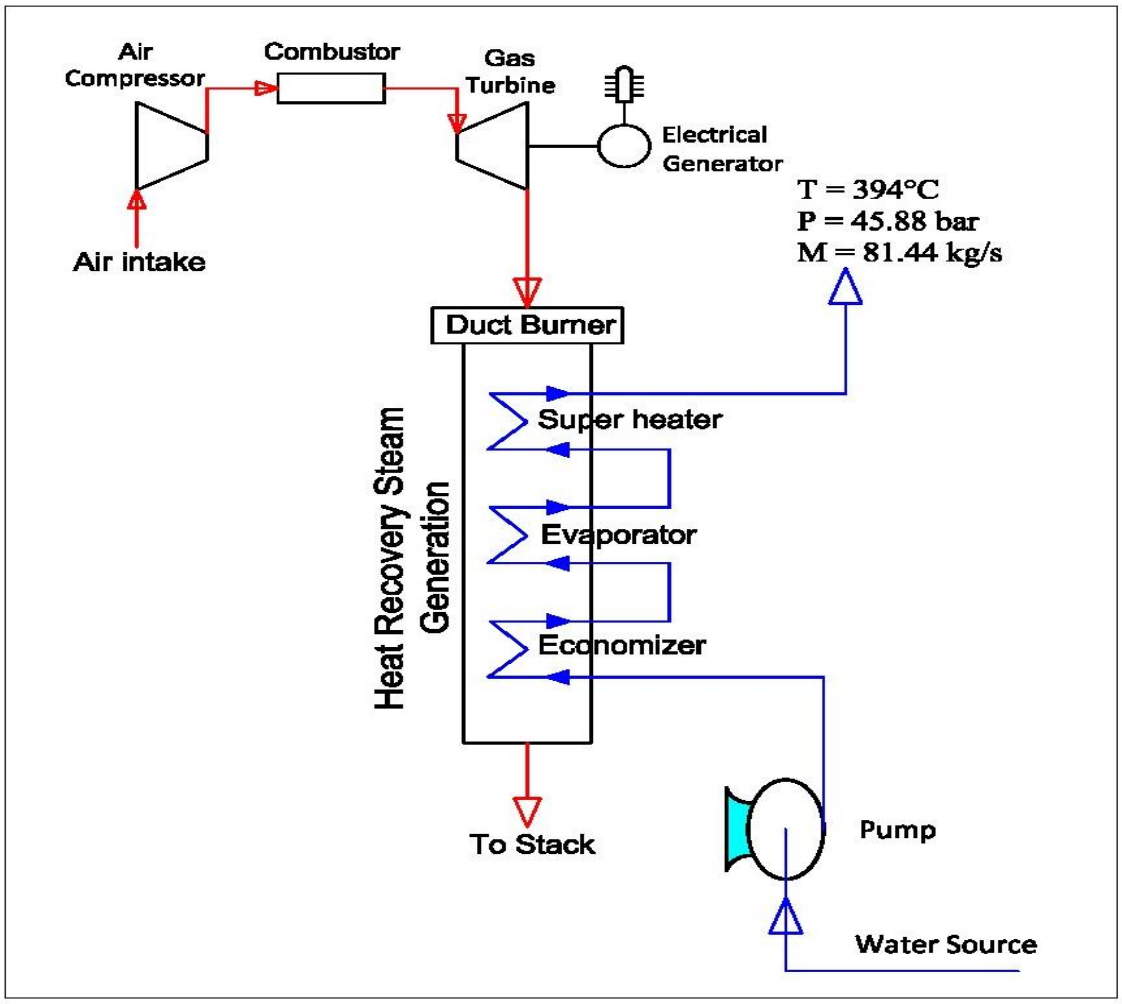

Figure 4.1: Schematic diagram of a conventional gas turbine cogeneration power plant.

The exhaust gases from the gas turbine are recovered through Heat Recovery Steam Generation (HRSG) system to produce the steam. As shown in Figure 4.1, when exhaust gases enter the HRSG system it first passes through the superheater where it exchanges heat with the steam produced by the evaporator, raising the steam temperature before it enters the proses. The exhaust gas then passes through the evaporator where it again gives away part of its heat to water to be transformed to steam. When passing through the last piece of equipment: the economizer; the exhaust exchanges heat once again giving it

this time to liquid water to increase its temperature at the entrance of the evaporator. This helps to improvement of the power given by the plant and the plant's efficiency. At this point the exhaust gases exit the plant and goes to the stack. On the other hand, water transforms into steam by the heat power received by exhaust gases. The resultant heated steam goes to the industrial process. This cycle was used as a reference cycle.

In the present study, different gas turbine sizes for cogeneration system have been investigated to give constant thermal load from the plant. So for the capacity of gas turbine sizes smaller than 150 MW, the required thermal power was provided by the duct burner. Also, a duct burner is installed in the HRSG to raise additional steam when the solar generator is unavailable.

The first phase of the study is to investigate the thermo-economic performance when the gas turbine size is changing (reference cycle), whereas the second phase of the study is to investigate the effect of integrating three different concentrating solar technologies to the gas turbine cogeneration system with different gas turbine sizes. In this part of the study the required size of the solar collector was estimated in addition to the installation and operation costs. Other thermo-economical and environmental performance metrics have been evaluated and compared for each of the gas turbine sizes suggested for each integration mode

4.1.1 Systems to Be Analyzed

This study focuses on the thermo-economic analysis of four different configurations. The following systems are representing the main idea of the present work. The reference system is shown in Fig. 4.1 which is a schematic diagram of the conventional gas turbine cogeneration power plant, whereas, the other systems are gas turbine cogeneration power plants assisted by three different solar concentration technologies, namely Parabolic Trough collector (PTC) technology, Linear Fresnel Reflector (LFR) technology, and Solar Tower (ST) technology. The four specific systems to be analyzed in this study are the following:

1. Reference conventional gas turbine cogeneration power plant which is basically a simple gas turbine cycle with HRSG and duct burner as shown in Fig.4. 1.
2. Parabolic Trough Collector (PTC) system integrated with steam generation side in gas turbine cogeneration plant as shown in Fig. 4.2.
3. Linear Fresnel Reflector (LFR) system integrated with steam generation side in a gas turbine cogeneration plant as shown in Fig.4. 3.
4. Solar Tower (ST) system integrated with a gas side of cogeneration plant, where solar energy is used to pre-heat compressed air before entering combustion chamber as shown in Fig. 4.4.

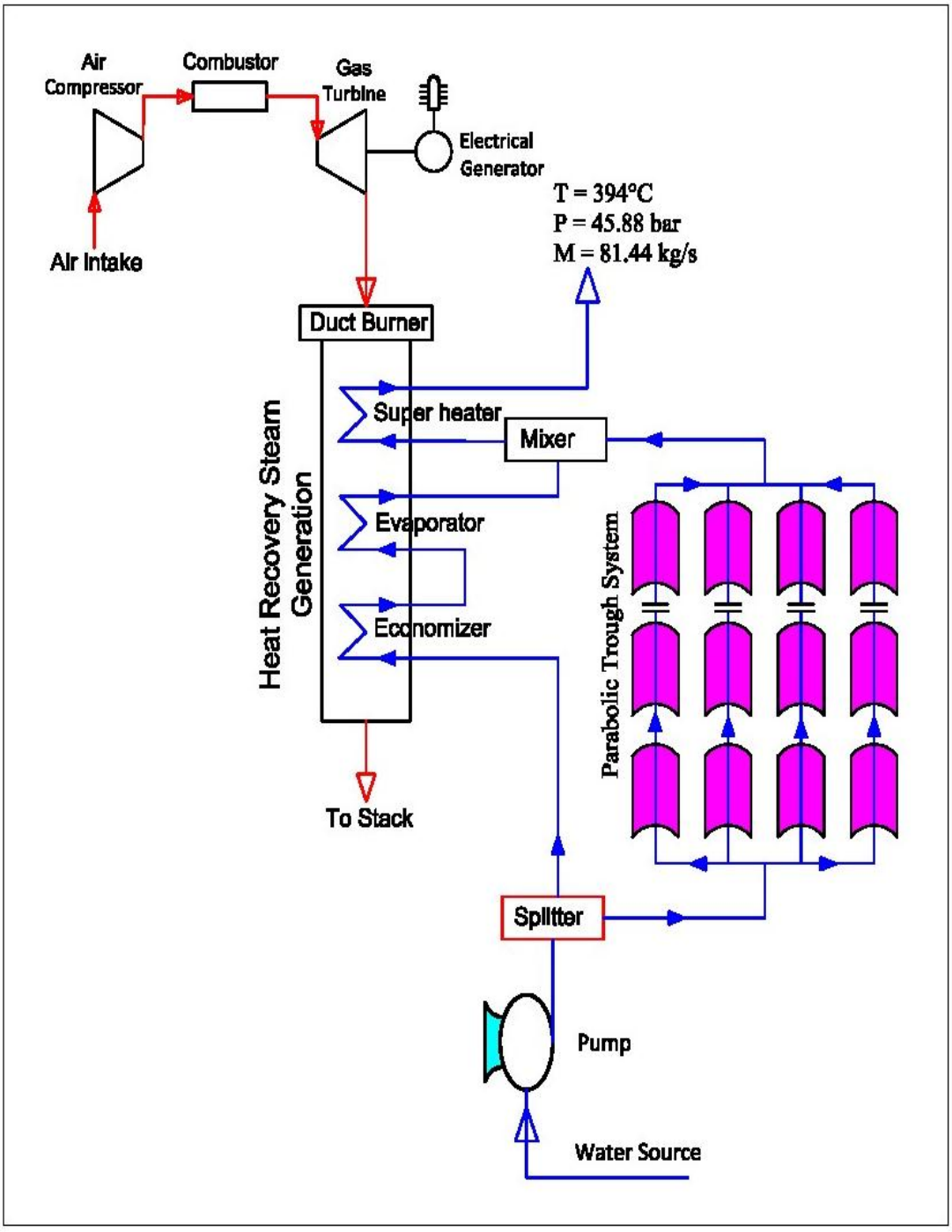

Figure 4.2: Schematic diagram of a PTC integrated with steam generation side in a gas turbine cogeneration plant

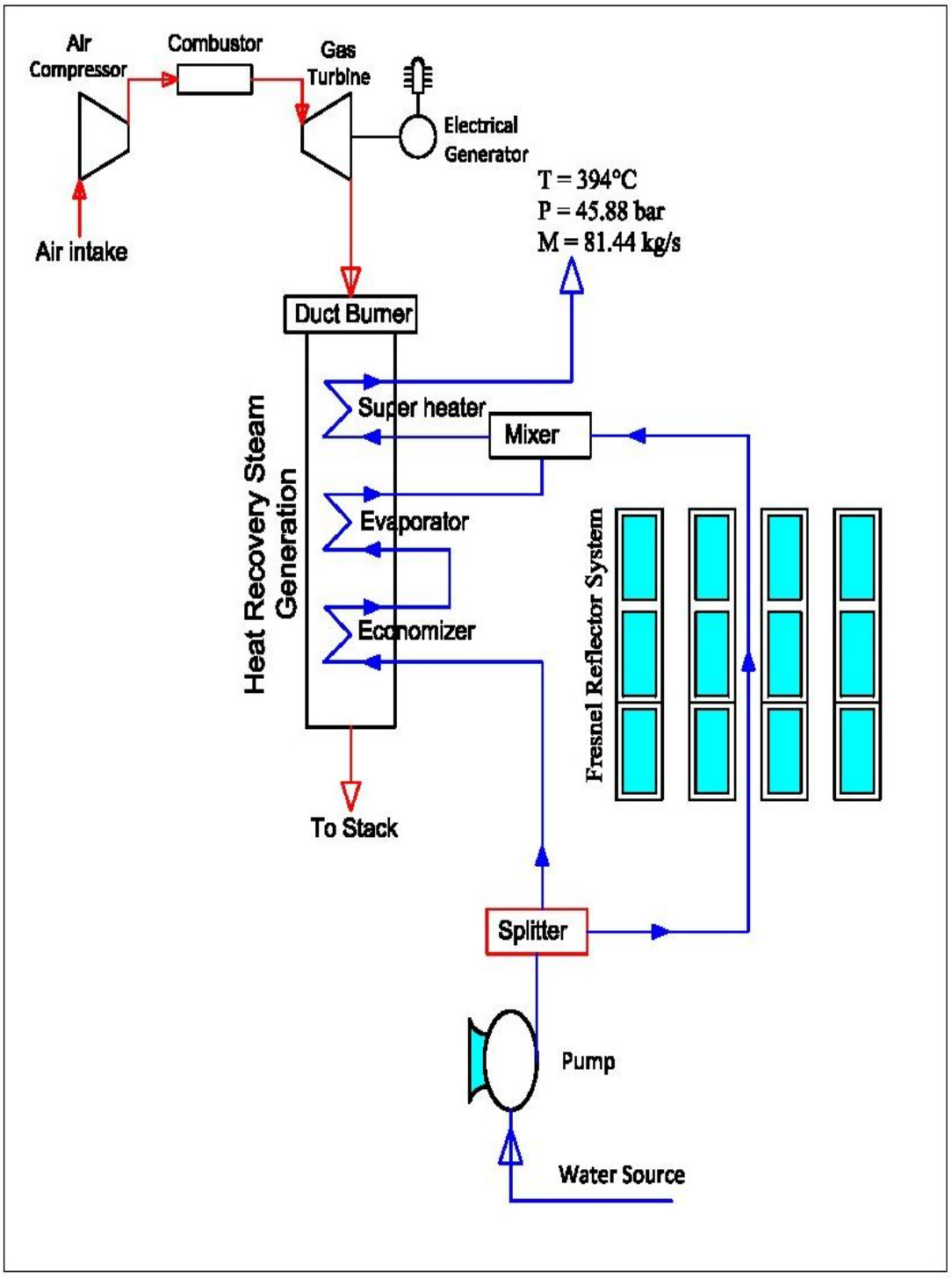

Figure 4.3: Schematic diagram of a LFR system integrated with steam generation side in a gas turbine cogeneration plant

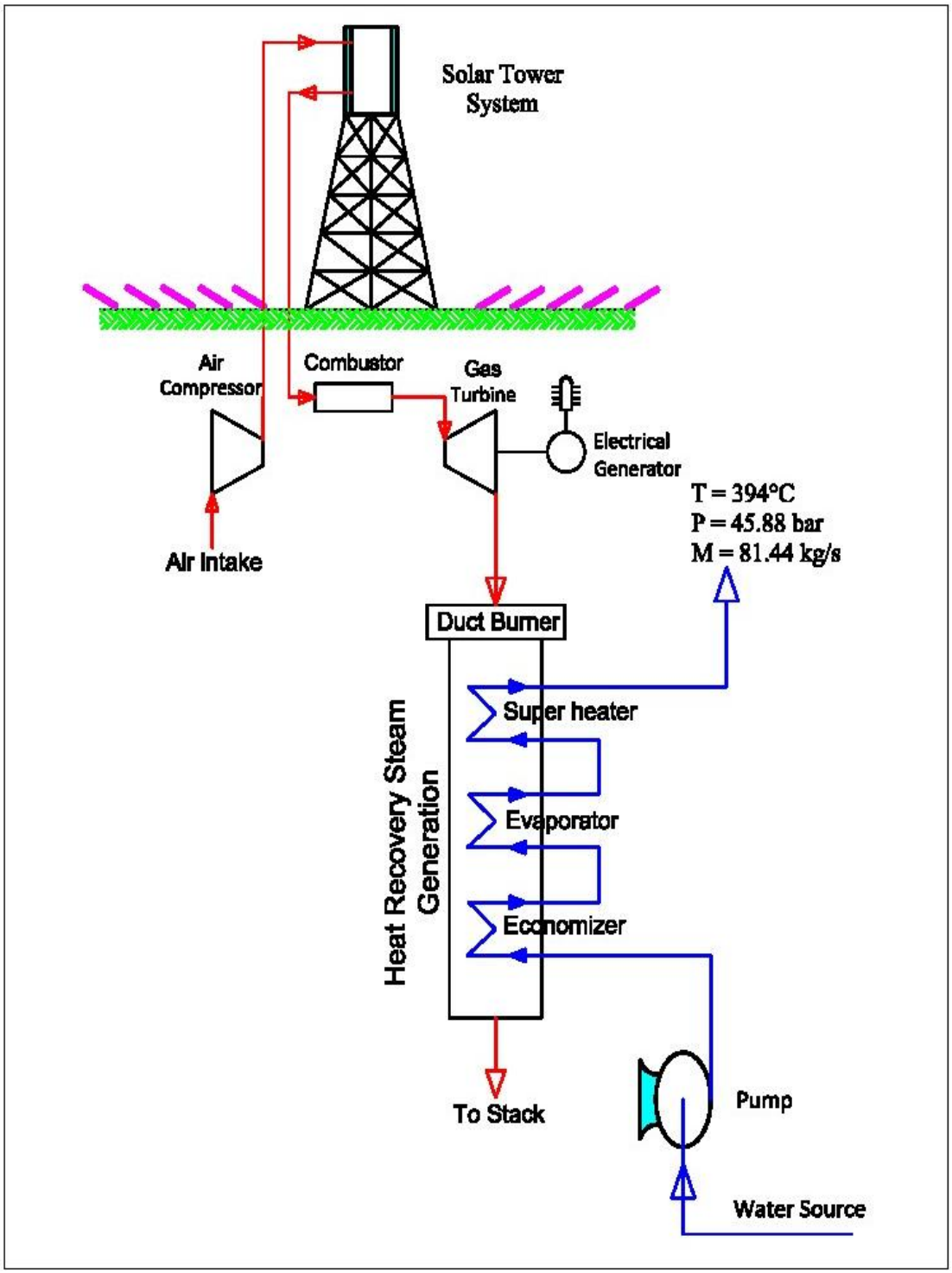

Figure 4.4: Schematic diagram of a ST system integrated with a gas side of gas turbine in cogeneration plant

4.2 Approach

To achieve the above stated objectives the THERMOFLEX with PEACE software was used to assess different integrating design. Actually, THERMOFLEX + PEACE software has a model library containing all components necessary for the simulation of a conventional and solar assisted cogeneration power plant including models for the three CSP technology considered design of the proposal work. Moreover, many thermo-economic performance matrices were evaluated so as to asses and optimize the thermo-economic performance of each of the proposed integrating designs of the CSP technology with cogeneration system.

The first step was to optimize the size of a gas turbine and duct burner in a conventional gas turbine cogeneration system. The second step was to investigate the optimal integration of different solar CSP technology with a conventional gas turbine cogeneration system.

4.2.1 Solution Methodology

THERMOFLEX with PEACE software was used for thermo-economic analysis of the gas turbine cogeneration system assisted by solar power systems.

The following are the steps to simulate and analyze the system:

1. Determine the latitude and longitude of the industrial plant location
2. Gather the weather data of that location; these data include:

- Average hourly direct normal irradiance; dry bulb temperature; and relative humidity.
- Average daily direct normal irradiance; dry bulb temperature, and relative humidity.
- Average monthly direct normal irradiance; dry bulb temperature, and relative humidity

3. Build the configurations by using THERMOFLEX software.
4. Determine the technical characteristics of the solar collector assembly.

These characteristics are available for solar collectors installed in many solar power plants, which are include the aperture length and width of the collector, the optical efficiency of the collector, the outer and inner receiver diameter and the concentrating ratio of the collector.

5. Assume different scenarios of operation and integration modes that include:
   - Conventional gas turbine cogeneration system
   - Gas turbine cogeneration system assisted by solar energy
6. Calculate all thermo-economic parameters for each integration mode.
7. Compare all configurations according to thermo-economical performance.

The definitions and significance of all the thermo-economic matrices to be used during the proposed work to assess and optimize the integrated solar gas turbine cogeneration system are given here after.

4.2.2 Simulation Parameters and Performance Metrics

Different parameters have been used to evaluate the performance of integrating different solar field sizes with different sizes of gas turbine such as solar multiple, annual solar share, instantaneous solar share, net incremental solar efficiency, and incremental CO_2 avoidance.

4.2.2.1 Efficiency of gas turbine cogeneration plant

For a cogeneration plant producing electricity and heat, the first law total energy efficiency is defined as the ratio of delivered usable energy to the energy input [1]:

$$\eta_{cogen} = \frac{(W_{net} + Q_{heat})}{E_{inp}} \tag{4.1}$$

Where, W_{net} is the net electrical power output, Q_{heat} is the rate heat is supplied from the plant, and E_{inp} is the rate of energy input to the plant. This relation is referred to as the utilization efficiency to differentiate it from the thermal efficiency, which is commonly used for a power plant with single output power.

$$E_{inp} = \dot{m}_{fuel} * LHV \tag{4.2}$$

where

$\dot{m}_{fuel}$: Fuel mass flow rate,

LHV : Lower heating value of fuel.

4.2.2.2 Solar Multiple

Solar multiple represents the amount of solar energy provided by the solar field relative to the power block size under reference conditions. In the proposed work, the solar field was integrated to gas turbine cogeneration power plant in two ways, one of them the solar field (PTC or LFR) was integrated to steam side in the cogeneration power plant. The other one solar field (ST) was integrated to gas side in cogeneration power plant. For that matter, the definition of solar multiple is different for the two methods.

Solar multiple for integrating solar field in steam side is representing ratio of thermal power produced by solar field to the total thermal power needed for the proses [40,and 42].

$$SM = \frac{P_{th,solar}}{P_{th,total}} \tag{4.3}$$

Increasing or decreasing of solar multiple (solar field size) can be carried out by increasing or decreasing the mass follow rate of heat transfer fluid through the solar field with fixing inlet and outlet temperatures of the solar field (in design mode). In other words, the design of different solar field sizes was performed at the same design hour but for different mass flow rates.

$$Solar\ \ thermal\ \ \ power = \dot{m}_w * (h_{outlet,SF} - h_{inlet,SF}) \tag{4.4}$$

Where

$\dot{m}_w$: Water flow rate through solar collector field

$h_{outlet,SF}$: Enthalpy of water at outlet of solar collector field

$h_{inlet,SF}$: Enthalpy of water at inlet of solar collector field

Solar multiple in other configuration where the solar field is integrated to the gas turbine side is defined as the ratio of the produced thermal power by solar tower system to the required thermal power for gas cogeneration cycle as shown in eq. (4.5). The reason behind this way of defining the solar multiple in this configuration, solar thermal energy is contributing in the production of the electric and thermal powers of the cogeneration plant.

$$SM_{st} = \frac{P_{th,solar}}{P_{th,Gas\ Turbine} + P_{th,duct\ burner}} \tag{4.5}$$

$P_{th,solar}$,$P_{th,Gas\ Turbine}$, and $P_{th,duct\ burner}$ can be calculated using the following formulas:

$$P_{th,solar} = \dot{m}_{gas}(\ h_{out,SF} - h_{in,SF}) \tag{4.6}$$

$$P_{th,Gas\ Turbine} = \dot{m}_{gas} * C_P * T_{inlet,GT} \tag{4.7}$$

$$P_{th,duct\ burner} = \dot{m}_{fuel,duct\ burner} LHV \tag{4.8}$$

Where

$P_{th,solar}$:Thermal power produced by solar tower system

$P_{th,Gas\ Turbine}$:Thermal power enter to turbine

$P_{th,duct\ burner}$:Thermal power produced by duct burner

$\dot{m}_{gas}$: Flow rate of compressed air through solar collector field

$h_{outlet,SF}$: Enthalpy of compressed air at outlet of solar collector field

$h_{inlet,SF}$: Enthalpy of compressed air at inlet of solar collector field

C_P :Specific heat

$T_{inlet,GT}$:Temperature of gases entering the turbine

$\dot{m}_{fuel,duct\ burner}$:Fuel flow rate entry to duct burner

LHV :Lower heat value of fuel

4.2.2.3 Annual Solar Share (SS)

Annual solar share is the ratio of the energy generated from the solar energy input to the total energy generated from both the solar and fuel energy input to the plant over the year [34, and 40].

$$Annual\ Solar\ Shar\ (SS) = 1 - \frac{(Annual\ Fuel\ consumption/\ KWh)_{ISGCP}}{(Annual\ Fuel\ consumption/\ KWh)_{GCP,Reference}} \quad (4.9)$$

Where

$\left(\frac{Annual\ Fuel\ consumption}{KWh}\right)_{\text{ISGCP}}$: Annual fuel consumption per kWh of integrated solar with gas turbine cogeneration power plant.

$\left(\frac{Annual\ Fuel\ consumption}{KWh}\right)_{GCP,Referen}$: Annual fuel consumption per kWh of gas turbine cogeneration power plant (GCP) that produce same electric and thermal power of the ISGCP cycle.

4.2.2.4 Net Incremental Solar Efficiency

Net incremental solar efficiency indicates to the efficiency of converting the solar energy into the generated energy [34, 36, and40].

$$\eta_{net\_incr\_solar} = \frac{P_{gen,ISGCP} - \eta_{ref} * \dot{m}_{fuel,\text{ISGCP}} * LHV}{P_{th,solar}/\eta_{th,collector}} \quad (4.10)$$

Where

$P_{gen,ISGCP}$:Total power generated from integrated solar gas turbine cogeneration power.

η_{ref} : Net efficiency of the reference power plant.

$\dot{m}_{fuel,\mathrm{ISGCP}}$: Total fuel flow rate of integrated gas turbine solar cogeneration.

$P_{th,solar}$: Thermal power produced by solar field.

4.2.2.5 Instantaneous Solar Share

Instantaneous solar share is the ratio of the power generated from the solar field to the total power generated from both of the solar and fuel energy input to the plant at the design hour [34], [36], and [40].

$$X_{net,eng,solar} = \frac{\eta_{net\_incr\_solar} * P_{th,solar}/\eta_{th,collector}}{P_{gen,IGSCP}} \tag{4.11}$$

Or

$$X_{net,eng,solar} = \frac{P_{gen,Solar}}{P_{gen,\mathrm{ISGCP}}} = \frac{P_{gen,\mathrm{ISGCP}} - \eta_{ref} * \dot{m}_{fuel,\mathrm{IGSCP}} * LHV}{P_{gen,\mathrm{ISGCP}}} \tag{4.12}$$

Where

$P_{gen,Solar}$:Power generated from the solar field

$P_{gen,\mathrm{ISGCP}}$: Total power generated solar from integrated gas turbine cogeneration power plant (ISGCP)

4.2.2.6 Incremental CO_2 Avoidance

Incremental CO_2 avoidance is the annual reduction of CO_2 emission due to the utilization of solar energy [40].

$$\Delta \mathrm{co}_2(\%) = \frac{\mathrm{co}_{2_{GCP,\mathrm{Ref}}} - \mathrm{co}_{2_{\mathrm{ISGCP}}}}{\mathrm{co}_{2_{GCP,\mathrm{Ref}}}} * 100\% \tag{4.13}$$

$co_{2_{GCP,\text{Ref}}}$: Annual emission of CO_2 from of gas turbine cogeneration power plant (GCP)

$co_{2_{\text{ISGCP}}}$: Annual emission of CO_2 from integrated solar gas turbine cogeneration power plant (ISGCP)

4.2.2.7 Economic Analysis:

Economic analysis is a decisive factor and is the most important factor in the design of a power plant. The power plant must not only be sufficient from the technical study, but also from the economic viewpoint. Therefore, the plant must satisfy the energy demand, with an optimal combination of investment and running costs which gives the lowest total cost. For this reason, it is important to clear some feature related to the economic analysis, which are taken into account in the proposed work.

Economic analysis will perform in terms of levelized energy cost (LEC) and solar levelized Energy Cost (SLEC). Both terms can be calculated from the following formulations.

4.2.2.7.1 Levelized Energy Cost

Levelized Energy Cost can be defined as the ratio of the total annual cost in USD$ to the total annual energy generated from power plant.

$$LEC = \frac{total\ annualized\ cost}{total\ energy\ produced\ per\ year} \quad (\$/KWh) \tag{4.14}$$

It is well known in the cogeneration system there are two main products, which are steam and electric energy. According to literature [44, 45, 46, 47, and 48] one can calculate the Levelized Energy Cost of cogeneration system by fixing the cost of one of the products (usually steam) at its local market price, and calculate the "net cost" of the other (usually power). For example, references [44, and 45] calculated the LEC by fixing the steam cost at local market. In their calculations, a steam price 20% higher than the respective fuel price was assumed. Whereas the reference [46] evaluated the costs and benefits of new diesel cogeneration systems that were suitable for rural Alaska and determined the extent to which these systems could potentially reduce the cost or improve the reliability of electricity for rural communities. They concluded that, where the electricity is the primary product and the steam is the byproduct, the steam energy was priced between $4.00 and $14.20 per MMBtu, when the steam is the primary product and the electricity is the byproduct, the electricity is priced between $0.04/kWh and $0.13/kWh.

The thermal load is a constant for all design plants which are considered in the proposed work, so one can fix the cost of steam and calculate the net cost of the electrical energy. In present calculations a steam price was assumed higher than the respective fuel price by 20% [44, and 45]. Levelized electricity Cost (LEC) could be defined as follows;

$$LEC = \frac{I_{tot} * fcr + OM_{ann} + F_{ann} - steam\ energy\ cost}{E_{el,ann}} \tag{4.15}$$

Where

I_{tot} : Total investment cost.

fcr : Annuity factor.

OM_{ann} : Annual Operation and Maintenance costs.

F_{ann} : Annual fuel consumption cost.

E_{ann} : Annual total electrical energy (kWh).

$$fcr = \frac{K_d * (1 + K_d)^n}{(1 + K_d)^n - 1} + K_{insurance} \quad (4.16)$$

Where K_d is the real debt interest; $K_{insurance}$ is annual insurance rate; n is depreciation period in years.

Table 4.1: Parameters for performance and LEC evaluation [36, 40]

Debt interest rate (K_d)	9 %
Annual insurance rate ($K_{insurance}$)	1%
Depreciation period (n)	20 Year
Fuel heat rate (LHV)	50046.7 KJ/Kg
Fuel cost	4.4 US$/GJ
Steam cost	4.4*1.2= 5.28 US$/GJ
Annuity factor	0.11955 %
Fixed O&M cost	20 US$/ (Net electrical power kW/year)
Variable O&M cost	0.002 US$/ kWh
Solar field specific O&M costs (US$)	1% from solar field installation cost
Total operation hour in the year	8760 hour

4.2.2.7.2 Solar levelized Energy Cost (SLEC)

Solar levelized Energy Cost (SLEC) is the second important parameter of economic analysis. SLEC has been defined in different forms in literature but with the same physical meanings as follows [40]:

1- Calculation of solar levelized energy cost can be considered by the ratio of solar field cost to the annual energy produced by solar as shown in the following formula:

$$SLEC = \frac{Cost_{solar\ field}}{W_s} \tag{4.17}$$

2- Calculation of solar levelized energy cost when annual solar share is based on output data (annual energy produced by solar) as shown in the following formula [37, and 40].

$$SLEC = \frac{LEC_{\mathrm{ISGCP}} - \left[(1 - X_s) * LEC_{GCP,\mathrm{Ref}}\right]}{X_s} \tag{4.18}$$

Based on this option, there are two ways to calculate SLEC as follows:

a) Calculate SLEC when reference cycle produces the same annual energy of integrated gas turbine solar cogeneration power plant (IGSCP).

b) Calculate SLEC when reference cycle consumes the same fuel amount of integrated gas turbine solar cogeneration power plant (IGSCP).

3- According to Dersch at el. [34] the calculation of solar levelized energy cost can be considered when the annual solar share is based on input and output data (fuel consumption/kWh) as shown in the following formula.

$$SLEC = \frac{LEC_{ISGC} - \left[(1 - SS) * LEC_{GCP,Ref}\right]}{SS} \tag{4.19}$$

Mokheimer [58] proved in KFUPM-MIT report that all forms for calculation $SLEC$ have the same physical meanings which lead to the same results.

CHAPTER 5

WEATHER DATA AND TECHNICAL ASSESSMENT

The solar collector field subsystem is the basic building block of the integrated gas turbine solar cogeneration power plant. Collector costs are the highest capital cost of that plant at all temperatures and power levels and are the major high contributor to the levelized energy cost.

Performance of the system strongly depends on the site chosen. The comprehensive performance analysis in this study was conducted for a site in Dhahran (Saudi Arabia). However, the performance of the optimal configuration has been assessed at five main regions in the kingdom. For the thermo-economic analysis of the power cycles, THERMOFLEX with PEACE simulation program was used. Actually, THERMOFLEX with PEACE software has a model library containing all components necessary for the simulation of a conventional and solar assisted cogeneration power plant including models for the three CSP technology considered design of the proposal work. The main data input to the program are latitude (for Dhahran 26.5°), altitude (for Dhahran 90 m), Day of the year, gas turbine size, and steam requirement.

5.1 A Procedure for the Simulation of a Solar Energy Assisted Gas Turbine Cogeneration System for the Whole Year

As known, the incident solar radiation hourly and seasonally change, as a result of the outlet energy from solar field will also change over a time. To calculate thermo-economic parameters for one year, it is necessary to calculate thermal power obtained from solar field in one year, so one can calculate that by using averaging method; this method focuses on calculating thermal power obtained from solar field on an average day in a month based on average daily solar radiation then multiply that number by the days in the month to get monthly thermal energy obtained from solar field; after that add up monthly thermal energy obtained to get the total thermal energy obtained for one year. Actually, the averaging method has been proven in the present study in two steps. These steps target to compare thermal energy obtained from solar field by using averaging method and hourly method. The averaging method can be conducted using either of the following approaches:

1. One can calculate monthly thermal energy obtained from solar field on an average day in a month rather than for every day in the month.

2. One can use daily average solar radiations rather than hourly solar radiations to calculate thermal energy obtain from solar field on a day.

To prove the validity of the aforementioned approaches, one can use a simple solar power plant as shown in Figure 5.1. This simple plant consists of parabolic solar field, pump, water supply, and process output. The plant has 61 hectares for solar field sizes. Steam output from the plant considered with constant flow rate (81.44 kg/s) at 45.88 bar output pressure, but the output temperature was changing during different solar radiations.

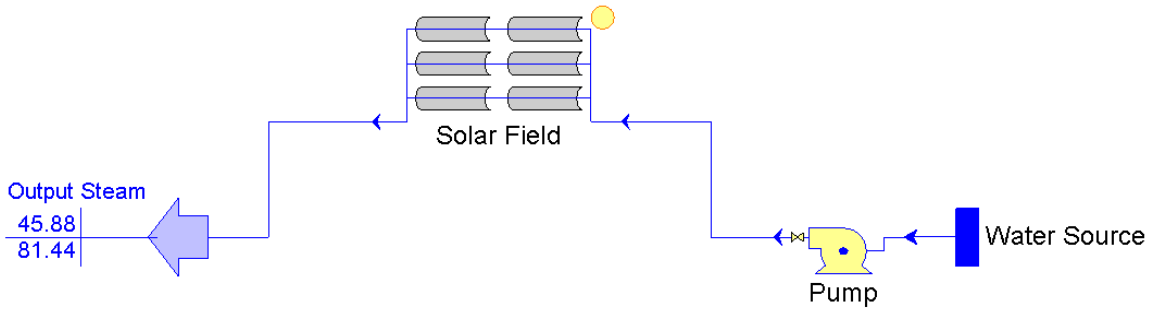

Figure 5.1: Simple solar thermal power plant

Also, it is important to know an average day in a month to prove the previous two concepts. Many books have shown the average day in a month as presented in Table 5.1. For example, Solar Engineering of Thermal Processes book by Duffie and Beckman [57].

Table 5.1: Recommended average days for months [57]

Month	Date	Day of the year (n)	Month	Date	Day of the year (n)
January	17	17	**July**	17	198
February	16	47	**August**	16	228
March	16	75	**September**	15	258
April	15	105	**October**	15	288
May	15	135	**November**	14	318
June	11	162	**December**	10	344

To prove the validity of the first approach that summed up in the use of the average day in a month rather than every day in the month to calculate monthly obtained thermal energy from solar field, one can compare monthly thermal energy obtained from solar field based on first approach with the monthly obtained thermal energy based on every day in a month.

The monthly thermal energy obtained from solar field based on first approach can be calculated as follows; calculate hourly thermal energy obtained from solar field of the average day in a month then multiply by number of days in the month to get monthly thermal energy obtained from solar field. Where the monthly thermal energy obtained from solar field based on all days in a month can be calculated with this sequence; calculate hourly thermal energy obtained from solar field at every day in a month, and then add up that thermal energy for all days in a month to get monthly thermal energy.

Since parabolic solar collector is linked with aperture solar radiations rather than direct normal solar radiations, aperture solar radiations would be presented in this section. Tables 5.2 and 5.3 present average hourly aperture solar radiations for two months in Dhahran city. The first month is January which is a winter month, and the second month is June which is a summer month. The aperture solar radiation was used to calculate the thermal energy obtained from solar field. The simple plant in Figure 5.1 with 61 hectare for solar field size was used for the simulations.

Monthly thermal energy obtained from solar field in Figure 5.1 has been calculated for January and June by using two methods. The first method is based on every day in the month; the second method is based on average day in the month (Tables 5.4, 5.5, 5.6, and 5.7).

As can be seen on the Tables 5.4 and 5.5, at the early morning the solar radiation is very low, as a result, the obtained thermal energy from solar field equals to zero. This is because the calculated losses exceeded these values of solar radiation during that time period because these calculated losses assumed that the fluid entering the collector was at 25ºC. In reality, no fluid would be circulating and the absorbed solar energy would heat the collector without reducing the useful energy gain.

By comparing the obtained monthly thermal energy, one can conclude that the difference doesn't exceed 0.195 % for both months. So, using monthly average day for simulation will not affect performance of the integrating solar collectors to gas turbine cogeneration systems if and only if we use proper averaging method in the first concept.

Table 5.2: Average hourly aperture solar radiation for January (W/m^2)

Month	Date	Day of the Year	Hour												
			6	7	8	9	10	11	12	13	14	15	16	17	18
January	1	1	0	17.8	230.7	448.1	484.9	487.7	485.4	487.7	484.9	448.1	230.7	17.8	0
January	2	2	0	18.1	232.2	449.2	486.0	488.8	486.6	488.8	486.0	449.2	232.2	18.1	0
January	3	3	0	18.5	233.8	450.4	487.2	490.1	487.9	490.1	487.2	450.4	233.8	18.5	0
January	4	4	0	18.9	235.6	451.8	488.6	491.4	489.2	491.4	488.6	451.8	235.6	18.9	0
January	5	5	0	19.3	237.5	453.2	490.0	492.9	490.7	492.9	490.0	453.2	237.5	19.3	0
January	6	6	0	19.7	239.5	454.7	491.5	494.4	492.2	494.4	491.5	454.7	239.5	19.7	0
January	7	7	0	20.2	241.6	456.3	493.0	496.0	493.9	496.0	493.0	456.3	241.6	20.2	0
January	8	8	0	20.7	243.9	458.0	494.7	497.7	495.6	497.7	494.7	458.0	243.9	20.7	0
January	9	9	0	21.2	246.3	459.8	496.5	499.6	497.5	499.6	496.5	459.8	246.3	21.2	0
January	10	10	0	21.8	248.9	461.7	498.4	501.5	499.4	501.5	498.4	461.7	248.9	21.8	0
January	11	11	0	22.4	251.6	463.7	500.3	503.5	501.4	503.5	500.3	463.7	251.6	22.4	0
January	12	12	0	23.0	254.4	465.7	502.3	505.6	503.6	505.6	502.3	465.7	254.4	23.0	0
January	13	13	0	23.7	257.4	467.9	504.5	507.7	505.8	507.7	504.5	467.9	257.4	23.7	0
January	14	14	0	24.3	260.4	470.1	506.7	510.0	508.1	510.0	506.7	470.1	260.4	24.3	0
January	15	15	0	25.0	263.7	472.4	508.9	512.3	510.4	512.3	508.9	472.4	263.7	25.0	0
January	16	16	0	25.8	267.0	474.8	511.3	514.8	512.9	514.8	511.3	474.8	267.0	25.8	0
January	17	17	0	26.6	270.5	477.3	513.8	517.3	515.4	517.3	513.8	477.3	270.5	26.6	0
January	18	18	0	27.4	274.1	479.8	516.3	519.9	518.1	519.9	516.3	479.8	274.1	27.4	0
January	19	19	0	28.2	277.9	482.4	518.9	522.5	520.8	522.5	518.9	482.4	277.9	28.2	0
January	20	20	0	29.1	281.7	485.1	521.5	525.3	523.6	525.3	521.5	485.1	281.7	29.1	0
January	21	21	0	30.0	285.7	487.9	524.3	528.1	526.4	528.1	524.3	487.9	285.7	30.0	0
January	22	22	0	30.9	289.9	490.7	527.1	531.0	529.4	531.0	527.1	490.7	289.9	30.9	0
January	23	23	0	31.9	294.1	493.6	530.0	533.9	532.4	533.9	530.0	493.6	294.1	31.9	0
January	24	24	0	33.0	298.5	496.6	532.9	537.0	535.4	537.0	532.9	496.6	298.5	33.0	0
January	25	25	0	34.0	303.0	499.6	535.9	540.1	538.6	540.1	535.9	499.6	303.0	34.0	0
January	26	26	0	35.1	307.7	502.7	539.0	543.2	541.8	543.2	539.0	502.7	307.7	35.1	0
January	27	27	0	36.3	312.4	505.8	542.1	546.4	545.1	546.4	542.1	505.8	312.4	36.3	0
January	28	28	0	37.5	317.3	509.0	545.3	549.7	548.4	549.7	545.3	509.0	317.3	37.5	0
January	29	29	0	38.8	322.3	512.2	548.5	553.1	551.8	553.1	548.5	512.2	322.3	38.8	0
January	30	30	0	40.1	327.4	515.5	551.8	556.5	555.2	556.5	551.8	515.5	327.4	40.1	0
January	31	31	0	41.5	332.7	518.9	555.2	559.9	558.7	559.9	555.2	518.9	332.7	41.5	0

Table 5.3: Average hourly aperture solar radiation for June (W/m^2)

Month	Date	Day of the Year	Hour														
			5	6	7	8	9	10	11	12	13	14	15	16	17	18	19
June	1	152	0	119.5	532.0	705.4	794.9	842.8	865.7	872.4	865.7	842.8	794.9	705.4	532.0	119.5	0
June	2	153	0	120.9	533.9	705.6	795.0	843.0	865.9	872.7	865.9	843.0	795.0	705.6	533.9	120.9	0
June	3	154	0	122.3	535.8	705.7	795.1	843.1	866.1	872.9	866.1	843.1	795.1	705.7	535.8	122.3	0
June	4	155	0	123.5	537.5	705.8	795.2	843.2	866.3	873.1	866.3	843.2	795.2	705.8	537.5	123.5	0
June	5	156	0	124.7	539.2	705.9	795.2	843.3	866.5	873.3	866.5	843.3	795.2	705.9	539.2	124.7	0
June	6	157	0	125.9	540.8	706.1	795.3	843.4	866.6	873.4	866.6	843.4	795.3	706.1	540.8	125.9	0
June	7	158	0	127.0	542.2	706.2	795.4	843.5	866.8	873.6	866.8	843.5	795.4	706.2	542.2	127.0	0
June	8	159	0	128.0	543.6	706.2	795.4	843.6	866.9	873.7	866.9	843.6	795.4	706.2	543.6	128.0	0
June	9	160	0	128.9	544.9	706.3	795.5	843.7	867.0	873.8	867.0	843.7	795.5	706.3	544.9	128.9	0
June	10	161	0	129.8	546.1	706.4	795.5	843.8	867.1	874.0	867.1	843.8	795.5	706.4	546.1	129.8	0
June	11	162	0	130.7	547.2	706.4	795.5	843.8	867.2	874.1	867.2	843.8	795.5	706.4	547.2	130.7	0
June	12	163	0	131.4	547.9	706.5	795.6	843.9	867.3	874.1	867.3	843.9	795.6	706.5	547.9	131.4	0
June	13	164	0	132.1	548.1	706.5	795.6	843.9	867.3	874.2	867.3	843.9	795.6	706.5	548.1	132.1	0
June	14	165	0	132.7	548.3	706.6	795.6	844.0	867.4	874.3	867.4	844.0	795.6	706.6	548.3	132.7	0
June	15	166	0	133.3	548.5	706.6	795.6	844.0	867.4	874.4	867.4	844.0	795.6	706.6	548.5	133.3	0
June	16	167	0	133.7	548.6	706.7	795.6	844.0	867.5	874.4	867.5	844.0	795.6	706.7	548.6	133.7	0
June	17	168	0	134.1	548.7	706.7	795.6	844.0	867.5	874.5	867.5	844.0	795.6	706.7	548.7	134.1	0
June	18	169	0	134.5	548.8	706.7	795.6	844.1	867.6	874.5	867.6	844.1	795.6	706.7	548.8	134.5	0
June	19	170	0	134.7	548.9	706.7	795.6	844.1	867.6	874.5	867.6	844.1	795.6	706.7	548.9	134.7	0
June	20	171	0	134.9	549.0	706.7	795.7	844.1	867.6	874.5	867.6	844.1	795.7	706.7	549.0	134.9	0
June	21	172	0	135.0	549.0	706.7	795.7	844.1	867.6	874.6	867.6	844.1	795.7	706.7	549.0	135.0	0
June	22	173	0	135.1	549.0	706.7	795.7	844.1	867.6	874.6	867.6	844.1	795.7	706.7	549.0	135.1	0
June	23	174	0	135.0	549.0	706.7	795.7	844.1	867.6	874.6	867.6	844.1	795.7	706.7	549.0	135.0	0
June	24	175	0	134.9	549.0	706.7	795.7	844.1	867.6	874.5	867.6	844.1	795.7	706.7	549.0	134.9	0
June	25	176	0	134.7	548.9	706.7	795.6	844.1	867.6	874.5	867.6	844.1	795.6	706.7	548.9	134.7	0
June	26	177	0	134.5	548.8	706.7	795.6	844.1	867.6	874.5	867.6	844.1	795.6	706.7	548.8	134.5	0
June	27	178	0	134.1	548.7	706.7	795.6	844.0	867.5	874.5	867.5	844.0	795.6	706.7	548.7	134.1	0
June	28	179	0	133.7	548.6	706.7	795.6	844.0	867.5	874.4	867.5	844.0	795.6	706.7	548.6	133.7	0
June	29	180	0	133.3	548.5	706.6	795.6	844.0	867.4	874.4	867.4	844.0	795.6	706.6	548.5	133.3	0
June	30	181	0	132.7	548.3	706.6	795.6	844.0	867.4	874.3	867.4	844.0	795.6	706.6	548.3	132.7	0

Table 5.4: Thermal energy obtained from the solar field based on all days in January (kW)

Month	Date	Day of the Year	Hour											Total for 9 hours
			7	8	9	10	11	12	13	14	15	16	17	
January	1	1	0	35848	69538	75197	75628	75274	75628	75197	69538	35848	0	587696
January	2	2	0	36082	69707	75366	75797	75459	75797	75366	69707	36082	0	589363
January	3	3	0	36331	69892	75551	75996	75658	75996	75551	69892	36331	0	591198
January	4	4	0	36612	70107	75766	76196	75858	76196	75766	70107	36612	0	593220
January	5	5	0	36908	70323	75981	76426	76088	76426	75981	70323	36908	0	595364
January	6	6	0	37219	70554	76211	76657	76319	76657	76211	70554	37219	0	597601
January	7	7	0	37547	70800	76442	76902	76580	76902	76442	70800	37547	0	599962
January	8	8	0	37905	71061	76703	77163	76841	77163	76703	71061	37905	0	602505
January	9	9	0	38279	71338	76979	77455	77132	77455	76979	71338	38279	0	605234
January	10	10	0	38684	71631	77271	77746	77424	77746	77271	71631	38684	0	608088
January	11	11	0	39105	71938	77562	78053	77731	78053	77562	71938	39105	0	611047
January	12	12	0	39541	72246	77869	78330	78069	78330	77869	72246	39541	0	614041
January	13	13	0	40008	72584	78207	78698	78406	78698	78207	72584	40008	0	617400
January	14	14	0	40475	72923	78544	79051	78759	79051	78544	72923	40475	0	620745
January	15	15	0	40989	73276	78882	79404	79112	79404	78882	73276	40989	0	624214
January	16	16	0	41502	73645	79250	79787	79496	79787	79250	73645	41502	0	627864
January	17	17	0	42047	74029	79634	80170	79879	80170	79634	74029	42047	0	631639
January	18	18	0	42607	74414	80017	80569	80293	80569	80017	74414	42607	0	635507
January	19	19	0	43198	74813	80416	80968	80707	80968	80416	74813	43198	0	639497
January	20	20	0	43789	75228	80814	81397	81136	81397	80814	75228	43789	0	643592
January	21	21	0	44411	75658	81244	81826	81565	81826	81244	75658	44411	0	647843
January	22	22	0	45064	76088	81673	82270	82025	82270	81673	76088	45064	0	652215
January	23	23	0	45716	76534	82117	82715	82485	82715	82117	76534	45716	0	656649
January	24	24	0	46400	76994	82561	83190	82944	83190	82561	76994	46400	0	661234
January	25	25	0	47099	77455	83021	83664	83435	83664	83021	77455	47099	0	665913
January	26	26	0	47829	77931	83496	84139	83925	84139	83496	77931	47829	0	670715
January	27	27	0	48559	78406	83971	84629	84430	84629	83971	78406	48559	0	675560
January	28	28	0	49319	78897	84461	85134	84935	85134	84461	78897	49319	0	680557
January	29	29	0	50095	79388	84950	85655	85456	85655	84950	79388	50095	0	685632
January	30	30	0	50886	79894	85456	86175	85976	86175	85456	79894	50886	0	690798
January	31	31	0	51708	80416	85976	86695	86512	86695	85976	80416	51708	0	696102
Thermal energy obtained from solar field based on all days in the month														**19,618,995**

Table 5.5: Thermal energy obtained from the solar field based on all days in June (kW)

Month	Date	Day of the Year	Hour													Total for 11 hours
			6	7	8	9	10	11	12	13	14	15	16	17	18	
June	1	152	0	82424	109239	123222	130710	134311	135364	134311	130710	123222	109239	82424	0	1295176
June	2	153	0	82715	109270	123238	130742	134342	135411	134342	130742	123238	109270	82715	0	1296025
June	3	154	0	83006	109286	123254	130758	134374	135442	134374	130758	123254	109286	83006	0	1296798
June	4	155	0	83266	109301	123269	130773	134405	135474	134405	130773	123269	109301	83266	0	1297502
June	5	156	0	83526	109317	123269	130789	134436	135505	134436	130789	123269	109317	83526	0	1298179
June	6	157	0	83772	109348	123285	130805	134452	135521	134452	130805	123285	109348	83772	0	1298845
June	7	158	0	83986	109364	123301	130821	134484	135552	134484	130821	123301	109364	83986	0	1299464
June	8	159	0	84200	109364	123301	130836	134499	135568	134499	130836	123301	109364	84200	0	1299968
June	9	160	0	84399	109379	123316	130852	134515	135584	134515	130852	123316	109379	84399	0	1300506
June	10	161	0	84583	109395	123316	130868	134531	135615	134531	130868	123316	109395	84583	0	1301001
June	11	162	0	84751	109395	123316	130868	134546	135631	134546	130868	123316	109395	84751	0	1301383
June	12	163	20325	84859	109410	123332	130884	134562	135631	134562	130884	123332	109410	84859	20325	1301725
June	13	164	20434	84889	109410	123332	130884	134562	135647	134562	130884	123332	109410	84889	20434	1301801
June	14	165	20528	84920	109426	123332	130899	134578	135662	134578	130899	123332	109426	84920	20528	1301972
June	15	166	20623	84950	109426	123332	130899	134578	135678	134578	130899	123332	109426	84950	20623	1302048
June	16	167	20685	84966	109426	123332	130899	134594	135678	134594	130899	123332	109426	84966	20685	1302112
June	17	168	20748	84981	109426	123332	130899	134594	135694	134594	130899	123332	109426	84981	20748	1302158
June	18	169	20811	84996	109426	123332	130915	134594	135694	134594	130915	123332	109426	84996	20811	1302220
June	19	170	20842	85012	109441	123332	130915	134609	135694	134609	130915	123332	109441	85012	20842	1302312
June	20	171	20873	85027	109441	123347	130915	134609	135694	134609	130915	123347	109441	85027	20873	1302372
June	21	172	20889	85027	109441	123347	130915	134609	135710	134609	130915	123347	109441	85027	20889	1302388
June	22	173	20905	85027	109441	123347	130915	134609	135710	134609	130915	123347	109441	85027	20905	1302388
June	23	174	20889	85027	109441	123347	130915	134609	135710	134609	130915	123347	109441	85027	20889	1302388
June	24	175	20873	85027	109441	123347	130915	134609	135694	134609	130915	123347	109441	85027	20873	1302372
June	25	176	20842	85012	109441	123347	130915	134609	135694	134609	130915	123347	109441	85027	20842	1302357
June	26	177	20811	84996	109441	123347	130915	134609	135694	134609	130915	123347	109441	84996	20811	1302310
June	27	178	20748	84981	109441	123332	130899	134594	135694	134594	130899	123332	109441	84981	20748	1302188
June	28	179	20685	84966	109441	123332	130899	134594	135678	134594	130899	123332	109441	84966	20685	1302142
June	29	180	20623	84950	109426	123332	130899	134578	135678	134578	130899	123332	109426	84950	20623	1302048
June	30	181	20528	84920	109426	123332	130899	134578	135662	134578	130899	123332	109426	84920	20528	1301972
Thermal power gained from solar field based on all days in the month																**39,026,120**

Table 5.6: Thermal energy obtained from the solar field based on the average day and all days in January (kW)

Month	Average day	Day of the Year	Hour											Total
			7	8	9	10	11	12	13	14	15	16	17	
January	17	17	0	42047	74029	79634	80170	79879	80170	79634	74029	42047	0	631639
Number of days in the month														31
Thermal energy obtained from solar field based on average day in January														**19,580,809**
Thermal energy obtained from solar field based on all days in January														19,618,995
Difference (%)														0.194638

Table 5.7: Thermal energy obtained from the solar field based on the average day and all days in June (kW)

Month	Average day	Day of the Year	Hour												Total
			6	7	8	9	10	11	12	13	14	15	16	17	18	
June	11	162	0	84751	109395	123316	130868	134546	135631	134546	130868	123316	109395	84751	0	1301383
Number of days in the month																30
Thermal power obtained from solar field based on average day in June																**39,041,490**
Thermal power obtained from solar field based on all days in June																39,026,120
Difference (%)																(0.039384)

Table 5.8 presents average hourly aperture solar radiations for Dhahran city at the average day in a month. The aperture solar radiation was used to calculate the thermal energy obtained from solar field. Table 5.9 illustrates the hourly thermal energy obtains from solar field for the average day in a month.

Table 5.8: Average hourly aperture solar radiations (W/m^2)

Month	Date	Day of the year	Hour												
			6	7	8	9	10	11	12	13	14	15	16	17	18
January	17	17	0	26.55	270.5	477.3	513.8	517.3	515.4	517.3	513.8	477.3	270.5	26.55	0
February	16	47	0	73.88	430.6	577.3	613.8	620.6	620.4	620.6	613.8	577.3	430.6	73.88	0
March	16	75	0	185.9	579	680.6	719.6	731.2	733.2	731.2	719.6	680.6	579	185.9	0
April	15	105	32.74	348.9	663.9	758.4	801.6	818.8	823.2	818.8	801.6	758.4	663.9	348.9	32.74
May	15	135	89.28	485.2	699.8	790.4	837.2	858.7	864.9	858.7	837.2	790.4	699.8	485.2	89.28
June	11	162	130.7	547.2	706.4	795.5	843.8	867.2	874.1	867.2	843.8	795.5	706.4	547.2	130.7
July	17	198	113.5	523.3	704.6	794.3	842.1	864.7	871.3	864.7	842.1	794.3	704.6	523.3	113.5
August	16	228	54.76	414.7	684.8	777.3	822.2	841.6	846.8	841.6	822.2	777.3	684.8	414.7	54.76
September	15	258	8.883	255.3	622	720.1	760.7	774.9	777.9	774.9	760.7	720.1	622	255.3	8.883
October	15	288	0	109.7	509.8	619.4	656.6	665.2	665.8	665.2	656.6	619.4	509.8	109.7	0
November	14	318	0	37.53	317.3	509	545.3	549.7	548.4	549.7	545.3	509	317.3	37.53	0
December	10	344	0	18.13	232.2	449.2	486	488.8	486.6	488.8	486	449.2	232.2	18.13	0

Table 5.9: Thermal energy obtained from the solar field based on hourly solar radiations (kW)

Month	Date	Day of the year	Hour												
			6	7	8	9	10	11	12	13	14	15	16	17	18
January	17	17	0	0	42047	74029	79634	80170	79879	80170	79634	74029	42047	0	0
February	16	47	0	0	66841	89382	95015	96063	96033	96063	95015	89382	66841	0	0
March	16	75	0	28854	89645	105382	111443	113257	113570	113257	111443	105382	89645	28854	0
April	15	105	0	54217	102788	117510	124260	126947	127634	126947	124260	117510	102788	54217	0
May	15	135	0	75242	108364	122510	129822	133200	134174	133200	129822	122510	108364	75242	0
June	11	162	0	84751	109395	123316	130868	134546	135631	134546	130868	123316	109395	84751	0
July	17	198	0	81088	109110	123119	130592	134143	135179	134143	130592	123119	109110	81088	0
August	16	228	0	64389	106035	120464	127478	130513	131330	130513	127478	120464	106035	64389	0
September	15	258	0	39680	96279	111521	117869	120088	120557	120088	117869	111521	96279	39680	0
October	15	288	0	0	79018	95878	101653	102990	103083	102990	101653	95878	79018	0	0
November	14	318	0	0	49318	78896	84459	85132	84933	85132	84459	78896	49318	0	0
December	10	344	0	0	36081	69706	75365	75795	75457	75795	75365	69706	36081	0	0

To prove the second concept that summed up in the use daily average solar radiations rather than hourly solar radiations to calculate thermal energy obtain from solar field in a day, five averaged values for every average day in a month have been calculated for aperture solar radiation (Figure 5.2). The first averaged value is based on 8 hours where

the second, third, fourth, and fifth averaged values are based on 9, 10, 11, and 13 hours respectively. Those averaged values have been applied to the previous simple solar power plant, which shown in Figure 5.1.

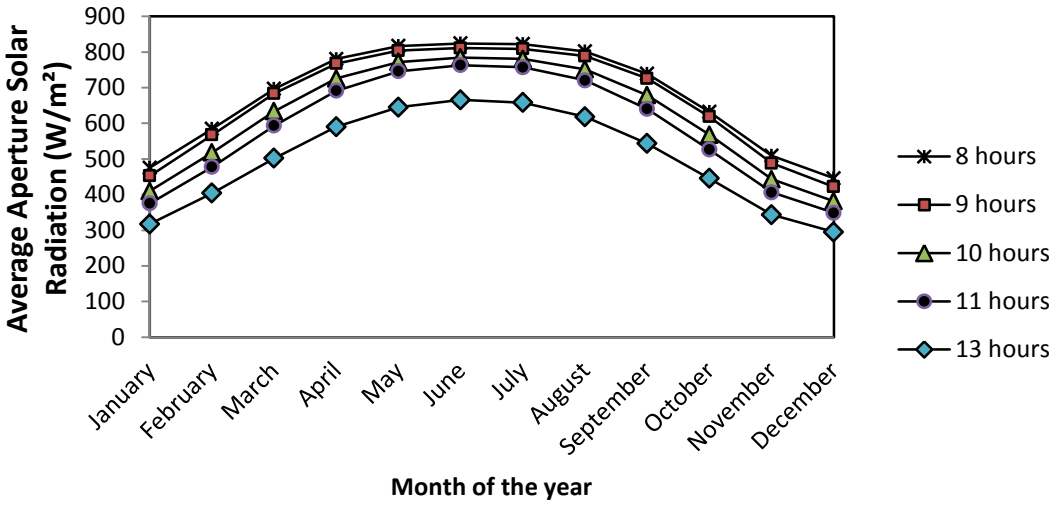

Figure 5.2: Average solar radiation based on different averaged values

Monthly average thermal energy obtained from solar field based on hourly solar radiation and based on daily average solar radiation have been calculated as shown in Table 5.10. Results reveal averaging based on 11 hours is better for seven months in the year which are March, April, May, June, July, August, and September. Whereas the averaging based on 9 hours is better for the other five months, which are October, November December January, and February.

In conclusion, the difference doesn't exceed 0.1% for each average day. So, using daily average solar radiation will not affect performance of the integrating solar collectors to gas turbine cogeneration systems if and only if we use proper averaging method in the second concept.

Table 5.10: Thermal energy obtained from the solar field based on hourly and average daily solar radiations

Month	Day of the year	Total Thermal energy obtained from solar field based on hourly solar radiation (Actual) (KW/day)	Total Thermal energy obtained from solar field based on daily average solar radiation multiplied by number of hours (KW/day)					Difference (%) for				
			8 hours	9 hours	10 hours	11 hours	13 hours	8 hours	9 hours	10 hours	11 hours	13 hours
January	17	631639	589776	632070	636650	641003	641407	-6.63	0.07	0.79	1.48	1.55
February	47	790635	723712	790398	802620	814660	815802	-8.46	-0.03	1.52	3.04	3.18
March	75	1010732	863352	952947	981390	1010394	1011699	-14.58	-5.72	-2.90	-0.03	0.10
April	105	1179078	967896	1070595	1124160	1177880	1187667	-17.91	-9.20	-4.66	-0.10	0.73
May	135	1272450	1013664	1121949	1196740	1271523	1298258	-20.34	-11.83	-5.95	-0.07	2.03
June	162	1301383	-	1131525	1216280	1300761	1340040	-	-13.05	-6.54	-0.05	2.97
July	198	1291283	-	1129122	1209870	1290619	1324752	-	-12.56	-6.30	-0.05	2.59
August	228	1229088	-	1100277	1164060	1227798	1244243	-	-10.48	-5.29	-0.10	1.23
Septemb	258	1091431	-	1011888	1051220	1090485	1093807	-	-7.29	-3.68	-0.09	0.22
October	288	862161	783000	861813	879150	896709	898183	-9.18	-0.04	1.97	4.01	4.18
Novemb	318	680543	631424	680922	687370	693517	693966	-7.22	0.06	1.00	1.91	1.97
Decembe	344	589351	553592	589779	592940	596057	596128	-6.07	0.07	0.61	1.14	1.15

5.2 Solar Radiation Estimation

In order to evaluate the performance of the solar field and its contribution to the cogeneration cycle, it is necessary to estimate the average daily solar radiation intensity. So the first step is to get the average hourly solar radiation at the corresponding date and location. Actually, THERMOFLEX was used to get the average hourly solar radiation. THERMOFLEX has a model library containing all ASHRAE climatic data, the main data input to program are latitude, altitude, day of the year. The proposed location is Dhahran city, Saudi Arabia (Altitude 90 m, latitude 26.5°). Table 5.11 presents the average hourly solar radiation for the average day in the months at Dhahran city.

Table 5.11: Average hourly direct normal solar radiations (W/m²)

Month	Date	Day of the Year	Hour												
			6	7	8	9	10	11	12	13	14	15	16	17	18
January	17	17	0	186	418.2	604.7	701	747.7	761.7	747.7	701	604.7	418.2	186	0
February	16	47	0	234.6	512.1	670	751.4	791.1	803.2	791.1	751.4	670	512.1	234.6	0
March	16	75	0	352.3	600.2	728.4	795.7	829.1	839.3	829.1	795.7	728.4	600.2	352.3	0
April	15	105	188.9	468.1	666.1	770	826.3	854.7	863.5	854.7	826.3	770	666.1	468.1	188.9
May	15	135	253.4	538	701.5	790.6	840.2	865.7	873.5	865.7	840.2	790.6	701.5	538	253.4
June	11	162	299.7	564.7	713.9	796.9	843.8	868.1	875.7	868.1	843.8	796.9	713.9	564.7	299.7
July	17	198	281.2	554.7	709.4	794.7	842.6	867.4	875.1	867.4	842.6	794.7	709.4	554.7	281.2
August	16	228	210.9	504.1	684.8	781.1	834	861	869.3	861	834	781.1	684.8	504.1	210.9
September	15	258	184.7	407.4	632.9	749.3	811.3	842.3	851.8	842.3	811.3	749.3	632.9	407.4	184.7
October	15	288	0	277	548.9	694.7	770.2	807.3	818.6	807.3	770.2	694.7	548.9	277	0
November	14	318	0	192.5	449	626.6	718	762.3	775.7	762.3	718	626.6	449	192.5	0
December	10	344	0	184.7	390.2	584.3	685.2	733.9	748.6	733.9	685.2	584.3	390.2	184.7	0

5.3 Ambient Temperature and Relative Humidity Estimation

Temperature and relative humidity are the most important weather parameters affecting electric load generated by power utilities in many parts of the world. Recorded hourly average temperatures and hourly relative humidity are provided by many weather services in Saudi Arabia. Those two parameters are important in the proposed work.

Since we used average solar radiation in the average day in a month for the designs, it was necessary to use the average ambient temperature and relative humidity at the same days and the same hours in the day. So we used the averaging method based on 11 hours for seven months in the year which are March, April, May, June, July, August, and September to calculate daily average ambient temperature and relative humidity. Whereas the averaging based on 9 hours was used for the other five months, which are October, November December January, and February. At non-solar time (night) the performance of plant would be evaluated at the average temperature and relative humidity at non-solar time, which is the day time minus solar time.

Tables 5.12 and 5.13 present the average hourly and daily ambient temperature and relative humidity respectively in Dhahran at solar time. On other hand, Tables 5.14 and 5.15 present the average hourly and daily ambient temperature and relative humidity respectively in Dhahran at non-solar time.

Table 5.12: Statistics of average hourly temperatures in Dhahran, Saudi Arabia during solar time

Month	Date	Hour													Solar time	Average temperature for solar time
		6:00 AM	7:00 AM	8:00 AM	9:00 AM	10:00 AM	11:00 AM	12:00 PM	1:00 PM	2:00 PM	3:00 PM	4:00 PM	5:00 PM	6:00 PM		
January	17	11.5	11	12	15	17.5	20	21.5	22.5	23	22.5	21	19.5	18	9	19.4
February	16	13	14	16	19	20.5	23	24.5	24	24.5	24	23.5	22.5	21.5	9	22.1
March	16	16	17	20	23.5	25.5	27.5	28.5	29.5	29	29	28.5	26.5	24.5	11	25.9
April	15	25	24	25.5	25.5	26.5	27	27.5	28	26	25	25	25	24.5	11	25.9
May	15	29	31	33	36.5	38	39	39.5	40.5	39.5	38.5	36.5	35	34	11	37.0
June	11	31	33.5	36	38	40.5	42.5	44	43.5	43	41	39.5	37.5	36.5	11	39.9
July	17	36	37.5	39.5	41	43	43.5	43.5	43.5	43	42	41.5	41	39.5	11	41.7
August	16	31.5	33	30.5	37	39	41	41.5	42.5	42.5	43	41.5	40.5	39	11	39.3
Septembe	15	27.5	29	33.5	36.5	38	40	41	42	41.5	40.5	38	36	35	11	37.8
October	15	23.5	24.5	26	27.5	30	32.5	34.5	35.5	36	35	33.5	32.5	30.5	9	32.3
Novembe	14	16	16	19.5	23.5	25.5	27.5	28.5	29.5	30	30.5	28	26.5	25	9	26.9
Decembe	10	11	11.5	14	16	19.5	20.5	22	23.5	23.5	23	21.5	20.5	18.5	9	20.4
Observation period: 2010 - 2011.																

Table 5.13: Statistics of average hourly relative humidity in Dhahran, Saudi Arabia during solar time

Month	Date	Hour													Solar time	Average Relative Humidity for solar time
		6:00 AM	7:00 AM	8:00 AM	9:00 AM	10:00 AM	11:00 AM	12:00 PM	1:00 PM	2:00 PM	3:00 PM	4:00 PM	5:00 PM	6:00 PM		
January	17	80%	79%	72%	53%	49%	44%	40%	39%	38%	36%	44%	50%	53%	9	46%
February	16	87%	85%	80%	62%	46%	38%	34%	38%	32%	37%	38%	48%	57%	9	45%
March	16	55%	59%	53%	39%	32%	30%	28%	21%	21%	23%	22%	24%	29%	11	32%
April	15	44%	54%	47%	48%	47%	42%	41%	41%	45%	43%	45%	45%	49%	11	45%
May	15	50%	44%	39%	22%	18%	18%	19%	15%	16%	22%	29%	29%	38%	11	24%
June	11	44%	32%	26%	23%	20%	15%	14%	14%	15%	23%	29%	35%	41%	11	22%
July	17	37%	39%	33%	28%	23%	22%	22%	22%	23%	22%	23%	25%	27%	11	25%
August	16	52%	48%	48%	49%	43%	38%	36%	33%	27%	23%	29%	29%	40%	11	36%
Septembe	15	40%	34%	27%	30%	22%	24%	20%	23%	21%	22%	36%	43%	47%	11	27%
October	15	72%	67%	64%	65%	54%	43%	34%	29%	27%	30%	35%	36%	45%	9	42%
Novembe	14	65%	82%	48%	29%	23%	24%	23%	20%	49%	19%	25%	32%	41%	9	29%
Decembe	10	82%	69%	65%	59%	46%	42%	37%	27%	35%	37%	39%	41%	46%	9	43%
Observation period: 2010 - 2011.																

Table 5.14: Statistics of average hourly temperatures in Dhahran, Saudi Arabia during non-solar time

Month	Date	Hour															Non solar time	Average temperature for non-solar time
		12:00 AM	1:00 AM	2:00 AM	3:00 AM	4:00 AM	5:00 AM	6:00 AM	7:00 AM	5:00 PM	6:00 PM	7:00 PM	8:00 PM	9:00 PM	10:00 PM	11:00 PM		
January	17	14	14	13	12.5	12.5	11.5	11.5	11	19.5	18	17	16.5	15.5	15	14.5	9	14.4
February	16	16	15.5	14.5	14.5	13.5	13.5	13	14	22.5	21.5	20	19	19	18	18	9	16.8
March	16	18	17.5	15.5	15.5	16	15.5	16	17	26.5	24.5	23.5	23.5	22.5	22.5	21.5	11	19.4
April	15	25	25	25	26	25.5	24.5	25	24	25	24.5	24	24	23	22.5	22.5	11	24.3
May	15	31	30	29.5	29	29	29	29	31	35	34	33.5	33.5	34	33	32.5	11	31.3
June	11	32.5	31.5	32	32	31	31	31	33.5	37.5	36.5	36.5	35.5	35.5	35.5	35	11	33.5
July	17	32.5	32.5	32.5	33.5	35	35.5	36	37.5	41	39.5	38.5	37.5	37	36	35	11	35.5
August	16	34.5	34	34	34.5	32.5	31.5	31.5	33	40.5	39	37.5	36.5	36	36	35	11	34.8
Septembe	15	29.5	29	28	28.5	27	27	27.5	29	36	35	34	33.5	33	32.5	31.5	11	30.5
October	15	27	25.5	25	24.5	24	24	23.5	24.5	32.5	30.5	29.5	29	28.5	27.5	26.5	9	26.8
Novembe	14	18.5	17.5	17.5	17	18.5	16	16	16	26.5	25	25	23	22.5	22	21.5	9	20.2
Decembe	10	13.5	12.5	12	11	11	10.5	11	11.5	20.5	18.5	17	16	15	14.5	13.5	9	13.9

Observation period: 2010 - 2011.

Table 5.15: Statistics of average hourly relative humidity in Dhahran, Saudi Arabia during non-solar time

Month	Date	Hour															Non solar time	Average Relative Humidity for non-solar time
		12:00 AM	1:00 AM	2:00 AM	3:00 AM	4:00 AM	5:00 AM	6:00 AM	7:00 AM	5:00 PM	6:00 PM	7:00 PM	8:00 PM	9:00 PM	10:00 PM	11:00 PM		
January	17	73%	75%	75%	78%	80%	80%	80%	79%	50%	53%	59%	66%	75%	77%	75%	15	71%
February	16	71%	73%	75%	75%	77%	80%	87%	85%	48%	57%	62%	60%	65%	69%	71%	15	70%
March	16	37%	47%	46%	48%	52%	52%	55%	59%	24%	29%	37%	39%	37%	37%	41%	13	43%
April	15	54%	59%	52%	43%	47%	48%	44%	54%	45%	49%	53%	53%	50%	49%	49%	13	50%
May	15	47%	50%	44%	52%	49%	54%	50%	44%	29%	38%	37%	35%	36%	38%	43%	13	44%
June	11	31%	37%	40%	40%	44%	44%	44%	32%	35%	41%	46%	50%	50%	50%	50%	13	43%
July	17	48%	47%	39%	36%	35%	39%	37%	39%	25%	27%	28%	31%	32%	32%	35%	13	35%
August	16	47%	47%	48%	46%	49%	51%	52%	48%	29%	40%	48%	50%	51%	52%	53%	13	48%
Septembe	15	51%	53%	50%	49%	47%	46%	40%	34%	43%	47%	53%	54%	61%	58%	38%	13	49%
October	15	67%	68%	70%	72%	71%	71%	72%	67%	36%	45%	53%	62%	66%	70%	77%	15	64%
Novembe	14	63%	70%	70%	73%	55%	75%	65%	82%	32%	41%	59%	69%	73%	76%	78%	15	65%
Decembe	10	80%	83%	82%	88%	85%	86%	82%	69%	41%	46%	51%	55%	61%	68%	74%	15	70%

Observation period: 2010 - 2011.

5.4 Design Conditions

Obtained thermal energy from solar field is varying according to the average solar radiation intensity for every month in the year, this leads to get different solar multiple for each month. At the design mode, the conditions for calculating solar multiple for all configurations must be fixed; that will help making the proper comparison between different designs to get to the optimal design. The important parameters for a design conditions are average direct solar radiation, ambient temperature, and relative humidity.

According to the above, the maximum average direct solar radiation was used to calculate solar multiple at design modes, which occurs on June 11 according to Table 5.16. The average ambient temperature and relative humidity for the same day were used for the design conditions. Table 5.16 presents the design conditions at solar time. Where the design conditions at non-solar time presented in Table 5.17.

Table 5.16: Design conditions at solar time

Month	Date	Day of the year	Number of day	Number of solar hours in a solar time	Average daily direct solar radiation (W/m²)	Average temperature at solar time (°C)	Average relative humidity at solar time (%)
January	17	17	31	9	633.88	19.4	46%
February	16	47	28	9	694.71	22.1	45%
March	16	75	31	11	677.34	25.9	32%
April	15	105	30	11	730.35	25.9	45%
May	15	135	31	11	758.68	37.0	24%
June	11	162	30	11	768.23	39.9	22%
July	17	198	31	11	764.79	41.7	25%
August	16	228	31	11	745.39	39.3	36%
September	15	258	30	11	703.47	37.8	27%
October	15	288	31	9	717.87	32.3	42%
November	14	318	30	9	654.17	26.9	29%
December	10	344	31	9	615.09	20.4	43%

Table 5.17: Design conditions at non-solar time

Month	Date	Day of the year	Number of day	Number of hours in non solar time	Average temperature at non solar time (°C)	Average relative humidity at non solar time (%)
January	17	17	31	15	14.4	71%
February	16	47	28	15	16.8	70%
March	16	75	31	13	19.4	43%
April	15	105	30	13	24.3	50%
May	15	135	31	13	31.3	44%
June	11	162	30	13	33.5	43%
July	17	198	31	13	35.5	35%
August	16	228	31	13	34.8	48%
Septembe	15	258	30	13	30.5	49%
October	15	288	31	15	26.8	64%
Novembe	14	318	30	15	20.2	65%
Decembe	10	344	31	15	13.9	70%

5.5 Natural Gas Price

Figure 5.3 depicts the price fluctuations of natural gas from 1994 to 2011. The price of natural gas in 1994 was $2.04/GJ and increased to a peak high of $9.51 /GJ in 2005. Even though there seems to be a downward price trend since 2005, the fluctuations have continued [50]. The price of natural gas in 2011 was $4.25/GJ. Natural gas averaged 5.4 USD/GJ in the last three years, which was used for economic analysys.

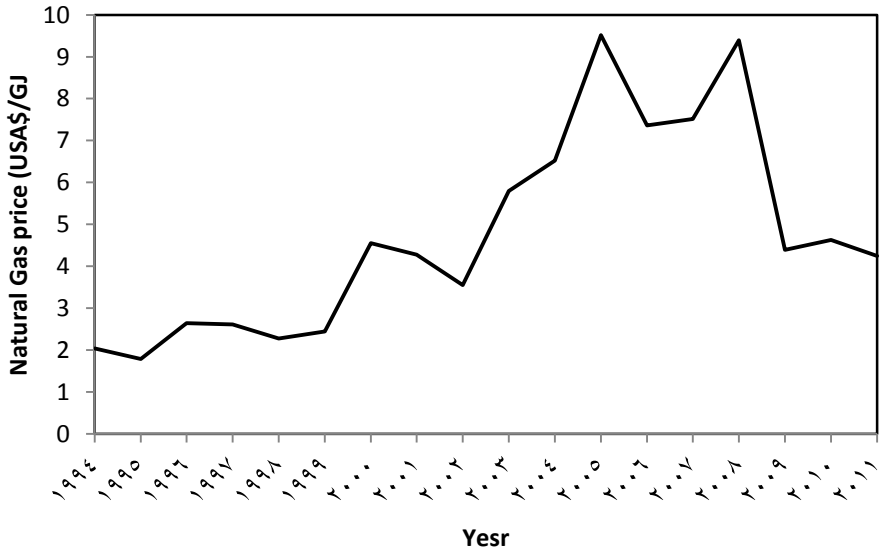

Figure 5.3: Average annual natural gas price in USA

5.6 Electricity Price

The retail price of electricity is a matter of concern to all affected sectors of society. Electricity and power is a major cost to residential consumers, commercial consumers, as well as industrial consumers. Figure 5.4 depicts the average retail price of electricity to the ultimate customers from 2003 to 2012 in the USA [51]. Figure 5.5 depicts the electricity price in different countries in 2012. As shown, the price in Saudi Arabia is very low because the kingdom supports the electricity sector, so the electricity price is not realty price of the power unit.

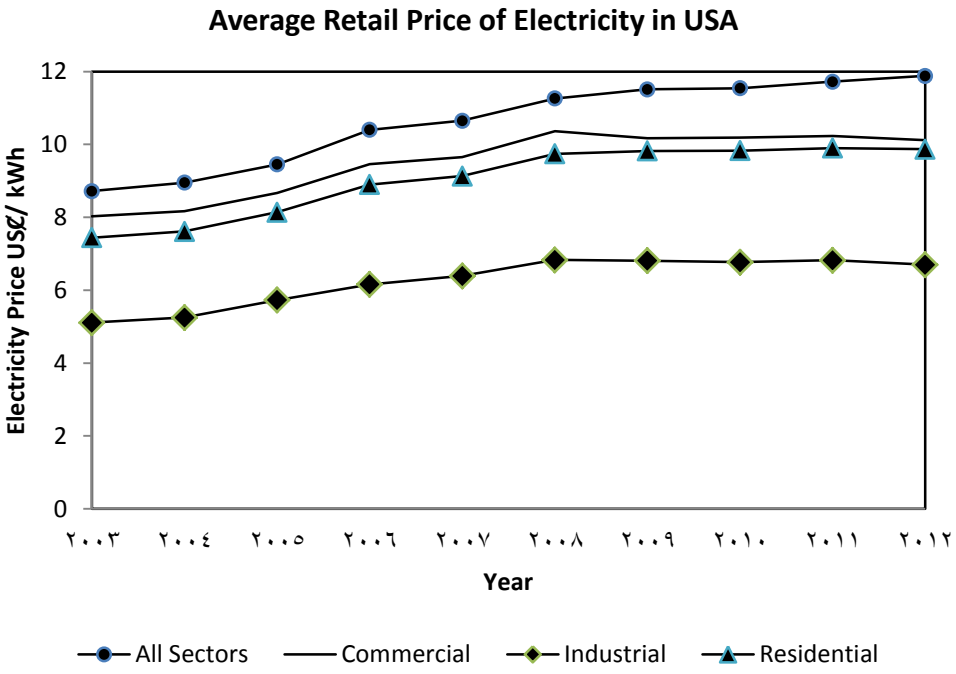

Figure 5.4: Average retail price of electricity to ultimate customers in USA

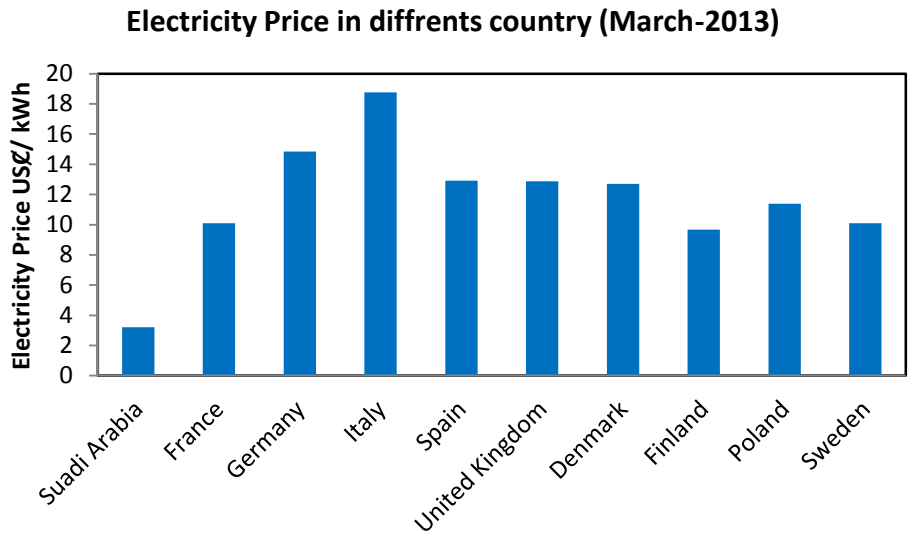

Figure 5.5: Comparison of average electricity price in the Kingdom with several countries

5.7 Thermal Energy (Steam) Price

According to literature [44] the purchase prices in Croatia 2006 were in the range of 2.5 US¢/kWh (6.94 USA $/GJ), for customers connected to the big district heating systems, to 5.4 US¢/kWh (15 USA $/GJ) for customers connected to the small heating networks. The price of steam in an Eastern Asia is high. For exampl, the price ranges from 12.6 to 96.9 US$/Tonne depending on the type of fuel used in Philippines; the price ranges from 10.7 to 82.6 US$/ Tonne also depending on the type of fuel used in Thailand; and the prices in Malaysia, Taiwan are (11-46.2), (16-78) US$/ Tonne respectively [52].

5.8 THERMOFLEX with PEACE Simulation Program

THERMOFLEX is a modular program with a graphical interface that allows to assemble a model from icons. The program contains a large library of components and fluid properties. Also the program covers both design and off-design simulation. It models all types of power plants, including cogeneration power plants, combined cycles, conventional steam cycles, and solar power plant. THERMOFLEX can operate on its own using virtual models of components, or together with PEACE which provides a set of physical components whose weights and dimensions provide the basis for estimated cost.

First of all, one needs to build a graphic model. In this regards; one can connect components in a flexible fashion in the THERMOFLEX, then one can edit the inputs describing each component, after calculate proposed cycle, and finally view the outputs. Figure 5.6 shows the four stages of working with a THERMOFLEX model, with transitions between them. For more detail see the appendix.

Stage 1: Draw System. Flowsheet border is white and the icon selector is shown along the bottom edge. Select components, place them on the screen, and connect them to construct your system. THERMOFLEX includes about 180 components, arranged under tabs at the bottom of the screen. Each component is represented by a graphic icon, with color-coded nodes to represent fluid inlet and exit ports. Color coding is used extensively to indicate fluid type.

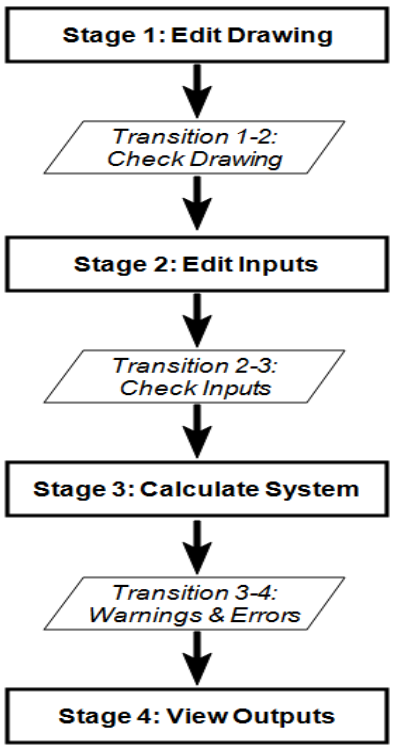

Figure 5.6: Specific simulation steps in THERMOFLEX

Transition 1-2: Check Drawing. Check that all component connections are sound. Check Drawing is triggered by the F3 key, or by pressing the green arrow button ( ) beside Edit Drawing on the navigator bar, above the flowsheet.

Stage 2: Edit Inputs. Flowsheet border area is grey, and the icon selector window is not shown. Double-click on a component to open its menu and specify its characteristics. Clicking the Edit Inputs button itself summons the *Site Menu* and provides access to all other program input menus.

Transition 2-3: Check Inputs. Performs cursory checks to prevent inconsistent or unreasonable component inputs, and automatically launch the computation if all input

checks pass. Check Inputs is invoked by the F4 or F5 keys, or by pressing green arrow button () beside Edit Inputs on the navigator bar, above the flowsheet.

Stage 3: Calculate System. THERMOFLEX calculates the model and displays its progress in a command window layered over the flowsheet. The intermediate results show the iteration number and progress as the model iterates toward a converged solution.

Transition 3-4: Computation Messages, Warnings & Errors. This transition warns you of inconsistencies and/or problems with your calculation's results, and suggests corrective actions. It is triggered automatically following the computation, if needed.

Stage 4: View Outputs. Flowsheet border area is light yellow. One or more of the yellow output topic buttons are enabled on the navigator bar, above the flowsheet. Double-click a component to view its text and graphic results.

You move from stage to stage by invoking the transition commands. You can move backward one or more stages by clicking the desired stage button from the navigator bar.

CHAPTER 6

TECHNO-ECONOMIC PERFORMANCE ANALYSIS OF PARABOLIC TROUGH COLLECTOR IN DHAHRAN, SAUDI ARABIA

This chapter is devoted to the modeling and simulation of PTC under Dhahran KSA weather conditions. To understand how the model of Parabolic Trough Collector (PTC) works, a brief description of the collector is provided in this section. A schematic cross section of the PTC is shown in Figure 6.1. The arc shape of PTC as shown in Fig. 6.1 is selected because of its focusing properties. The axis is the line that passes through the vertex and the focal point. The rim angle is measured from the axis to the line connecting the focus to the rim (edge) of the parabola. The aperture area is the distance from rim to rim multiplied by the reflective length of the reflector. Three characteristic dimensions are labeled in this diagram. 'f_n' is the parabola's focal length. 'B' is the parabola's depth. 'Wa' is the parabola's aperture width. This collector shape focuses incoming solar radiation that is parallel to the axis and normal to the aperture to the focal point.

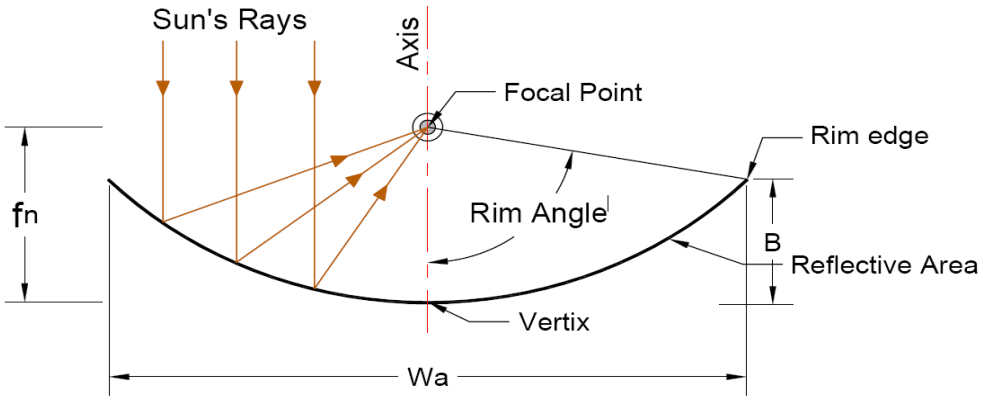

Figure 6.1: A schematic cross section of the parabolic trough collector.

To maximize energy capture, the solar collector trough is rotated by a drive system so it faces the sun as much as possible. The tracking system operates to keep the axis coplanar with the sun's central ray. Collector troughs are often aligned along meridians and rotate so they can track the sun from sunrise to sunset. However, other orientations are used, including perpendicular to meridians to more evenly balance the amount of captured energy throughout the year.

The Heat Collection Element (HCE) is carefully aligned with the parabolic trough's focal line, which shown as a point in the Figure 6.1. A cross section of the HCE is shown in Figure 6.2. It consists of the receiver tube that carrying the fluid being heated. The receiver tube is coated with an optically selective coating so it absorbs much of the incident solar radiation while emitting only a small amount of thermal radiation.

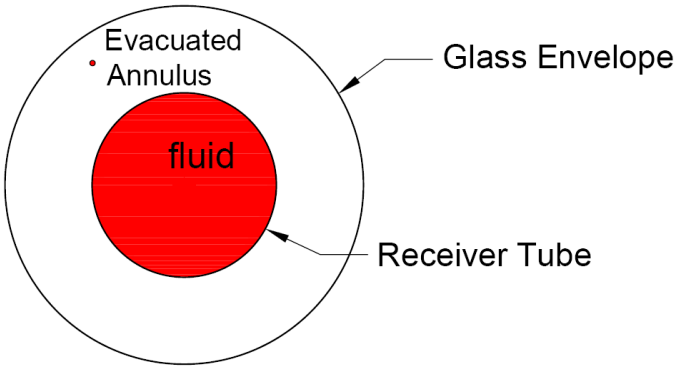

Figure 6.2: A cross section of the heat collection element

The receiver tube is surrounded by a glass envelope to reduce heat losses from the receiver tube. The envelope should be highly transparent to incoming solar radiation and highly opaque to outgoing thermal radiation emitted from the wall tube. The annulus

between receiver tube and the envelope is evacuated to virtually eliminate convective heat transfer between the tube and envelope.

Concentrating collectors only focus Direct Normal Irradiance (DNI), which is the radiation streaming directly from the sun without having been scattered by atmosphere. Indirect (diffuse) irradiance cannot be focused by these collectors. Furthermore, PTC can only focus the component of DNI normal to the aperture, which called Aperture Normal Irradiance (ANI). One can compute ANI from the DNI based on the collector's orientation on the earth; it is tilted away from horizontal, and the sun position in the sky. Assume that the collector is tracking the sun in one direction to makes the geometry straightforward that is because the sun central ray and the parabola's axis are coplanar.

The performance parameters of the PTC are listed as follows:

i. Concentration ratio; which gives indication of the maximum temperature produced by the collector.
ii. Optical efficiency; which gives information of the fraction of total solar energy incident on collector area absorbed by the absorber.
iii. Thermal efficiency; which gives information of the fraction of total energy incident on the collector area that we get in the form of heat from the collector.

The thermal efficiency of the parabolic trough solar collector system depends on the optical efficiency of the system. More is the optical efficiency of the reflector better will be the thermal efficiency and hence the overall performance of the system.

6.1 Assessment of the Optical Efficiency of a PTC System in Dhahran

The incident solar radiation fluctuates hourly and seasonally. As a result, the Aperture Normal Irradiance (ANI) changes also with time. Not all ANI is absorbed by the receiver tube. The surfaces of the reflector, the glass envelope, and the tube itself are not optically perfect. The optical efficiency of the collector accounts for losses at these surfaces. Optical efficiency is a characteristic of the reflector/absorber system and depends on the materials, coating, and alignment. Figure 6.3 shows the different parameters that affect the optical efficiency of the parabolic solar collector.

Nominal optical efficiency applies when the sun's central rays are perpendicular to the collector aperture. The optical efficiency is reduced from the nominal value as a function of incidence angle for other than normal ray strikes. The optical efficiency determines the percentage of ANI absorbed by the receiver tube. Peak nominal optical efficiencies can be as high as 80%, but in real practice, it may be as much as 10 to 15% below the peak value.

The design point collector nominal optical efficiency characterizes the collector's ability to focus incoming beam radiation on the receiver tube. This value applies when the sun's central rays are perpendicular to the collector aperture. Corrections to this efficiency are applied when the central rays strikes the aperture at other angles. The corrected optical efficiency dictates the percentage of ANI that is absorbed by the receiver tube. Some of the absorbed energy is lost to the surroundings by radiation, convection, and conduction.

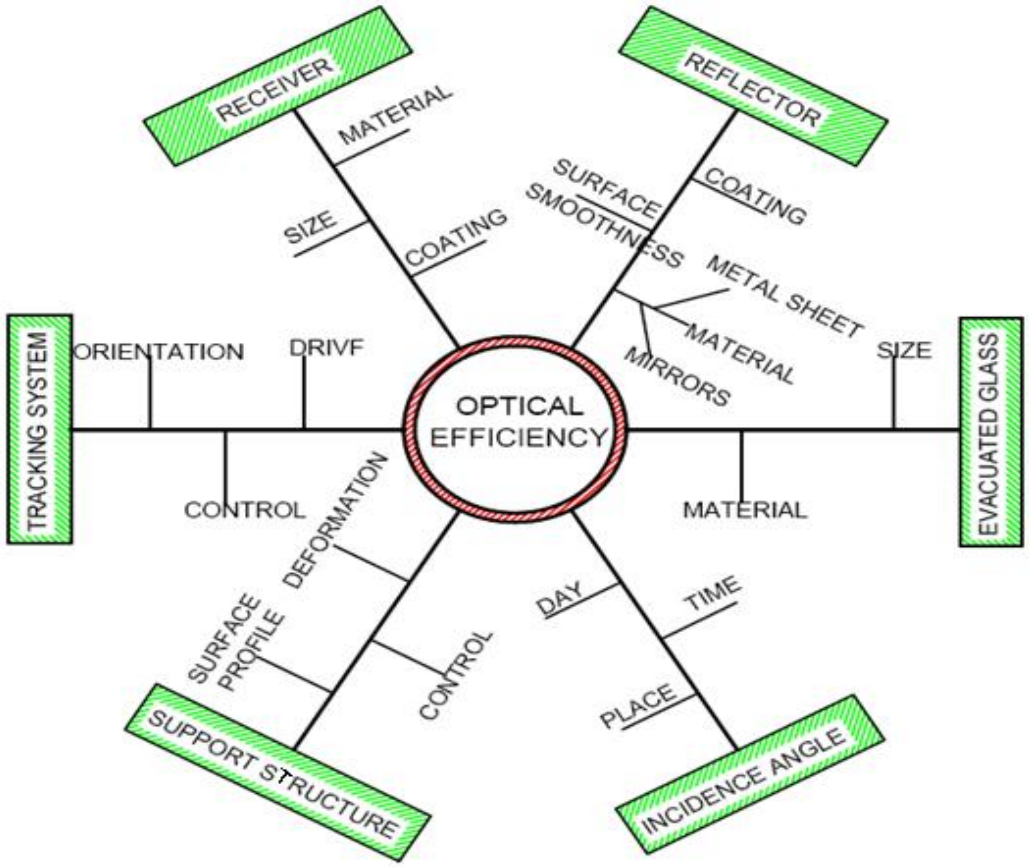

Figure 6.3: Parameters affecting optical efficiency

The absorbed radiation Q_{abs} is defined as the incidence solar energy on the collector that is actually absorbed by the heat transfer fluid through the HCE. The absorbed radiation is a fraction of the direct normal irradiance is adjusted due to the effects of incidence angle, row shading, solar field availability, collector cleanliness, and the collector field and HCE surface properties. The gross energy absorbed by the receiver tube is as follows:

$$Q_{abs} = ANI * \eta_{opt} \tag{6.1}$$

where:

Q_{abs} : Solar radiation absorbed by the receiver tubes [W/m²].

η_{opt} :Optical efficiency

ANI :Aperture normal irradiance (W/m²) that can be calculated by:

$$ANI = DNI * \cos(\Theta) \quad (6.2)$$

DNI : Direct normal irradiance (W/m²).

Θ : Angle of incidence (deg.).

The optical efficiency could be calculated by the following Eq.:

$$\eta_{opt} = \eta_{nominal} * IAM * f_{end\ loss} * f_{clean} * f_{rowshadow} \quad (6.3)$$

Where:

$\eta_{nominal}$: Nominal optical efficiency.

IAM : Incidence angle modifier.

$f_{end\ loss}$: Performance factor that accounts for losses from ends of the heat collector element.

f_{clean} : Cleanliness factor.

$f_{rowshadow}$: Performance factor that considers the mutual shading of parallel collector rows during early morning and late evening.

The nominal efficiency ($\eta_{nominal}$) can be expressed as

$$\eta_{nominal} = \rho_{cl} * (\tau\alpha_c)_n * \gamma \quad (6.4)$$

where

ρ_{cl} Clean mirror reflectivity

τ Transmittance of the glass envelope.

α_c Absorptance of the absorber surface coating.

$(\tau\alpha_c)_n$ The effective product of τ and α_c. A modified value of $(\tau\alpha_c)_n$ is recommended by Ref [53] as $1.01(\tau\alpha_c)$.

γ Intercept factor (fraction of the reflected radiation that is intercepted by the receiver)

The nominal optical efficiency depends on selected solar collector type. There are currently several collectors for concentrated solar power plants applications that have been successfully tested under real operating conditions. For example, the Luz International Ltd (Luz) developed and designed three parabolic trough collectors, called LS-1, LS-2 and LS-3 (see Table 6.1 and Fig. 6.4), these collectors were installed in solar electric generating system plants. The EuroTrough collector model (Table 6.2) was the result of analysis of several different collector structures.

Table 6.1: Dimensions and properties of the Luz PTC system [54]

Model	LS-1	LS-2		LS-3
Year	1984	1985	1988	1989
Max. Operating temp. (°C)	307	349	390	390
Aperture area (A_a)(m^2)	128	235.5	235.5	570.2
Aperture width (W_a)(m)	2.55	5	5	5.76
Length (L_{SCA})(m)	50.2	47.1	47.1	99
Focal length (f_n)(m)	0.68	1.4	1.4	1.71
Mean focus distance (m)	0.94	1.84	1.84	2.12
Absorber tube diameter (D_o)(mm)	40	70	70	70
Cover tube diameter (D_{co})(mm)	*	0.115	0.115	0.115
Rim angle (Θ_r) (°)	85	80	80	80
Acceptance angle (°)	1.918	1.59	1.59	1.37
Geometric concentration ratio	18.95	22.74	22.74	26.2
Peak optical efficiency (η_{opt})	0.734	0.74	0.74	0.77
Reflectance (ρ_{cl})	0.94	0.94	0.94	0.94
Intercept factor (γ)	0.87	0.89	0.89	0.93
Transmittance (τ)	0.94	0.95	0.95	0.96
Absorptance (α)	0.94	0.94	0.94	0.96
Emittance (at temp. (°C)) (Ɛ)	0.30 (300)	0.24 (300)	0.24 (300)	0.15 (350)

* Unavailable datum.

(a) The back structure of an LS-2 parabolic trough solar collector assembly at Kramer Junction, California [54].

(b) The back structure of an LS-3 parabolic trough solar collector assembly at Kramer Junction, California [54].

Figure 6.4: Luz system collectors (LS-2 and LS-3).

Table 6.2: Main characteristic parameters of EuroTrough ET-100 [55]

Type	**Euro-Trough (ET-100)**
Aperture width ($W_{a)}$ [m]	5.76
Receiver tube outside diameter (D_o)[m]	0.07
Receiver tube inside diameter (D_i)[m]	0.063
Glass envelope outside diameter (D_{co}) [m]	0.136
Reflector rime angle (Θ_r)	80
Concentration ratio [%]	82
Optical efficiency(η_{opt}) [%]	78
Receiver absorptivity (α)	0.96
Mirror reflectivity (ρ_{cl})	0.94
Receiver emittance (ε)	0.15
Focal length (f_n) [m]	1.71

Figure 6.5: EuroTrough collector [55].

As stated earlier, the main objective of the proposed work in this chapter is to evaluate the optical efficiency of PTC throughout a year under Dhahran's weather conditions. In this regard, a computer simulation code was developed using the available software (e.g. EES), this simulation code was validated against the results achieved by THERMOFLEX code; the data for EuroTrough solar collector (ET-100) and for LUZ solar collector LS-3 have been considered in the simulation; the solar collector was rotated about horizontal north-south axis with continues adjustment to minimize the angle of incidence.

6.1.1 Development of an EES Code to Estimate Optical Efficiency of a PTC System

As stated earlier, solar radiation follows a direct line from the sun to the Earth is called extraterrestrial solar radiation. At entering the earth's atmosphere, some solar radiation is diffused by air, water molecules, and dust within the atmosphere [57]. The direct normal irradiance is defined as the solar radiation received from the sun without having been scattered by the atmosphere [57]. Direct normal irradiance (DNI) is measured by an instrument pointing directly at the sun and shaded from diffuse radiation. Beam radiation is often referred to as direct solar radiation.

Only the direct normal irradiance can be focused by linear concentrated solar collectors. The angle between the direct normal irradiance (DNI) on a surface and the plane normal to that surface is called the angle of incidence (θ). The angle of incidence is varying over the whole day as well as throughout the year. As a result, the performance of the solar collector is heavily influenced with that variation. Angle of incidence (θ) for a parabolic solar collector rotates about a horizontal north-south axis with continuous adjustment to minimize the angle of incidence that could be calculated by the following equation [57].

$$\cos(\Theta) = \sqrt{cos^2(\delta) * \sin^2(\omega) + cos^2(\Theta_z)} \tag{6.5}$$

On the right hand side of this equation, there are three angles, which are declination angle (δ), angular hour (ω), and zenith angle (Θz). These angles can be estimated:

The declination (δ) is the angular position of the sun at solar noon (i.e., when the sun is on the local meridian) with respect to the plane of the equator, north positive; the declination angle is varies as -23.45°≤ δ ≥ 23.45° according to the Eq. (6.6) [57].

$$\delta = 23.45 \sin\left(360\ \frac{284 + n}{360}\right) \tag{6.6}$$

where

n The day number of the year, from 1 (corresponding to January 1) to 365 (corresponding to December 31).

The hour angle, ω, is the angular displacement of the sun east or west of the local meridian due to rotation of the earth on its axis at 15° per hour, morning negative, afternoon positive. The hour angle, ω, is 0° at solar noon time [57]. Calculation of angular hour could be done by the following Eq.

$$\omega = (\text{solar time} - 12) * 15°/\text{hr} \tag{6.7}$$

where ω is the hour angle [deg.], and solar time is the solar time [hr.].

$$\text{Solar time} = \text{standard time} - 4(L_{st} - L_{loc}) + E \tag{6.8}$$

where:

standard time : Based on a standard meridian for the local time zone [h].

L_{st} : Standard meridian for the local time zone [deg].

For Saudi Arabia ($L_{st} = 45°$)

L_{loc} : The longitude of the location of the collector site [deg].

E : Equation Time [min].

$$\mathrm{E} = 229.2[0.00075 + .001868\cos(\mathrm{B}) - 0.032077\sin(\mathrm{B}) - 0.014615\cos(2\mathrm{B}) - .04089\sin(2\mathrm{B})] \quad (6.9)$$

where

$$\mathrm{B} = (\mathrm{n} - 1)\frac{360}{365} \quad (6.10)$$

The third important solar angle is zenith angle (Θz) which is the angle between the vertical and the line to the sun that is, the angle of incidence of direct normal irradiance on a horizontal surface. Zenith angle could be calculated by Eq. (6.11).

$$\cos(\Theta_z) = \cos(\phi)\cos(\delta)\cos(\omega) + \sin(\phi)\sin(\delta) \quad (6.11)$$

Where Ø is a latitude location of the solar field.

As mentioned before, the energy absorbed in the solar receiver is affected by the optical properties and imperfections of the solar collector ensemble. The optical efficiency of a PTC field (η_{opt}) can be defined as the fraction of the direct solar irradiance incident on the aperture of the collector which is absorbed at the surface of the HCE. One can rewrite the Eq. (5.1) as following:

$$\eta_{opt} = \frac{Q_{abs}}{ANI} \quad (6.12)$$

By substituting Eq. 6.4 into Eq. 6.3, one can get

$$\eta_{opt} = \rho_{cl} * (\tau\alpha_c)_n * \gamma * IAM * f_{rowshadow} * f_{end\ loss} \quad (6.13)$$

According to Eq. (6.13), the solar field optical efficiency considers mirror reflectivity, the transmittance of the receiver glass envelope, the absorptance of the absorber surface coating, the intercept factor, the incident angle effects, the cleanliness of the mirrors, the row to row shadowing, and the receiver end losses.

Intercept Factor (γ)

In this study, the effect of correction parameters for the parabolic solar collector assembly; mirrors and heat collection element are accounted the intercept factor, γ, which is a fraction of the reflected radiation that is incident on the absorbing surface of the receiver. The factors that affect the intercept factor are [29, 59]:

- Losses from shading of ends of Heat collection element due to bellows, shielding, and supports, γ_1.
- Twisting and tracking error associated with the collector type, γ_2.
- Geometry accuracy of the collector mirrors, γ_3.
- Losses due to shading of HCE by dust on the envelope, γ_4.
- Miscellaneous factors to adjust for other HCE losses, γ_5.

Thus, the intercept factor is defined as:

$$\gamma = \prod_{i=1}^{i=5} \gamma_i \tag{6.14}$$

where, the values for γ_i are shown in Table 6.3.

Table 6.3: Effective optical efficiency terms, adapted from [29, 59, 60, 70, and 40]

Factor and Optical properties	Value
Luz Black Chrome (γ_1)	0.974
Luz Cermet (γ_1)	0.971
Twisting and tracking error (γ_2)	0.994
Geometry accuracy of the collector mirrors (γ_3)	0.98
Dirt on HCE (γ_4)	0.98
Miscellaneous factor (γ_5)	0.96

Incidence Angle Modifier (IAM)

For a PTC system, the nominal optical efficiency occurs when the direct beam radiation is normal to the collector aperture area. In addition to losses due to the normal angle of incidence, there are other losses from the collector that can be correlated to the angle of incidence greater than 0º [57]. So a factor called incident angle modifier (*IAM)* is used when the beam radiation is not normal. The IAM is taken into consideration in all optical and geometric losses due to an incident angle greater than 0º. The incident angle modifier depends on the geometry and the optical characteristics of the solar collector. The incident angle modifier is defined as [62, 63]:

$$IAM = \frac{\eta_{(\Theta)}}{\eta_{nominal}} \tag{6.15}$$

The incident angle modifier function is defined by:

$$IAM = \max[0, IAM(\Theta)] \tag{6.16}$$

Incidence angle modifier is given as an empirical formula in term of incidence angle (Θ). Each specific solar collector has its formula. Table 6.4 shows the incident angle modifier function for different solar collectors. These functions were plotted and shown in Figure 6.6.

Table 6.4: Incident angle modifier for different solar collectors

Solar Collector	Incident Angle Modifier function (IAM)	Reference
LS-2	$1 + 8.84 * 10^{-4}\frac{\theta}{\cos(\theta)} - 5.369 * 10^{-5}\frac{\theta^2}{\cos(\theta)}$	[63,40]
IST	$1 + 3.178 * 10^{-4}\frac{\theta}{\cos(\theta)} - 3.985 * 10^{-5}\frac{\theta^2}{\cos(\theta)}$	[64]
LS-3	$1 - 2.2307 * 10^{-4}\theta - 1.1 * 10^{-4}\theta^2 + 3.18596 * 10^{-6}\theta^3 - 4.85509 * 10^{-8}\theta^4$	[65]
Euro rough ET-100	$1 - 5.25097 * 10^{-4}\frac{\theta}{\cos(\theta)} - 2.859621 * 10^{-5}\frac{\theta^2}{\cos(\theta)}$	[66,67]

θ: incident angle in degrees

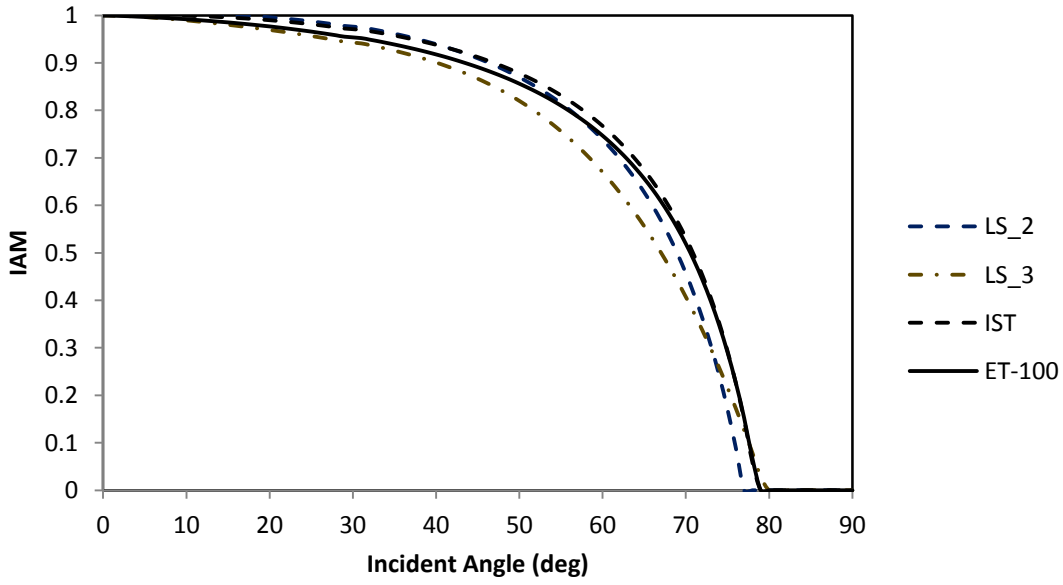

Figure 6.6: Incident angle modifiers for different parabolic trough solar collectors.

Row Shadowing

The positioning and geometry of the collector troughs and HCEs can introduce further losses, due to shading of parallel rows in the Sunrise and Sunset as well as end losses from the HCE.

The collectors are arranged in parallel rows, and they track the sun during the day time. Due to the sunrise and sunset row shading is occurs. For example, due to the low solar altitude angle of the sun in the morning, the eastern-most row of collectors can receive full sun, but this row will shade all subsequent rows to the west. As the sun rises and the collectors track the sun, this mutual row shading effect decreases, until a critical zenith angle is reached at which no row shading occurs. Collector rows remain un-shaded through the middle of the day. Figure 6.7 shows tracking of the solar collectors from early to mid-morning, and the consequent row shading occurs over this period.

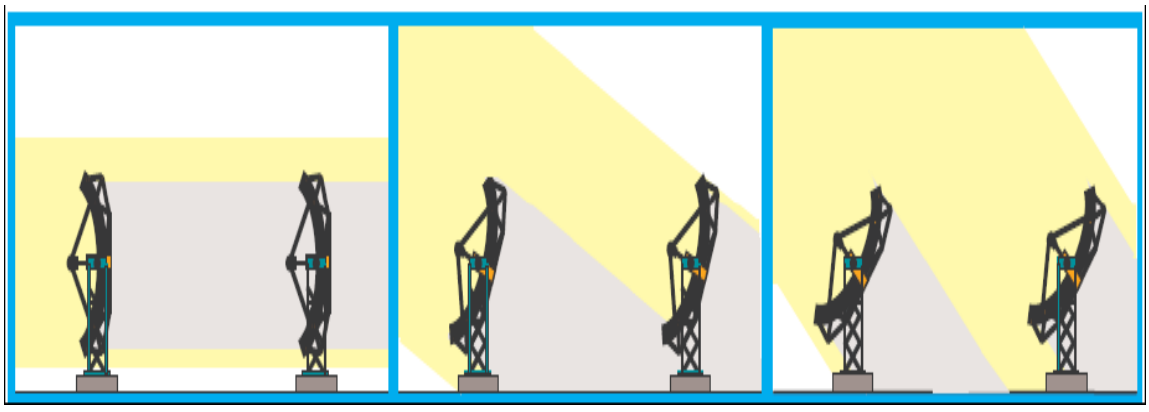

Figure 6.7: Collector tracking throughout the morning, showing digression of collector shading as the day progresses [53, 59, and 40]

Shading factor could be calculated by Eq. (6.17) [53, 59, and 40].

$$f_{row\ shadow} = \frac{L_{space}}{W_a} * \frac{\cos(\Theta_z)}{\cos(\Theta)} \tag{6.17}$$

where:

L_{space} : Distance between two parallel collectors [m].

W_a : Aperture width [m].

Θ_z :Zenith angle

Shading factor equation is bounded with a minimum value of 0 (rows are fully shaded) and a maximum value of 1 (rows are not shaded).

$$f_{row\ shadow} = \min\left(max\left(0.0\ ;\ \frac{L_{space}}{W_a} * \frac{cos(\Theta_z)}{cos(\Theta)}\right)\ ;\ 1.0\right) \tag{6.18}$$

End Losses

In a solar collector field, some length of the absorber tube is not illuminated by reflected solar radiation from the mirrors. As a result, the solar collectors end losses. In other words, End losses occur at the ends of the heat collection elements, where there is no focused radiation on those portions as shown in Fig. 6.8. End losses depend on the solar collector average focal length, the solar incidence angle, and the length of solar collector.

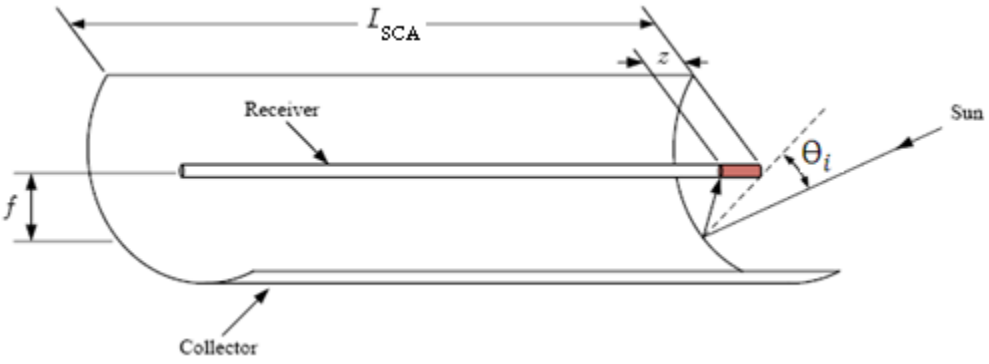

Figure 6.8: End losses from heat collector element

As shown in Figure 6.8, the part of the receiver that is not illuminated (z) is as follows:

$$Z = r * tan(\Theta) \tag{6.19}$$

The distance r is shown in Figure 6.9 and can be defined by [68]:

$$r = f_n + \frac{x^2}{4f} \tag{6.20}$$

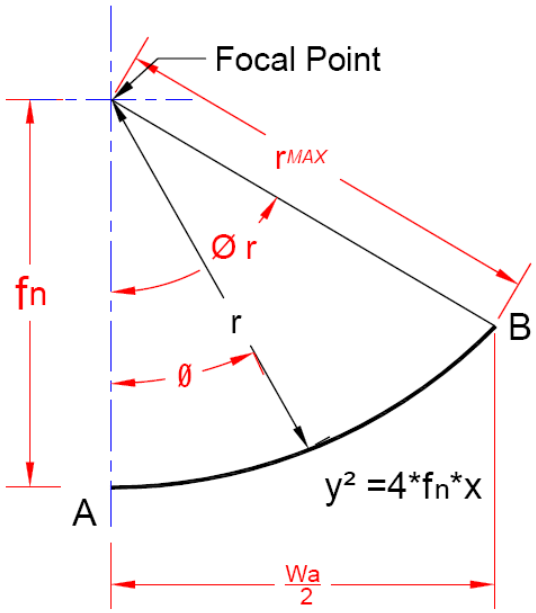

Figure 6.9: Parabola geometry for a rim angle of Θ_r [57, 68].

The fraction of the receiver that is illuminated is:

$$f_{end\ loss} = 1 - \frac{r}{L_{SCA}} \tan(\Theta) \tag{6.21}$$

where

r Local mirror radius [m].

L_{SCA} Length of a single solar collector [m].

f_n Focal length of the collectors [m].

Lippke et al. [69] proposed that r = f_n . This assumption is widely used in other models [53, 59] and leads to minimum end losses for certain geometric configuration. A previous work developed by Gaul and Rabl [62] suggested the use of an average value of r. This value was used in this study as given by:

$$\bar{r} = \frac{1}{\frac{W_a}{2}} \int_0^{\frac{W_a}{2}} \left(f_n + \frac{x^2}{4f_n} \right) \mathrm{dx} \tag{6.22}$$

$$\bar{r} = f_n \left(1 + \frac{{W_a}^2}{48{f_n}^2} \right) \tag{6.23}$$

Replacing the value of r, then, the collector geometrical end losses [62, 70] is:

$$f_{end\ loss} = max \left[0;\ 1 - \frac{f_n}{L_{SCA}} \left(1 + \frac{{W_a}^2}{48{f_n}^2} \right) \tan(\Theta) \right] \tag{6.24}$$

Figure 6.10 compares the end loss factor for the model of Lippke et al. [69] and the model of Gaul and Rabl [62] for two collector geometries. As shown in the Figure, the model of Lippke shows higher end loss factor than that in the model of Gaul and Rabl for the two collectors. Also the losses are greater when the incidence angle is higher.

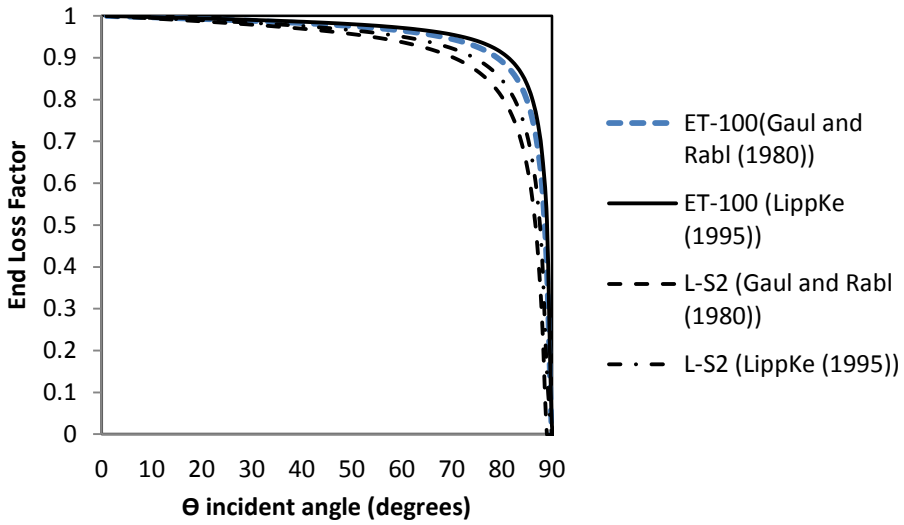

Figure 6.10: End loss factor for different parabolic trough collectors and assumptions. Lippke [69], Gaul and Rabl [62]

The annual optical efficiency as given by EES at noon time is shown in Figure 6.11. As shown, the maximum optical efficiency occurs at summer season in a year, the optical efficiency for ET-100 is better than that for LS-3 especially during a winter session. The difference between the two efficiencies comes from incidence angle modifier, where the incidence angle modifier for ET-100 is better than that for LS-3.

The daily optical efficiency of ET-100 at the average days in a month is shown in Figure 5.17. As shown in the Figure 5.17, the variations of daily optical efficiency in the winter months are greater than the variations in the summer months. Moreover, the optical efficiency of the summer months starts from lower values at early hours in the morning and increases to reach the maximum values at noon solar time.

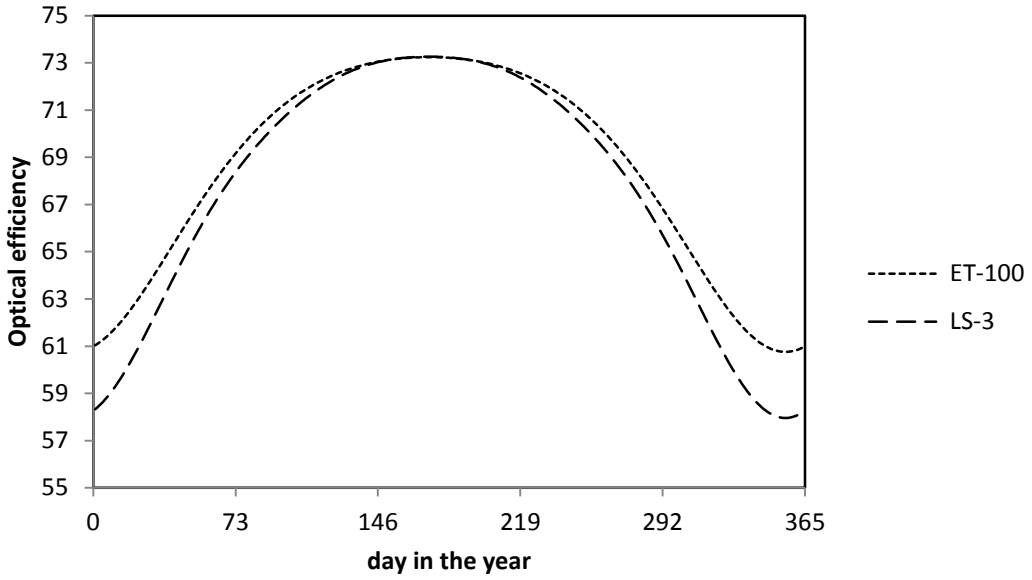

Figure 6.11: Optical efficiency of PTC throughout a year (at noon solar time) (using EES)

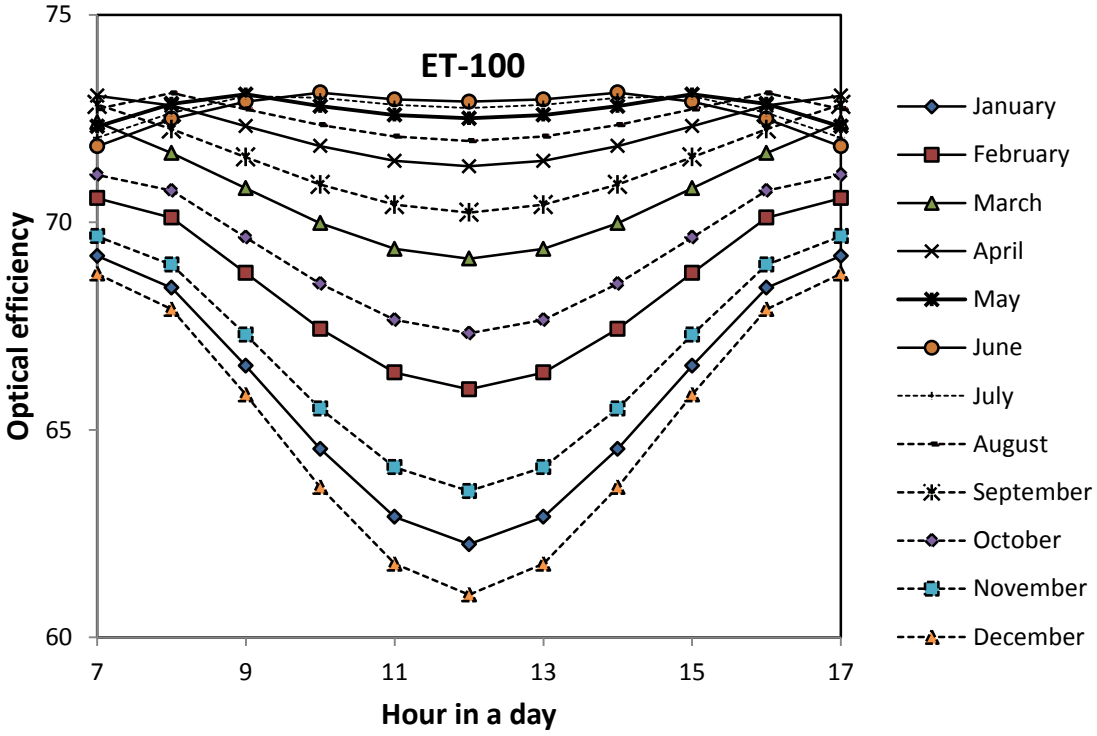

Figure 6.12: Hourly optical efficiency of PTC (ET-100) during an average day in the months (using EES)

On the other hand, the optical efficiency of the winter months starts from maximum values in early morning and decreases reach the lower values at noon. Figure 6.13 shows the monthly optical efficiency of ET-100 at the average days in a month.

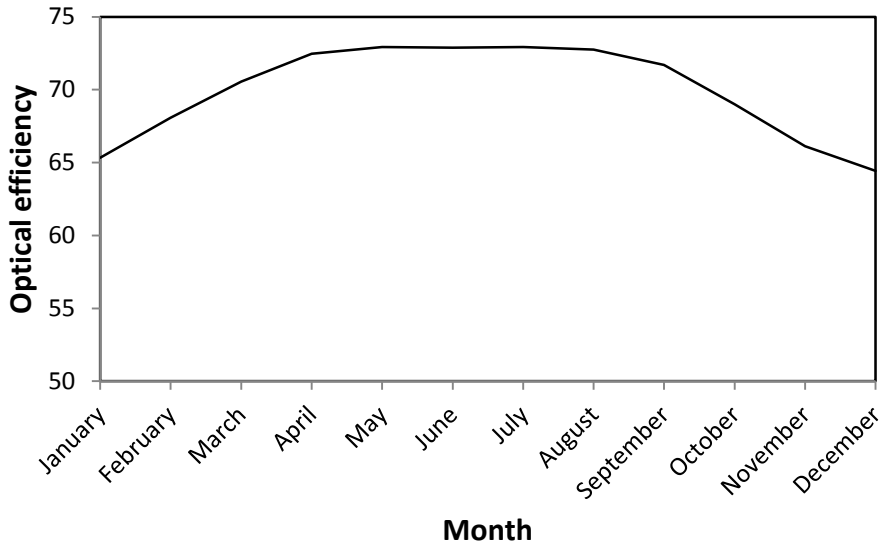

Figure 6.13: Average monthly optical efficiency of a parabolic solar collector throughout a year (using EES).

6.1.2 Estimation Optical Efficiency of PTC by Using THERMOFLEX Software

The model (in THERMOFLEX) uses an estimate of atmospheric transmissivity developed by Hottel [71] to determine the fraction of extraterrestrial flux that reaches the earth at the specified location. THERMOFLEX includes an option to use a model to compute the beam radiation at anytime and anywhere.

THERMOFLEX computes Aperture Normal Irradiance (ANI) from the Direct Normal Irradiance (DNI) based on the collector's orientation on the earth, its tilt away from

horizontal, and the sun's position in the sky. The model in THERMOFLEX assumes the collector is tracking in one dimension so the sun's central ray and the parabola's axis are coplanar.

The gross energy absorpted by the receiver tube is obtained by Eq. (6.1) where the Eq. 6.3 has been used by THERMOFLEX to calculate optical efficiency of solar collector. However the IAM is named by THERMOFLEX as $f_{incident}$.

The optical efficiency that obtained when the incident solar radiation is normal to the aperture ($\theta = 0°$) is called nominal efficiency, this simplified definition of nominal efficiency, $\eta_{nominal}$, includes the deleterious effects of misaligned mirrors and tubes. It also includes effects of radiation absorption and scattering when radiation interacts the mirrors, as well as it includes effects of reflection, absorption, and scattering from the glass envelope and the receiver tube itself.

The nominal efficiency ($\eta_{nominal}$) and cleanliness factor (f_{clean}) are inserted directly to THERMOFLEX program, and the end loss factor ($f_{end\ loss}$) is computed by the program. The incident angle correction factor (IAM) accounts for changes in optical efficiency due to non-normal rays strike on real the mirror surfaces. This factor is inserted in a table to the program as a function of incident angle. Figure 6.14 shows the variations of correction factor (IAM) with incident angle for a typical solar collector characteristic in the THERMOFLEX.

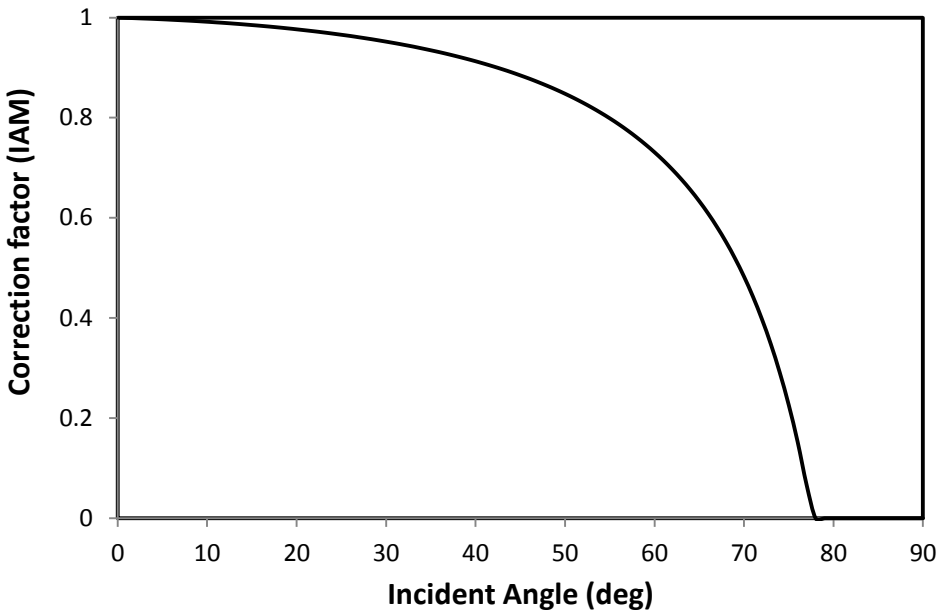

Figure 6.14: Variations of correction factor (IAM) with incident angle (from THERMOFLEX)

To study the variations of the optical efficiency for the PTC by using THERMOFLEX program; the data for EuroTrough solar collector (ET-100) has been used; the data of Dhahran Saudi Arabia has been used; the solar collector was rotated about horizontal north-south axis with continues adjustment to minimize the angle of incidence.

The annual optical efficiency as given by THERMOFLEX at noon solar time is shown in Figure 6.15. As shown, the maximum optical efficiency occurs at the summer season in a year. The daily optical efficiencies of ET-100 at the average days in the months are shown in Figure 6.16.

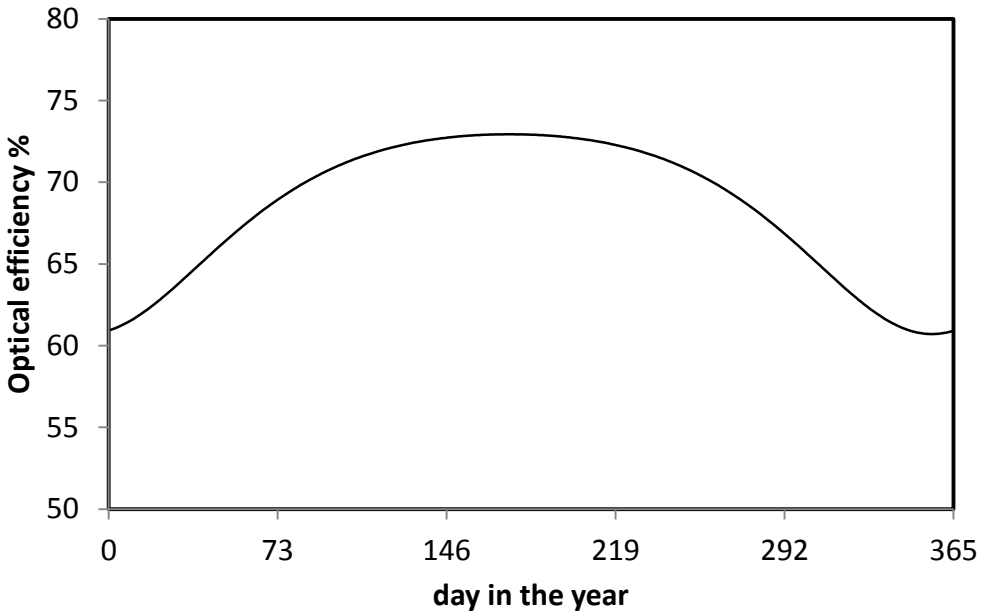

Figure 6.15: Optical efficiency of PTC (ET-100) throughout a year (at noon solar time) (using THERMOFLEX)

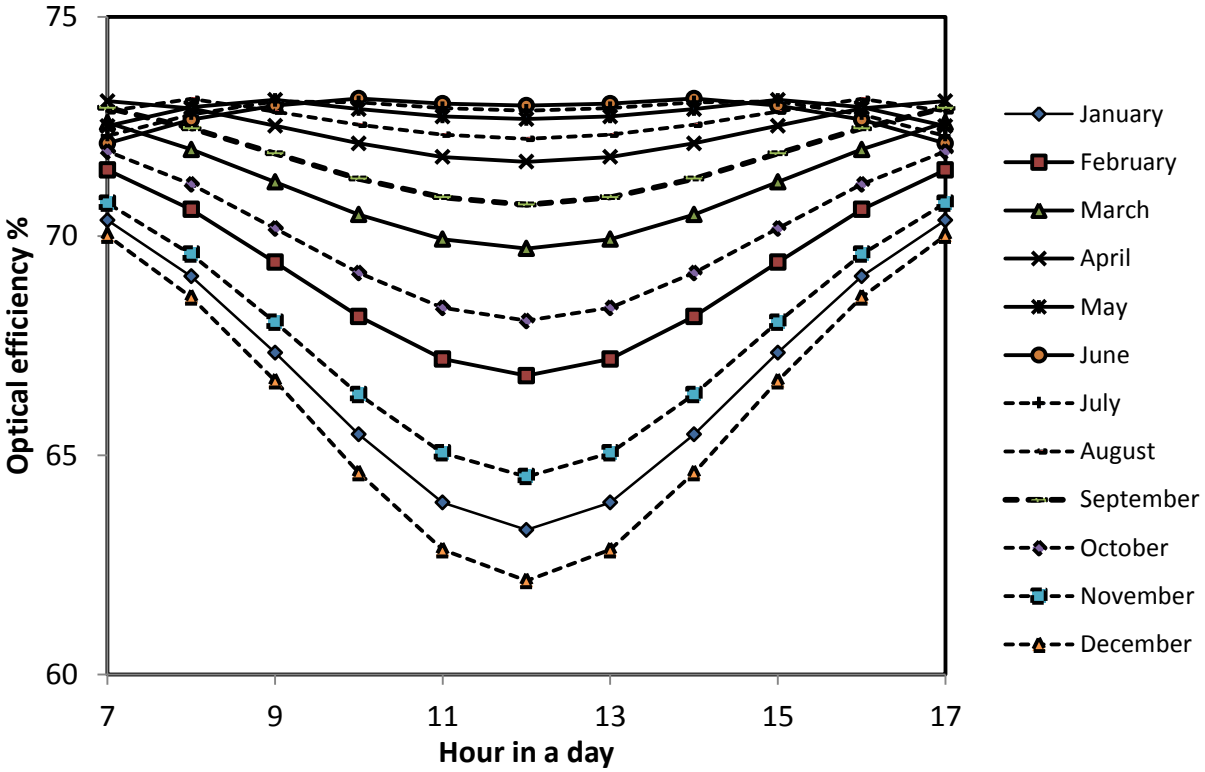

Figure 6.16: Hourly optical efficiency of PTC (ET-100) during an average day in the months (using THERMOFLEX)

As shown in the Figure 6.16, the variations of daily optical efficiencies in the winter months are greater than those in the summer months. Moreover, the optical efficiencies of the summer months start from lower values in early morning and increase to reach the maximum value at noon time. On the other hand, the optical efficiency of the winter months starts decrease from maximum values in early morning and increase to reach the lower values at noon. Figure 6.17 depicts the monthly optical efficiency for ET-1100 at the average days in the months.

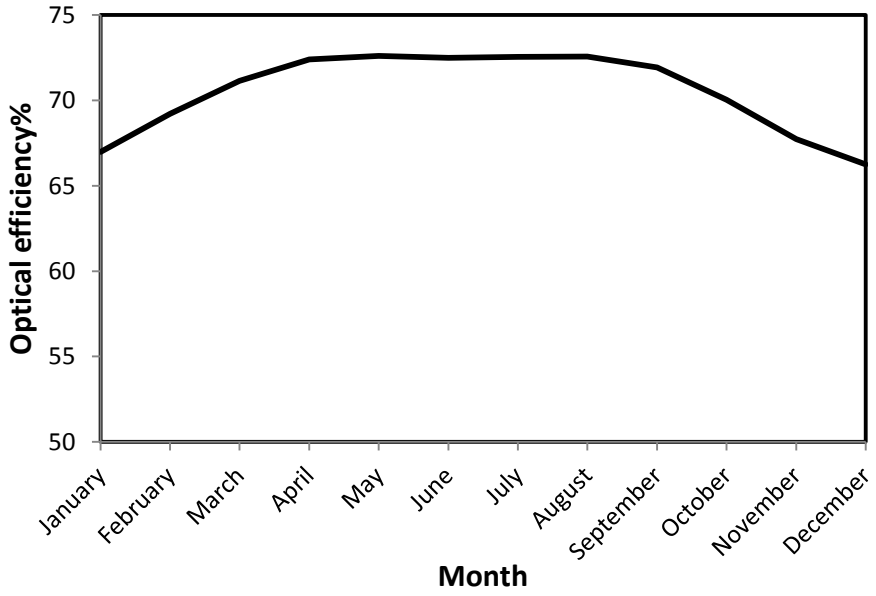

Figure 6.17: Average monthly optical efficiency of the PTC throughout a year (using THERMOFLEX).

6.1.3 Comparison of the Optical Efficiency of the PTC System between EES Code and THERMOFLEX

Figure 6.18 shows the comparison between results obtained by EES code and those by THERMOFLEX code for the same solar collector characteristics (EuroTrough solar collector ET-100). Figure 6.19 shows the same comparison for LS-3.

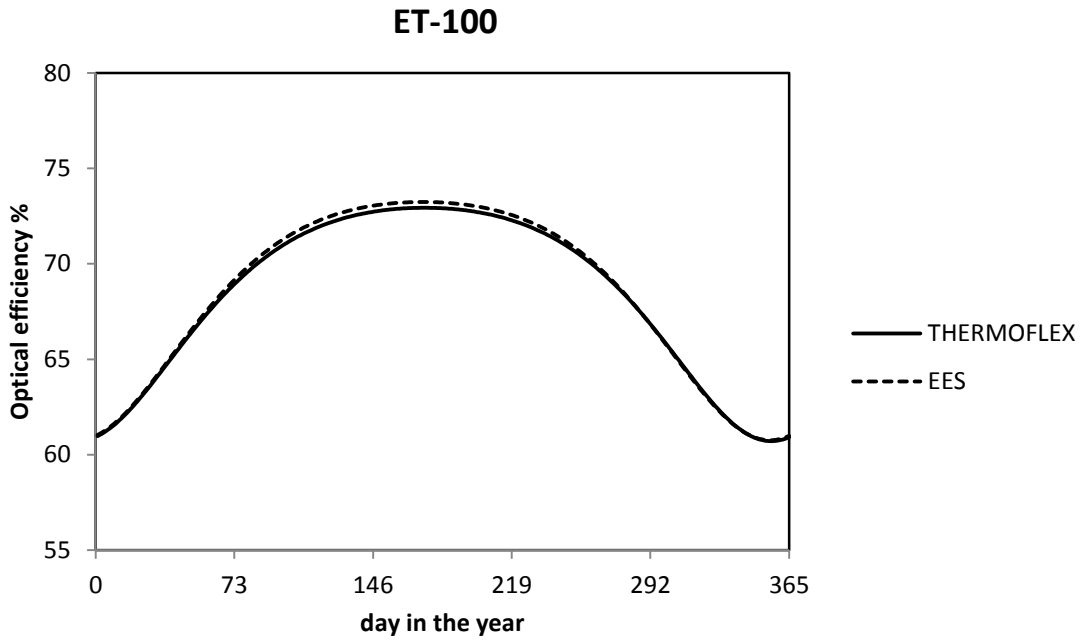

Figure 6.18: Comparison of daily optical efficiency of ET-100 between presently developed code in EES and THERMOFLEX code (at noon solar time).

As shown in Figure 6.18, the optical efficiency obtained by THERMOFLEX for ET-100 solar collector is matching very well with the results from EES code. This is because the IAM for both the typical model in the THERMOFLEX and the ET-100 are almost the same.

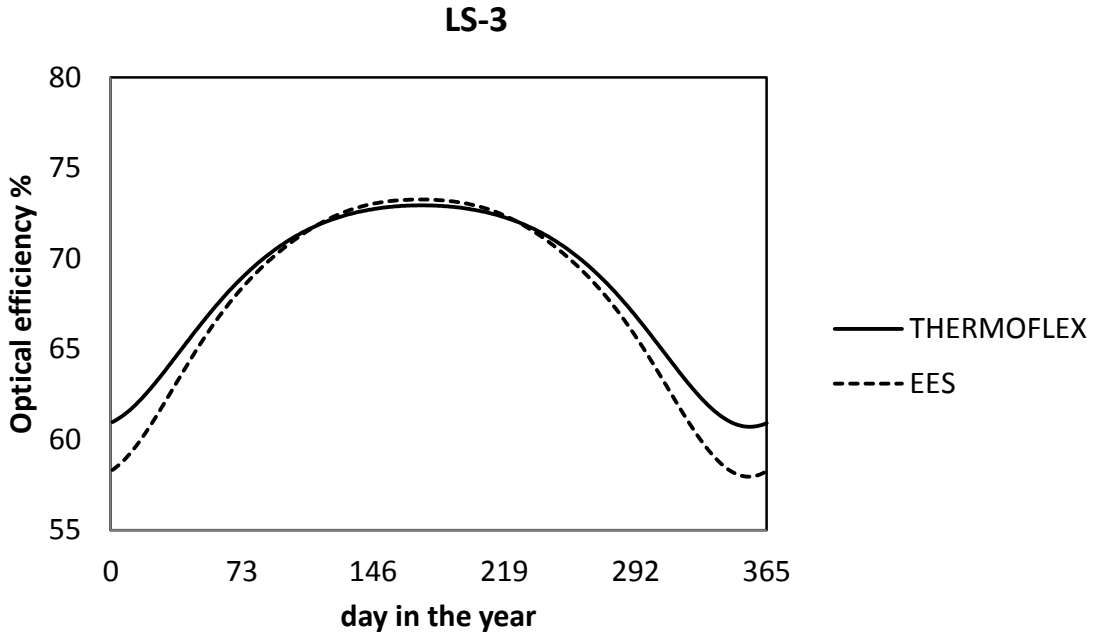

Figure 6.19: Comparison of daily optical efficiency of LS-*3* between presently developed code in EES and THERMOFLEX code (at noon solar time).

Figures 6.20-a, and 20-b shows the comparison between the results obtained by EES code and those by THERMOFLEX code for Euro Trough solar collector (ET-100). In general, the daily optical efficiencies obtained by THERMOFLEX for ET-100 solar collector show an excellent agreement with those obtained by EES code during all months in the year. The Figure 6.21 presents the comparison between the two codes at the average optical efficiency for each month.

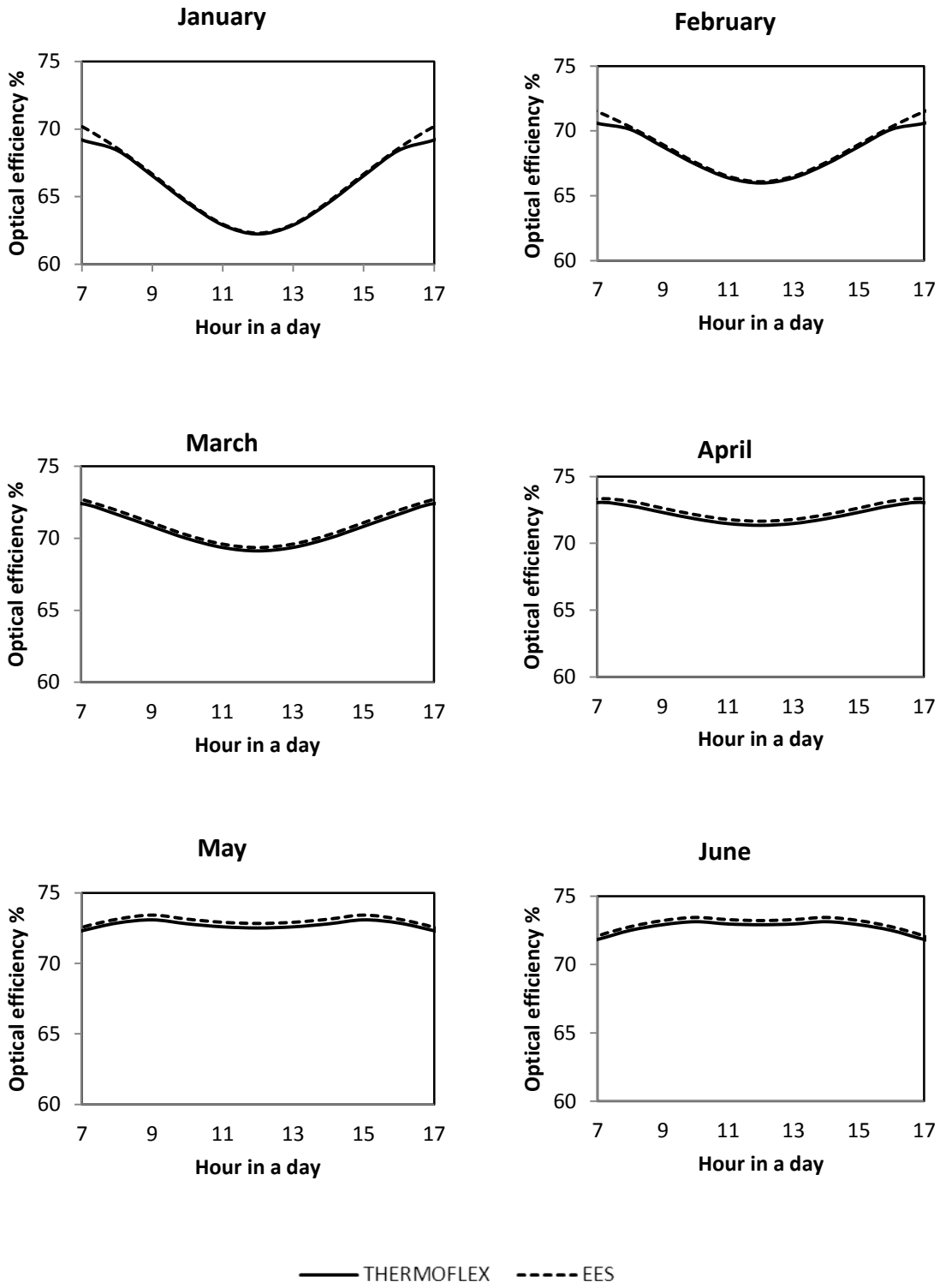

Figure 6.20-a: Comparison of hourly optical efficiency between presently developed code in EES and THERMOFLEX code for six months.

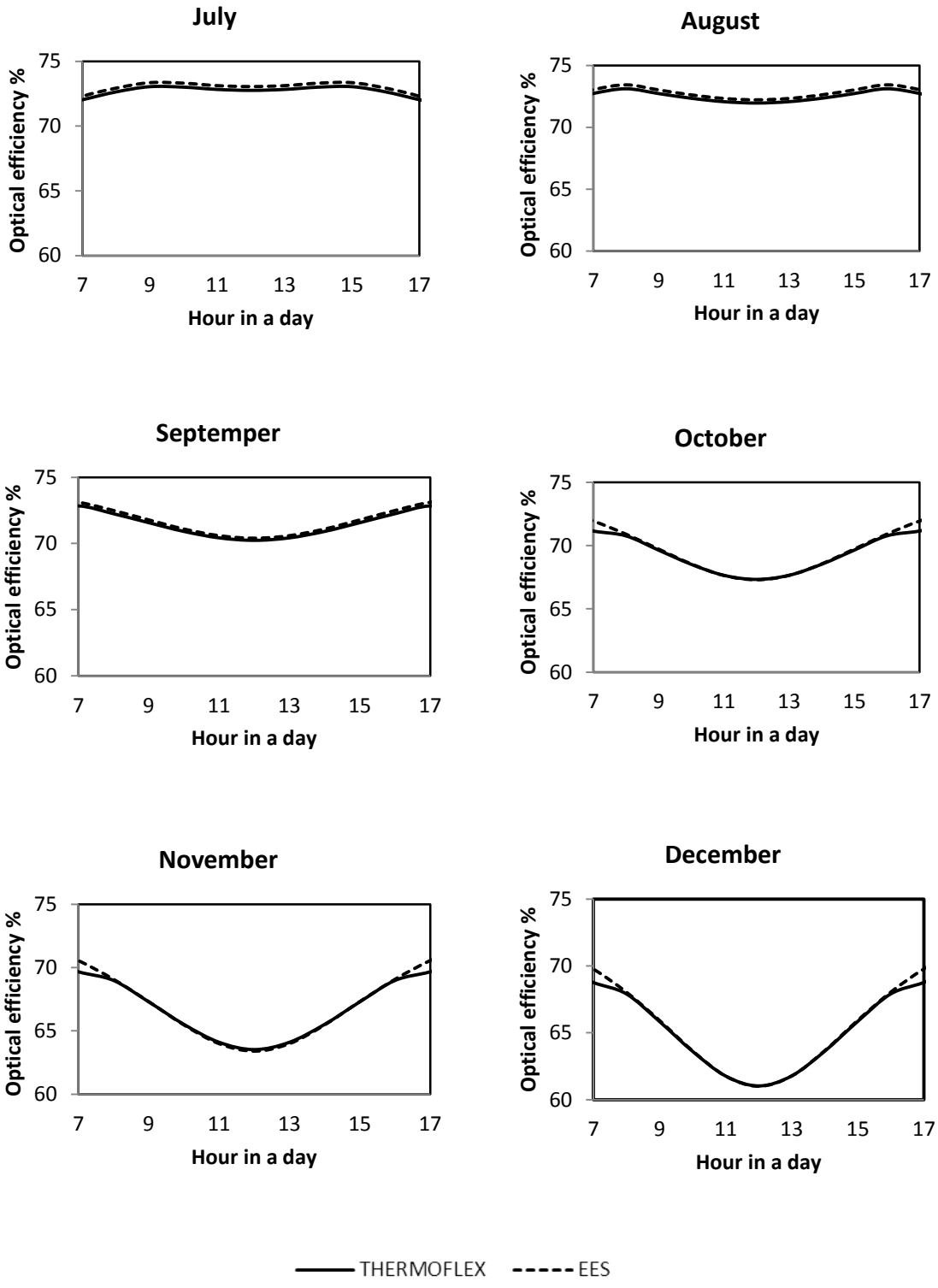

Figure 6.20-b: Comparison hourly optical efficiency between present developing code in EES and THERMOFLEX code for the other six months

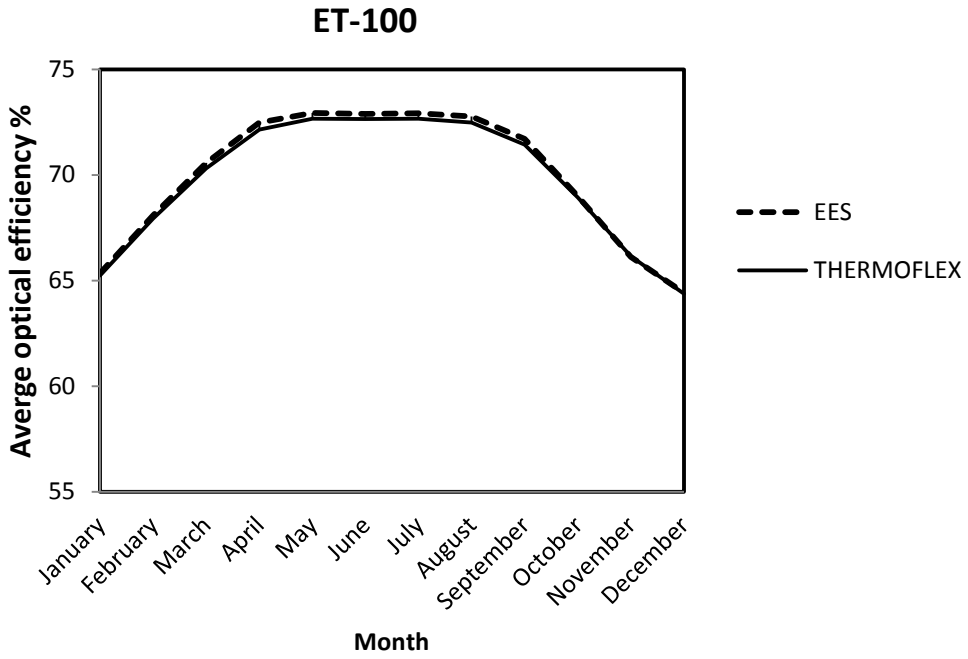

Figure 6.21: Comparison of monthly optical efficiency between presently developed code in EES and THERMOFLEX code.

In conclusion, the optical efficiency for parabolic solar collector proposed to install in Dhahran is varying with a time. However, the variation in optical efficiency in a summer months is very bigger than that in a winter months. The maximum optical efficiency can be reached in Dhahran is 73.5 %, whereas the minimum optical efficiency is 61%. The validation of EES code with THERMOFLEX has been done; the optical efficiency of PTC obtained by EES for ET-100 solar collector show an excellent agreement with those obtained by THERMOFLEX code.

6.2 Assessment the Thermal Efficiency of a PTC System in Dhahran

Collector thermal efficiency includes the effect of the collector's optical efficiency, end losses (resulting from collector geometry), and the thermal loss (from the hot receiver tube to the surroundings). It does not include heat losses at the inlet and exit header. If the receiver tube has zero heat loss and there were no end losses, the solar efficiency would equal the optical efficiency. Collector efficiency is the measure of the collector-only performance, independent of installation details. Thermal performance of solar collector is characterized by the thermal efficiency:

Thermal efficiency

$$= \frac{\text{Net energy transferred to the fluid in receiver tubes}}{\text{Energy impinging active focused aperture area}} \tag{6.25}$$

$$\eta_{th,collector} = \frac{\text{Qu}}{(ANI * A_a)} \tag{6.26}$$

where

$\eta_{th,collector}$	Thermal collector efficiency
Qu	Net energy transferred to the fluid in receiver tubes
ANI	Aperture normal irradiance
A_a	Aperture area

Some of absorbed energy heats the receiver tube and the fluid flowing inside. The balance is lost to the surroundings via radiation, convection, and conduction. The wall tube radiates to the glass envelope and the surroundings. In this model, the small

convective heat transfer from the tube to the ultra-low pressure gases in the annulus is ignored (evacuated glass envelope). The glass envelope loses heat to the environment by convection and radiation. According to reference [57], net heat transfer to the fluid in receiver tube is:

$$Q_u = F_R * A_a \left[Q_{abs} - \frac{\mathrm{A}_r}{\mathrm{A}_a} * \mathrm{U}_L(\mathrm{T}_i - \mathrm{T}_a) \right] \tag{6.27}$$

$$F^{"} = \frac{F_R}{F'} = \frac{\dot{m} * C_p}{\mathrm{A}_r * \mathrm{U}_L * F'} \left[1 - \exp\left(- \frac{\mathrm{A}_r * \mathrm{U}_L * F'}{\dot{m} * C_p} \right) \right] \tag{6.28}$$

$$F' = \frac{U_O}{U_L} \tag{6.29}$$

$$U_O = \frac{1}{U_L} + \frac{D_o}{h_{fi} * D_i} + \frac{D_o * \ln(\frac{D_o}{D_i})}{2 * k} \tag{6.30}$$

$$\mathrm{A}_a = (W_a - D_o) * L \tag{6.31}$$

$$\mathrm{A}_r = A = \pi * D_o * L \tag{6.32}$$

where

D_o : Outer diameter of absorber tube [m].

D_i : Inner diameter of absorber tube [m].

A_r : Receiver area

A_a : Aperture area

U_L : Collector over all heat losses

h_{fi} : Heat transfer coefficient inside tube

F' : Collector efficiency factor

$F^{"}$: Collector flow factor

F_R : Collector heat removal factor

$\dot{m}$: Flow rate

C_p : Specific heat

T_i : Fluid inlet temperature

T_a : Ambient temperature

Q_u : Useful energy

Q_{abs} : Absorbed energy

Now, one needs to calculate U_L and h_{fi} .

Calculation Collector over all Heat Losses (U_L)

The heat loss (Q_{loss}) is estimated for each step using a one dimensional heat transfer model. For each station along the tube, one can computes a one-dimensional heat balance using an energy balance with a gray body radiative exchange from the receiver tube to the glass envelope, and a combined radiative and convective heat loss from the glass envelope to the environment. The heat absorbed by the fluid conduct through the tube wall and heats the fluid by convection heat transfer from inner wall of the absorber tube to the bulk fluid.

Figure 6.22 illustrates the cross section at a location along the tube. The ambient temperature is the same as other site temperature. The other temperatures are computed for each step. The external heat transfer coefficient is assumed constant along the tube length; also the radiative properties of the surfaces are assumed constants. The mathematical code computes the thermal conductivity of the tube based on its material

and its local temperature. The mathematical code computes internal heat transfer coefficient based on the fluid properties at the local fluid conditions.

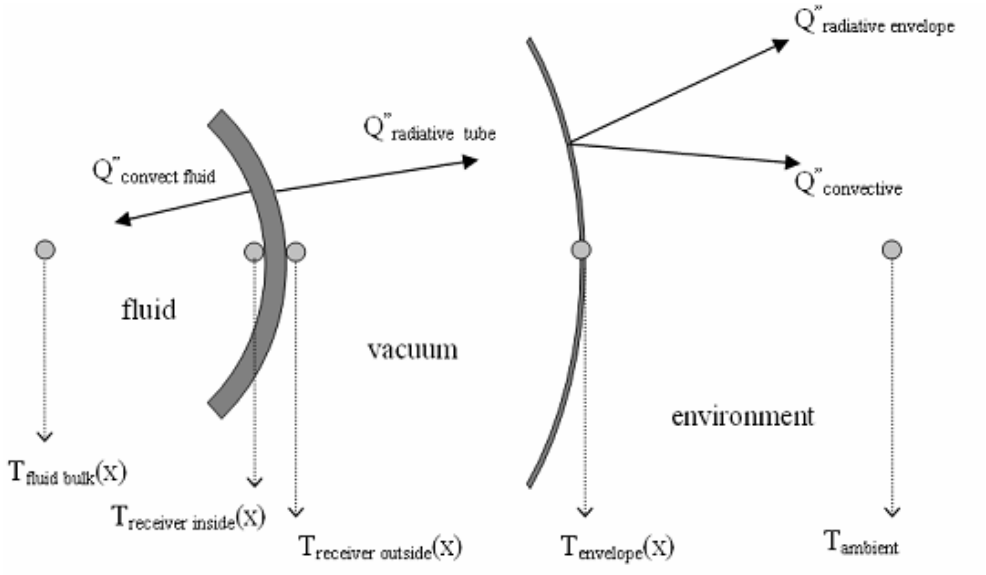

Figure 6.22: Temperature and heat flow from heat collection element

$$Q_{loss} = \pi * D_{co} * \mathrm{L} * \mathrm{h}_w(\mathrm{T}_{co} - \mathrm{T}_a) + \varepsilon_c * \pi * D_{co} * \mathrm{L} * \sigma\left(\mathrm{T}_{co}{}^4 - \mathrm{T}_{sky}{}^4\right) \qquad (6.33)$$

where

D_{co} : Outer diameter of glass envelops.

L : Collector length.

h_w : Wind heat transfer coefficient.

T_{co} : Outer glass envelope temperature.

ε_c Emittance for glass envelope.

T_{sky} Sky temperature = ambient temperature -5°C.

σ Stefan- Boltzman constant= $5.67*10^{-8}$.

Now, one needs to calculate $\mathbf{h}_{w}$ .The equations describing the loss can be solved by various equation-solving programs. At the beginning, assume the cover temperature is 290 K. To estimate the wind heat transfer coefficient, it is necessary to find the Reynolds number of the wind in which the physical properties depends on the average temperature between the cover and ambient temperatures).

$$Re = \rho * V * D_{co} \ /\mu \tag{6.34}$$

The wind heat transfer coefficient is then found from:

$$h_w = Nu_{out} * k/D_{co} \tag{6.35}$$

For flow of air across a single tube in an outdoor environment, the equations recommended by reference [57] have been used.

$$Nu_{out} = 0.4 + 0.54 * \mathrm{Re}^{0.52} \quad \text{For} \quad \text{o.1< Re >1000} \tag{6.36}$$

$$Nu_{out} = 0.30 * \mathrm{Re}^{0.6} \quad \text{For} \quad \text{o.1< Re >1000} \tag{6.37}$$

Now, one needs to calculate the inner cover temperature. That can be done through calculating the conduction heat transfer between the outer and the inner surface of the glass envelope. Where the (Q_{loss}) will be found from Eq. (6.33).

$$Q_{loss} = \frac{2 * \pi * k_c * L(T_{ci} + T_{co})}{\ln(\frac{D_{co}}{D_{ci}})} \tag{6.38}$$

where

T_{ci} : Inner temperature of glass envelope.

T_{co} : Outer temperature of glass envelope.

k_c : Thermal conductivity of the glass envelope.

D_{co} : Outer diameter of glass envelope.

D_{ci} : Inner diameter of glass envelope.

Thus, the heat loss by radiation from the receiver and inner surface of the glass envelope is the follows:

$$Q_{loss} = \frac{\pi * D_r * L * \sigma({T_r}^4 - {T_{ci}}^4)}{\frac{1}{\varepsilon_r} + \frac{1-\varepsilon_c}{\varepsilon_r}(\frac{D_r}{D_{ci}})} \quad (6.39)$$

The output of Eq. (6.39) has to equal the original heat losses. If they do not equal, it is necessary to make another guess of the outside cover temperature. Linear interpolation is also used to find the temperature, when the error is zero yields a cover temperature. Then one can calculate U_L from the following equation:

$$Q_{loss} = U_L * A_r(T_r - T_a) \quad (6.40)$$

Calculate Heat Transfer Coefficient inside tube h_{fi}

Reynolds number for heat transfer element is given by the following equation:

$$Re_{HTF} = \frac{\rho_f * V * D_{i,r}}{\mu_f} = \frac{4 * \dot{m}_f}{\pi * A_{i,r}} \quad (6.41)$$

where:

V_f : Velocity of HTF inside the tube.

$D_{i,r}$: Inner diameter of absorber tube.

μ : Absolute viscosity for heat transfer fluid.

ρ_f : Density for heat transfer fluid.

$\dot{m}_f$: Mass flow rate of heat transfer fluid for each collector path.

$A_{i,r}$: Inside cross sectional area of the absorber tube.

$$A_{i,r} = \frac{\pi}{4} * D_{i,r}^2 \tag{6.42}$$

In order to calculate Reynolds number for the flow inside the tube, properties of HTF should be known such as absolute viscosity, and density. So, these properties are given at the mean fluid temperature (T_{fm}). By assuming the value of the temperature at the outlet of solar field (T_{fo}), the mean fluid temperature can be calculated by the following equation:

$$T_{fm} = \frac{T_{fo} + T_{fi}}{2} \tag{6.43}$$

In order to calculate Nusselt number inside the tube, properties of HTF are given at the mean fluid temperature (T_{fm}). Value of Nusselt number depends on status of fluid flow, laminar or turbulent. When the laminar option is selected and the Reynolds number (Re) is lower than 2300, the Nusselt number will be constant. For flow inside tube, the value will be 4.36 [57]. When the Reynolds number (Re) is higher than 2300, the Nusselt number is given by the following equation [82]:

$$Nu_{insid\ tube} = \frac{\frac{f_2}{8} * (Re - 1000) * Pr_1}{1 + 12.7 * \left(\frac{f_2}{8}\right)^2 * \left(Pr_1^{\frac{3}{2}} - 1\right)} \left(\frac{Pr_1}{Pr_2}\right)^{0.11} \tag{6.44}$$

Where

f_2 : Friction factor for the inner surface of the absorber pipe.

Pr_1 : Prandtl number evaluated at the HTF temperature, (T_{fi}).

Pr_2: : Prandtl number evaluated at the absorber inner surface temperature (Ti), where (Ti) as a first guess Ti =T_{fm}+2.

T_{fm} : Main fluid temperature.

Ti : Inner reservoir temperature.

After determining the value of the Nusselt number, heat transfer coefficient (h_{fi}) can be calculated by the following equation:

$$h_{fi} = \frac{Nu_{inside\ tube} * k_f}{D_{i,r}} \quad (6.45)$$

where (k_f) is thermal conductivity of heat transfer fluid, also it should be found at the mean fluid temperature (T_{fm}).

6.2.1 Results and Discussion

The thermal efficiency of the parabolic trough solar collector system depends mainly on the optical efficiency of the system. More is the optical efficiency of the reflector better will be the thermal efficiency and hence the overall performance of the system. The annual thermal efficiency is shown in Figures 6.23 as determined by EES at noon solar time. As shown, the maximum thermal efficiency occurs at summer season in the year.

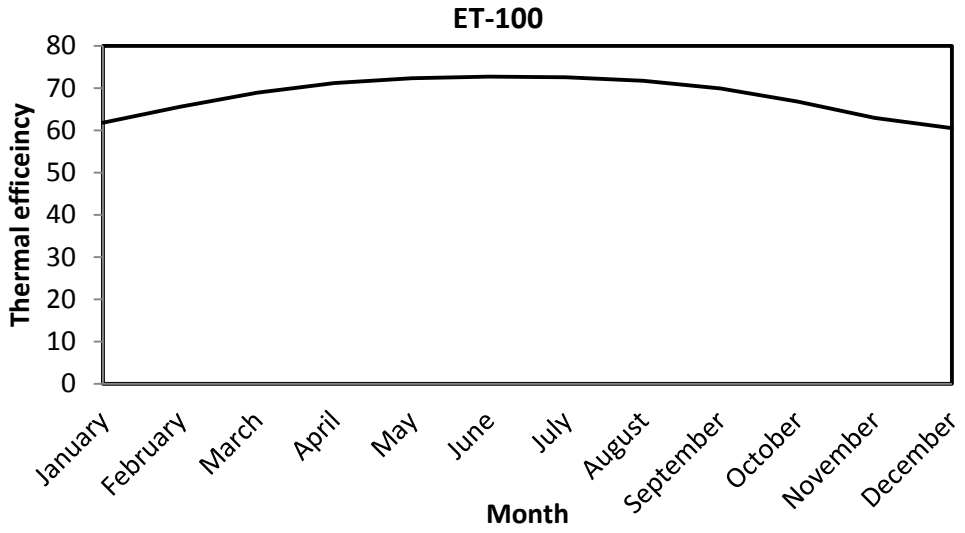

Figure 6.23: Thermal efficiency of PTC (ET-100) throughout a year (at noon solar time) (using EES)

Figure 6.24 depicts the comparison between results obtained by EES code and those by THERMOFLEX code for the same solar collector characteristics (EuroTrough solar collector ET-100). The thermal efficiency from THERMOFLEX for ET-100 solar collector is matching very well with the results from EES code.

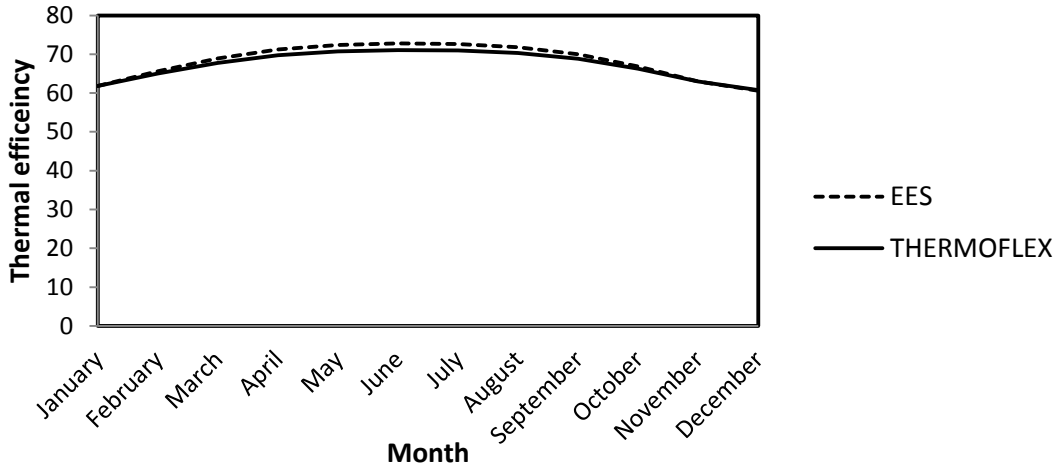

Figure 6.24: Comparison of daily thermal efficiency of ET-100 between presently developed code in EES and THERMOFLEX code (at noon solar time).

The daily thermal efficiency of ET-100 at the average day in each month is shown in Figures 5.25-a, and 5.25-b. The daily thermal efficiency in the winter months is less than that in the summer months. Moreover, the thermal efficiency in the summer months starts from lower values in early morning and increases to reach the maximum value at noon. Whereas the thermal efficiency in the winter months starts from lower values in early morning and increases to reach the maximum, and then starting decreases during the day time till reach minimum value at noon solar time and then starting to increases again. Furthermore, the daily solar time for summer months is greater than the daily solar time for winter months. As a result, the thermal obtained from solar collector during summer months is higher.

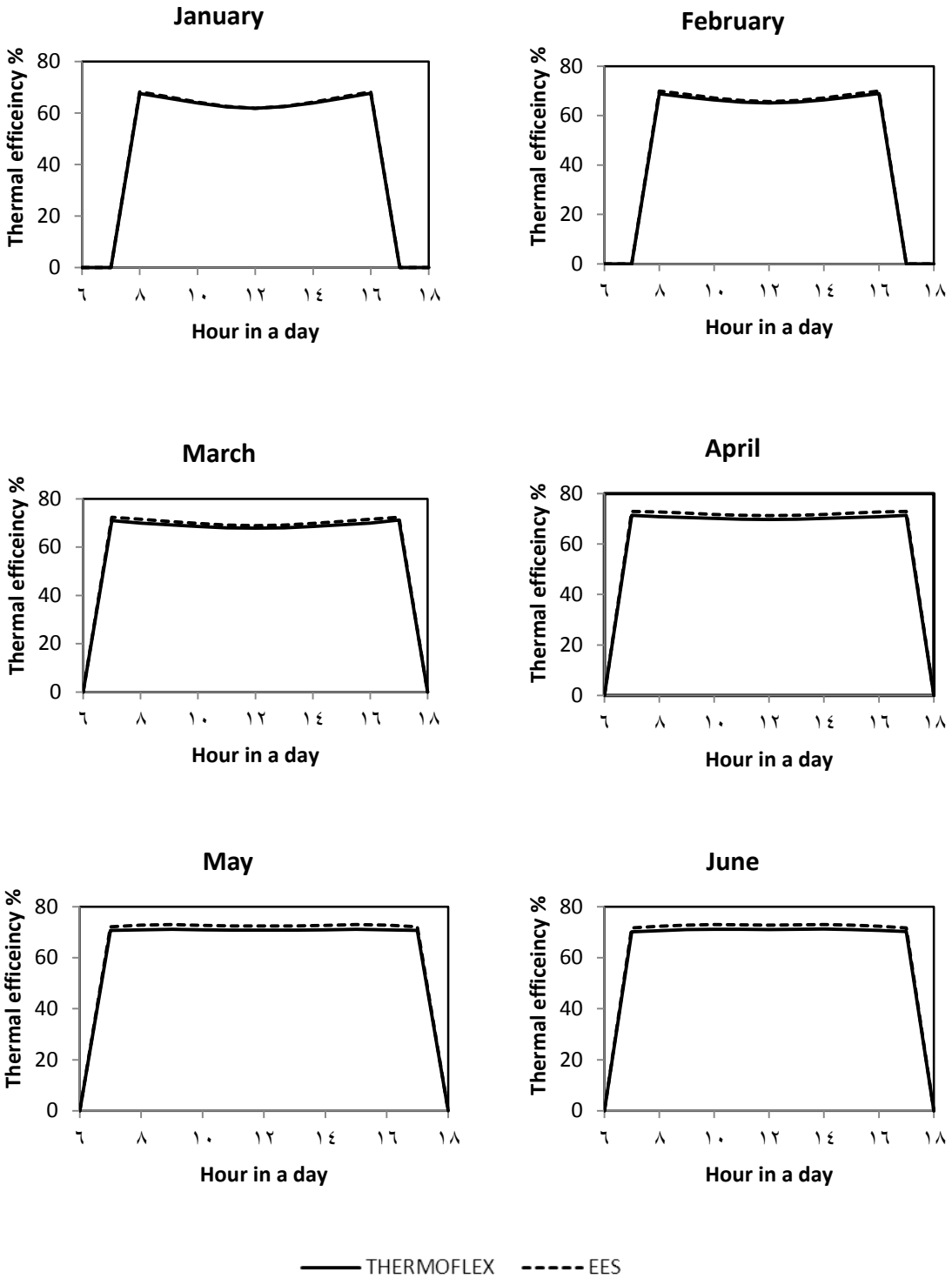

Figure 6.25: Comparison of hourly thermal efficiency between presently developed code in EES and THERMOFLEX code for six months.

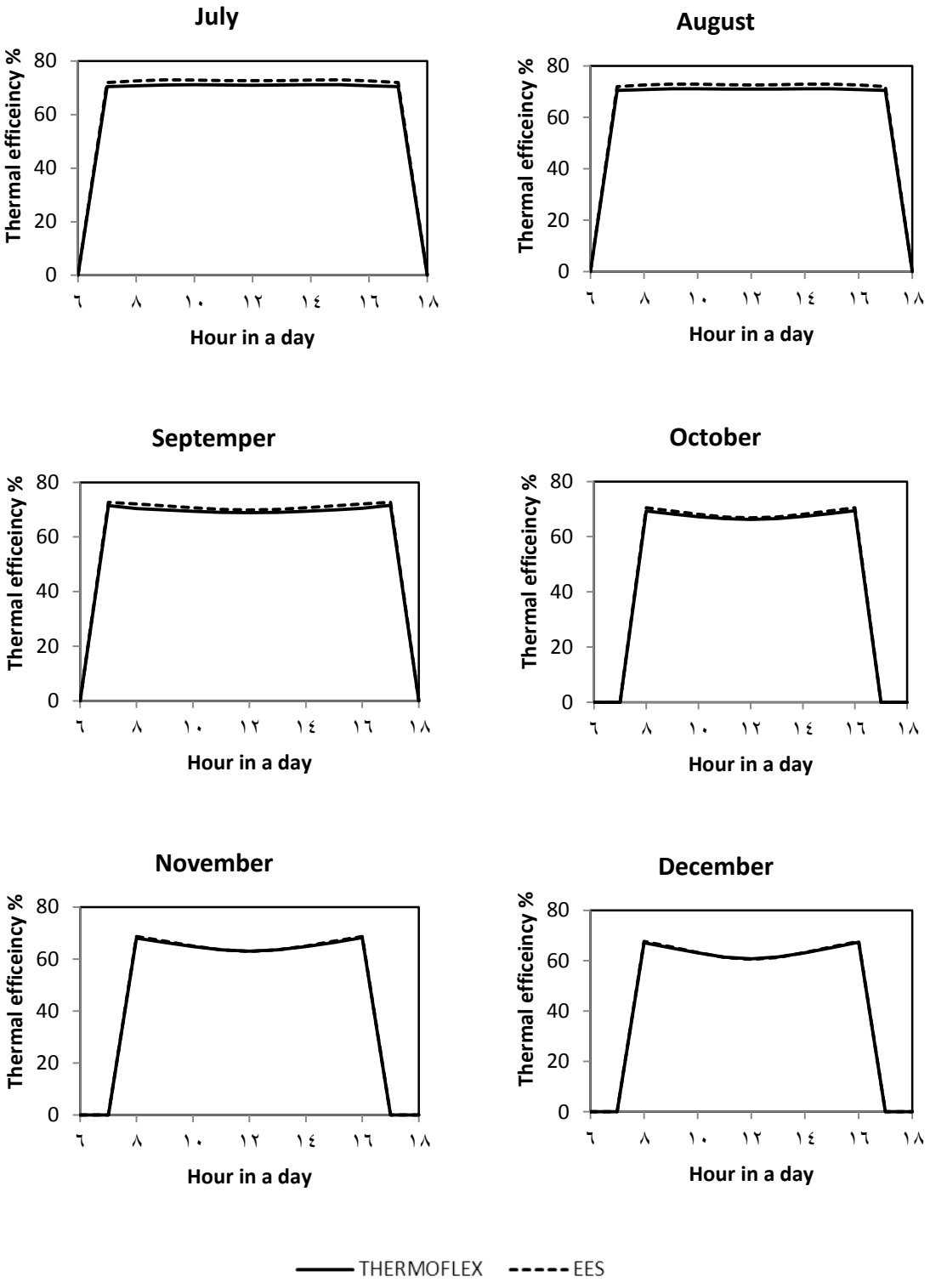

Figure 6.26: Comparison of hourly thermal efficiency between presently developed code in EES and THERMOFLEX code for the other six months.

6.3 Cost Reduction through Economies of Scale – Increasing the Plant Size

The costs of electric power generated by a line-focus solar power system are dependent on the capital equipment cost and the performance as well as the operating and maintenance costs. can also impact delivered energy costs. Increasing the scale of plants is an important cost reduction driver. This study focuses on the solar field cost only and how the cost varies increasing solar field area. The proposed parabolic trough power plant under study has a solar field area of 2.8 hectare to 160 hectare.

The major equipment for a concentrated solar power (CSP) plant involves the important solar components (solar collector field, heat transfer piping, and storage subsystem) and more-or-less conventional thermodynamic power cycle components. We will focus on the solar components and address the suitable opportunities for both cost reduction and performance improvement.

Increasing plant size is one of the easiest ways to reduce the cost of the solar electricity from parabolic trough power plants. Previous studies have shown that doubling the size of the plant reduces the capital cost by approximately 12-14% [72, 73, 74, and 75]. For example, Pilkington Solar International report [72] has shown that the specific cost for a parabolic trough power plant with 40 MW can be cut by 14.5 % at 80 MW and by 28% at 160 MW. A similar analysis identified that the specific cost for a parabolic trough power plant can be cut by 12.1% if the plant size is increased from 50 MW to 100 MW and by 20.3% if it is increased from 50 MW to 200 MW [73, and 74]. Also Nieto [75] came to

the conclusion that the capital costs for a parabolic trough power plant could be reduce by 13% if the plant size is increased from 50 MW to 120 MW.

According to NREL report [76] (Renewable Energy Technology Characterizations), the specific cost for a parabolic trough power plant with 10 MW can be cut by 19% at 20MW , by 37% at 40 MW, by 48 at 80 MW , and by 61% at 160 MW.

This section describes the typical cost structure of a PTC, which is the most commercially advanced. Like any other industry, PTC business actors are not willing to disclose internal information on the cost structures in an unlimited way. Still, some commercial cost information has been made available, which is analyzed and referenced in this section.

To study the cost reduction of PTC by increase solar field size, one can use a simple solar power plant as shown in Figure 6.27. This simple plant has a parabolic solar field, one pump, one water supply, and process output. Steam output from this plant was considered with constant flow rate (81.44 kg/s) at 45.88 bar output pressure, but the output temperature was changing during increasing solar field size. The solar field area of the simple power plant (under study) varies from 2.8 hectare to 160 hectare.

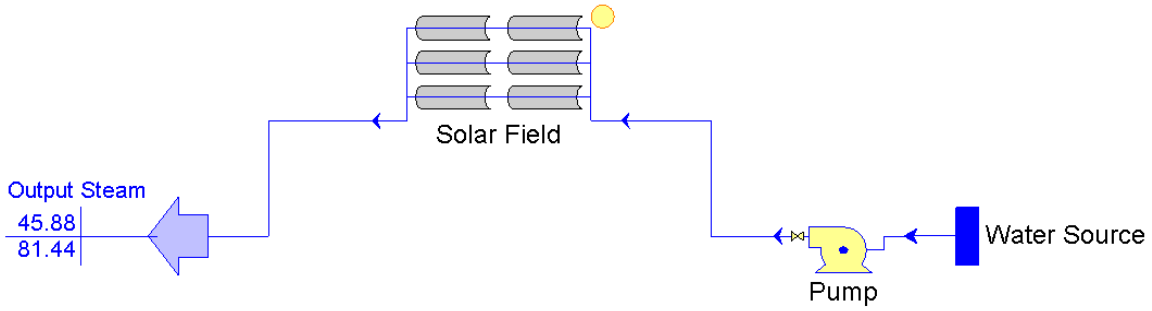

Figure 6.27: Simple solar thermal power plant

One can increase the solar field size by increasing number of solar collector's rows. The variations of total installed cost of parabolic solar field with solar field size are shown in Figure 6.28. The total installed cost of parabolic solar field involves the cost of mechanical and civil works. As shown in Fig. 6.28, the cost of mechanical works is the major contributor to total installed cost.

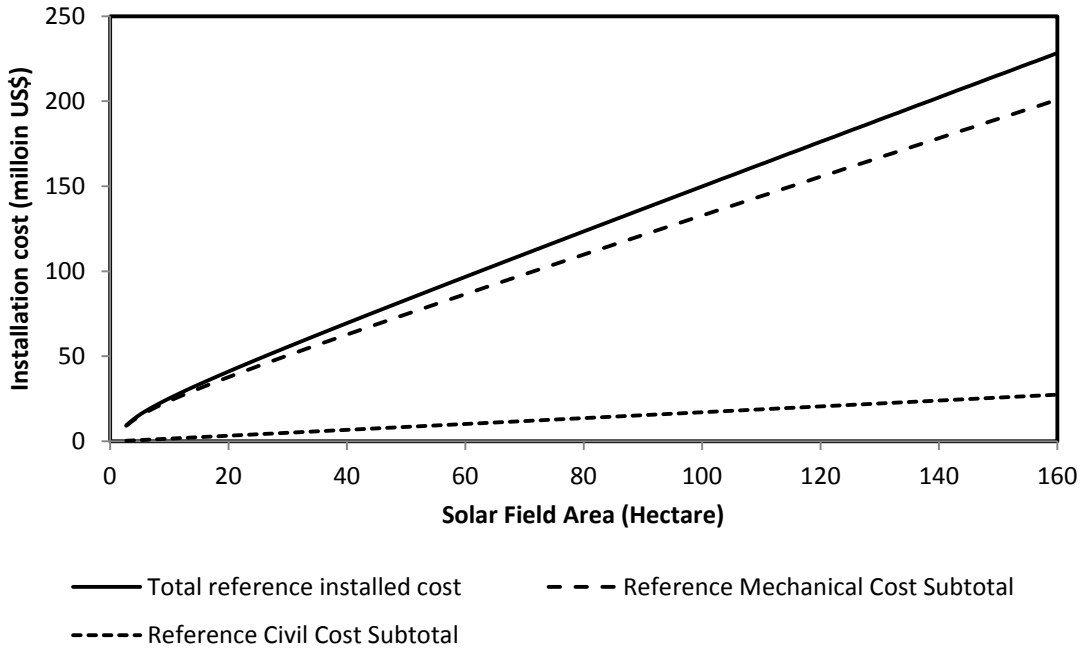

Figure 6.28: Variation of installation costs of PTC with solar field size.

The mechanical cost includes the cost of receiver, reflector, structure and drives system, piping with headers system, and mechanical labor. The civil cost includes the cost of foundation material and equipment, excavation/backfill material and equipment, and civil labor. The cost variations of mechanical works with increasing solar field size are shown in Figure 6.29. Whereas the cost variations of civil works with increasing solar field size are shown in Figure 6.30.

For parabolic collectors, there are three important different areas; one of them is called reflective area, the other one is called aperture area, and the third one called solar field area (size). The reflective area is that covered by shiny material on the parabolic reflector surface. It is the area you would get if you flattened out the trough. Aperture area is the distance between rim to rim multiplied by the reflective length of the reflector. The solar field area is a required area for solar collector field (land area). Figure 6.31 shows the variation of aperture and reflective area of solar collector with required land area solar field (solar field size).

The cost per unit area is important scale for solar collector works. Figure 6.32 shows how the total installation cost per unit area varies with solar field size. As shown, the total installation cost is calculated for three different unit areas, which are reflective, aperture, and land unit area. However, the most popular one is the total installed cost per unit aperture area. The total installation cost is reduced by increasing the solar field size; the cost reduction is filled down by increasing solar field size from 2.8 hectare to 10 hectare, then the cost declination is rapidly when the solar field size is increased from 10 hectare

to 60 hectare, after that the cost declination is almost gradual with increasing the solar field size.

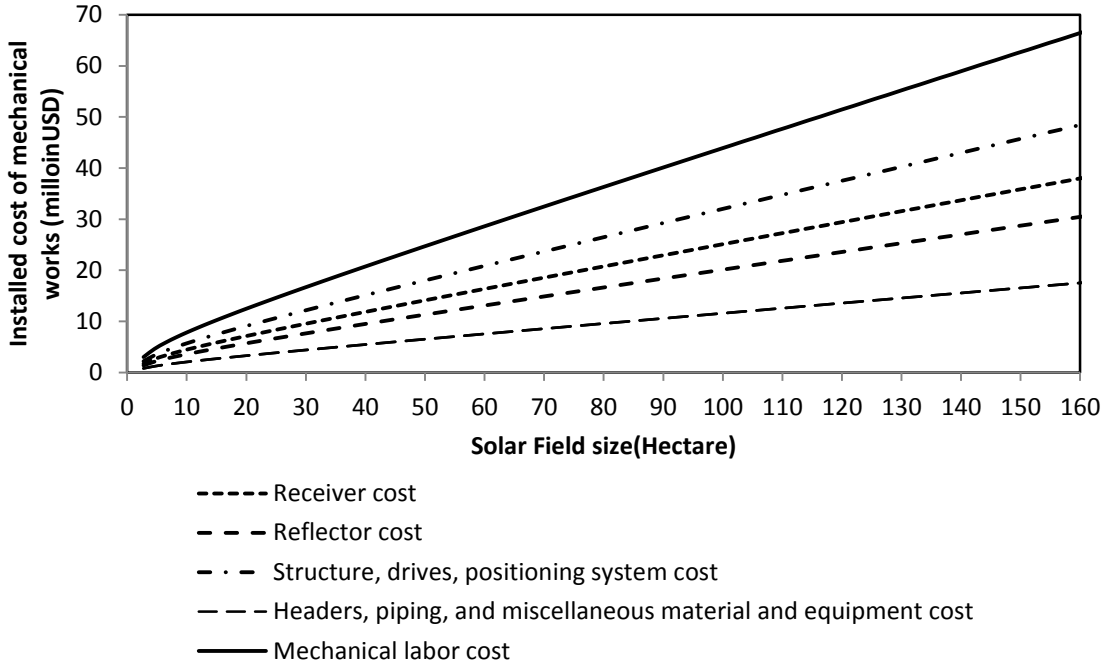

Figure 6.29: Variation of installation costs of mechanical works with solar field size (for PTC)

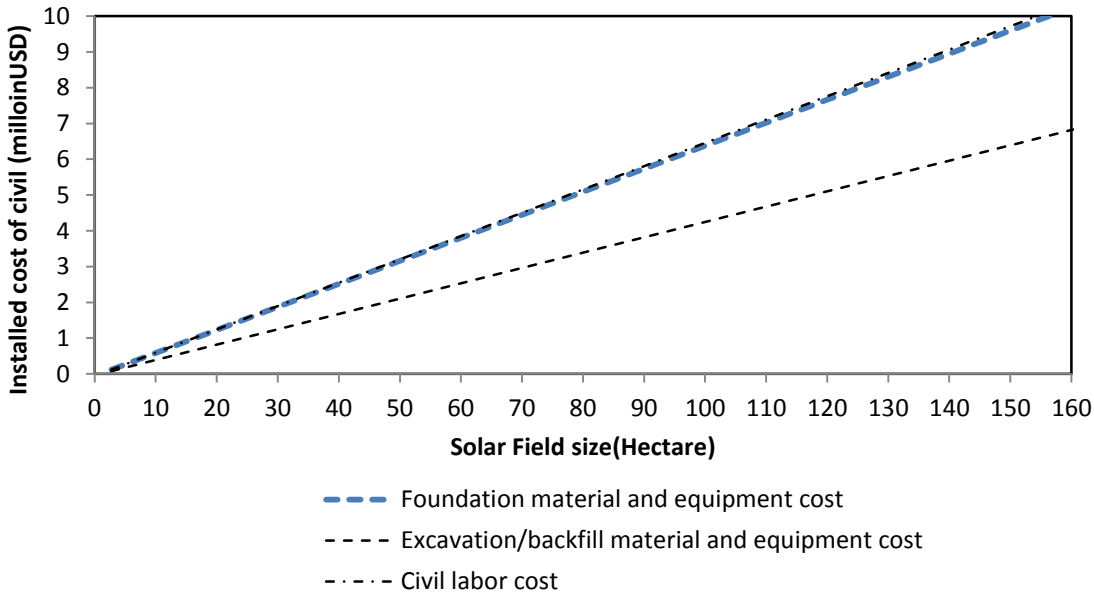

Figure 6.30: Variation of installation costs of civil works with solar field size (for PTC)

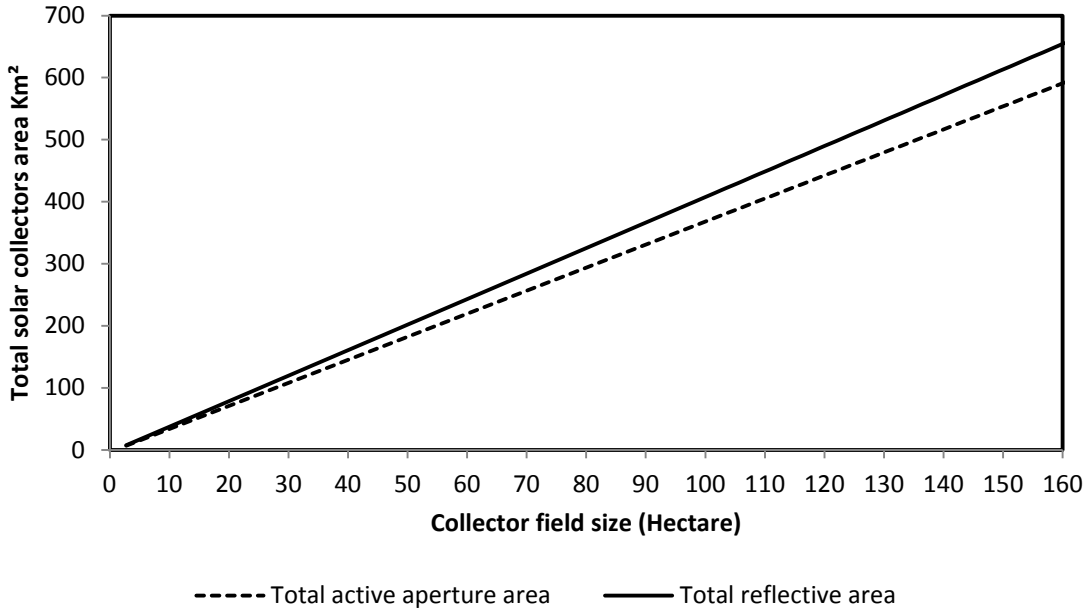

Figure 6.31: Variation of total collector area with solar field size (for PTC)

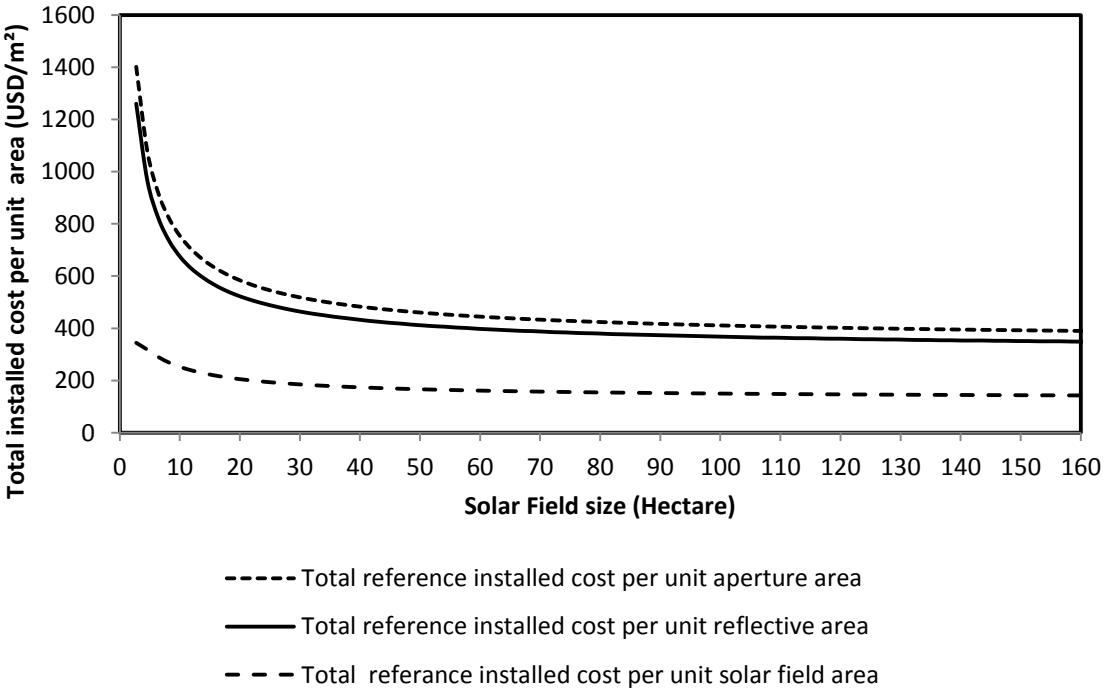

Figure 6.32: Variation of installation cost per unit area with solar field size (for PTC)

The key components to reduce the solar field material cost are the support structures including tracking system, and receivers. Figure 6.33 shows the percentage of the material cost of PTC. As shown, the structure and drives systems represent about 36 % of the collector field material cost, the receiver tubes and fittings represent about 28% of the collector field material cost, the reflector system represents about 23% of the collector field material cost, The other percentage (13%) is for headers, piping, and miscellaneous material and equipment cost.

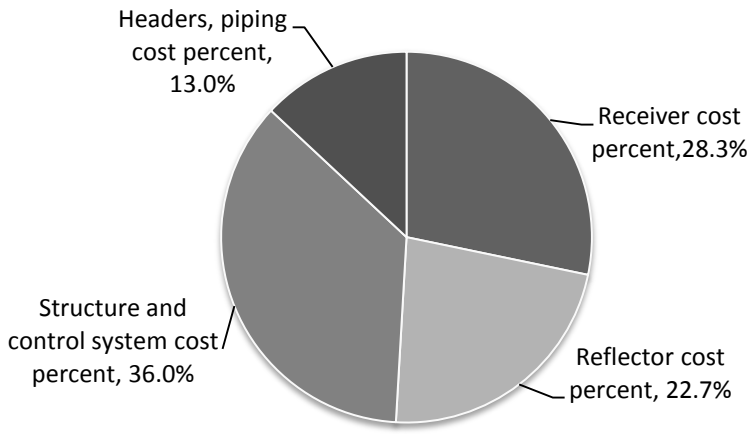

Figure 6.33: Cost breakdown for parabolic trough collector components

As shown in Figure 6.33, the structure and drives system represent 36 % of the collector field material cost. This factor was presented with the solar field size. Figure 6.34 shows that the specific structure and tracking system cost per unit aperture area with 2.8 hectares can be cut by almost 140 USD at 10 hectares while by almost 218 USD at 160 hectares.

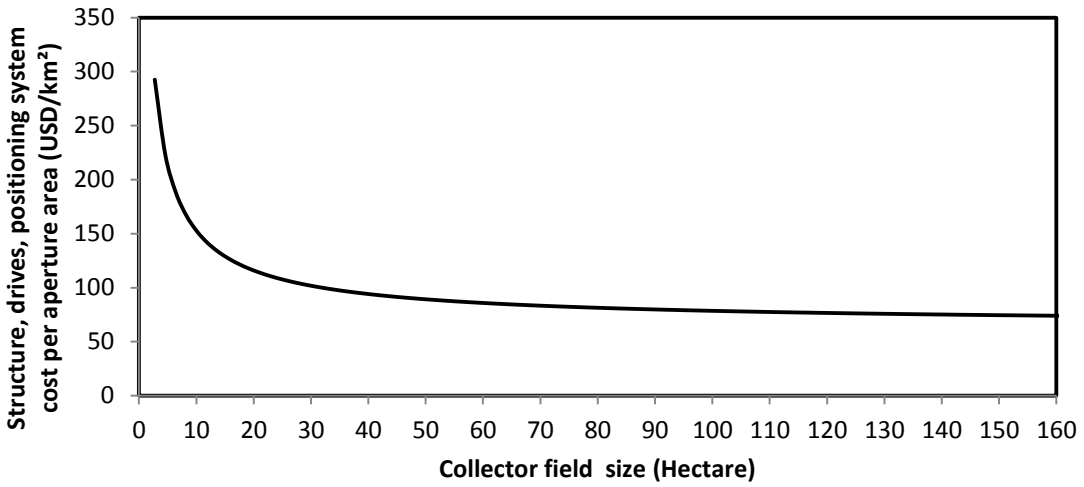

Figure 6.34: Variation of structure and drives system cost per unit aperture area with solar field size (for PTC)

The receivers (heat collection elements) are a major contributor to trough solar field performance. The heat collection elements constitute a major portion of the direct capital cost; the vacuum receiver cost about (200-300) € per m receiver length [74]. When the solar field size is increased of course the total receiver length will be increased. Figure 6.35 illustrates that increment.

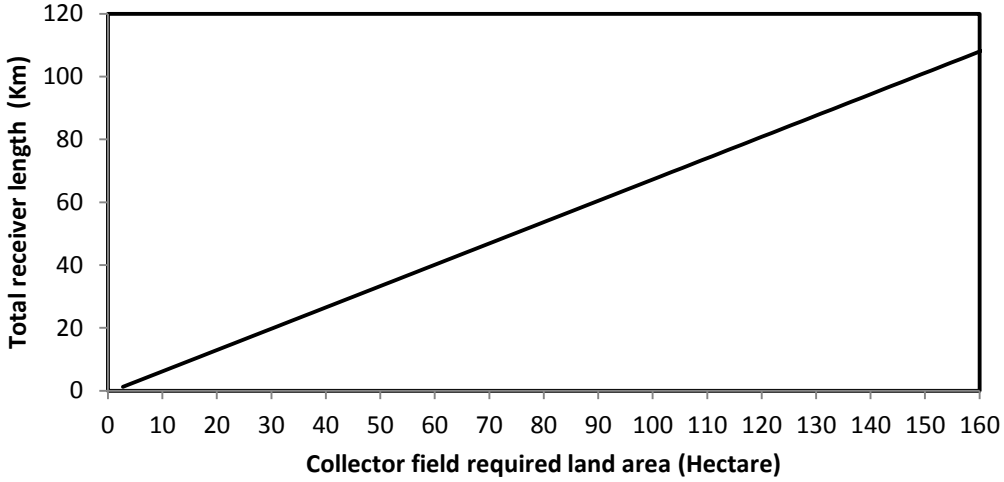

Figure 6.35: Variation of total receiver length with solar field size (for PTC).

Figure 5.36 shows how the receiver cost per unit length varies with solar field size. The unit length receiver cost is reduced by increase the solar field size. The receiver unit cost is almost halved by increase solar field size from 2.8 hectare to 10 hectare (-760 USD), then it continues sharply declined by increase the solar field size from 10 hectare to 60 hectare, After that the declination was almost gradual from 408 USD/km to 352 USD/km by increase the solar field size from 60 hectare to 160 hectare.

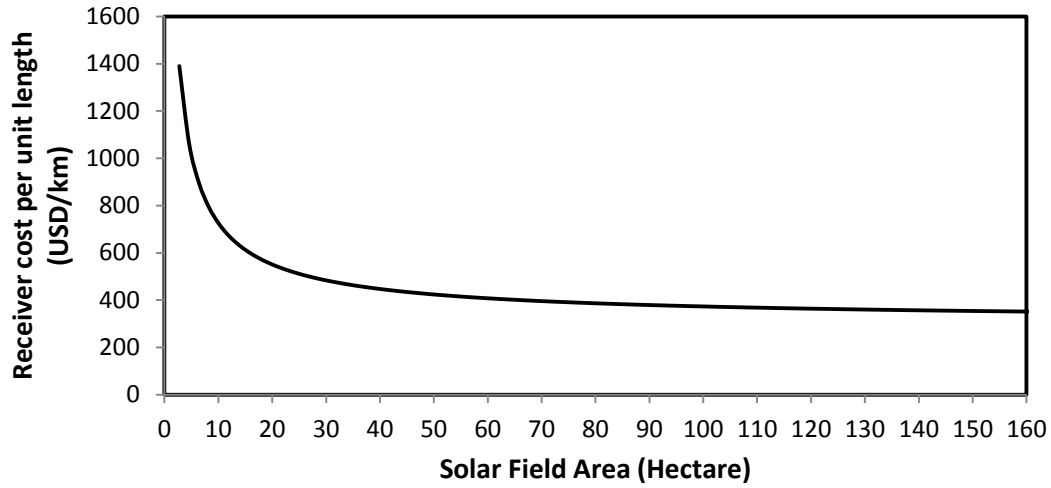

Figure 6.36: Variation of receiver cost per unit length with solar field size (for PTC)

The other important factor is the reflector cost per unit aperture area. Figure 6.37 presents the variation of the reflector cost per unit aperture area with solar field size. According to the Figure, the specific receiver cost with 2.8 hectare can be cut by almost 98 USD (48%) at 10 hectare and by almost 152 USD (75%) at 160 hectare referred to the cost at 2.8 hectare.

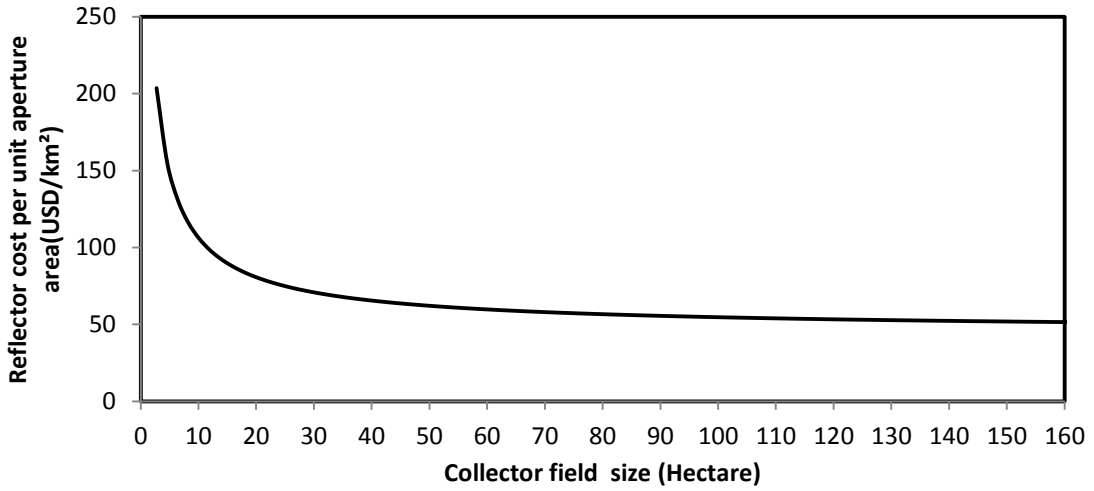

Figure 6.37: Variation of reflector cost per unit aperture area with solar field size (for PTC)

Figure 6.38 shows variation of the headers, piping, and miscellaneous material cost per unit receiver length. The Figure shows that the specific receiver cost with 2.8 hectare can be cut by around 450 USD at 60 hectare (70%), and by around 480 USD (75%) at 160 hectare referred to the cost at 2.8 hectare

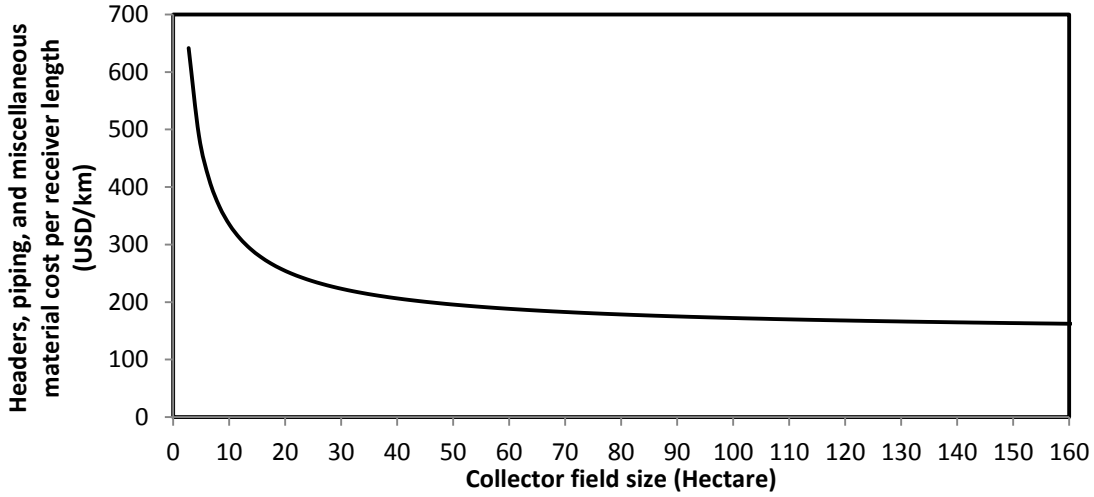

Figure 6.38: Variation of headers, piping, and miscellaneous material cost per unit receiver length with solar field size (for PTC)

The variation of mechanical labor cost per unit aperture area with increase solar field size is shown in Figure 6.39. The mechanical labor cost was almost halved by increasing solar field size from 2.8 hectare to 10 hectare (-213USD), then the unit cost continue to decline significantly by increase solar field size from 10 hectare to 60 hectare, After that the declination is almost gradual from 130.6 USD/km to 112 USD/km by increase solar field size from 60 hectare to 160 hectare.

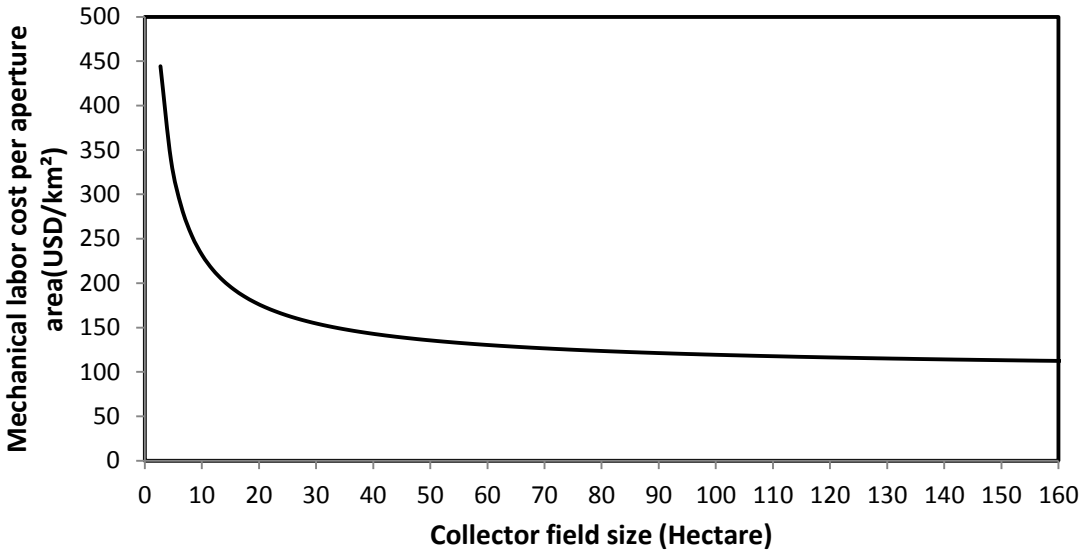

Figure 6.39: Variation of mechanical labor cost per unit aperture area with solar field size (for PTC)

The cost of civil works per unit aperture area with increasing solar field size is shown in Figure 6.40. The civil works include foundation work (material and equipment); excavation/backfill work (material and equipment); and civil labor. As shown, the costs of different civil works per unit aperture area are constants when the solar field size is increasing.

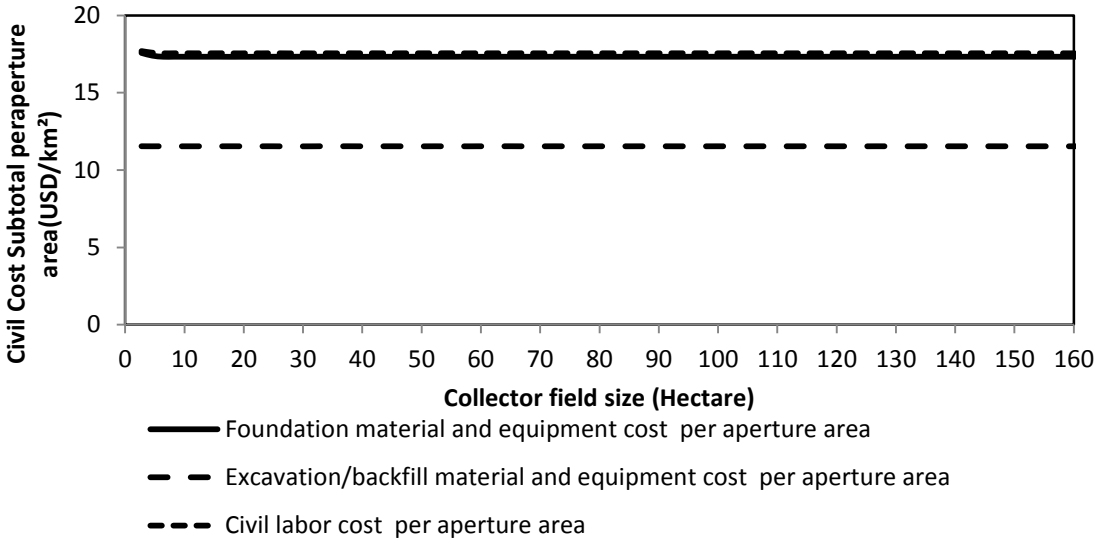

Figure 6.40: Variation of civil cost per unit aperture area with solar field size (for PTC)

Figure 6.42 presents the comparison between the results in present study and those results in Pilkington report [72] and kistner [73] in terms of PTC installation cost per unit reflective area. As shown, the cost per unit area of solar field collector in the current study is matching very well with the results from the others studies.

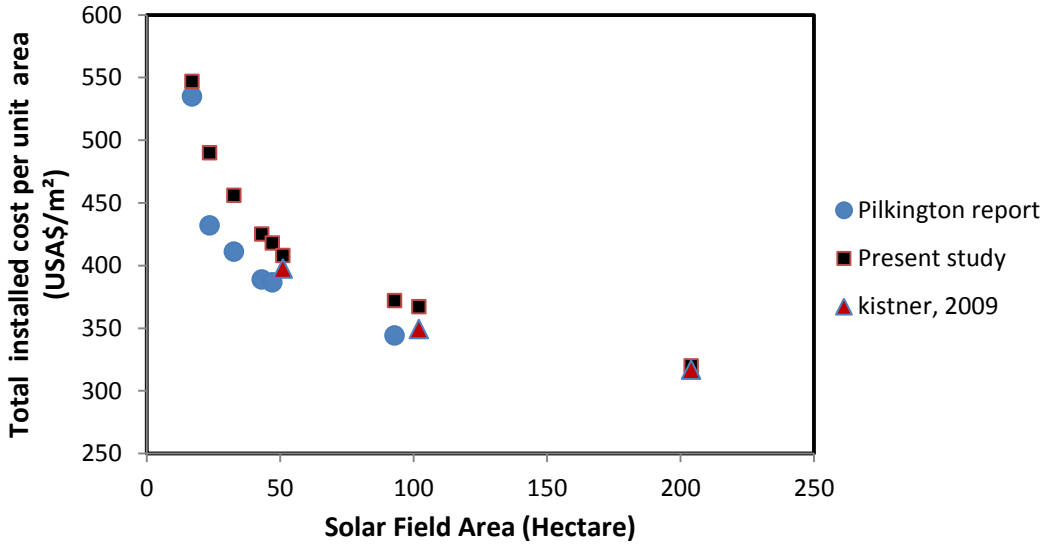

Figure 6.42: Comparison between the present study and literatures in terms of PTC installation cost per unit reflective area

6.4 Conclusions

This study came to the following conclusions:

- The specific cost for a PTC field per unit aperture area with 2.8 hectare can be cut by about 46 percent at 10 hectare and by about 72 percent at 160 hectare (compared with the cost at 2.8 hectare).

- The study shows that the relative contribution of the different cost shares to the economies of scale varies the same trend for the mechanical works and is constant for the civil works.

- The economy of scale can be realized in mechanical labor cost, structure and drives system cost, receiver cost, and reflector cost, the specific cost can be cut by about 75 percent in these areas.

- The specific cost of different mechanical works drops by about 48 percent at 10 hectare and by about 75 percent at 160 hectare, where the specific civil cost remains a constant. Hence, these cost items almost remain constant in absolute numbers, independent of the plant size.

- Since costs of solar field depend on the plant size, only small changes can be observed regarding the labor, and the collector material, as material cost is the dominant cost fraction in these areas.

- The PTC cost per unit area in the present study shows an excellent agreement with those results from the others studies.

CHAPTER 7

CONVENTIONAL GAS TURBINE COGENERATION POWER PLANT

As mentioned earlier, the cogeneration plant of Ras Tanura with 150 MWe and 81.44 kg/s steam has been the target of simulation and design modification in the this study. The schematic diagram of the conventional gas turbine cogeneration power plant can be shown the Figure 4.1. According to the Figure 4.1, the plant has one gas turbine, one duct burner, one superheater, an evaporator, one economizer, and a pump. The gas turbine was connected to heat recovery steam generation through a supplementary duct burner. The plant was used to generate steam with 394°C, 45.88 bars, and 81.44 kg/s for steam temperature, steam pressure, and steam flow rate respectively. The gas turbine was ranged between 30 MWe to150 MWe.

7.1 Simulation Procedures of a Conventional Gas Turbine Cogeneration Plant

As stated earlier, THERMOFLEX with PEACE software was used for the simulation. The schematic diagram of the conventional cogeneration plant as simulated in THERMOFLEX is shown in Figure 7.1. As can be seen in the Figure, the plant has one gas turbine: (4); one duct burner: (1); one superheater: (8); an evaporator: (12); one economizer: (9); and a pump: (11). In order to explain the plant's operating in the clearest

way it is essential to remember that this plant works with two different working fluids: air/gas and steam/water.

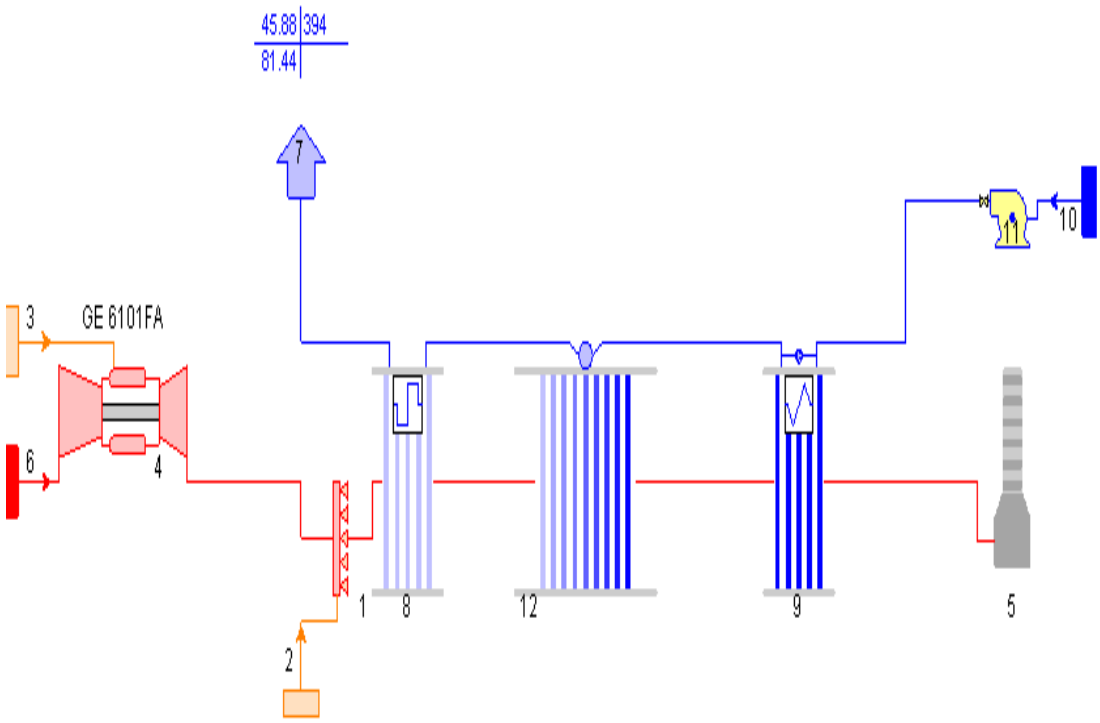

Figure 7.1: Schematic diagram of the conventional gas turbine cogeneration plant as simulated in THERMOFLEX.

Table 7.1: Components name of conventional gas turbine cogeneration plant.

Number	Component Name	Number	Component Name
1	Duct Burner	7	Process
2	Fuel Source	8	Superheater
3	Fuel Source	9	Economizer
4	Gas Turbine	10	Water/Steam Source
5	Stack	11	Pump
6	Gas/Air Source	12	Evaporator

As shown in the Figure 7.1, when exhaust gases entering the HRSG system it first passes through the superheater: (8), where it exchanges heat with the steam produced by the evaporator, rising the steam's temperature before it enters the proses. The exhaust gas then passes through the evaporator (12) where it again gives away part of its heat to liquefied water to transformat to steam. When passing through the last piece of HRSG: the economizer (9); the exhaust once again exchanges heat, giving it this time to liquid water to raise its temperature to the saturated temp at the entrance of the evaporator. This helps in the increasing the power given by the plant and raises the plant's efficiency. At this point the exhaust gases exits the plant and goes to the stack (5). The generated steam is taken to the industrial process (7).

Figure 7.2 shows the flowchart of the conventional power plant simulation. The specific steps to simulate the conventional power plant are listed below. Those steps were explained step by step in the Appendix

1. The first step of the simulation is to build the configuration by using THERMOFLEX program as explained step by step in the Appendix.
2. The second step is to edit the data of the operating conditions. This conditions includes the latitude (for Dhahran 26.5°), and altitude (for Dhahran 90 m) of the industrial plant location.
3. Then select and fix gas turbine size starting from 30 to 150 MWe. In this study, the products manufacturing by General Electric Company as listed in THERMOFLEX program have been used; an air source has been used to specify

the conditions of a flow of air into a gas turbine; and the ambient air method (specify conditions in site menu) has been used to satisfy an air source conditions.

4. After that enter and fixe the output steam conditions. These conditions are 394°C, 45.88 bars, and 81.44 kg/s for steam temperature, steam pressure, and steam flow rate respectively.
5. Make a control loops to operate duct burner to cover the thermal load of the plant when the exhaust gases for gas turbine couldn't cover that load.
6. Evaluate performance of plant at design hour based on figures of merit in section 4.2.2.
7. Make multi runs for one year. So, to start multiple runs for one year, one needs to operate the plant at solar times and non-solar times. The operation for solar time is 11 hours for seven months in the year which are March, April, May, June, July, August, and September. Whereas the operating based on 9 hours is used for the other five months. The operation for non-solar time is the remaining daily time from 24 hours. It is important to enter all operating conations for all months to the program. The operating conations are described in sections 5.2, 5.3, and 5.4.
8. Evaluate performance of plant for one year based on figures of merit in section 4.2.2.

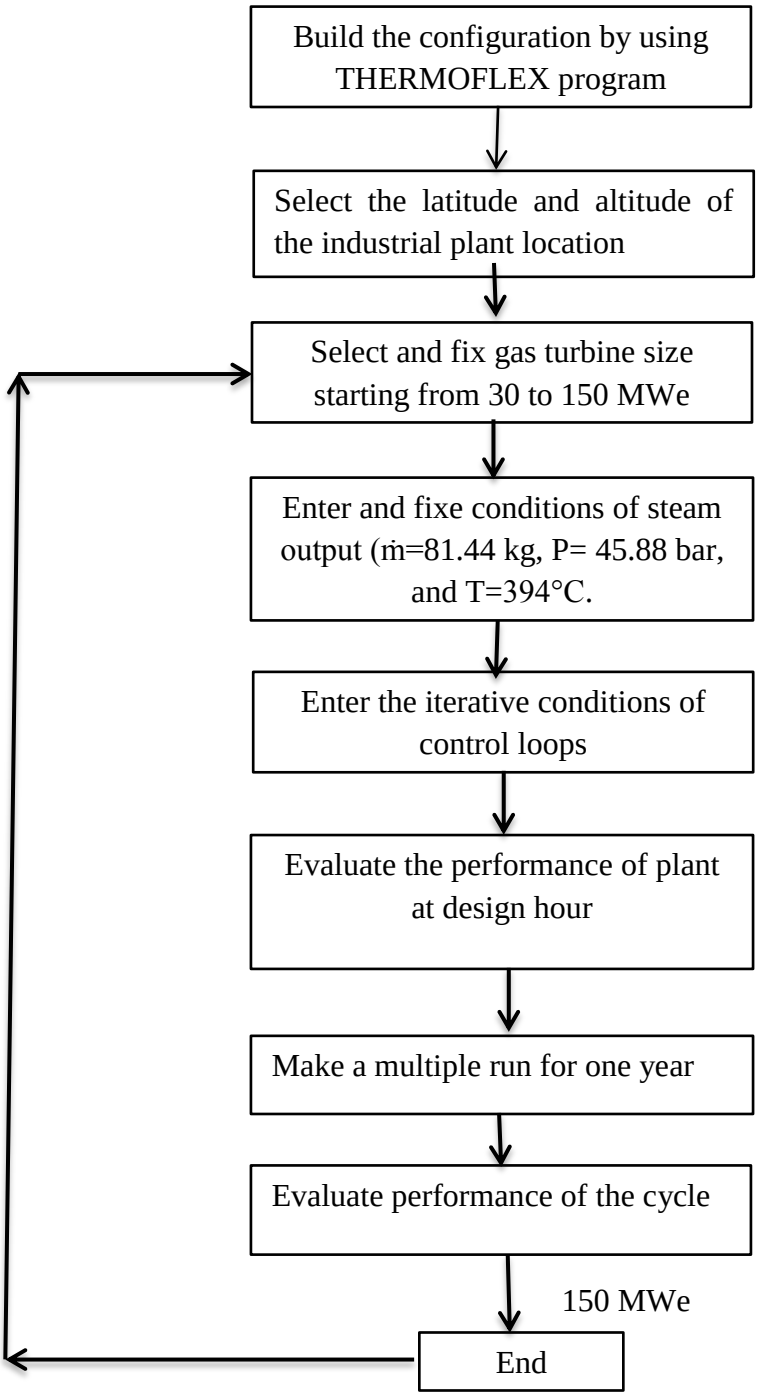

Figure 7.3: The specific steps to simulate a conventional gas turbine cogeneration power plant.

7.2 Simulation Results

As stated earlier, energy required to generate the steam is provided by a gas turbine exhaust gases and duct burner, the size of the gas turbine investigated in this study was varied between 30 to 150 MWe.

The result of this simulation was the amount of energy provided by the gas turbine exhaust gases and that is provided by (needed from) the duct burner. Figure 7.3 depicts the annual percentage of required energy from the duct burner with the gas turbine size so as to satisfy the thermal load of the plant. The result of this simulation was important to find out how much energy would be required from the duct burner so as to assist the gas turbine to satisfy the thermal load of the plant. This simulation was also useful to find out what size of the gas turbine would give enough room for solar energy to be integrated economically to the plant. This simulation was also used to estimate the carbon dioxide emission, and the levelized energy cost for each of the conventional gas turbine cogeneration plant that satisfies the constant load of the industrial process.

The result of the simulation shows that the large gas turbine of 150 MWe does not need much energy from the duct firing (about 24%). So, it has no much room for solar energy integration. However, the small gas turbine of 30 MWe has a large amount of energy supplied via the duct firing which leaves a large room for solar energy integration to the steam side in a plant. To answer the question of which gas turbine size would result in an economic integration of the solar energy to the gas turbine cogeneration conventional

plant, a simulation of the integrated solar gas turbine cogeneration was carried out in the second part of the study in following chapters.

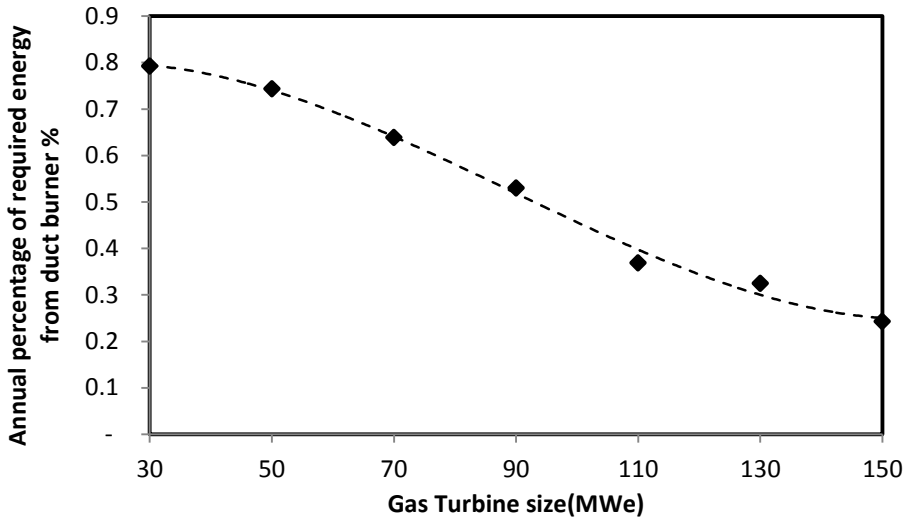

Figure 7.3: Annual percentage of the required energy from the duct firing

Figures of merit such as annual CO_2 emissions, and LEC have been calculated for each gas turbine size. Figure 7.4 shows the annual CO_2 emission in K tonne for different gas turbine size. The simulation result shows that the minimum CO_2 emission was for 30 MWe gas turbine size (almost 512 K tonne of CO_2), and this emission is increased with increasing gas turbine size, which leaves with almost 792 K tonne of CO_2 for 150 gas turbine size. The results of this simulation are very important to find out how much CO_2 would be avoided by integrating solar energy to conventional gas turbine cogeneration power plant.

The thermal load is a constant for all design plants which are considered in the proposed work, so one can fix the cost of steam and calculate the net cost of the electrical energy.

In present calculations a steam price was assumed higher than the respective fuel price by 20% [44, and 45]. Levelized electricity Cost (LEC) could be calculated as follows;

$$LEC = \frac{I_{tot} * fcr + OM_{ann} + F_{ann} - steam\ energy\ cost}{E_{el,ann}} \quad (7.1)$$

The LEC was evaluated for the conventional gas turbine cogeneration plant. Figure 7.5 shows the variation of the levelized electricity cost for conventional gas turbine cogeneration power plant with the gas turbine size. The LEC increases by increasing gas turbine size from 30 to 70 MWe. After that the LEC remains almost constant with increasing gas turbine size which leaves with 3.09 US¢/kWh for 150 MWe.

For a cogeneration plant producing electricity and heat, the first law total energy efficiency is defined as the ratio of delivered usable energy to the energy input [1]:

$$\eta_{cogen} = \frac{(W_{net} + Q_{heat})}{E_{inp}} \quad (7.2)$$

Where, W_{net} is the net electrical power output, Q_{heat} is the rate heat is supplied from the plant, and E_{inp} is the rate of energy input to the plant. The result of the simulation presented in Figure 7.6 shows the annual total efficiency for conventional gas turbine cogeneration power plant at different gas turbine size. As can be seen, the large gas turbine of 150 MWe has a small total efficiency (about 85.6 %). Whereas, the small gas turbine of 30 MWe has a large amount of total efficiency.

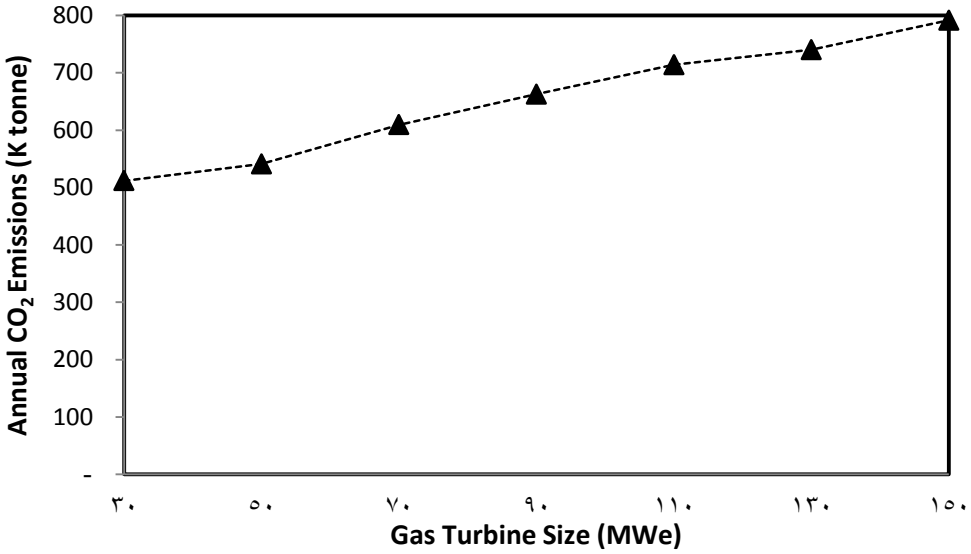

Figure 7.4: Annual CO_2 emissions from the conventional gas turbine cogeneration power plant for different gas turbine sizes

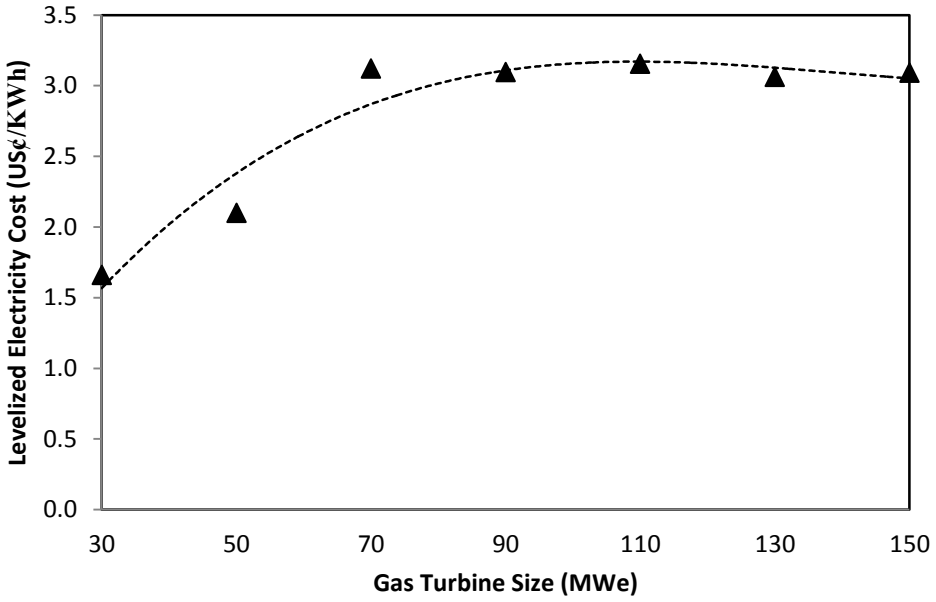

Figure 7.5: Levilized electricity cost for the conventional cogeneration plant for different gas turbine sizes.

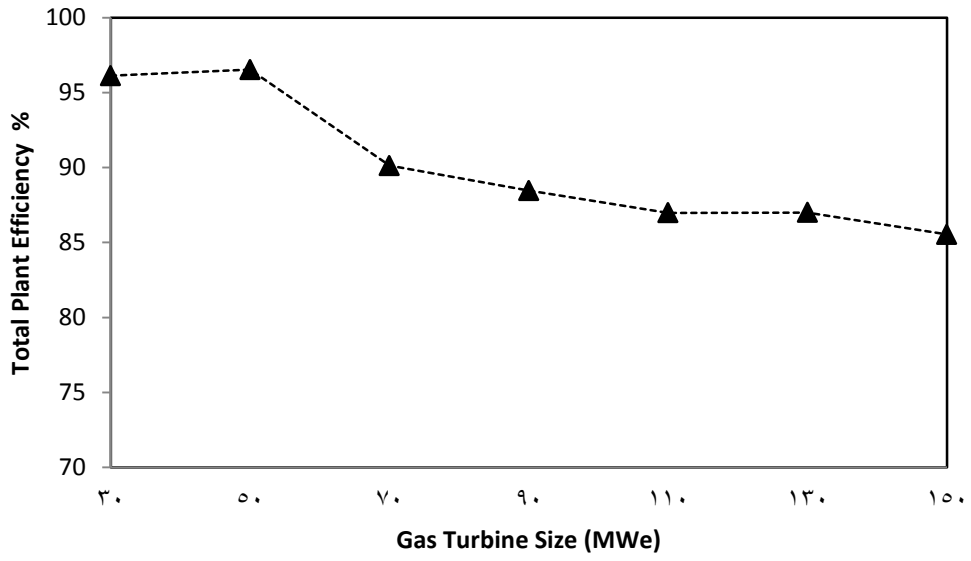

Figure 7.6: Annual total efficiency for conventional gas turbine cogeneration power plant for different gas turbine sizes.

7.3 Concluding Remarks

A conventional gas turbine cogeneration system that generates steam at a constant flow rate of 81.44 kg/s at P = 45.88 (bar) and temperature of T = 394°C around the year in addition to generation of electricity have been simulated and assessed for different sizes of the gas turbine. The energy required to generate the steam was provided by the gas turbine exhaust gases and burning fuel in duct burner. The size of the gas turbine investigated in this study was ranged between 30 to 150 MWe. The performance analysis was conducted for a site in Dhahran city at the eastern province of Saudi Arabia. Finding from case study point to the following conclusions:

- The amount of energy provided by the gas turbine exhaust and that is provided by the duct burner were determined.

- The result of the simulation was important to find out how much energy would be required from the solar field so as to assist the gas turbine to satisfy the industrial process requirements.

- The results of the simulation have proved that the large gas turbine of 150 MWe does not need much energy from the duct firing (about 24%). So, it has no much room for solar energy integration. However, the small gas turbine of 30 MWe has a large amount of energy supplied via the duct firing which leaves a large room for solar energy integration to the steam side in a plant.

- The results indicate that the large gas turbine of 150 MWe has less total efficiency (about 85.6 %). Whereas, the small gas turbine of 30 MWe has a large value of total efficiency (about 96.1 %).

- The results have proved that the integrated duct burner with gas turbine less than 70 MWe has more economical feasibility than integrated it with large gas turbine.

- The results show that the minimum CO_2 emission was for 30 MWe gas turbine size (almost 512 K tonne of CO_2), and this emission was increased with increasing gas turbine size, which left with almost 792 K tonne of CO_2 for 150 gas turbine size.

CHAPTER 8

PARABOLIC TROUGH COLLECTOR SYSTEM INTEGRATED WITH STEAM GENERATION SIDE IN A GAS TURBINE COGENERATION PLANT.

An integrated Parabolic Trough Collector (PTC) system with steam generation side in a gas turbine cogeneration plant, which considered in this work, was used to generate the same amount of steam at the same conditions mentioned in chapter 7. The same range of gas turbine sizes was also investigated here. Figure 8.1 shows a schematic diagram of PTC integrated with steam generation side in a gas turbine cogeneration plant.

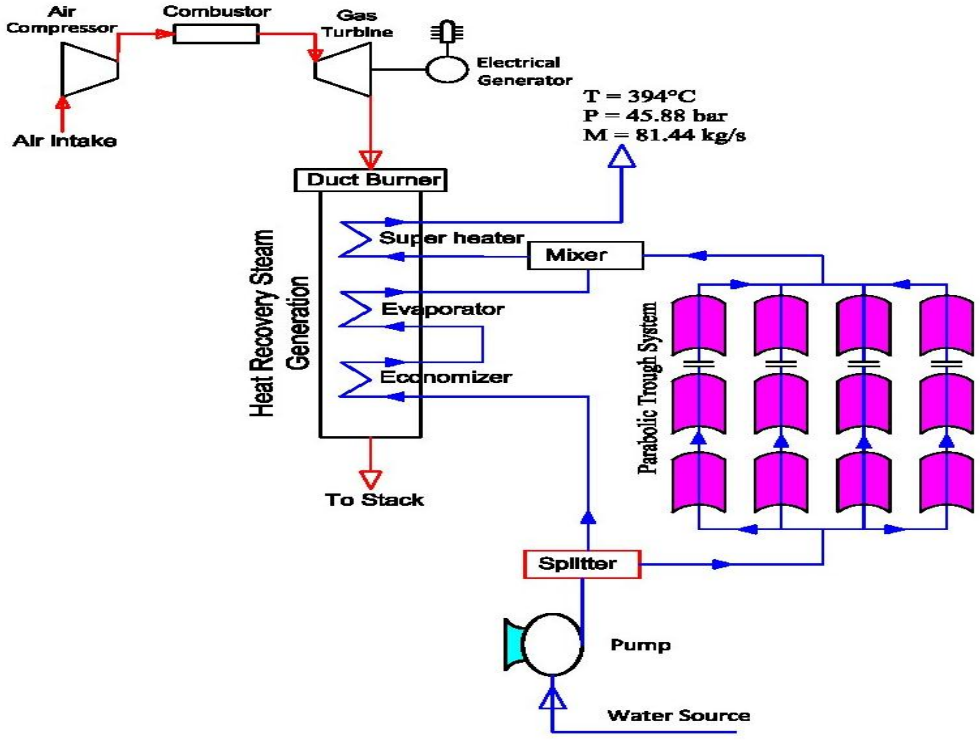

Figure 8.1: Schematic diagram of PTC integrated with steam generation side in a gas turbine cogeneration plant.

8.1 Simulation Procedures of a Gas Turbine Cogeneration Plant Integrated with PTC System

As stated earlier, THERMOFLEX with PEACE software was used for the simulation. The schematic diagram of the integration PTC system with steam generation side in a gas turbine cogeneration plant as simulated in THERMOFLEX is shown in Figure 8.2. As can be seen in the Figure, the plant has one gas turbine: (4); one duct burner: (1); one superheater: (8); an evaporator: (12); one economizer: (9); solar field (14); one splitter (13); one mixer (15): and a pump: (11).

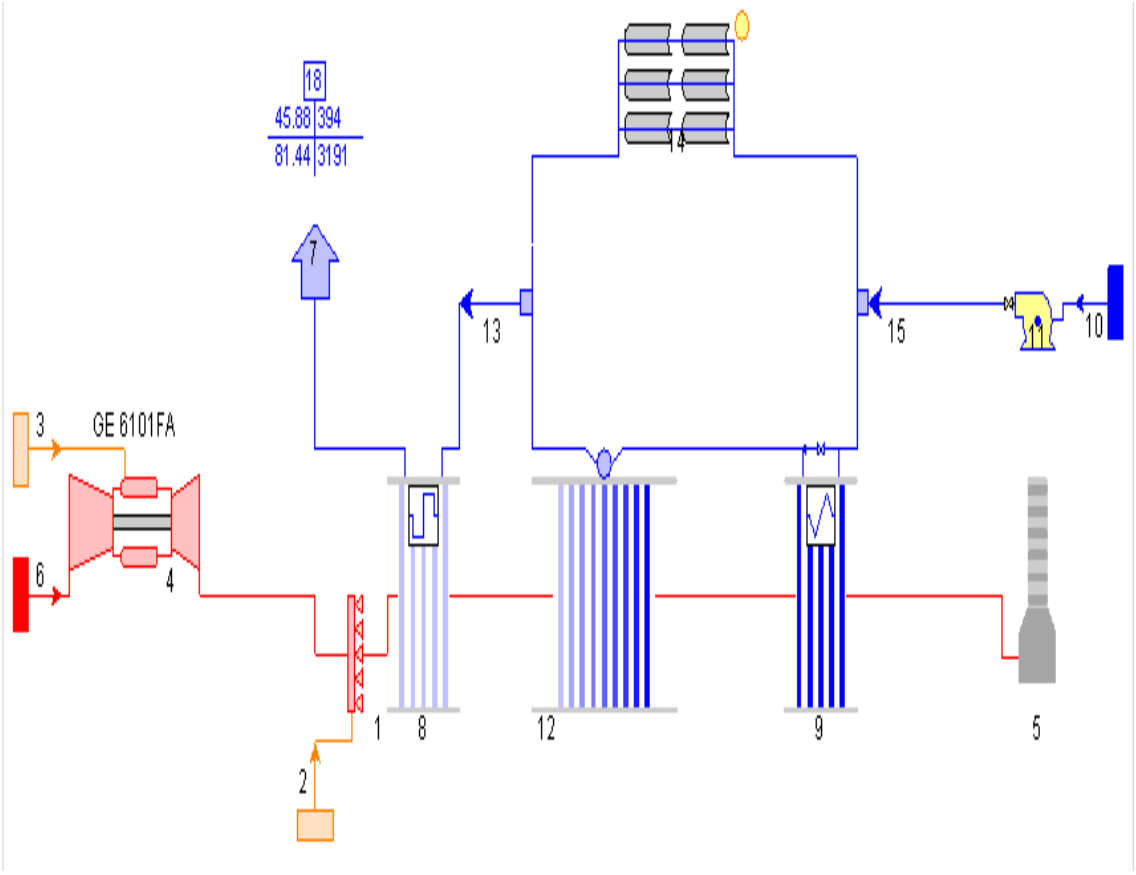

Figure 8.2: Schematic diagram of the gas turbine cogeneration plant integrated with PTC as simulated in THERMOFLEX.

Table 8.1: Components name of the gas turbine cogeneration plant integrated with PTC

Number	Component Name	Number	Component Name
1	Duct Burner	9	Economizer
2	Fuel Source	10	Water/Steam Source
3	Fuel Source	11	Pump
4	Gas Turbine	12	Evaporator
5	Stack	13	Splitter
6	Gas/Air Source	14	Solar Field
7	Process	15	Mixer
8	Superheater		

In this cycle, water transforms into steam due to the heat power received from exhaust gases and thermal energy from solar field. Pump (11) was used to raise water pressure to high enough for giving output steam pressure. Pressurized water after the pump spilt to two different paths (15); one of them passes through the solar collector field (14), and the other one passes through the economizer (9) then the evaporator (12). In this work, the solar collector field was connected to the power cycle parallel to the economizer and evaporator. The output steam from solar field and evaporate mixed again, and then passes through superheater. The generated steam is taken to industrial process (7).

The specific steps to simulate gas turbine solar cogeneration plant integrated with PTC system are listed in Figure 8.3. As shown in this Figure, the first step of the simulation is building the configuration by using THERMOFLEX program as shown in Figure. 8.2.

For study integrated PTC with gas turbine cogeneration plant by using THERMOFLEX program; the data of Euro-Trough solar collector (ET-100) were considered (Table 6.2);

the weather data of Dhahran, Saudi Arabia was also considered. The solar collector was rotated about horizontal north-south axis with continues adjustment to minimize the angle of incidence. The latitude (for Dhahran 26.5°), and altitude (for Dhahran 90 m) of the industrial plant location was selected from the program.

In this chapter, all the operating conditions of the conventional power plant in chapter 7 have been used. For examples; the plant was considered to generate steam with a constant flow rate of 81.44 kg/s at P = 45.88 (bar) and temperature of T = 394°C throughout a year in addition to generate an electricity; the products manufacturing by General Electric Company as listed in THERMOFLEX program have been used except the 90 MWe gas turbine size was selected from ASTM; the gas turbine was ranged between 30 MWe to 150 MWe. In this cycle, for water source component, all the default values in the THERMOFLEX were used, which are 25 °C and 1.014 bars for water temperature and pressure respectively were selected. For the fuel component, all the default values were also used, which are 25 °C and 20.68 bar for fuel temperature and pressure respectively.

As stated above, the output thermal power from the plant was considered as a constant throughout the year, and as known, the thermal power from solar field varies according to the solar radiation intensity. As a result, the outlet mass flow rate of the steam from solar filed was also changing, but duct burner was operated to substitute the rest of the required output thermal energy from the system. At any time solar field will not be able to cover specific load, duct burner was operated by using control loops.

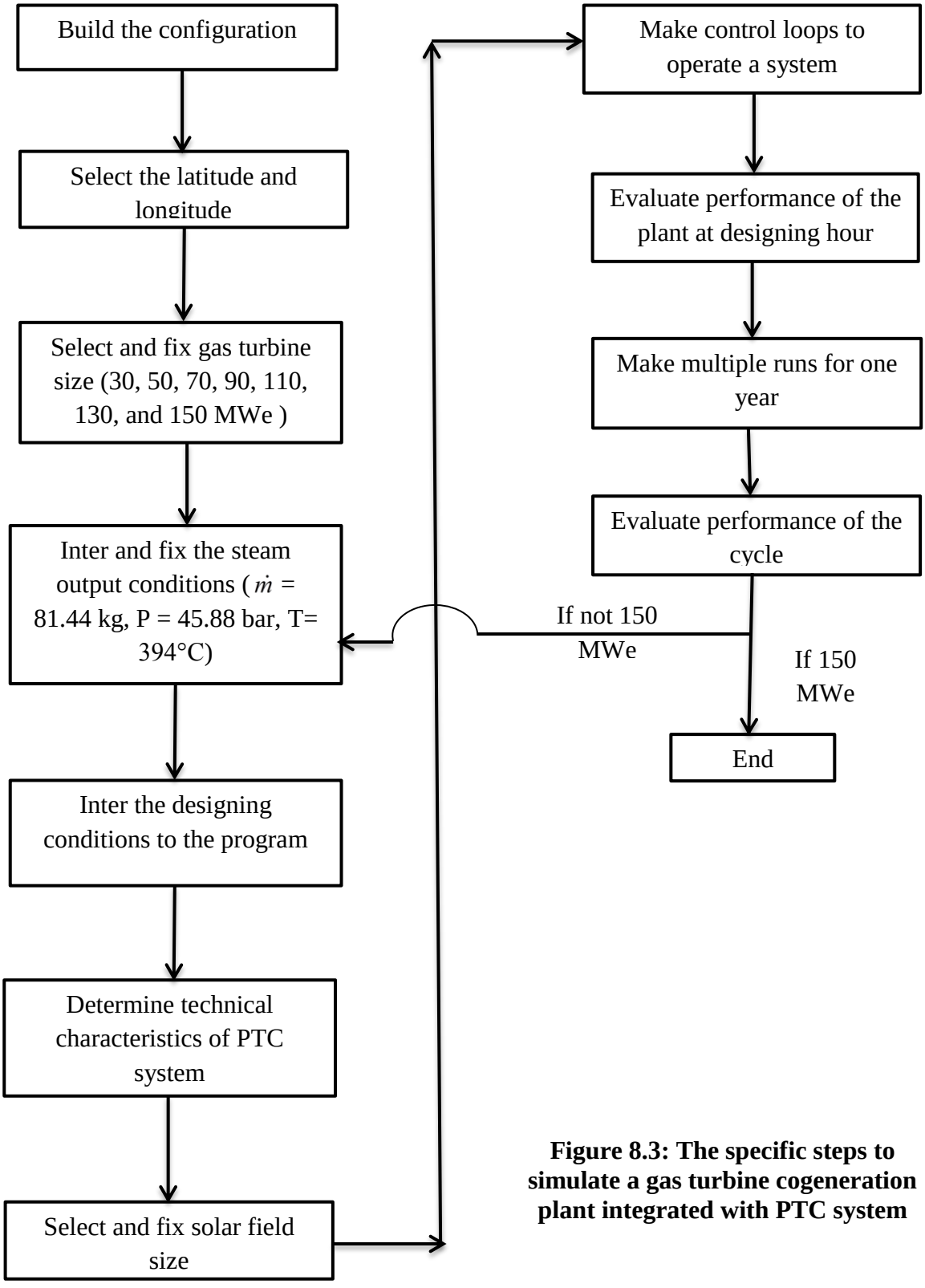

Figure 8.3: The specific steps to simulate a gas turbine cogeneration plant integrated with PTC system

In order to make a proper comparison between different designs, one should fix all the design and operates conditions of the system. The important parameters for the design conditions are average direct solar radiation, average ambient temperature, and average relative humidity (section 5.4). In this study, the maximum average direct solar radiation was used to calculate solar multiple at the design condition, which occurs at 11 June according to Table 5.16. The averages of ambient temperature and relative humidity for the same day were used as the design conditions.

In this cycle, to carry out multiple runes for one year simulation, one needs to enter the operating conditions to the program for solar time and non-solar time (sections 5, 2, 5.3, and 5.4). The operating solar time based on 11 hours has been used for seven months in the year which are March, April, May, June, July, August, and September. Whereas the operating based on 9 hours has been used for the other five months. The operation of non-solar time was the remaining daily time from 24 hours. In this configuration the operation at non-solar times was the same as the operation of reference cycle at non-solar time. It is important to enter the all operation conations for all months to the program

After that, one needs to evaluate performance of plant for each gas turbine size based on figures of merit in section 4.2.2 such as CO_2 emission, levelized energy cost, and solar levelized energy cost.

The purpose of changing gas turbine size was to find out how much energy would be required from solar field and duct burner so as to satisfy the thermal load of the plant, and the purpose of changing solar multiple was to achieve the best solar share for gas turbine size based on figures of merit. The results of this simulation were the basis to find out what would be the optimal solar multiple for each gas turbine size, and what would be the optimal gas turbine size that can be integrated with PTC solar technology to satisfy the same thermal load of the plant.

8.2 Simulation Results

Solar field size was estimated at maximum average direct solar radiation at Dhahran city, which occurs at 11 June according to Table 5.16. Also the averages ambient temperature and relative humidity for the same day were used for the design conditions.

The solar multiple represents the ratio of thermal power produced by solar field to the thermal power input to industrial process at design hour. The thermal load of industrial process is 259860 kW, where the thermal power at design hour can be obtained from PTC's field by using THERMOFLEX. The performance of the integrated solar gas turbine cogeneration cycle with different solar multiple higher and lower than that calculated at the design conditions have been assessed.

Thermal power required from solar field at design hour is a function of mass flow rate and outlet temperature from solar field (at design mode). Since the mass flow rate and outlet temperature from solar field are a function of solar field size, so increasing or decreasing solar multiple could be carried out by increasing or decreasing solar field size. In other words, design of different solar field sizes has been done at the same design hour but with different mass flow rates and different outlet temperature from solar field. The maximum outlet temperature from solar field could be reached is 394ºC. As shown in Figure 8.4, solar field size has increasing behavior with increasing solar multiple. This increasing of solar multiple save more amount of fuel as well as prevent more amount of CO_2 emissions.

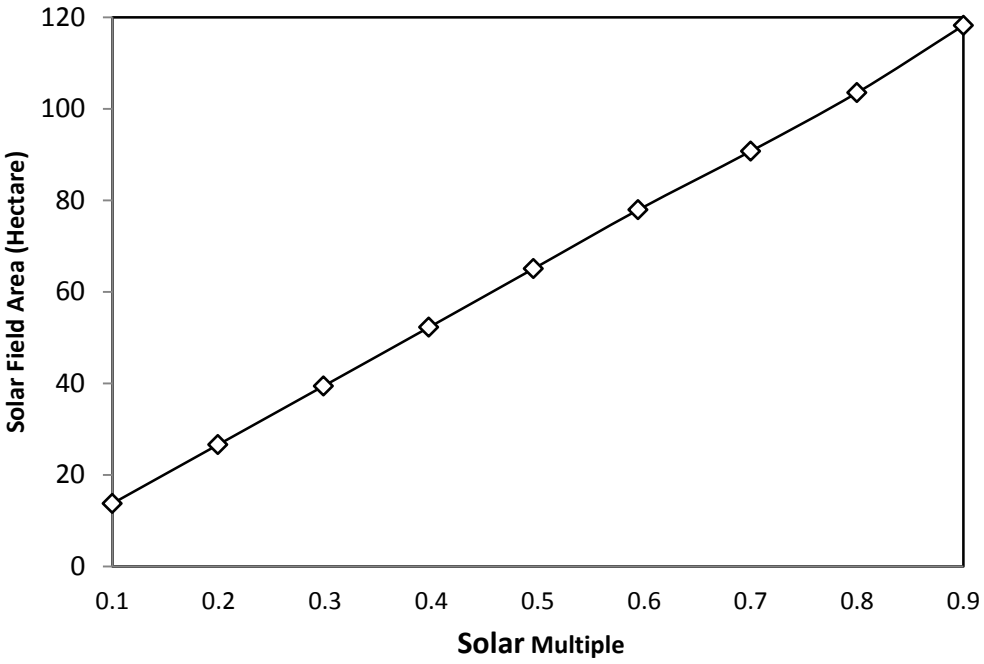

Figure 8.4: PTC field Area versus solar multiples.

As stated earlier, the exhaust gases from gas turbine recovered through Heat Recovery Steam Generation (HRSG) system to produce steam. In this study, thermal load of power plant is the output of three energy sources, which are energy content in hot exhaust gases from the gas turbine; burning fuel in duct burner; and solar energy.

It is important to note that increasing or decreasing gas turbine size leads to increasing or decreasing energy obtained from HRSG. The energy content in the exhaust gases must be recovered at any deigned mode. So it is impossible to reach a value of solar multiple that equal one, according to the definition of the solar multiple adapted for integrating solar to the steam generation.

Also it is worth noting that at any time solar field has more than enough energy, which is needed to cover specified load. One of the following scenarios might take place:

1. Extra thermal power is generated.
2. Solar field collectors are operated partially which means some loops are out of service.
3. Gas turbine is operated partially.

Since the first and third scenarios are impossible occurs because the thermal load and gas turbine were fixed, the second scenario is the one which occurs. Solar thermal power obtained from solar field at different solar multiple for different gas turbine size has been calculated using THERMOFLEX. Figure 8.5 depicts thermal power obtained from solar field which integrated with different gas turbine size at different solar multiples.

As can be seen in Figure 8.5, thermal power obtained from solar field increases significantly with the solar multiple up to specific value beyond which the solar thermal power needed by the load remains constant. The maximum specific thermal power required from solar field occurs when fuel consumption by duct burner is much closed to zero during solar time. That means there is no more room for solar energy integration to the plant after that point, this is because the energy content in the exhaust gases from gas turbine must be recovered. According to Figure 8.5, the large gas turbine of 150 MWe does not need much energy from the solar integration at design hour (about 63.8 MW). However, the small gas turbine of 30 MWe has a large amount of thermal power obtained from solar field (about 209MW).

.

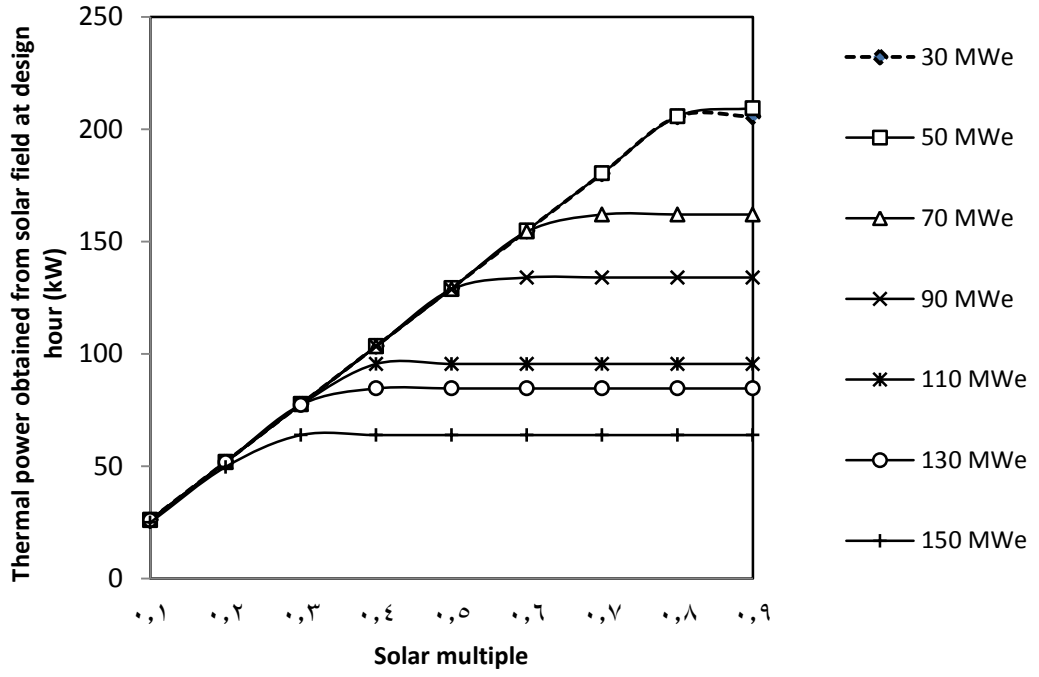

Figure 8.5: Thermal power obtained from solar field of PTC versus solar multiple.

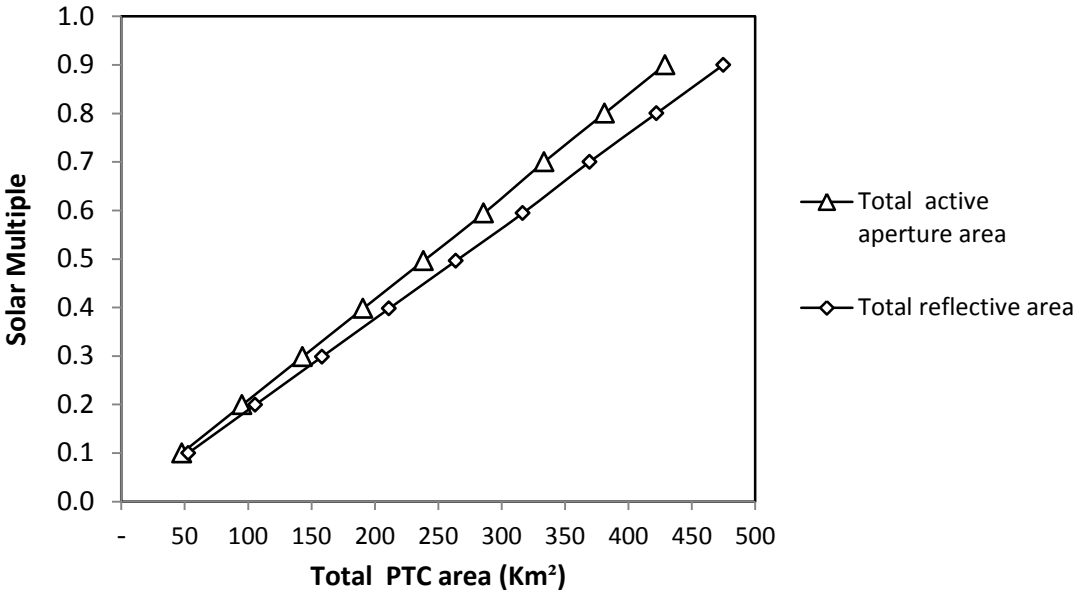

Figure 8.6: Reflective and aperture areas of PTC system versus solar multiple.

Figure 8.6 presents total aperture and reflective area of PTC for different solar multiple. The results shown; the PTC's reflective area is greater than PTC's aperture area, and the difference between them is increased by increasing solar multiple. These results are important for comparing integrations of different solar technologies. Figure 8.7 shows the maximum possible solar multiple with gas turbine size. One can note that the optimal solar multiple is much closed to this point as can be seen later on.

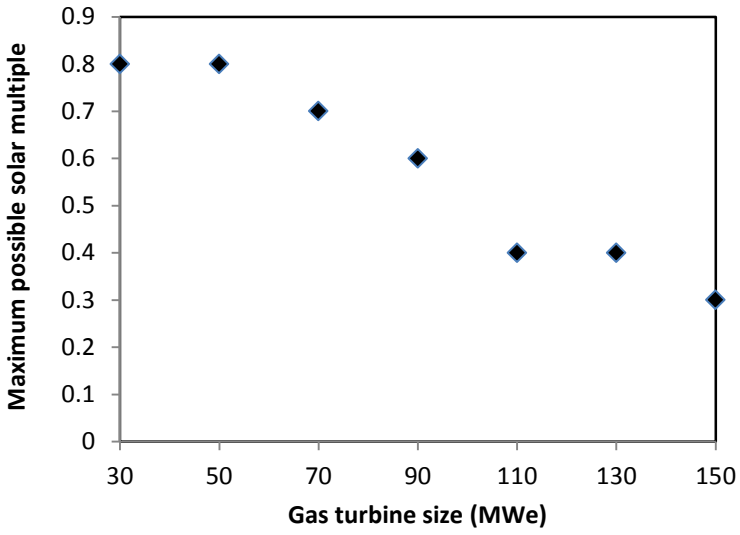

Figure 8.7: Maximum possible solar multiple with gas turbine size.

Figures of merit such as instantaneous solar share, annual solar share, annual CO_2 avoidance, LEC, and SLEC have been calculated for each gas turbine size at different solar multiple in order to assess the performance of integrated PTC to steam generation side for gas turbine cogeneration system.

First of all, instantaneous solar share is the ratio of the power generated from the solar field to the total power generated from both of the solar and fuel energy input to the plant at the design hour Eq. (4.12). Figure 8.8 presents instantaneous solar share for integrating different solar multiples of PTC system with different gas turbine sizes. As shown in the Figure 8.8, the instantaneous solar share is increased significantly with increasing solar multiple up to specific solar multiple for each gas turbine size. Beyond that specific point, instantaneous solar fraction remains a constant. The reason behind this behavior, is the over sizing of solar field area for solar multiple beyond this shown in Figure 8.8.

To calculate how much percent of the energy produced annually from the integrated solar gas turbine cogeneration power plant is due to the solar energy utilization, one needs to calculate the annual solar share. Figure 8.9 shows the variation of this parameter with solar multiple for different gas turbine sizes. According to the Figure the Figure 8.9, the large gas turbine of 150 MWe does not need much energy from the solar integration (about 5.16 % at the maximum solar multiple). However, the small gas turbine of 30 MWe has a large amount of annual solar share (about 24.65% at the maximum solar multiple).

Economic analysis has been carried out in terms of levelized electricity cost (LEC) and solar levelized electricity cost (SLEC). The LEC and SLEC are very important thermo-economical figures of merits that are used to estimate the cost of energy production from a given power plant design. Figure 8.10 depicts the variation of the LEC for different gas turbine sizes integrated with different solar multiples, whereas Figure 8.11 shows the

variation of the SLEC for different gas turbine sizes. As can be seen in Figure 8.11, the optimal SLEC is for integrate 0.5 solar multiple with 90 MWe.

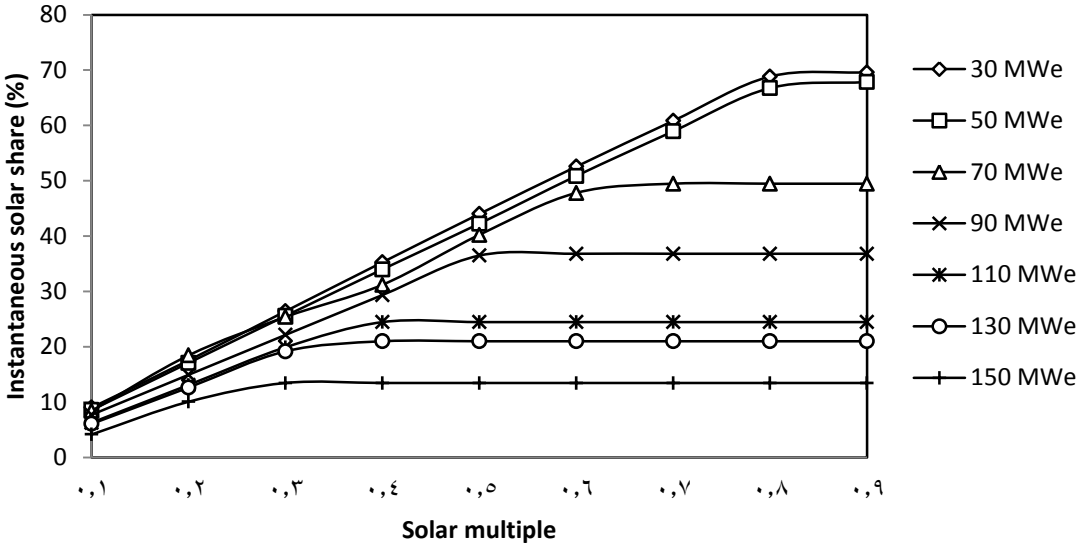

Figure 8.8: Instantaneous solar share for integrating different field sizes of a PTC with different gas turbine sizes.

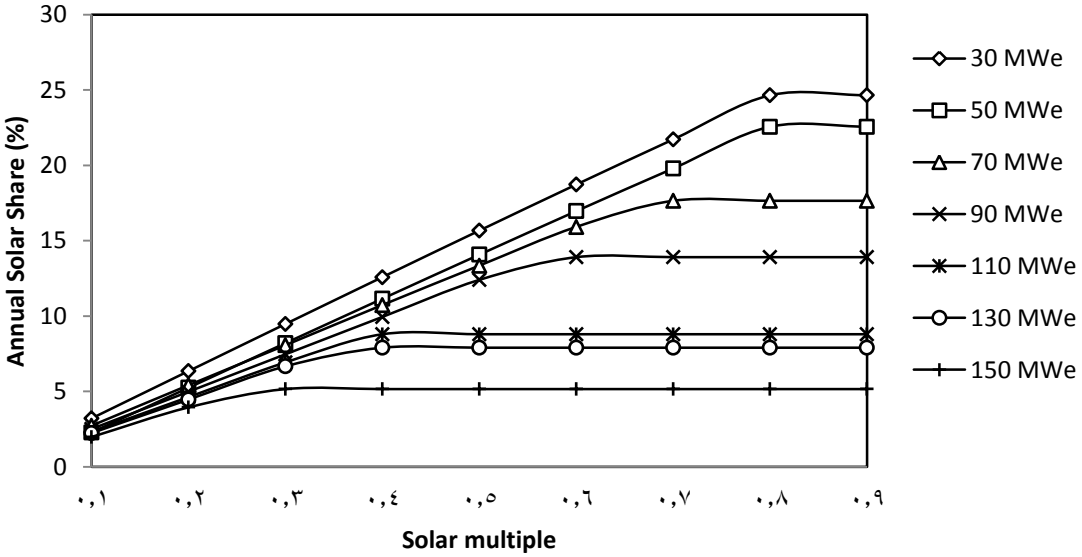

Figure 8.9: Annual solar share for integrating different field sizes of a PTC with different gas turbine sizes.

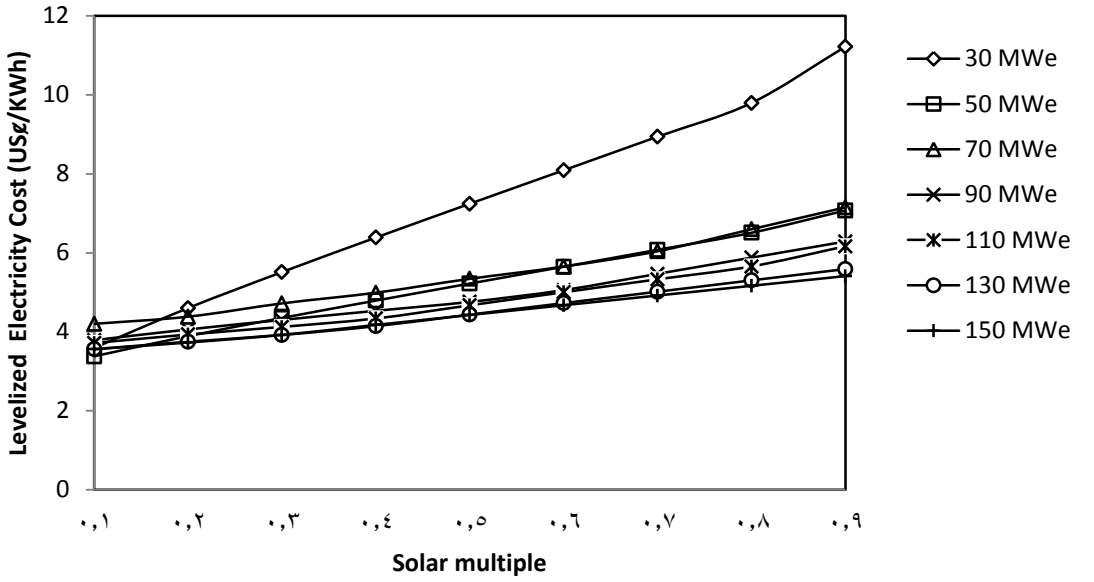

Figure 8.10: Levilized electricity cost for integrating different field sizes of a PTC with different gas turbine sizes.

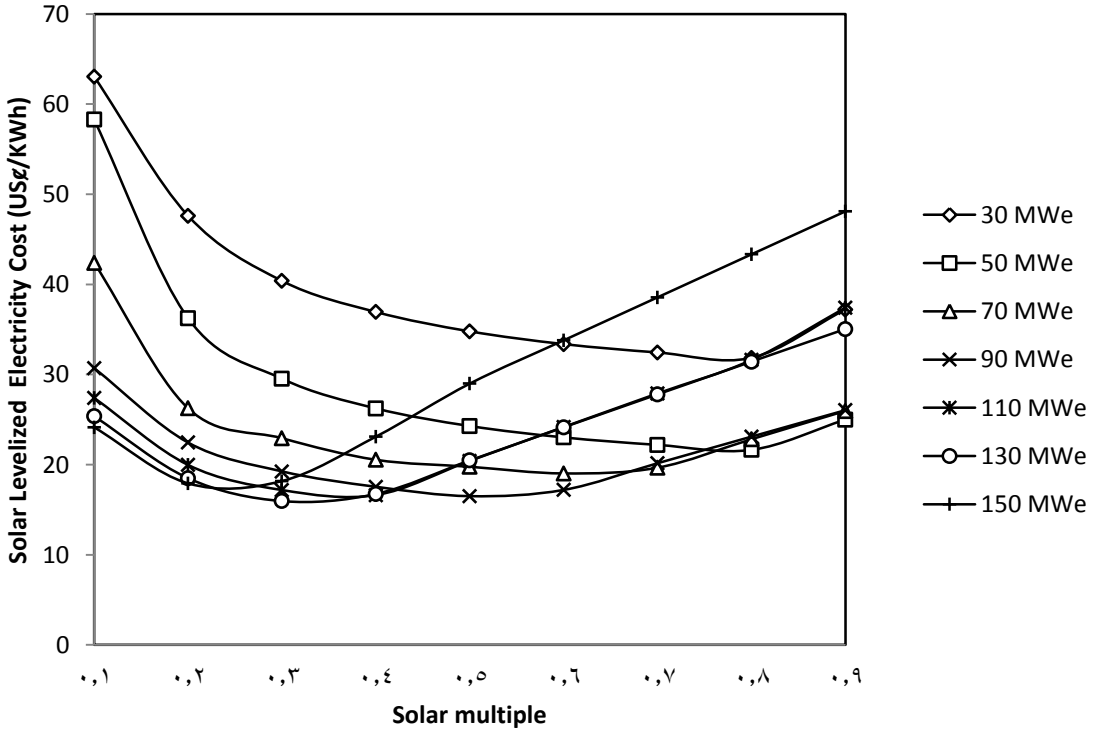

Figure 8.11: Solar levilized electricity cost for integrating different field sizes of a PTC with different gas turbine sizes.

The simulation results presented in in Figure 8.9 show that; there are minor increases in levelized energy cost with increase solar multiple, this incrementally incases is not the same for gas turbine sizes especially for 30 MWe. There is a negligible difference between LEC for integrating PTC with different gas turbine size. This is because there is an incremental in total investment cost by increasing solar multiple in one hand, but there is a reduction in annual fuel cost by increasing solar multiple in the other hand. This makes a balance between annual cast for different gas turbine sizes. LEC could not reveal optimal solar share. However, SLEC has minimal point, which is corresponding to the optimal solar multiple for each gas turbine size.

As shown in Fig. 8.11, Solar Levelized Electricity Cost (SLEC) decreased substantially when solar multiple increased up to optimal solar multiple for each gas turbine size. Beyond that value, SLEC increased sharply. The reason behind that behavior, there is over sizing of solar collector field which is not usable after that solar multiple.

The simulation results have shown that, the optimal solar multiple for different gas turbine sizes, which gives the minimum values of SLEC. The optimal solar multiples are different for gas turbine sizes, which can be found from Figure 8.11. The optimal solar multiples are 0.8, 0.8, 0.6, 0.5, 0.4, 0.3, and 0.3 for gas turbine size 30, 50, 70, 90, 110, 130, and 150 MWe respectively.

Integrating solar collector with gas turbine cogeneration has an environmental effect. Increasing of solar share results in reduction of total fuel consumption, which is required

for conventional cogeneration cycle to cover specific load, consequently, annual CO_2 emissions are reduced as shown in Fig. 8.12. Annual CO_2 emission for a reference gas turbine was presented at zero solar multiple in Figure 8.12.

The annual CO_2 avoidance could be defined as the annual reduction of CO_2 emission due to solar energy utilization. As can be seen in Figure 8.13, the annual CO_2 avoidance increased significantly by increasing solar multiple until reach specific point for each gas turbine size. After that specified point the annual CO_2 avoidance remained a constant. The best CO_2 avoidance was for integrating PTC with 30 MWe gas turbine size, where the reduction is greater than 140 k tonne of CO_2 from reference cycle (at 0 solar multiple).

The optimal solar multiples for integrated PTC with different gas turbine size have been determined, as 0.8, 0.8, 0.6, 0.5, 0.4, 0.3, and 0.3 for gas turbine size 30, 50, 70, 90, 110, 130, and 150 MWe respectively. One can select the optimal gas turbine size that can be integrated with solar collector by comparing all parameters corresponding to the optimal solar multiple for each gas turbine size

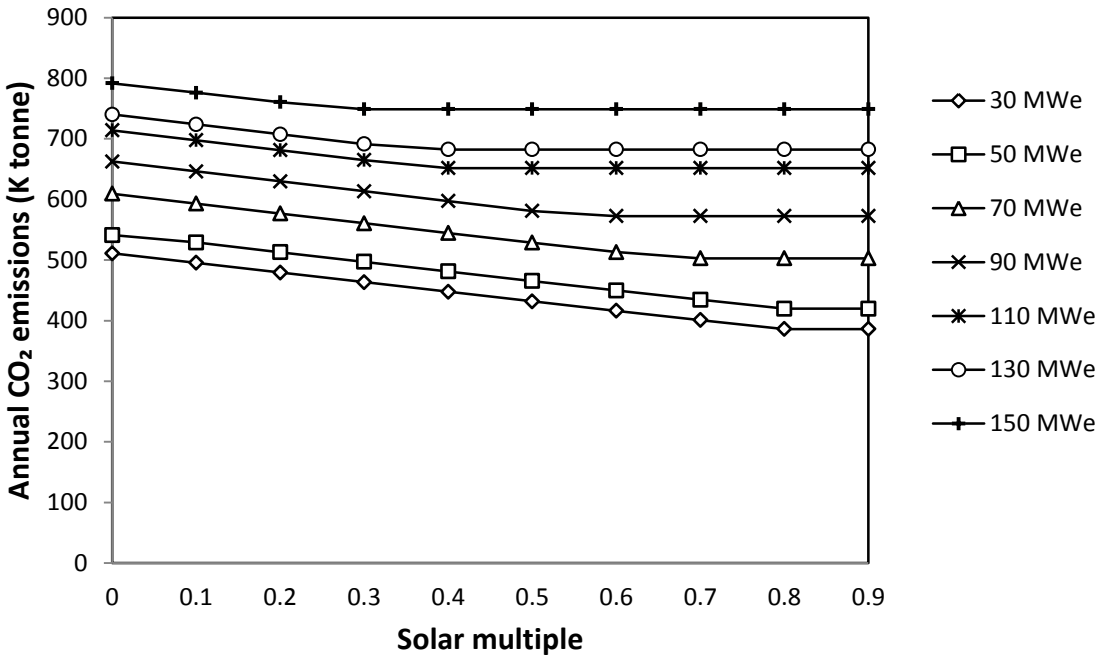

Figure 8.12: Annual CO_2 emissions from different gas turbine plants integrated with different solar field sizes of PTC.

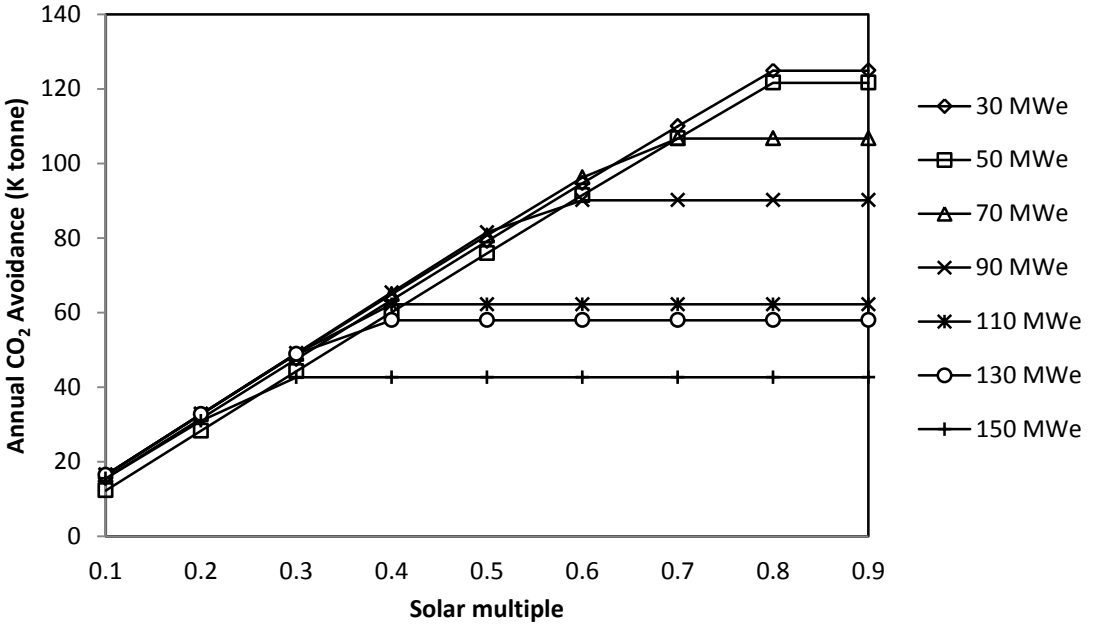

Figure 8.13: Annual CO_2 avoidance for integrating different field sizes of a PTC with different gas turbine sizes.

The optimal sizes of PTC field integrated with gas turbine cogeneration power plant have been determined for each gas turbine size at the minimum values of SLEC. Figure 8.14 shows that the optimal sizes of PTC field have decreased by increasing gas turbine size. As can be seen in Figure 8.14, the optimal solar field size integrated with 30 and 50 MWe gas turbine size are equal. This is because the optimal solar multiple for both gas turbine size are equal. The optimal size of solar field declined substantially while gas turbine size increasing from 50 MWe to130 MWe, but that declination was cut off at gas turbine size more than 130 MWe.

The instantaneous solar share achieved by integrating optimal solar multiple for different gas turbine size has been identified. Figure 8.15 shows that the instantaneous solar share decreases by increasing gas turbine size. Even though, the optimal solar multiple is equal for 30 MWe and 50 MWe gas turbine size, there is a decline in instantaneous solar share. This is because there is a difference in electrical power output from the two sizes.

The annual solar share achieved by integrating optimal solar multiple with different gas turbine size is presented in Figure 8.16. As expected, the annual solar share is higher when the PTC integrates with small gas turbine size. For example, the annual solar shares are 24.65% and 5.16% for integrating optimal solar multiple with 30 MWe and 150 MWe gas turbine size respectively.

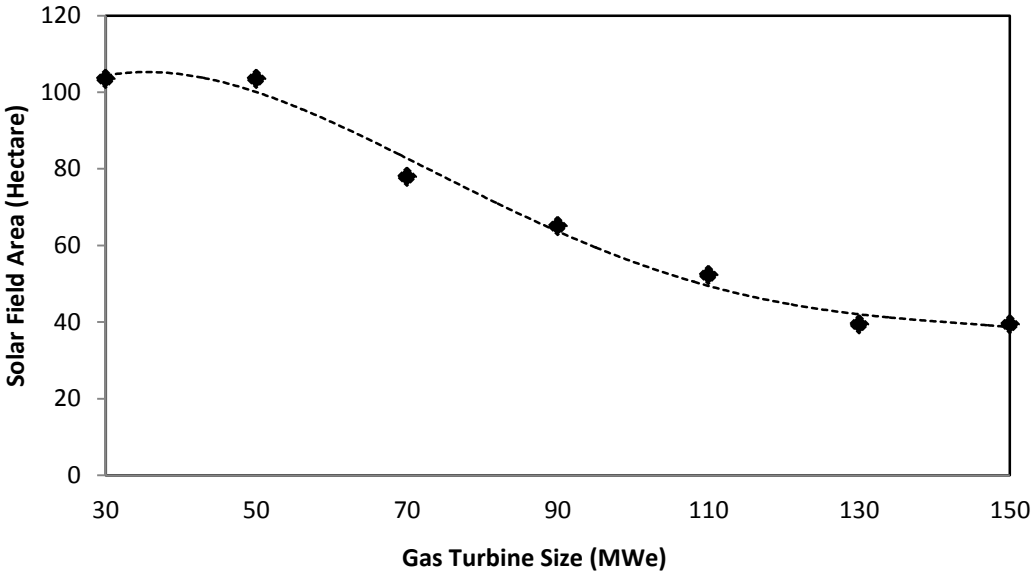

Figure 8.14: Solar field area of PTC system at the optimal solar integration for different gas turbine sizes.

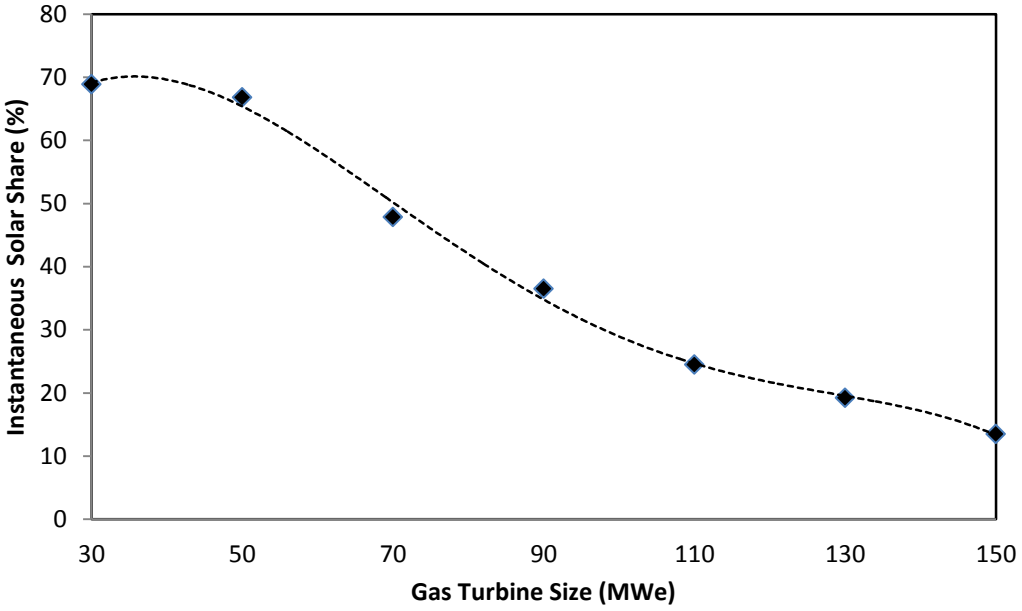

Figure 8.15: Instantaneous solar share at the optimal solar integration of PTC for different gas turbine sizes.

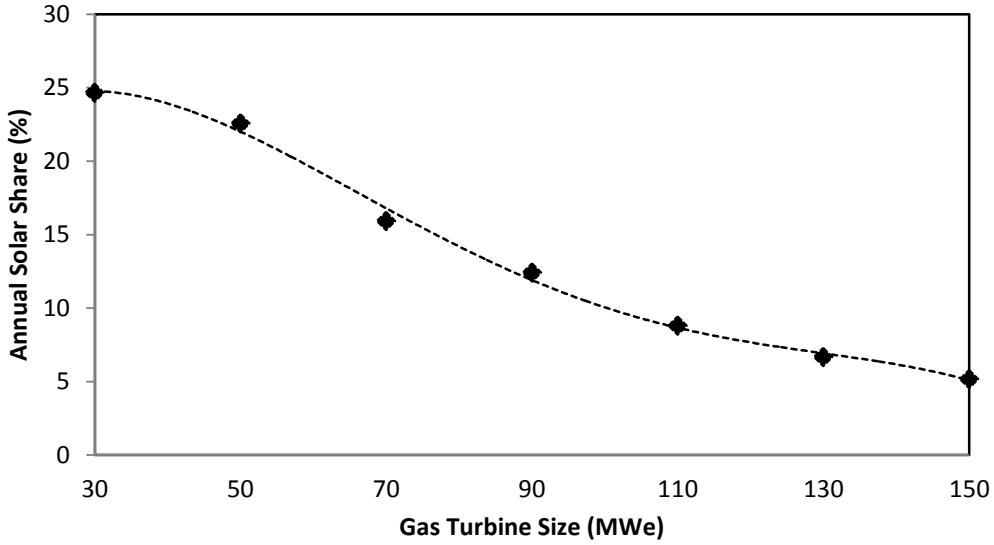

Figure 8.16: Annual solar share at the optimal solar integration of PTC for different gas turbine sizes.

Other thermo-economic figures of merits have been evaluated for both, the conventional and integrated PTC system with steam generation side in a gas turbine cogeneration plant. One of these economic parameters was the Levelized Energy Cost (LEC). Figure 8.17 shows the LEC for both, the conventional gas turbine cogeneration power plant and the integrated optimal size of PTC with different of gas turbine sizes.

The results presented in Fig. 8.17 indicate that integrating optimal solar multiple with the conventional gas turbine cogeneration plant will result in a logical increase in the LEC compared to the conventional cogeneration power plant. This is because of two main reasons, first one the industrial simulation land was located in the high insolation region, where the solar energy conversion system can produce the greatest amount of energy from specific PTC field size; the second one, the output thermal energy is greater than output electrical energy for all gas turbine sizes, which doesn't cost a lot.

According to Figure 8.17, the increase of LEC could be defined as the difference between LEC of integrated PTC system with gas turbine cogeneration plant and conventional gas turbine cogeneration plant.

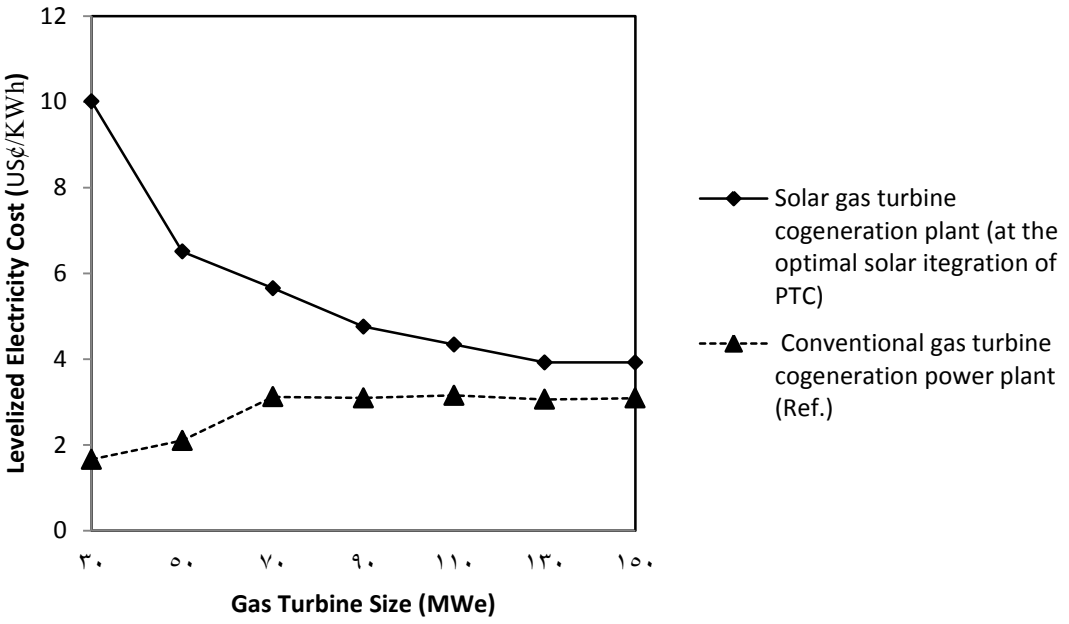

Figure 8.17: LEC for both the conventional gas turbine cogeneration plant and solar gas turbine cogeneration plant (at the optimal PTC integration).

The other economical parameter was the Solar Levelized Electrcity Cost (SLEC) for different gas turbine size. The SLEC achieved by integrating optimal size of PTC with different gas turbine size is presented in Figure 8.18. As shown, the integrated solar gas turbine cogeneration systems with the gas turbine range between 90 and130 have the lowest SLEC to convert solar energy into thermal energy for the cogeneration plant, which studied under Dhahran weather conditions.

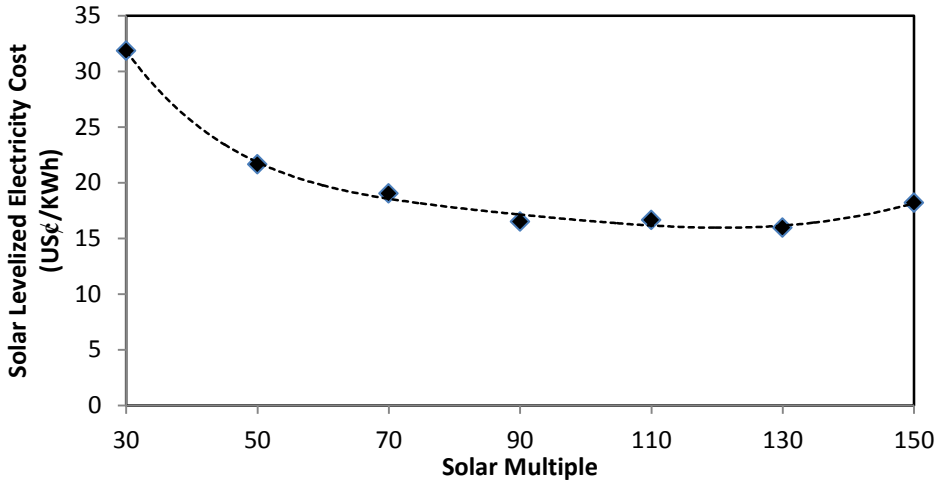

Figure 8.18: SLEC at the optimal solar integration of PTC for different gas turbine sizes.

Since the integrated PTC to steam side in a gas turbine cogeneration system leads to a logical increment in the levelized energy cost compared to the conventional gas turbine cogeneration power plant, the integration leads to a considerable reduction in CO_2 emission. Figure 8.19 depicts the annual CO_2 emission for both, integrated the optimal solar multiples with the gas turbine cogeneration system, and conventional gas turbine cogeneration system. Annual CO_2 avoidance could be defined as the annual reduction of CO_2 emission due to the solar energy utilization. Figure 8.20 shows the annual CO_2 avoidance, which is a difference between the amount of CO_2 emissions from conventional gas turbine cogeneration power plant and from the integrated optimal size of PTC system with gas turbine cogeneration plant.

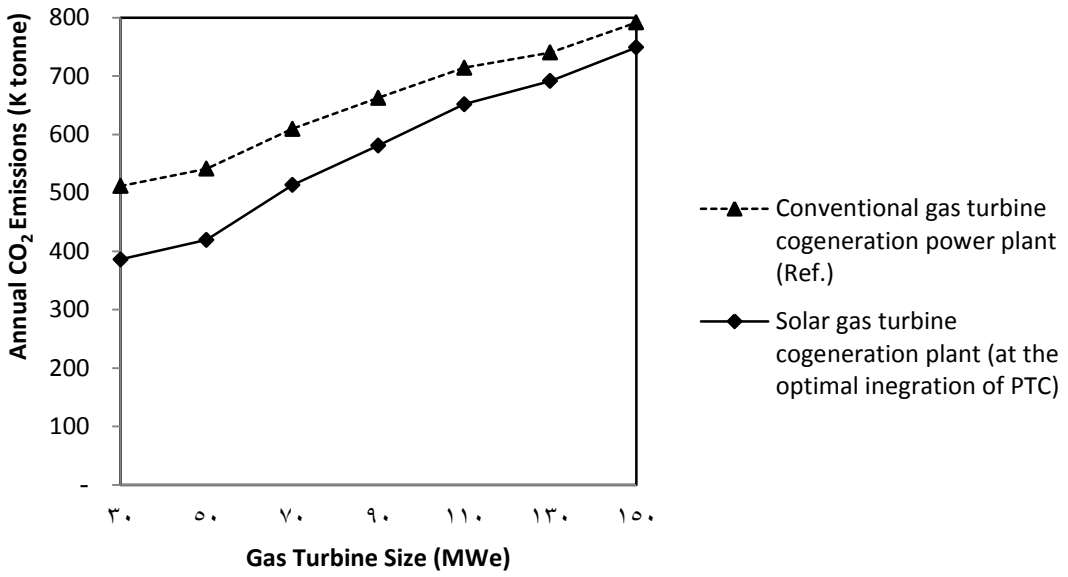

Figure 8.19: Annual CO_2 emissions from both conventional gas turbine cogeneration and solar gas turbine cogeneration (at the optimal PTC integration).

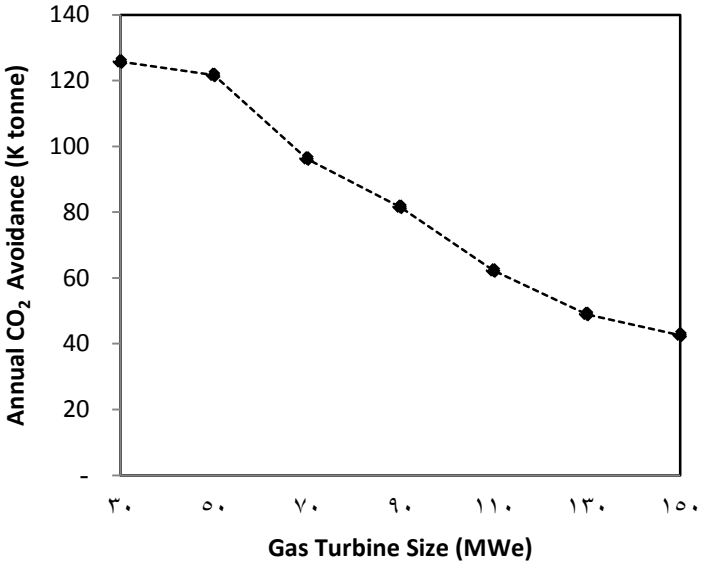

Figure 8.20: Annual CO_2 avoidance at the optimal solar integration of PTC for different gas turbine sizes.

As shown in Figure 8.20, the maximum annual CO_2 avoidance was for integrated PTC with 30 MWe gas turbine size (126 K tonne of CO_2), and this avoidance was decreased with increasing gas turbine size, which left with 42.6 K tonne of CO_2 . These results suggest that the cost of integrating solar energy with the conventional gas turbine cogeneration plant might be comparable to the integration of carbon dioxide elimination (avoidance) device to the conventional plant.

In reality, CO_2 capture technology is used to avoid CO_2 emissions from conventional power plants. One of the main importance reasons to integrate solar energy with cogeneration power plant is to avoid CO_2 emissions from power plants. So economical comparing of these two different technologies for CO_2 avoidance is very important to assess wither integrated solar energy with cogeneration power plant is economical feasible or not. One can use CO_2 capture technology with conventional gas turbine cogeneration power plant to avoid the same CO_2 which avoided by integrating the solar energy. So one can calculate a LEC for conventional power plant with CO_2 capture technology as follows:

First determine the annual CO_2 avoidance, which can be achieved by integrating solar technology. Then multiply that measure with cost of CO_2 capture technology. Divide the eventual by the annual electrical energy for each gas turbine size. Finally add up that amount with the LEC of conventional gas turbine cogeneration power plant. It is important to note the capturing one tonne of CO_2 required 160 US$ [77 and 40].

Figure 8.21 presents comparison between LEC by using different CO_2 avoiding technologies. As shown, integrated PTC to gas turbine cogeneration system has proved the economical feasibility more than CO_2 capture technology for gas turbine size less than 110 MWe. However, the integrated PTC to gas turbine cogeneration system has proved the same economical feasibility with CO_2 capture technology for gas turbine size greater than 110 MWe.

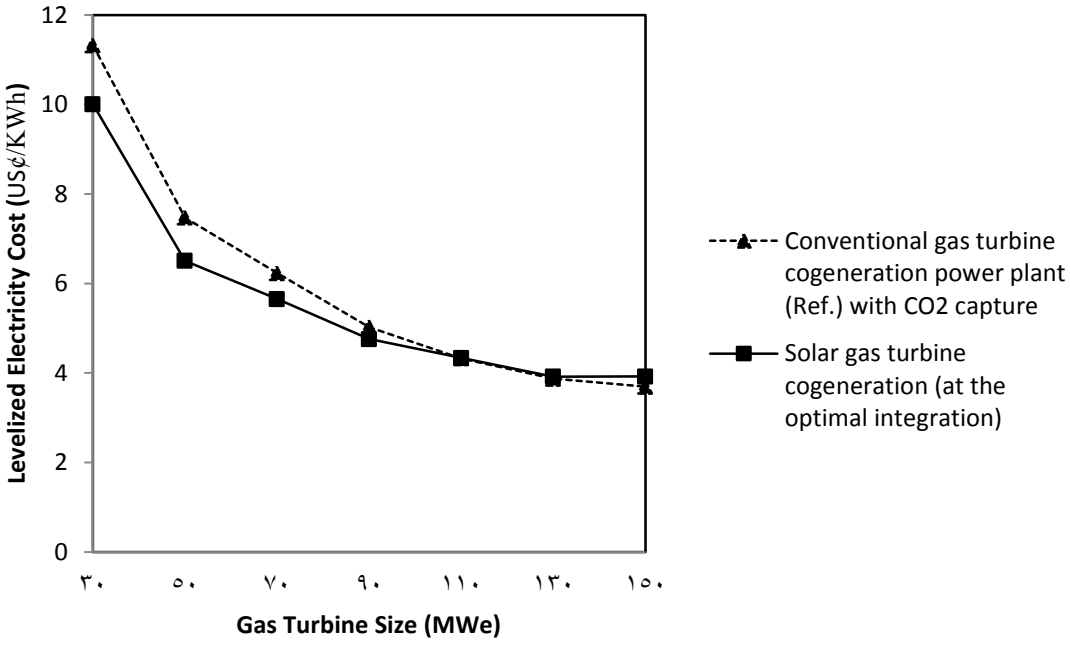

Figure 8.21: Comparison of LEC for different CO_2 avoiding technologies

The solar collector size at the optimal solar multiple has been determined for all gas turbine size integrated with PTC technology. Also levelized electricity cost and annual CO_2 emissions have been determined for all gas turbine size.

The International Renewable Energy Agency reported in 2012 that the LEC of parabolic trough plants were in the range 20 to 36 US¢/ kWh [78]. So one can compare the LEC of the present study with the minimum value of LEC reported by International Renewable Energy Agency, which is 20US¢/ kWh.

Figure 8.22 depicts the Levelized Electricity Cost (LEC) versus annual CO_2 emission for different solar gas turbine plants at optimal design. Point one presents the LEC and annual CO_2 emission of reference cycle with 150 MWe. Where point three presents the minimum LEC and annual CO_2 emission (equal to zero) of parabolic solar thermal power plant [78]. Point two presents the LEC and annual CO_2 emission of the present design where annual CO_2 emission is lower. Since gas turbine size of 30 MWe integrated with PTC has the lower CO_2 emission, one can define point two at this design.

The line linked between point one and point three represents the literature reference lines. By comparing present designs with this lines. One can note that the Levelized Electricity Cost (LEC) is reduced by integrating CSP technologies with gas turbine cogeneration system and most present designs are under these lines. This is because two main reasons, first one the industrial simulation land was located in the high insolation region, where the solar energy conversion system can produce the greatest amount of energy from specific solar collector field size; the second one, the output thermal energy in the present design is greater than output electrical energy for all gas turbine size, which doesn't cost a lot.

The line linked between point one and point two represents the lowest values for the best designs in the present study. The best designs can be considered as the design when it's representing point located below the line.

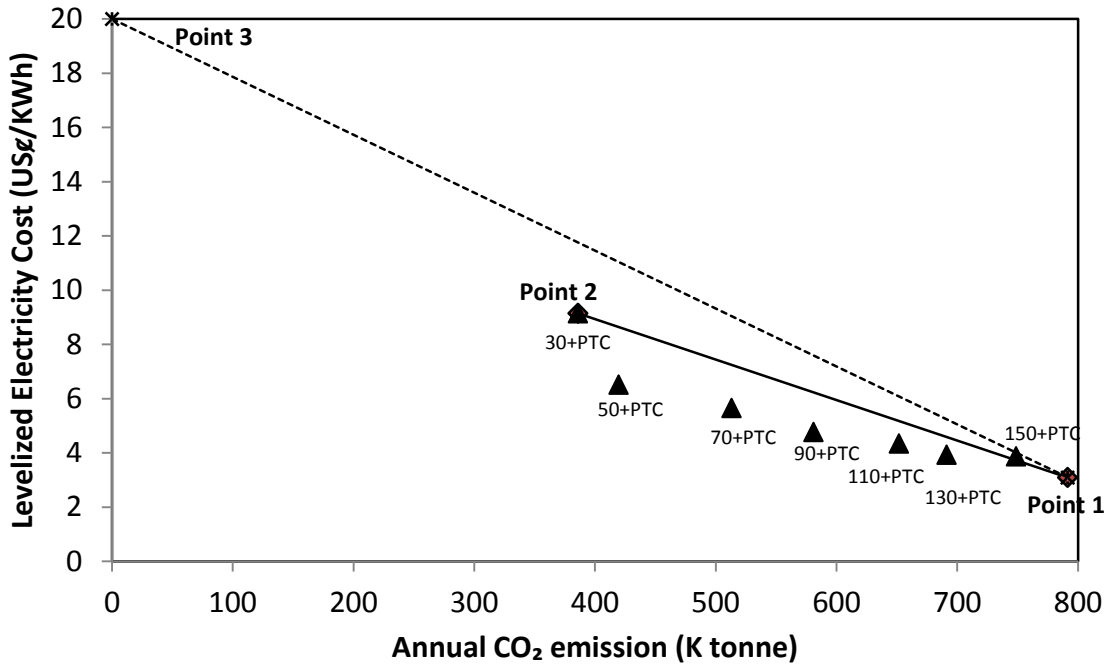

Figure 8.22: Levelized electricity cost versus annual CO_2 emission for different gas turbine sizes integrated with optimal solar multiple of PTC.

According to the results presented in the Figure 8.22, the annual CO_2 avoidance is higher when the PTC was integrated with small gas turbine size. But there is a logical increase in LEC for the integration with small gas turbine size compared to that with large gas turbine sizes. So one can conclude that the integration of the optimal solar multiple of PTC with gas turbine size range between 50 to 90 MWe have a sufficient ability for solar energy utilization with a logical increase in the LEC of energy generated.

Figure 8.23 depicts the total plant efficiency versus annual CO_2 emission for different solar gas turbine plants at optimal design. Point one presents the total plant efficiency and annual CO_2 emission of reference cycle with 150 MWe. Where Point two presents the total plant efficiency and annual CO_2 emission of the present design where annual CO_2 emission is lower. Since gas turbine size of 30 MWe integrated with PTC has the lower CO_2 emission, one can define point two at this design. The line linked between point one and point two represents the higher values for the best designs in the present study. The best designs can be considered as the design when it's representing point located on or above the line.

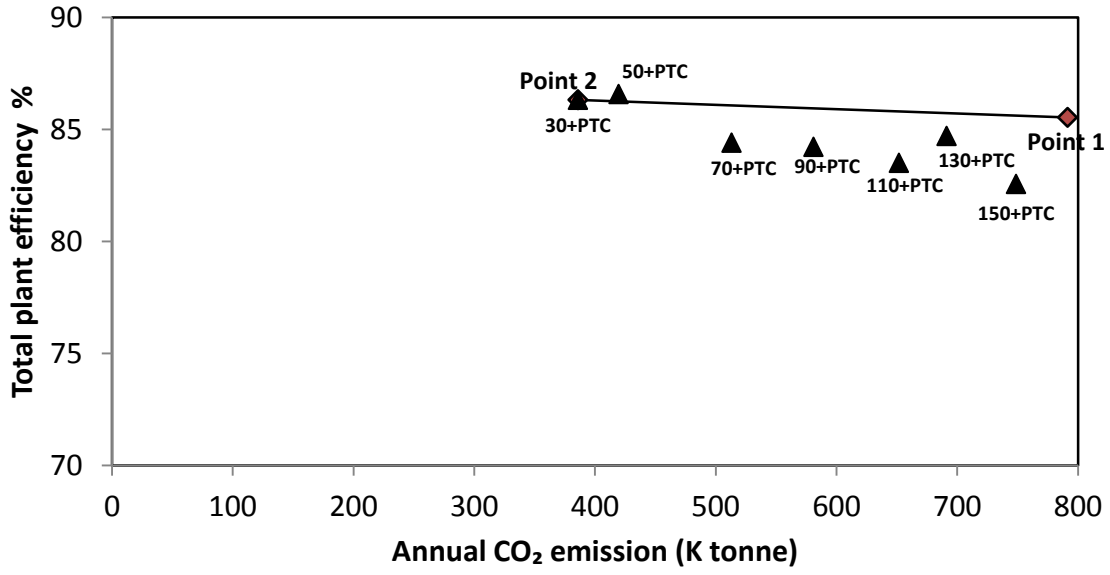

Figure 8.23: Total plant efficiency versus annual CO_2 emission for different gas turbine sizes integrated with optimal solar multiple of PTC.

According to the results presented in the Figure 8.23, the annual CO_2 avoidance and total plant efficiency are higher when the PTC was integrated with small gas turbine size. So

one can note that the integration of the optimal solar multiple of PTC with gas turbine size range between 30 to 50 MWe have a higher total plant efficiency. But there is a major increase in LEC for the integration with 30 MWe gas turbine size compared that with 50 MWe gas turbine sizes (Figure 8.22). So one can conclude that the integration of the optimal solar multiple (0.8) of PTC with 50 MWe gas turbine size has a sufficient ability for solar energy utilization.

8.3 Concluding Remarks

An integrated solar gas turbine cogeneration system that generates steam at a constant flow rate of 81.44 kg/s at P = 45.88 (bar) and temperature of T = 394°C throughout a year in addition to the generation of electricity have been simulated and assessed for different gas turbine sizes. THERMOFLEX with PEACE simulation software was used to assess the performance of each proposed integration designs. The Thermo-economical analysis was conducted for a site in Dhahran city at the eastern province of Saudi Arabia. From this study, one can draw the following conclusions:

- Solar energy is a promising technology and introducing integrated PTC with gas turbine cogeneration system offers much potential for large-scale application with stable power supply.

- The optimal solar multiple have been determined for integrating the PTC with different gas turbine sizes, which are 0.8, 0.8, 0.6, 0.5, 0.4, 0.3, and 0.3 for gas turbine size 30, 50, 70, 90, 110, 130, and 150 MWe respectively. The optimal

solar multiple have been determined to gives the minimum SLEC. At the optimal solar multiple, one can determined solar field sizes, which are 104, 104, 78, 65, 52, 39, and 39 hectare for gas turbine size listed above.

- The LEC is in the range 3.7 US¢ to 10 US¢/ kWh in the present study, Where the International Renewable Energy Agency reported in 2012 that the LEC of parabolic trough power plants was in the range 20 US¢ to 36 US¢/ kWh [78].

- The results have proved that the integrated PTC with gas turbine cogeneration system has more economical feasibility than CO_2 capture technology for gas turbine size less than 110 MWe.

- The results have proved that the integration of the optimal solar multiple (0.8) of PTC with 50 MWe gas turbine size has a sufficient ability for solar energy utilization.

CHAPTER 9

LINEAR FRESNEL REFLECTOR SYSTEM INTEGRATED WITH STEAM GENERATION SIDE IN A GAS TURBINE COGENERATION PLANT.

An Integrated Linear Fresnel Reflector (LFR) system with steam generation side in a gas turbine cogeneration plant considered in this work was used to generate the same amount of steam at the same conditions mentioned in chapters 7 and 8. The same range of gas turbine sizes was also investigated here. Figure 9.1 depicts the schematic diagram of the integration LFR with steam generation side in a gas turbine cogeneration plant.

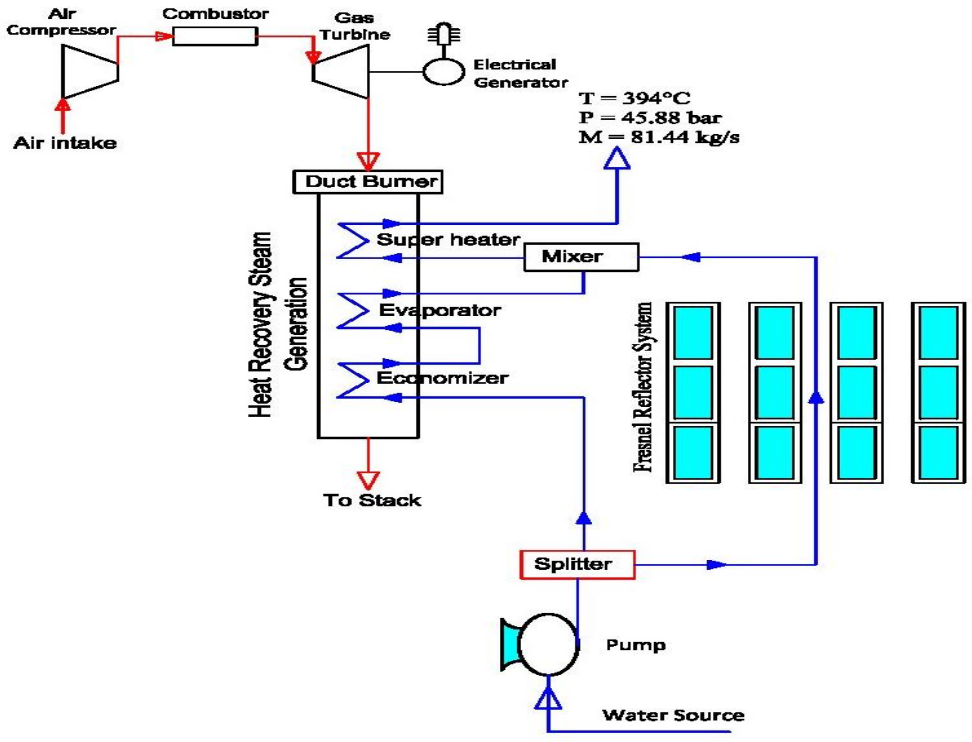

Figure 9.1: Schematic diagram of LFR integrated with steam generation side in gas turbine cogeneration plant

9.1 Simulation Procedures of a Gas Turbine Cogeneration Plant Integrated with LFR System

As stated earlier, THERMOFLEX with PEACE software has been used for a simulation. A schematic diagram of the integration LFR system with steam generation side in a gas turbine cogeneration plant as simulated in THERMOFLEX is shown in Figure 9.2. As can be seen in the Figure, the plant has one gas turbine: (4); one duct burner: (1); one superheater: (8); an evaporator: (12); one economizer: (9); LFR solar field (14); one splitter (15); one mixer (13): and a pump: (11).

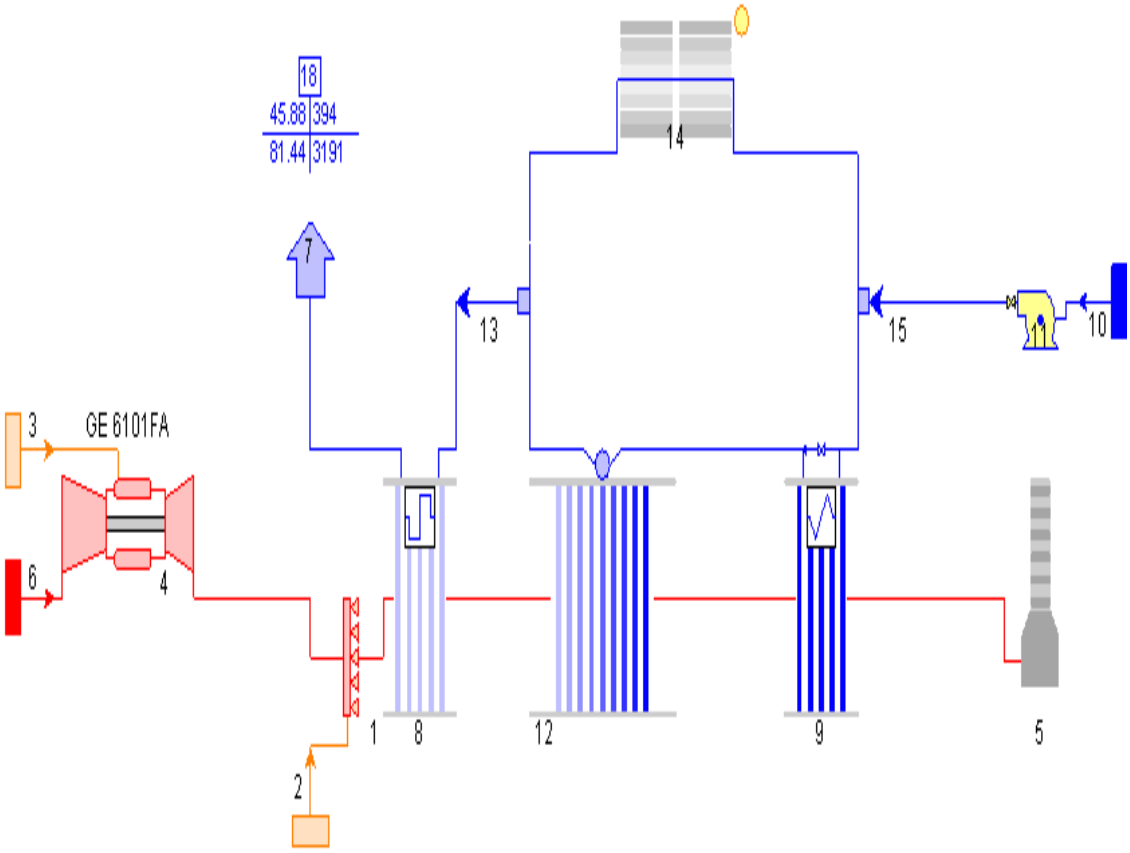

Figure 9.2: Schematic diagram of the gas turbine solar cogeneration plant integrated with LFR as simulated in THERMOFLEX.

Table 9.1: Components name of the gas turbine solar cogeneration plant integrated with LFR.

Number	Component Name	Number	Component Name
1	Duct Burner	9	Economizer
2	Fuel Source	10	Water/Steam Source
3	Fuel Source	11	Pump
4	Gas Turbine	12	Evaporator
5	Stack	13	Splitter
6	Gas/Air Source	14	LFR Solar Field
7	Process	15	Mixer
8	Superheater		

The specific steps to simulate gas turbine solar cogeneration plant integrated with LFR system are listed in Figure 9.3. As shown in this Figure, building a configuration by using THERMOFLEX program is the first steps of the simulation. For the simulation; the data of Novatec Solar superheating section (linear Fresnel) have been considered (Table 9.1); the data of Dhahran region which is located in the east part in Saudi Arabia have been considered. In this study; a solar collector was rotated about horizontal north-south axis with continues adjustment to minimize the angle of incidence; the latitude (for Dhahran 26.5°), and altitude (for Dhahran 90 m) of the industrial plant location was selected from the program.

In this chapter, all the operating conditions power plants in chapter 7and 8 have been used. For examples; the plant was considered to generate steam with a constant flow rate of 81.44 kg/s at P = 45.88 (bar) and temperature of T = 394°C throughout a year in addition to generate an electricity; the products manufacturing by General Electric Company as listed in THERMOFLEX program have been used except the 90 MWe gas

turbine size was selected from ASTM; the gas turbine was ranged between 30 MWe to 150 MWe.

Table 9.1: Parameters of LFR system and solar field

Reflector type: Fresnel		
Optical efficiency at 0 degrees incidence	67	%
Receiver outside diameter	70	mm
Receiver wall thickness	4.191	mm
Receiver inside diameter	61.62	mm
Reflector unit width	16	m
Reflector aperture width	12	m
Reflector focal length	7.4	m
Geometric concentration	171.4	
Ratio of reflector focal length to aperture width	0.6167	
collector Row pitch	20.5	m

As stated above, the output thermal power from the plant was considered as a constant throughout the year, and as known, producing thermal power from solar field varies according to the solar radiation intensity. Consequently, the outlet mass flow rate of the steam from solar filed was also changing. In this regards, a control loops have been constructed to operate the duct burner to cover the thermal load of the plant when the exhaust gases for gas turbine and thermal energy from solar field couldn't cover the thermal load of the plant.

In order to make a proper comparison between different designs, all the simulation conditions in the chapter 8 have been used in this chapter.

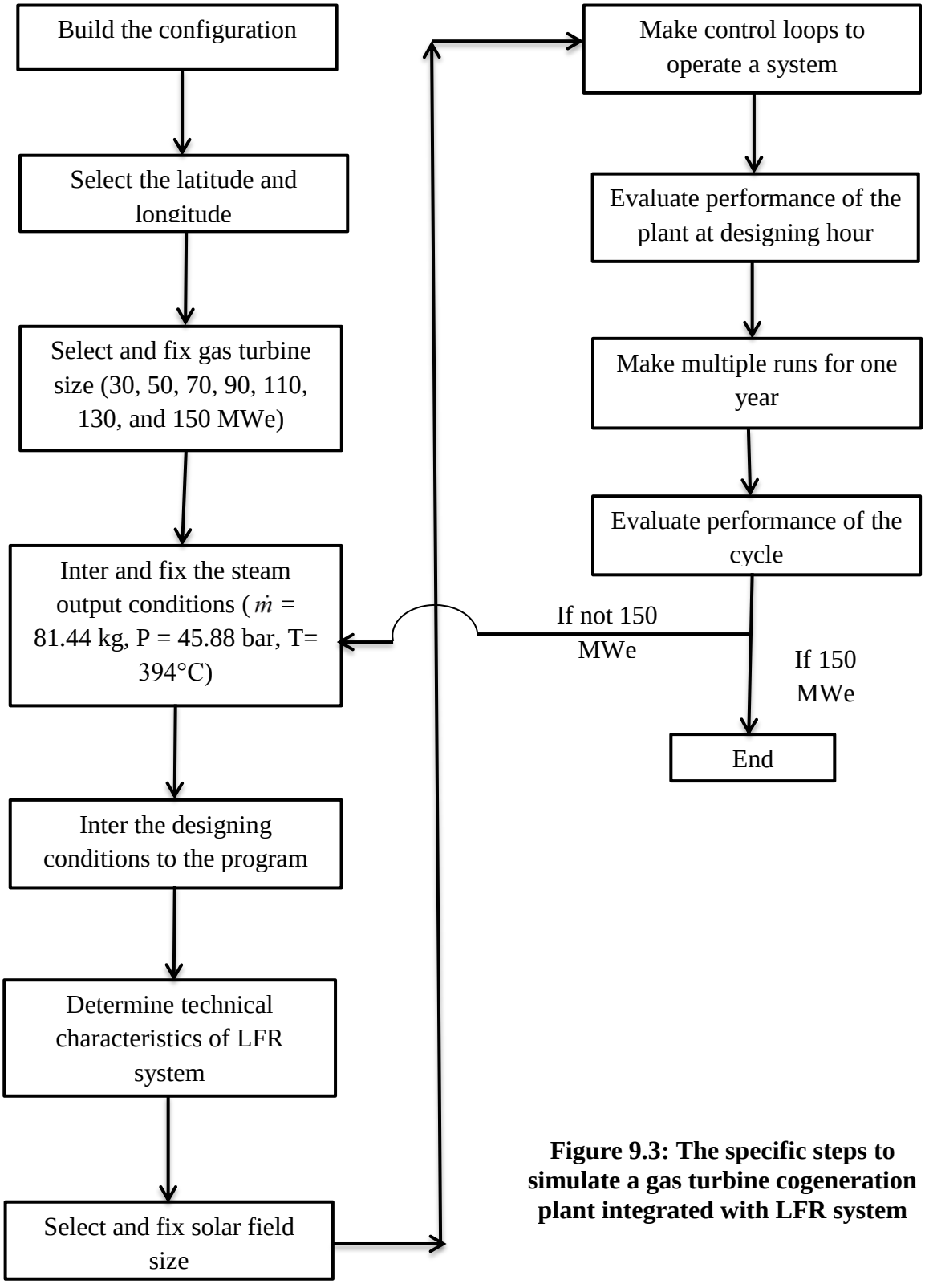

Figure 9.3: The specific steps to simulate a gas turbine cogeneration plant integrated with LFR system

9.2 Simulation Results

A LFR solar field size was estimated at the same design conditions (design hour) of PTC as described in chapter 8. The designing conditions include ; the maximum average direct solar radiation at Dhahran city, which occurs on June 11 according to Table 5.16; and an averages ambient temperature and relative humidity at the same day.

As mentioned previously, solar multiple represents the ratio of thermal power produced by solar field to the plant thermal load at design hour. The plant thermal load is the same as the thermal load in chapters seven and eight, which is 259860 kW, whereas the thermal power at design hour can be obtained from LFR field by using THERMOFLEX. Furthermore, the fixed thermal load in chapter eight (Figure 8.4) should be achieved in these designs for different solar multiples.

As stated above, thermal power required from a LFR field at design hour is a function of steam mass flow rate and outlet temperature from solar field (at design mode). Since the mass flow rate and outlet temperature from solar field are a function of solar field size, so increasing or decreasing solar multiple could be carried out by increasing or decreasing solar field size. In other words, design of different solar field sizes have been done at the same design hour but for different mass flow rates and different outlet temperature from solar field. The maximum outlet temperature from solar field can be reached is 394ºC.

At the design mode, the conditions for calculating solar multiple for solar field size corresponding to all gas turbine size must be fixed; that will help make the proper comparison between different designs to reach at the optimal design. Figure 9.4 shows that the solar field size increases with increasing solar multiple. This increasing of solar multiple save more amount of fuel as well as prevent more amount of CO_2 emissions. Figure 9.5 presents total reflective area of a LFR for different solar multiple. This result is an important for comparing integration of different solar technologies.

Solar thermal power obtained from solar field at different solar multiple for different gas turbine size has been estimated using THERMOFLEX. Figure 9.6 depicts thermal power obtained from solar field which integrated with different gas turbine size at different solar multiples.

As can be seen in Figure 9.6, the thermal power obtained from solar field increases with solar multiple up to specific value for each gas turbine size. After those points, the thermal power obtained remaining a constant. This is because there is over sizing of a LFR field size, which is not usable after that specified solar multiple. According to the Figure, the plant with large gas turbine of 150 MWe does not need much energy from the solar integration at design hour (about 63.9 MW). However, the plant with small gas turbine of 30 MWe has a large amount of thermal power obtained from solar field (about 207.8MW). Figure 9.7 shows the maximum possible solar multiple with gas turbine size. One can note that the optimal solar multiple is much closed to this point as can be seen later on.

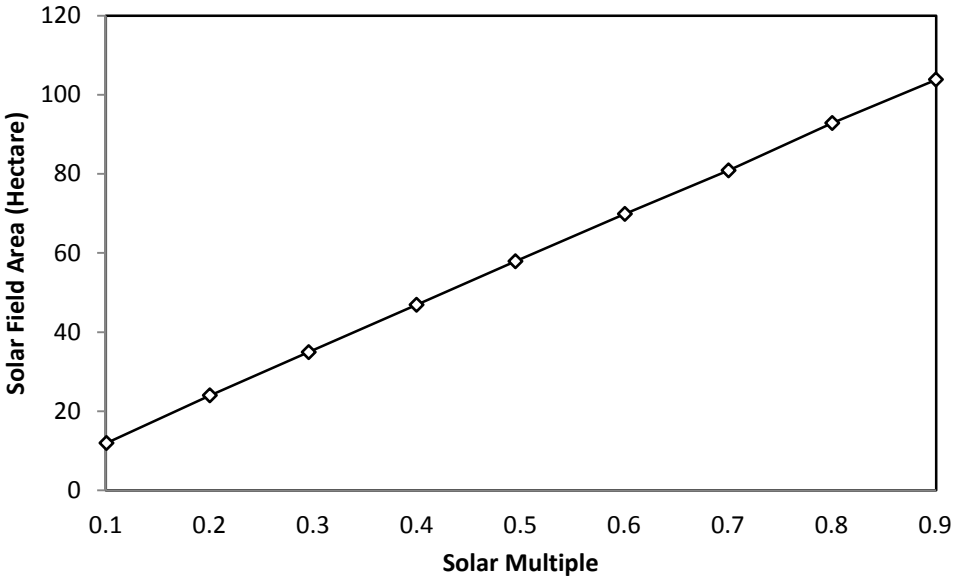

Figure 9.4: Solar field area of LFR solar field versus solar multiples.

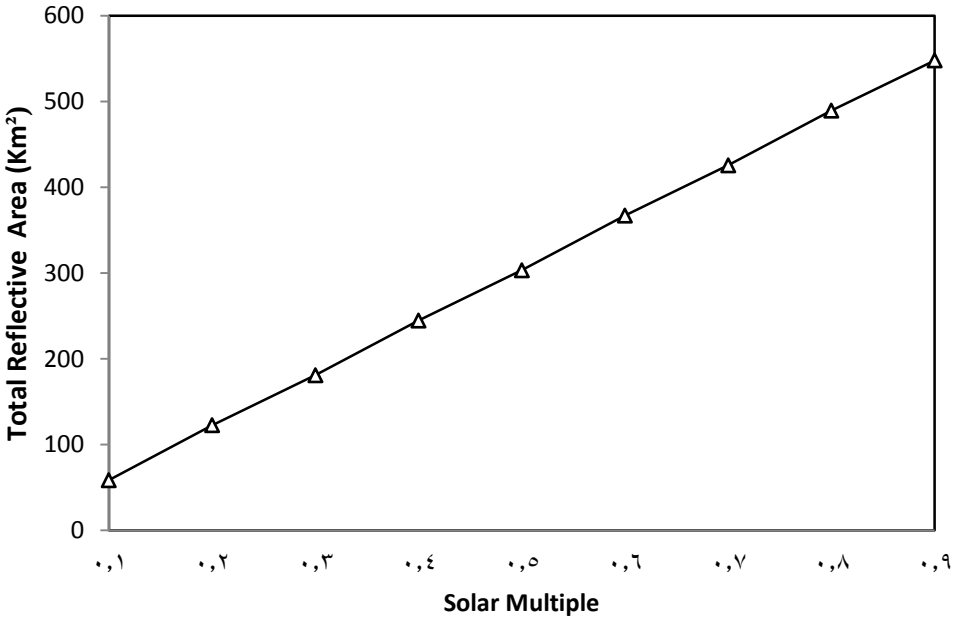

Figure 9.6: Reflective area of an LFR system versus solar multiples

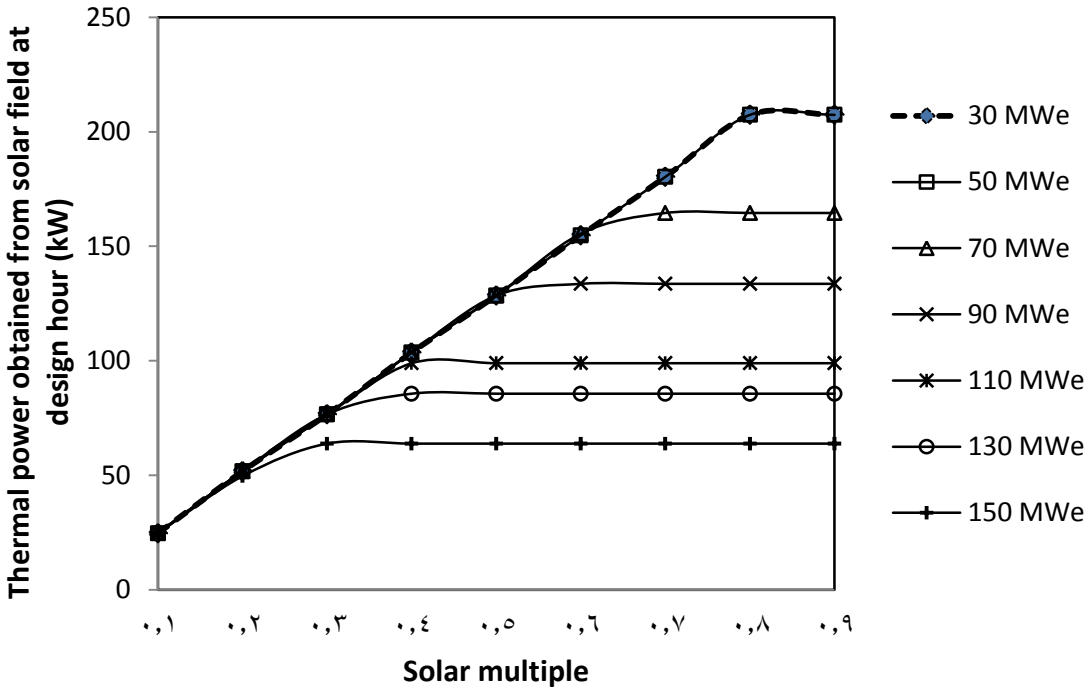

Figure 9.6: Thermal power obtained from solar field of an LFR integrated with different gas turbine sizes.

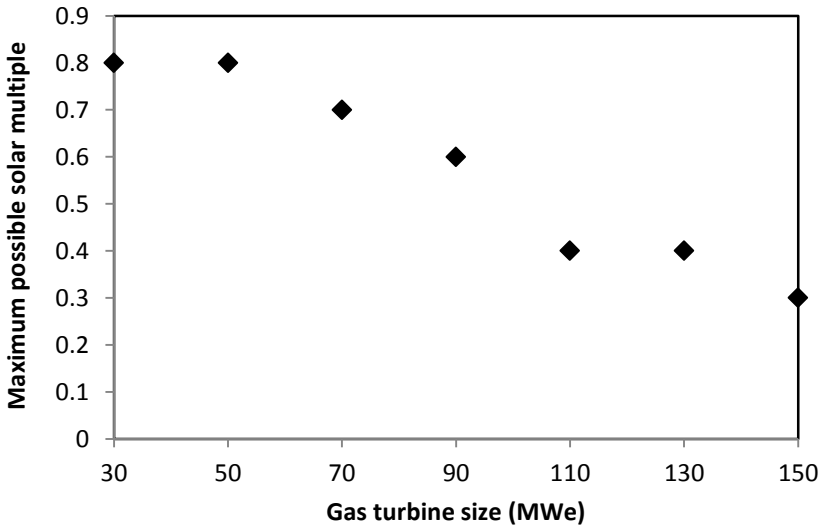

Figure 9.7: Maximum possible solar multiple with gas turbine size (for LFR).

Figures of merit such as instantaneous solar share, annual solar share, annual CO_2 avoidance, LEC, and SLEC have been calculated for each designing mode in order to assess the performance of integrated LFR with steam generation side for different gas turbine sizes in cogeneration system.

First of all, instantaneous solar share can be defined as a ratio of the power generated from the solar field to the total power (electrical + thermal) generated from both of the solar and fuel energy input to the plant at the design hour. The instantaneous solar share can be calculated by Equations given in section 4.2.2. Figure 9.8 depicts the instantaneous solar share for integrating different solar multiples of LFR with different gas turbine sizes.

According to Figure 9.8, an instantaneous solar share is increasing while solar multiple is increasing up to specific value for each gas turbine size. Beyond that specific value, instantaneous solar share is remaining a constant. This is due to solar field area, which is not fully used after that specified solar multiple as stated above. The plant with large gas turbine of 150 MWe does not require much energy from the solar integration at design hour (about 13.11 %). However, the plant with small gas turbine of 30 MWe has a large amount of instantaneous solar share from the solar integration at design hour (about 70.66%).

To calculate what percent of the energy produced per year from the integrated solar gas turbine cogeneration power plant is due to the solar energy, one needs to calculate the

annual solar shares. Where annual solar share gives an indication of how much energy produced annually by a LFR system. Figure 9.9 shows how an annual solar share raises in response to rise in solar multiple for different gas turbine size.

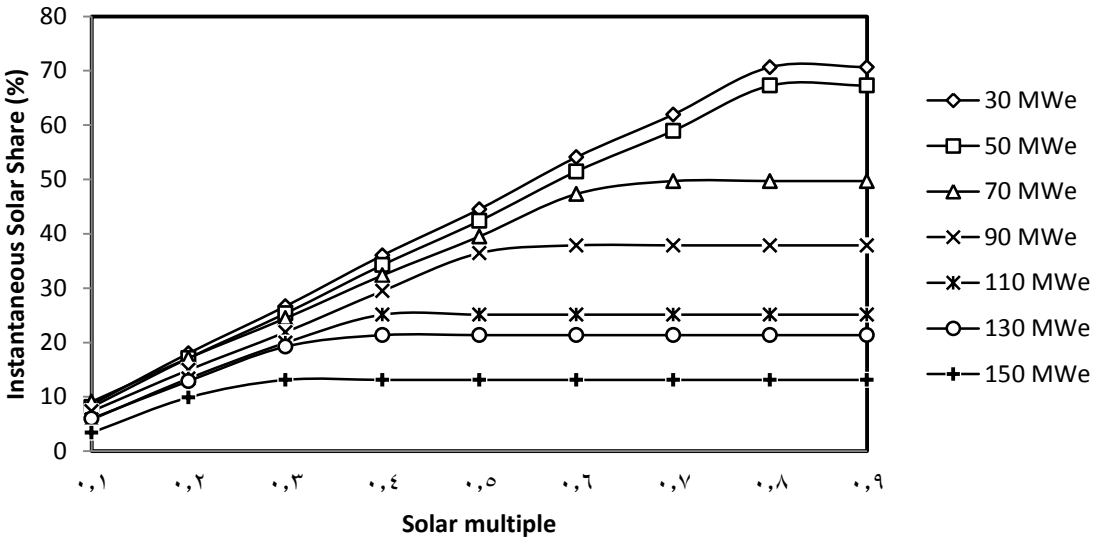

Figure 9.8: Instantaneous solar share for integrating different solar multiples of an LFR system with different gas turbine sizes.

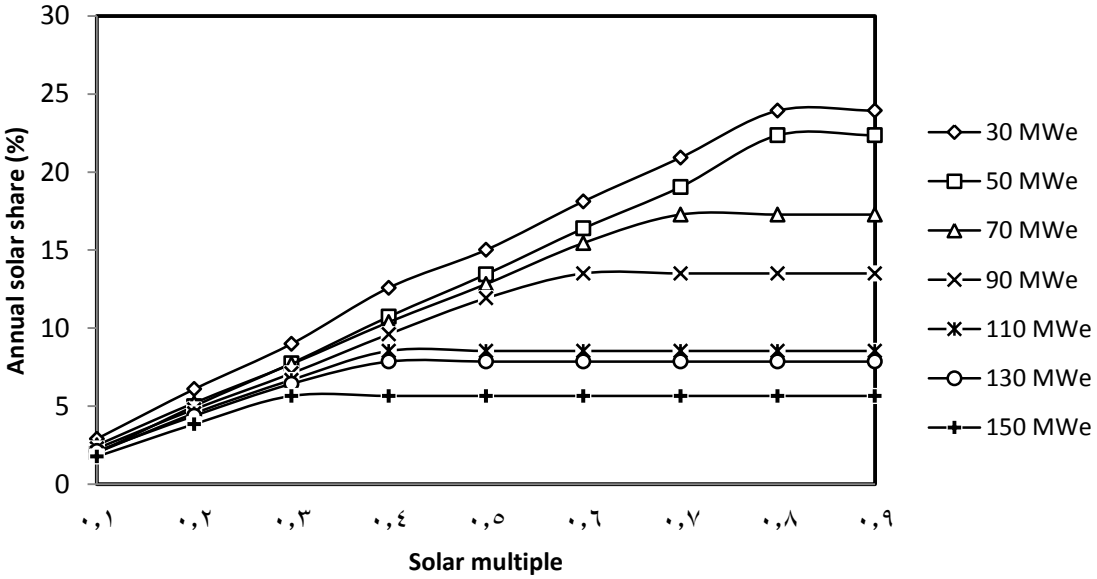

Figure 9.9: Annual solar share for integrating different field sizes of an LFR system with different gas turbine sizes.

According to Figure 9.9, the annual solar share rises significantly up to specific solar multiple for each gas turbine size. Beyond the specific value, annual solar share remains constant. The reason behind that behavior, there is no room for solar energy integration to the plant after that specified solar multiple as stated above. As shown, Plant with large gas turbine of 150 MWe does not require much annual energy from the solar integration (about 5.66 %). However, the small gas turbine of 30 MWe has a large amount of annual solar share (about 24%).

Economic analysis has been done in terms of levelized energy cost (LEC) and solar levelized energy cost (SLEC). The LEC and SLEC are very important thermo-economic figures of merits that used to estimate the cost of energy production from a given power plant design. Figure 9.10 illustrates the LEC in US¢/kWh at different solar multiple integrated with different gas turbine sizes. Whereas Figure 9.11 shows how the SLEC vary in response to rise in solar multiple for different gas turbine sizes.

According to simulation results presented in Figure 9.10, the LEC increased slightly by increasing solar multiple for each gas turbine size. This is because two main reasons, first one industrial simulation land locates in high insolation regions where the solar energy conversion system can produce the greatest amount of energy from specific LFR field size; the second one, the output thermal energy is greater than electrical energy output from all gas turbine size where the thermal energy doesn't cost a lot.

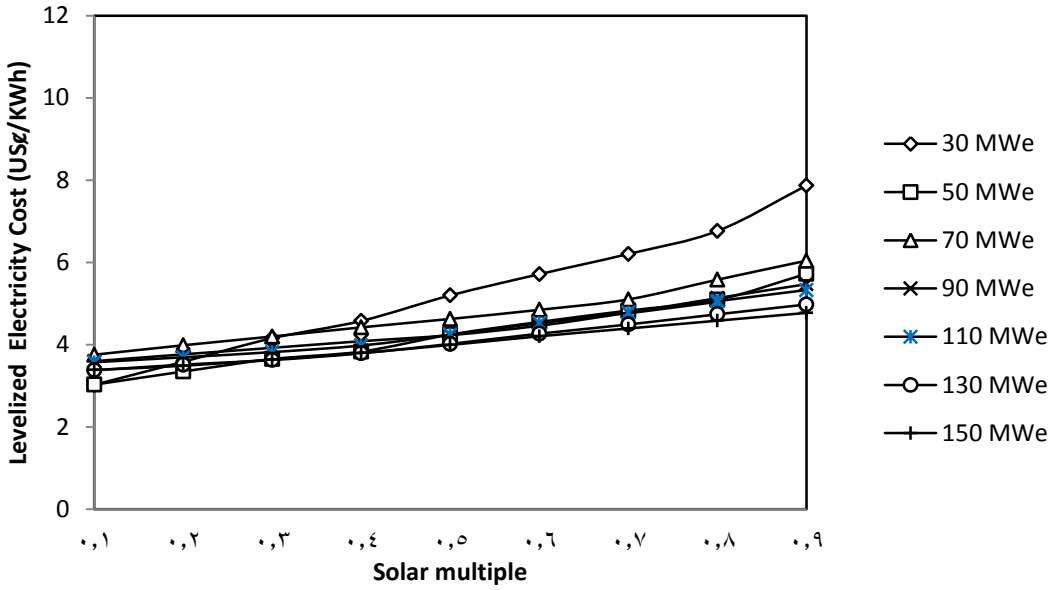

Figure 9.10: Levilized electricity cost for integrating different field sizes of an LFR with different gas turbine sizes.

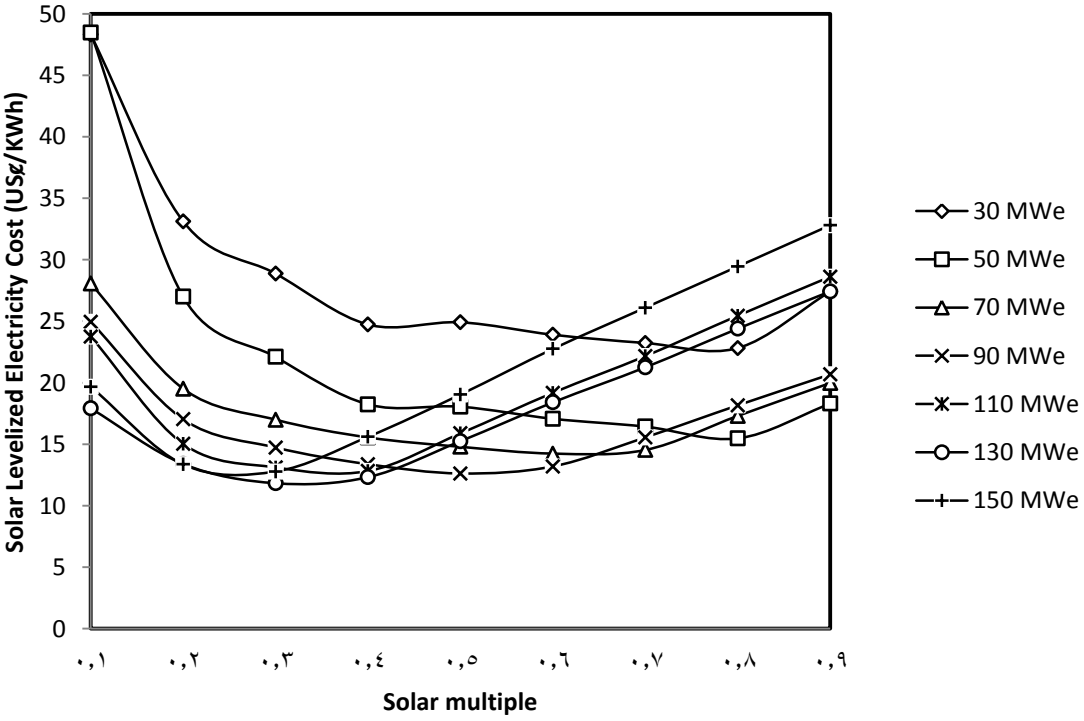

Figure 9.11: Solar levilized electricity cost for integrating different field sizes of an LFR with different gas turbine sizes.

Also according to Figure 9.10, there is a negligible difference between LEC for integrating LFR with different gas turbine size. This is because there is an incremental in total investment cost by increasing solar multiple in one hand, but there is a reduction in total fuel cost by increasing solar multiple in the other hand. So that leads to make a balance between annual cast for different gas turbine size. The LEC couldn't give the optimal solar multiple, but SLEC has minimal point, which is corresponding to the optimal solar multiple for each gas turbine size.

As shown in Figure 9.11, solar levelized electricity cost (SLEC) declined significantly up to specific point for each gas turbine size. Beyond that specific point, SLEC increased dramatically by increasing solar multiple. The simulation results show that the optimal solar multiple for each gas turbine size, which can be determined at the minimum value of SLEC. The optimal solar multiples are 0.8, 0.8, 0.6, 0.5, 0.4, 0.3, and 0.3 for gas turbine size 30, 50, 70, 90, 110, 130, and 150 MWe respectively.

Integrating solar collector with gas turbine cogeneration has an environmental effect since increasing of solar share result in reduction of total fuel consumption, which required for conventional combined cycle to cover specific load, which leads to reduced CO_2 emissions (Fig. 9.12). The annual CO_2 emissions of conventional gas turbine cogeneration presented at zero solar multiple in Figure 9.12. The annual CO_2 avoidance could be defined as the annual reduction of CO_2 emission due to solar energy utilization. Figure 9.13 shows that the annual CO_2 avoidance for different gas turbine size at different solar multiples.

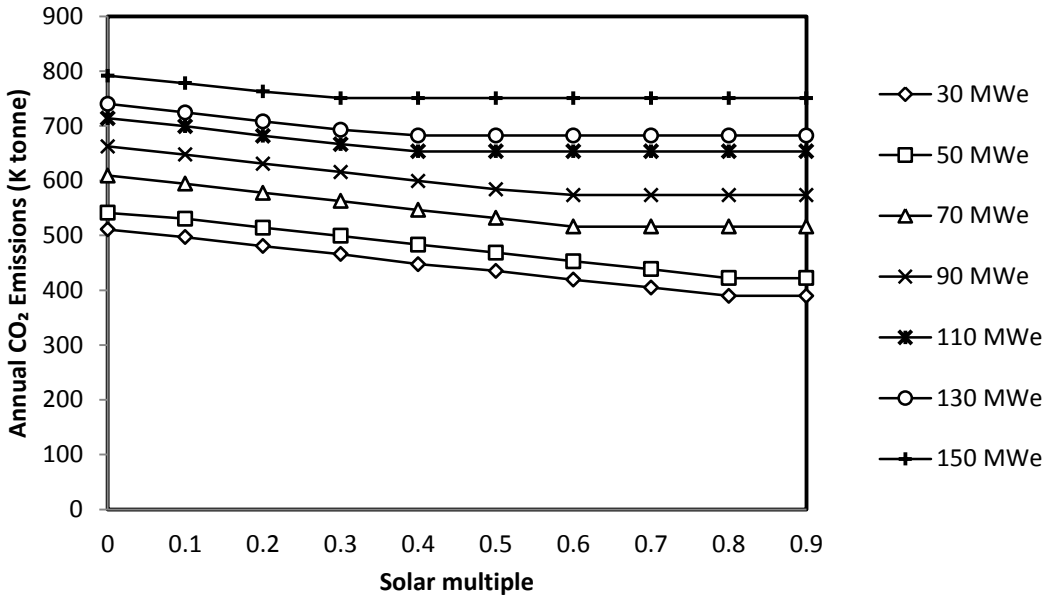

Figure 9.12: Annual CO_2 emissions from different gas turbine plants integrated with different solar field sizes of LFR.

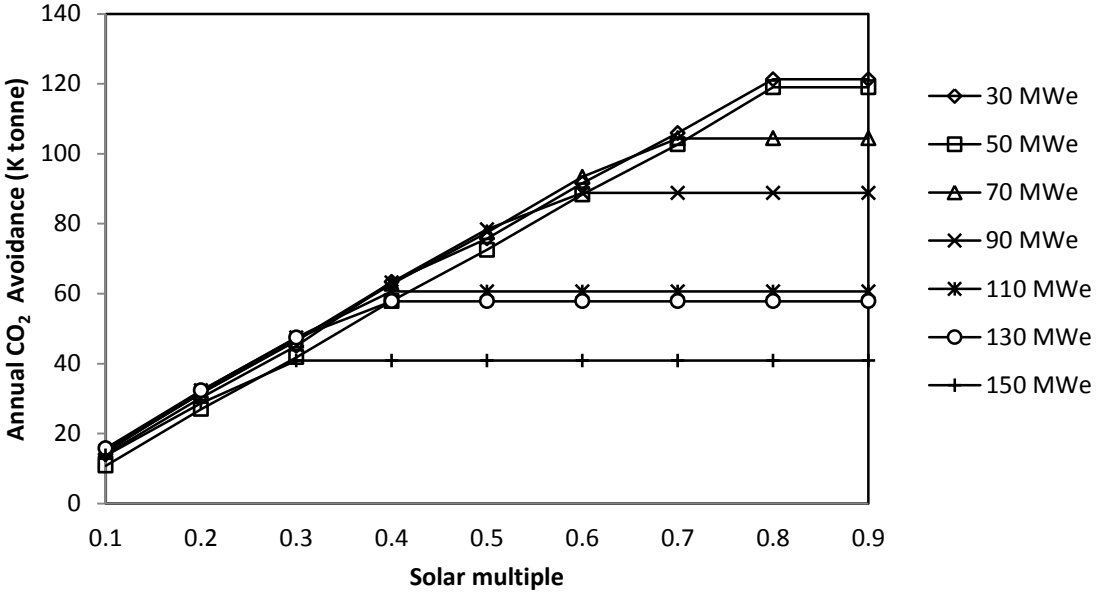

Figure 9.13: Annual CO_2 avoidance for integrating different field sizes of an LFR with different gas turbine sizes.

As can be seen in Figure 9.13, the CO_2 avoidance increases significantly by increasing solar multiple until reach specific value for each gas turbine size. After that specific value, the annual CO_2 avoidance remains a constant. The best CO_2 avoidance is for integrating LFR to cogeneration plant with 30 MWe gas turbine size, where the reduction is more than 122 k tonne of CO_2 from reference cycle (at 0 solar multiple).

The optimal solar multiples for integrated LFR with different gas turbine size have been determined, which are 0.8, 0.8, 0.6, 0.5, 0.4, 0.3, and 0.3 for gas turbine size 30, 50, 70, 90, 110, 130, and 150 MWe respectively. One can know study gas turbine size that can be integrated with optimal solar multiple by comparing all parameters corresponding to the optimal solar multiple for each gas turbine size.

First of all, the optimal LFR field size integrated with gas turbine cogeneration power plant has been determined for each gas turbine size. Figure 9.14 illustrates solar field area of the LFR system at the optimal solar integration for different gas turbine sizes. It can be seen that the solar field size integrated with 30 and 50 MWe gas turbine size are the same. This is because the optimal solar multiple for both gas turbine size are the same. The solar field size at the optimal integration declines substantially while gas turbine size increases from 50 MWe to130 MWe. The solar field size at the optimal solar integrated with 130 and 150 MWe gas turbine size are also the same, this is because the optimal solar multiple are the same for the two sizes.

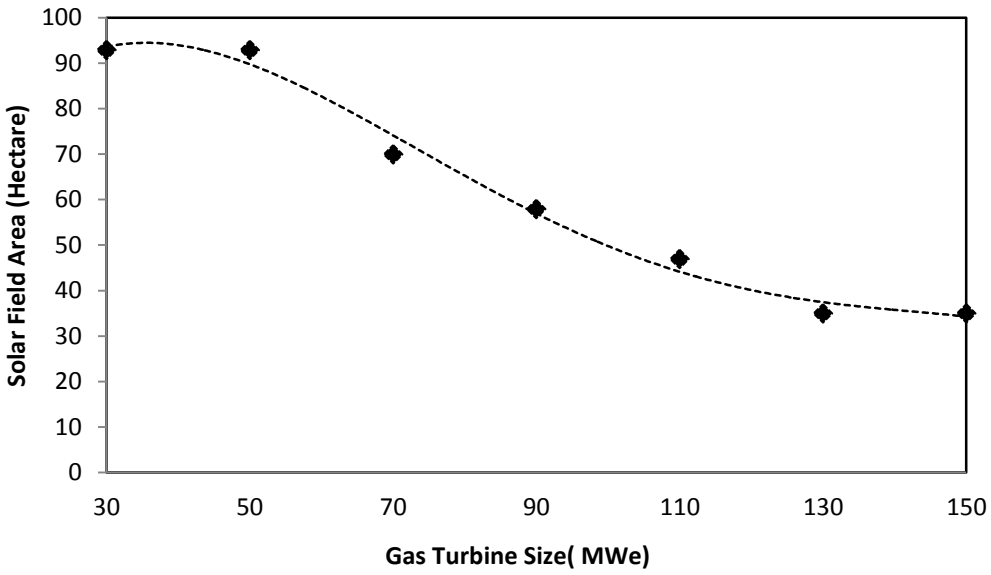

Figure 9.14: Solar field area of the LFR system at the optimal solar integration for different gas turbine sizes.

The instantaneous solar share achieved by integrating optimal solar multiple of LFR system for gas turbine cogeneration power plant has been identified. Figure 9.15 shows that the instantaneous solar share decreases substantially with gas turbine size. Even though, optimal solar multiple for gas turbine 30 MWe and 50 MWe are equal, there is a reduction in an instantaneous solar share. This is because electrical power output is a different from the two sizes.

An annual solar share achieved by integrating optimal solar multiple of LFR with different gas turbine sizes is presented in Figure 9.16. As expected the solar share is higher when the LFR is integrating with small gas turbine size. For example, the annual solar shares for this integration are 23.93%, 22.35%, and 15.44% for 30, 50, and 70 MWe gas turbine size respectively. The annual solar share decrease with increasing gas

turbine size which leaves almost 5.66% from annual total energy (electrical and thermal load) with a gas turbine size of 150 MWe.

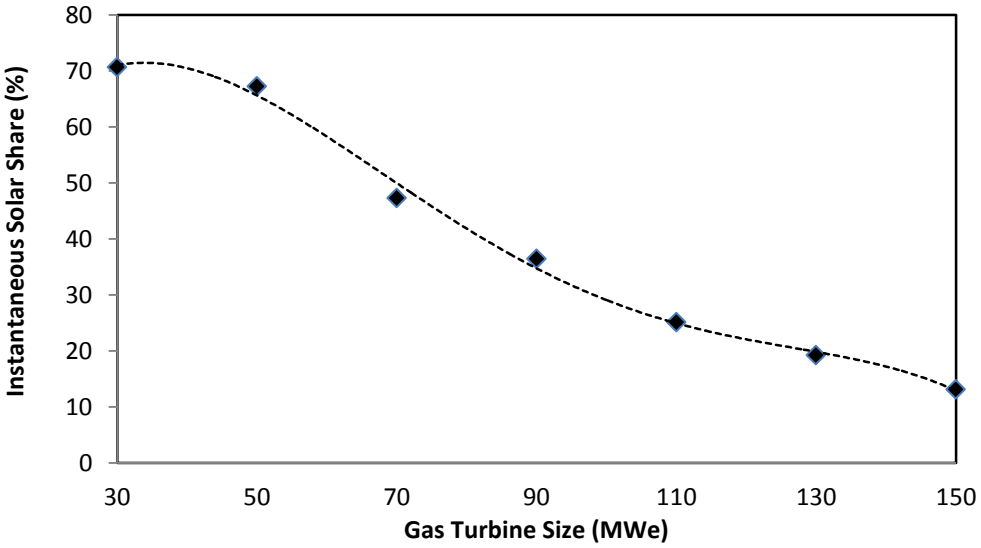

Figure 9.15: Instantaneous solar share at the optimal solar integration of LFR for different gas turbine sizes.

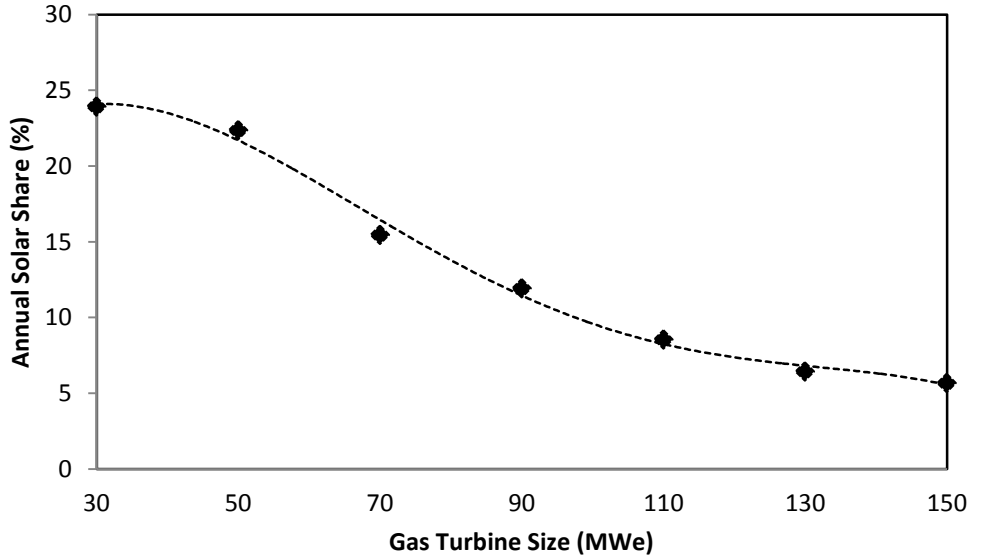

Figure 9.16: Annual solar share at the optimal solar integration of LFR for different gas turbine sizes.

Other thermo-economical figures of merits have been evaluated for both the conventional and integrated LFR system with gas turbine cogeneration plant. One of these economic parameters was the LEC. Figure 9.17 shows the levelized electricity cost for both, the conventional gas turbine cogeneration power plant, and the integrated LFR system with steam generation side in a gas turbine cogeneration plant.

The results in Fig. 9.17 shows that the integrating the optimal solar multiple of LFR system with a conventional gas turbine cogeneration plant will result in a logical increase in the levelized electricity cost compared to the conventional cogeneration power plant. This is because of two main reasons, first one the industrial simulation land was located in the high insolation region, where the solar energy conversion system can produce the greatest amount of energy from specific PTC field size; the second one, the output thermal energy is greater than output electrical energy for all gas turbine sizes, which doesn't cost a lot. An incremental in LEC due to using solar energy could be defined as the difference between LEC for solar gas turbine cogeneration plant and conventional gas turbine cogeneration plant, which presented as a gap between the two lines in Figure 9.17.

The other economical factor was the SLEC for different gas turbine sizes. This factor is presented in Figure 9.18 with different gas turbine sizes. As shown, the integrated solar gas turbines cogeneration systems with the gas turbine range between 90 and 130 have

the lowest SLEC to convert solar energy to useful energy for the cogeneration plant under Dhahran weather conditions.

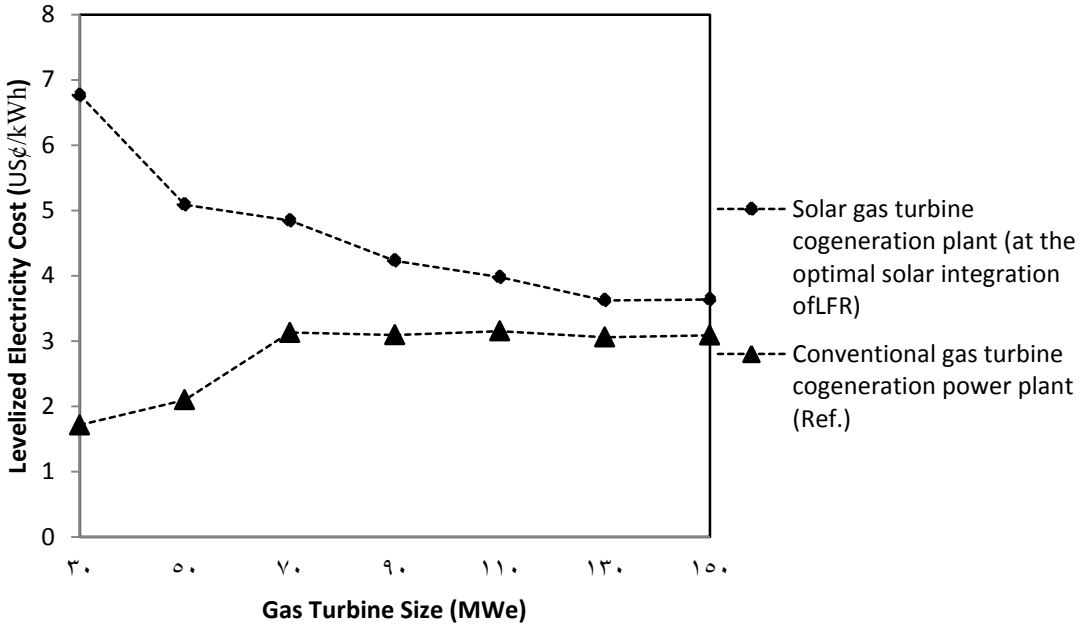

Figure 9.17: LEC for both the conventional gas turbine cogeneration plant and solar gas turbine cogeneration plant (at the optimal LFR integration).

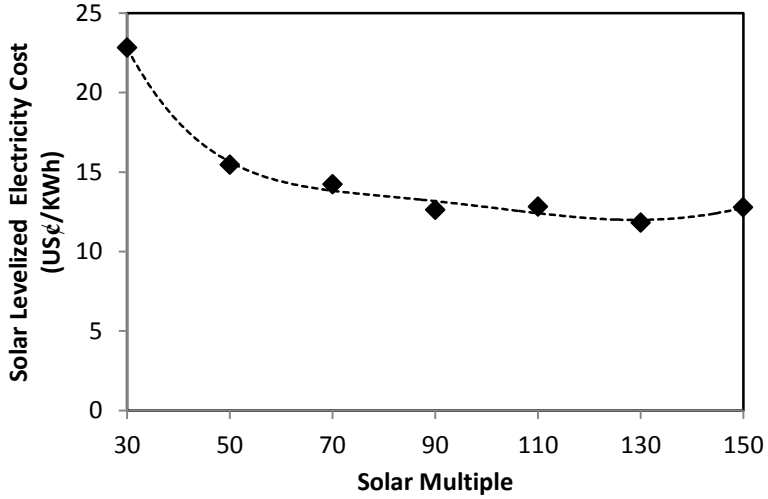

Figure 9.18: Solar levilized electricity cost at the optimal solar integration of LFR for different gas turbine sizes.

Since the integrated LFR with steam side in a gas turbine cogeneration system leads to a logical increment in the levelized energy cost compared to the conventional gas turbine cogeneration power plant, this integration leads to a considerable reduction in CO_2 emission. Figure 9.19 shows the annual CO_2 emission for both, the conventional gas turbine cogeneration power plant, and the integrated optimal solar multiple of LFR system with a gas turbine cogeneration plant.

Annual CO_2 avoidance is the annual reduction of CO_2 emission due to solar energy utilization. Figure 9.20 shows how this factor declined with increasing gas turbine sizes. These results suggest that the cost of integrating solar energy with the conventional gas turbine cogeneration plant might be comparable to integrate the carbon dioxide elimination (avoidance) device to the conventional plant.

As can be seen, the annual CO_2 avoidance for 30 and 50 MWe gas turbine sizes are almost the same. This is because the incremental in CO_2 emission by increasing gas turbine from 30 MWe to 50 MWe are equal (parallel) for both, the conventional gas turbine cogeneration power plant, and the integrated optimal size of LFR system with gas turbine cogeneration plant (Figure 9.18).

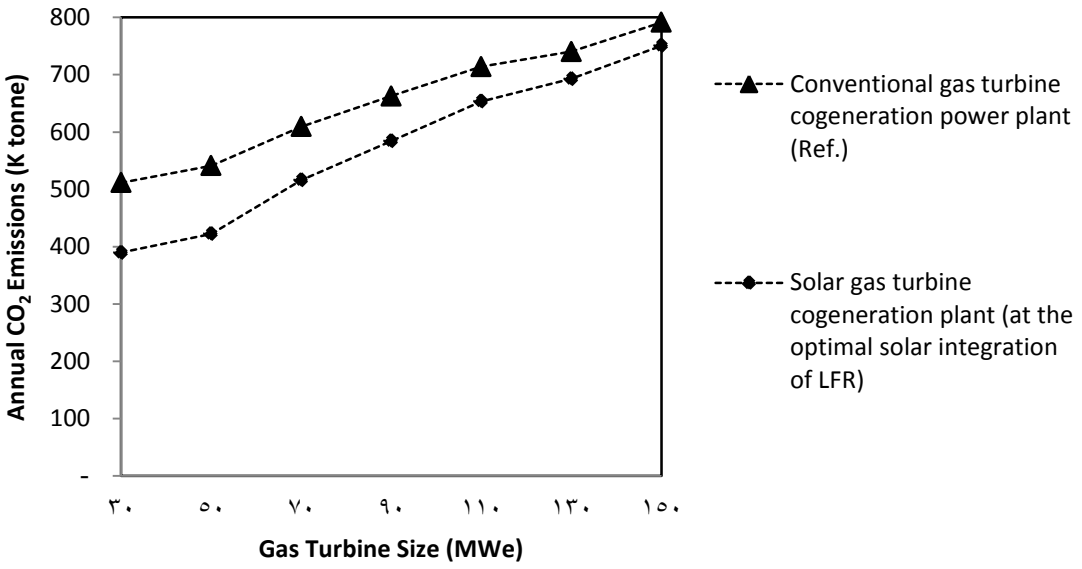

Figure 9.19: Annual CO_2 emissions from both conventional gas turbine cogeneration and solar gas turbine cogeneration plant (at the optimal LFR integration).

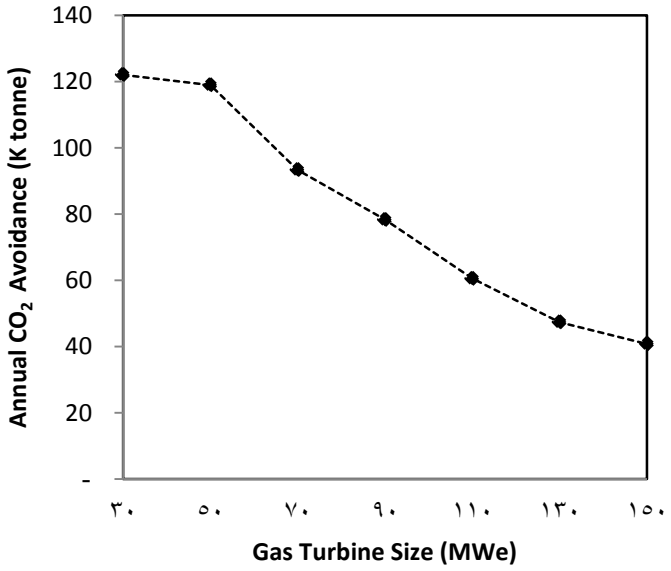

Figure 9.20: Annual CO_2 avoidance at the optimal solar integration of LFR for different gas turbine sizes.

In reality, CO_2 capture technology used to avoid CO_2 emissions from conventional power plants. One of the main importance reasons to integrate solar energy with cogeneration power plant is to avoid CO_2 emissions from power plants. So economical comparing of these two technologies is very importance to assess either integrated solar energy with cogeneration power plant is economical feasible or not. One can use CO_2 capture technology with conventional gas turbine cogeneration power plant to avoid the same CO_2 which avoided by integrating the solar energy. So one can calculate a LEC for conventional power plant with CO_2 capture technology as follows:

First determine the annual CO_2 avoidance, which can be achieved by integrating solar technology. Then multiply that measure with cost of CO_2 capture technology. Divide the eventual by the annual electrical energy for each gas turbine size. Finally add up that amount with the LEC of conventional gas turbine cogeneration power plant. It is important to note the capturing one tonne of CO_2 required 160 US$ [77].

Figure 9.21 illustrates comparison between LEC by using different CO_2 avoiding technologies. As shown, an integrated LFR to gas turbine cogeneration system has proved economical feasibility more than CO_2 capture technology for all gas turbine sizes.

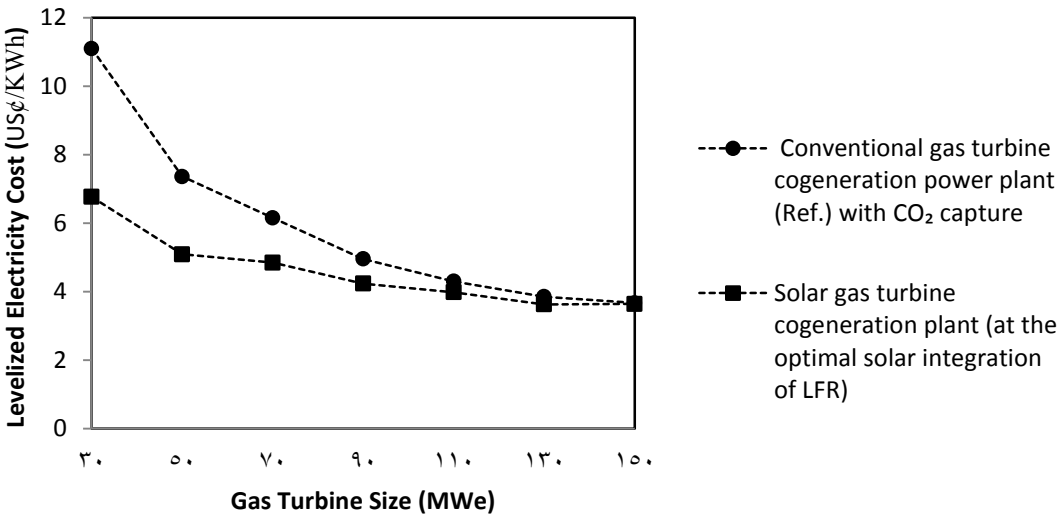

Figure 9.21: Comparison of LEC for different CO_2 avoiding technologies

The solar collector size at the optimal solar multiple has been determined for all gas turbine size integrated with PTC technology. Also levelized electricity cost and annual CO_2 emissions have been determined for all gas turbine size.

Figure 9.22 depicts the Levelized Electricity Cost (LEC) versus annual CO_2 emission for different solar gas turbine plants at optimal design. Point one presents the LEC and annual CO_2 emission of reference cycle with 150 MWe. Where point three presents the LEC and annual CO_2 emission (equal to zero) of linear Fresnel reflector power plant [83]. AREVA's compact linear Fresnel reflector (similar to Novatec Solar Espana's technology) was estimated to have a LEC of $0.137/kWh [83]. Point two presents the LEC and annual CO_2 emission of the present design where annual CO_2 emission is lower. Since gas turbine size of 30 MWe integrated with LFR has the lower CO_2 emission, one can define point two at this design.

The line linked between point one and point three represents the literature reference lines. By comparing present designs with this lines. One can note that the Levelized Electricity Cost (LEC) is reduced by integrating LFR technologies with gas turbine cogeneration system and most present designs are under these lines. This is because two main reasons, first one the industrial simulation land was located in the high insolation region, where the solar energy conversion system can produce the greatest amount of energy from specific solar collector field size; the second one, the output thermal energy in the present design is greater than output electrical energy for all gas turbine size, which doesn't cost a lot.

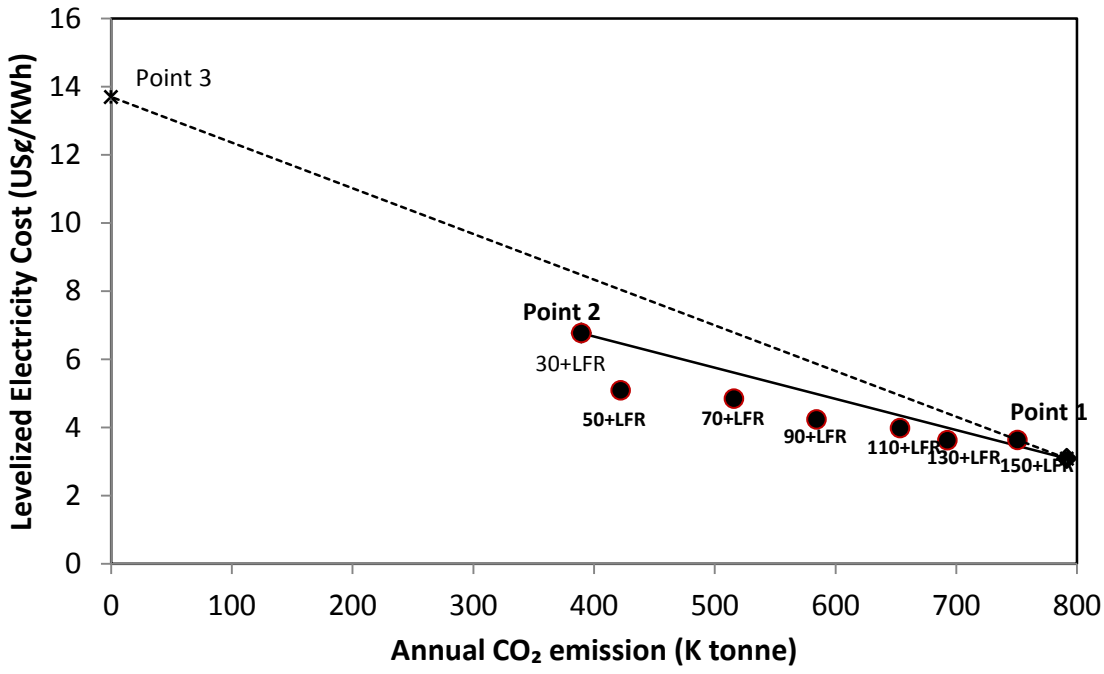

Figure 8.22: Levelized Electricity cost versus annual CO_2 emission for different gas turbine sizes integrated with optimal solar multiple of LFR.

The line linked between point one and point two represents the lowest values for the best designs in the present study. The best designs can be considered as the design when it's representing point located below the line.

According to the results presented in the Figure 8.22, the annual CO_2 avoidance was higher when the LFR was integrated with small gas turbine size. But there was a logical increase in LEC for the integration with small gas turbine size compared to that with large gas turbine sizes. So one can conclude that the integration of the optimal solar multiple of LFR with gas turbine size range between 50 to 90 MWe have a sufficient ability for solar energy utilization with a logical increase in the LEC of energy generated.

Figure 9.23 depicts the total plant efficiency versus annual CO_2 emission for different solar gas turbine plants at optimal design. Point one presents the total plant efficiency and annual CO_2 emission of reference cycle with 150 MWe. Where Point two presents the total plant efficiency and annual CO_2 emission of the present design where annual CO_2 emission is lower. Since gas turbine size of 30 MWe integrated with LFR has the lower CO_2 emission, one can define point two at this design. The line linked between point one and point two represents the higher values for the best designs in the present study. The best designs can be considered as the design when it's representing point located on or above the line.

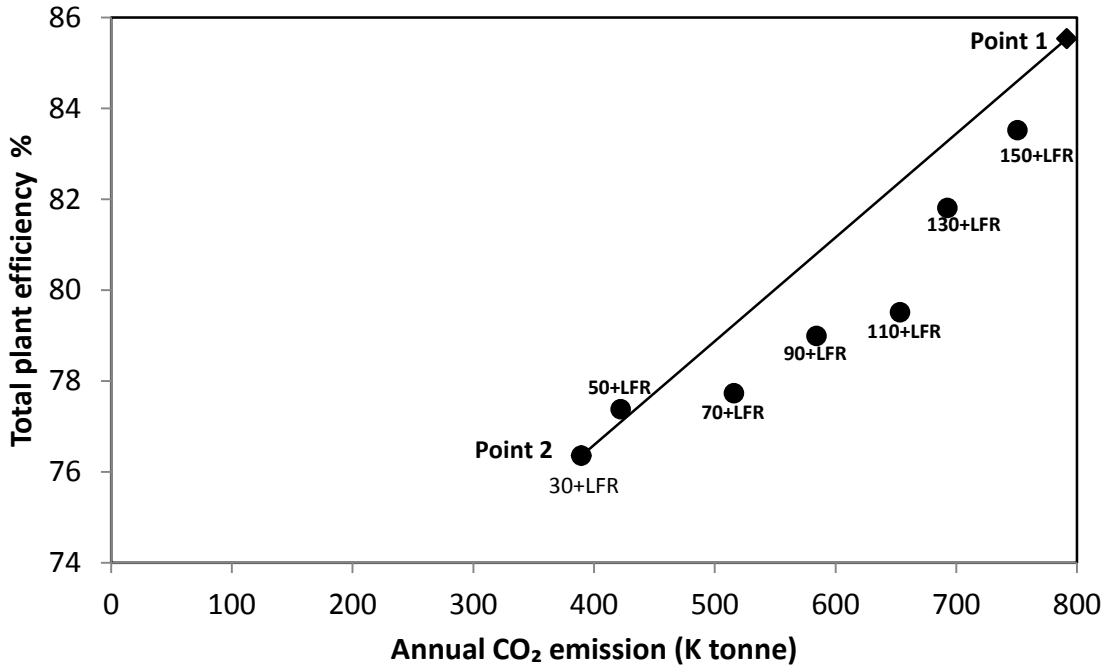

Figure 9.23: Total plant efficiency versus annual CO_2 emission for different gas turbine sizes integrated with optimal solar multiple of LFR.

According to the results presented in the Figure 9.23, the annual CO_2 avoidance and total plant efficiency are best when the LFR was integrated with gas turbine size range between 30 to 50 MWe. But there is a major increase in LEC for the integration with 30 MWe gas turbine size compared that with 50 MWe gas turbine sizes (Figure 9.22). So one can conclude that the integration of the optimal solar multiple (0.8) of LFR with 50 MWe gas turbine size has a sufficient ability for solar energy utilization.

9.3 Concluding Remarks

An integrated LFR with gas turbine cogeneration system that generates steam at a constant flow rate of 81.44 kg/s at P = 45.88 (bar) and temperature of T = 394°C throughout a year in addition to generation of electricity have been simulated and assessed for different sizes of the gas turbine. THERMOFLEX with PEACE simulation software was used to assess the performance of each proposed integration designs. The performance analysis was conducted for a site in Dhahran city at the eastern province of Saudi Arabia. From this study, one can draw the following conclusions:

- Solar energy is a promising technology and introducing integrated LFR with gas turbine cogeneration system offers much potential for large-scale applicability with stable power supply.

- The optimal solar multiple have been determined for integrating a LFR with different gas turbine sizes, which are 0.8, 0.8, 0.6, 0.5, 0.4, 0.3, and 0.3 for gas turbine size 30, 50, 70, 90, 110, 130, and 150 MWe respectively. The optimal solar multiple have been determined to gives the minimum SLEC. At the optimal solar multiple, one can determined solar field sizes, which are 93, 93, 70, 58, 47, 35, and 35 hectares for gas turbine size listed above.

- The LEC is in the range 3.6 US¢ to 6.8 US¢/ kWh in the present study, where the reference [83] reported that the LEC of linear Fresnel reflector power plants was 13.7 US¢/ kWh.

- The annual solar share is higher when the LFR is integrated with small gas turbine size; also the annual CO_2 avoidance is higher when the LFR is integrated with small gas turbine size.

- The results have proved that an integrated LFR with gas turbine cogeneration system has more economical feasibility than CO_2 capture technology for all gas turbine size especially with gas turbine size less than 90 MWe.

- The results have proved that the integration of the optimal solar multiple (0.8) of LFR with 50 MWe gas turbine size has a sufficient ability for solar energy utilization.

CHAPTER 10

SOLAR TOWER SYSTEM INTEGRATED WITH GAS SIDE IN A GAS TURBINE COGENERATION PLANT.

An integrated solar tower (ST) system with gas side in a gas turbine cogeneration plant is used to preheat air before entering the combustion chamber. The exhaust gases are recovered to generate steam with the same amount and at the same conditions mentioned in chapters 7, 8 and 9. The same range of gas turbine sizes was also investigated here. Figure (10.1) depicts a schematic diagram of a solar tower integrated with gas side in gas turbine cogeneration plant.

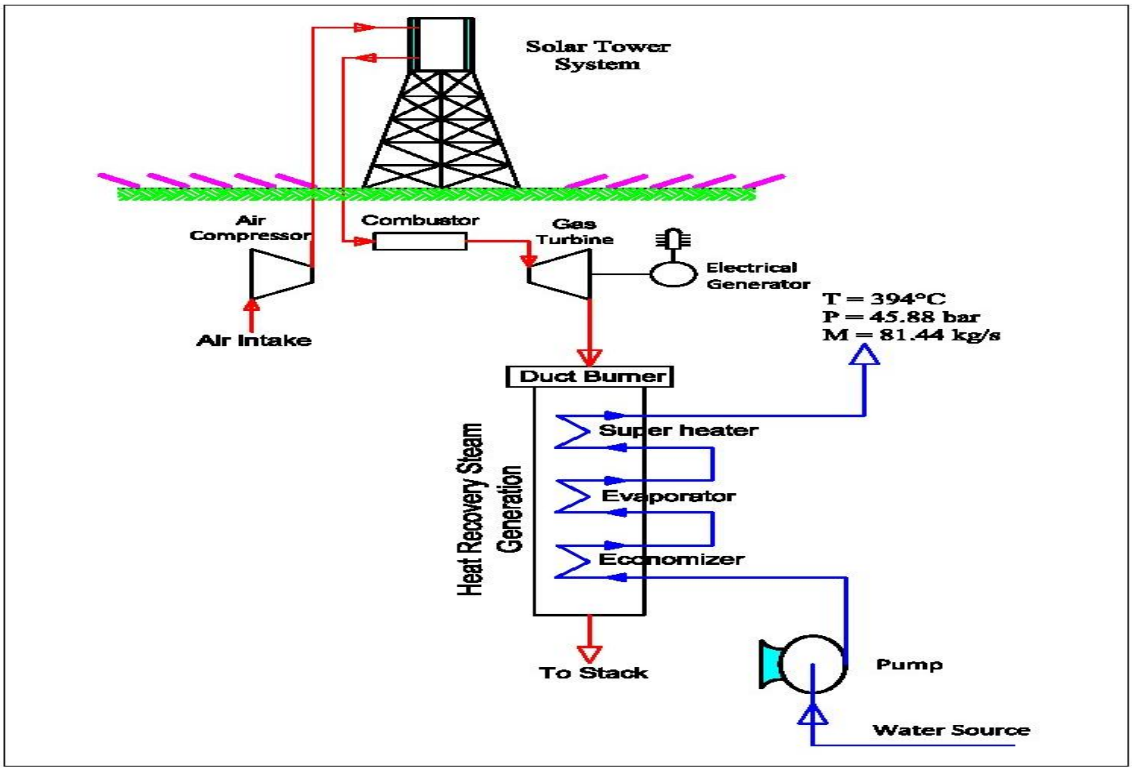

Figure 10.1: Schematic diagram of a solar tower system integrated with gas turbine in a cogeneration plant

10.1 Simulation Procedures of a Gas Turbine Cogeneration Plant Integrated with Solar Tower System

As stated earlier, THERMOFLEX with PEACE software has been used for a simulation. A schematic diagram of an integration ST system with gas side in a gas turbine cogeneration plant as simulated in THERMOFLEX is shown in Fig (10.2). In this study, thermo-economic analyses have been investigated to evaluate and to select the optimal solar tower and heliostat size to be integrated with different sizes of gas turbine.

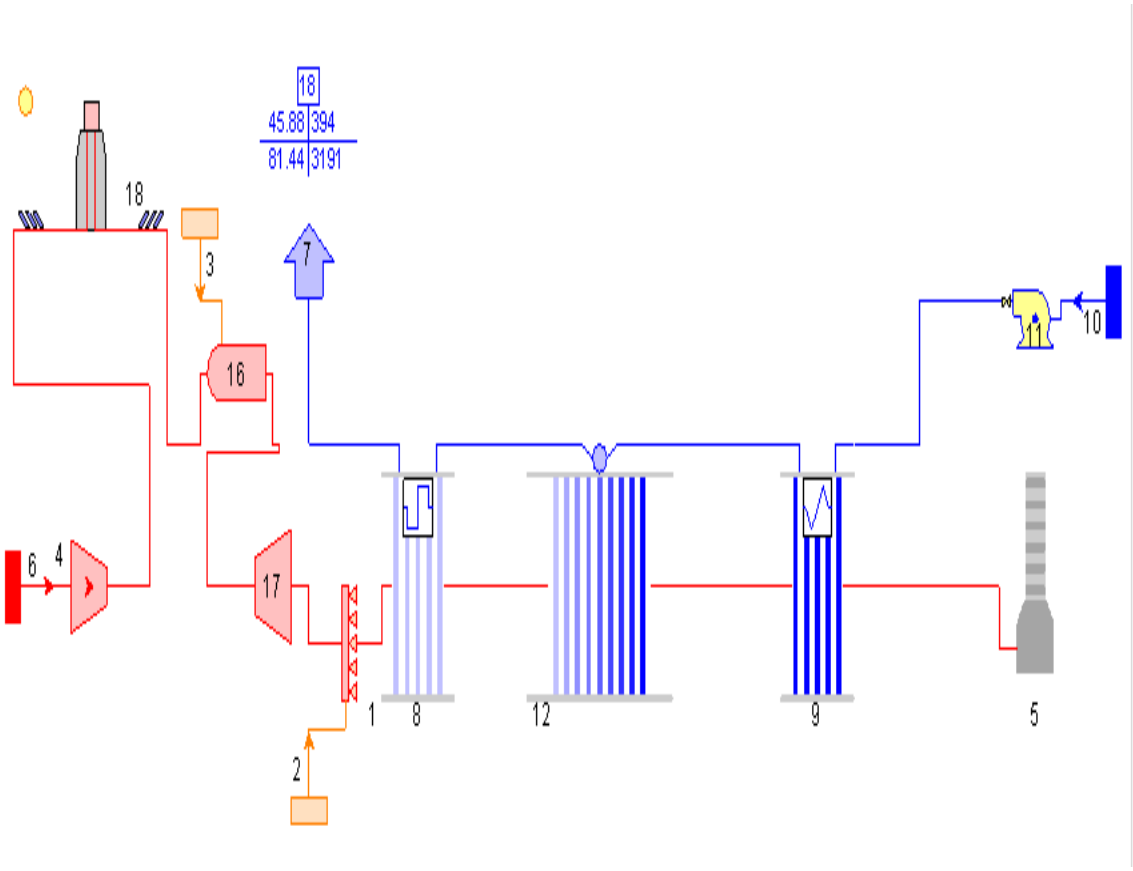

Figure 10.2: Schematic diagram of the gas turbine solar cogeneration plant integrated with a solar tower system as simulated in THERMOFLEX.

As can be seen in Figure 10.1, the plant has one compressor: (4); one gas turbine: (17); one combustion chamber: (16); one duct burner: (1); one superheater: (8); an evaporator: (12); one economizer: (9); solar tower (18); and a pump: (11). In order to simulate the plant's operation in the correct way it is important to bear understand that this plant works at same conditions of plants in chapters 8 and 9. In this cycle, air is preheated through solar tower collector before entering the combustion chamber. After the combustion chamber air is responsible to operate a gas turbine. The exhaust gases from gas turbine are recovered through Heat Recovery Steam Generation (HRSG) system to produce a steam.

Specific steps to simulate gas turbine cogeneration plant integrated with a solar tower system are listed in Figure 10.3. As shown in the Figure, building the configuration by using THERMOFLEX software is the first step of the simulation. After that one needs to enter the latitude (for Dhahran 26.5°), and altitude (for Dhahran 90 m) of the industrial plant location to the program.

In this study; all the operating conditions power plants in chapter 7, 8 and 9 have been used. For examples; the plant was considered to generate steam with a constant flow rate of 81.44 kg/s at P = 45.88 (bar) and T = 394°C throughout a year in addition to generate an electricity; the products manufacturing by General Electric Company as listed in THERMOFLEX program have been used except the 90 MWe gas turbine size was selected from ALSTOM company; the gas turbine was ranged between 30 MWe to 150 MWe.

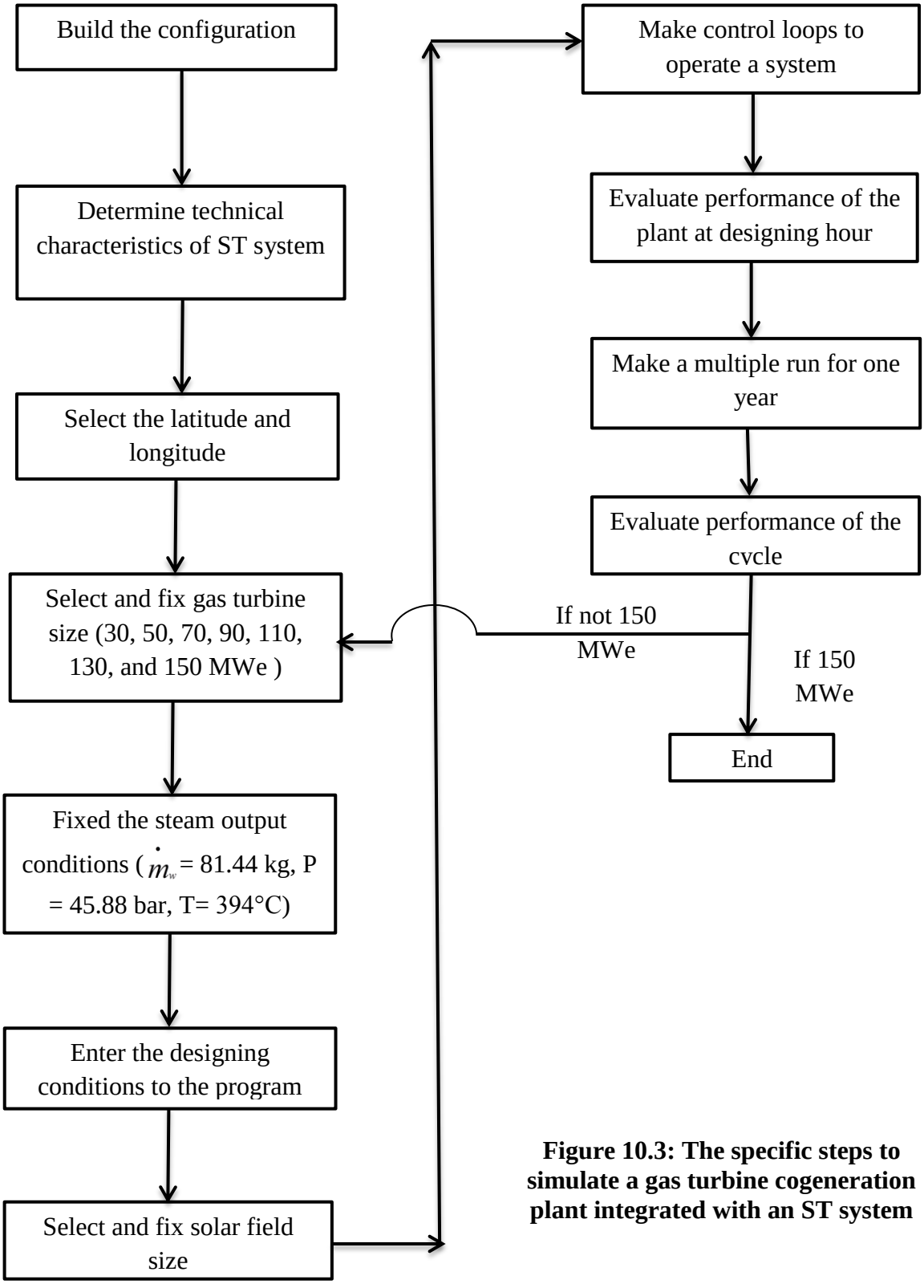

Figure 10.3: The specific steps to simulate a gas turbine cogeneration plant integrated with an ST system

In this cycle, all the default values of water source and fuel components have been used. For example, a 25 °C and 1.014 bars for water temperature and pressure have been selected; and a 25 °C and 20.68 bars for fuel temperature and pressure have been used.

Thermal energy from solar field varies according to the solar radiation intensity. For this reason at any time solar field would not be able to cover specific load, combustion chamber would be operated. In this regards, the control loops have been built to operate combustion chamber to cover the required energy for the gas turbine when the solar field doesn't work or when the output from solar field doesn't cover the required energy for the gas turbine. Furthermore, control loops have been built to operate the duct burner to cover the thermal load of the plant when the exhaust gases for gas turbine couldn't satisfy that thermal load.

In order to make a proper comparison between different designs, the design conditions for calculating solar multiple for solar field size corresponding to each gas turbine size must be fixed. The important parameters for a design condition are average direct solar radiation, average ambient temperature, and average relative humidity. In this study, the maximum average direct solar radiation has been used to calculate solar multiple at design modes, which takes as the average direct solar radiation of June 11 according to table 5.16. The average ambient temperature and relative humidity for the same day have been used for the design conditions.

In this cycle, at starting multiple run for one year, one needs to enter the operating conditions to the program for solar times and non-solar times (sections 5.2 ,5.3, and 5.4). The operating solar time based on 11 hours is used for seven months in the year which are March, April, May, June, July, August, and September. Whereas the operating based on 9 hours is used for the other five months. The operating non-solar time is the remaining daily time from 24 hours. In this configuration the operation at non-solar times is equal to the operation of reference cycle at non- solar time. It is important to enter the all operating conations for all months to the program.

After that, one needs to evaluate performance of the plant at each gas turbine size based on figures of merit in section 4.2.2 such as CO_2 emission, levelized energy cost, and solar levelized energy cost.

The purpose of changing gas turbine size is to find out how much energy would be required from solar field and combustion chamber so as to satisfy the required energy for gas turbine. Moreover, the purpose of changing solar multiple is to achieve the best solar share for each gas turbine size based on figures of merit. The results of this simulation are very importance to find out what will be the optimal solar multiple for each gas turbine size, and what will be the optimal gas turbine size that can be integrated with solar tower system to satisfy the industrial process requirements.

10.2 Simulation Results

A ST solar field size was estimated at maximum average direct solar radiation at Dhahran city, which occurs on June 11 according to Table 5.16. Also the averaged ambient temperature and relative humidity for the same day have been used for the designing conditions.

As mentioned previously, solar multiple is representing ratio of thermal power produced by solar tower system to the required thermal power for gas cogeneration cycle at design hour as shown in Eq. 10.1. The reason behind this way of defining solar multiple in this configuration, solar thermal energy has been utilized in two ways. The first way is direct usage which is preheating air before entering combustion chamber and the second way is indirect usage where exhaust gases have been used to super heat steam in HRSG.

$$SM_{st} = \frac{P_{th,solar}}{P_{th,Gas\ Turbine} + P_{th,duct\ burner}} \quad 10.1$$

$P_{th,solar}$,$P_{th,Gas\ Turbine}$, and $P_{th,duct\ burner}$ can be calculated using the following formulas:

$$P_{th,solar} = \dot{m}_{gas}(\, h_{out,SF} - h_{in,SF}) \quad 10.2$$

$$P_{th,Gas\ Turbine} = \dot{m}_{gas} * C_P * T_{inlet,GT} \quad 10.3$$

$$P_{th,duct\ burner} = \dot{m}_{fuel,duct\ burner} LHV \quad 10.4$$

$P_{th,solar}$: Thermal power produced by solar tower system.

$P_{th,Gas\ Turbine}$: Thermal power inlet to turbine.

$P_{th,duct\ burner}$: Thermal power produced by duct burner.

$\dot{m}_{gas}$: Flow rate of compressed air through solar collector field.

$\mathrm{h}_{\mathrm{outlet,SF}}$: Enthalpy of compressed air at outlet of solar collector field.

$h_{inlet,SF}$: Enthalpy of compressed air at inlet of solar collector field.

C_P : Specific heat.

$T_{inlet,GT}$: Temperature of gases at turbine inlet.

$\dot{m}_{fuel,duct\ burner}$: Fuel flow rate enter to duct burner.

LHV : Lower heat value of fuel.

The input thermal power for a gas turbine cogeneration system is presented in Table 10.1. As shown, the total thermal powers are different for a gas turbine size, which leads to generate different solar multiples for different gas turbine sizes with the same solar field area. In other words, the thermal output from the specific solar field size is constant when it is integrated with different gas turbine size, that means the numerator in Eq. (10.1) is constant for specific solar field size integrated with different gas turbine size, but the denominator in the same equation is different for each gas turbine size. As a result, we couldn't use the solar multiple to present the result in this chapter. The solar filed size has been used to present the results in this chapter.

Table 10.1: Input thermal power to a power plant

Gas turbine	Power enter to turbine $\dot{m} * C_p * T_{inlet\ to\ turbine}$ (kW)	Power enter to duct burner $\dot{m}_{fuel} * LHV$ (kW)	Total power enter to cycle (KW)	Percentage of power enter to turbine %	Percentage of power enter to duct burner %
30	135728.1	211697.5	347425.6	39.1	60.9
50	162540.0	192679.8	355219.8	45.8	54.2
70	255766.6	160399.7	416166.3	61.5	38.5
90	370912.0	136677.5	507589.5	73.1	26.9
110	482576.2	92686.5	575262.7	83.9	16.1
130	484332.2	85680.0	570012.1	85.0	15.0
150	539835.4	60706.6	600542.1	89.9	10.1

As shown in Figure 10.4, solar thermal required from solar field has increasing behavior with increasing solar field size. As a result, solar multiple has increasing behavior with increasing solar thermal obtained from solar field table (10.2). This increasing of solar multiple save more amount of fuel as well as prevent more amount of CO_2 emissions.

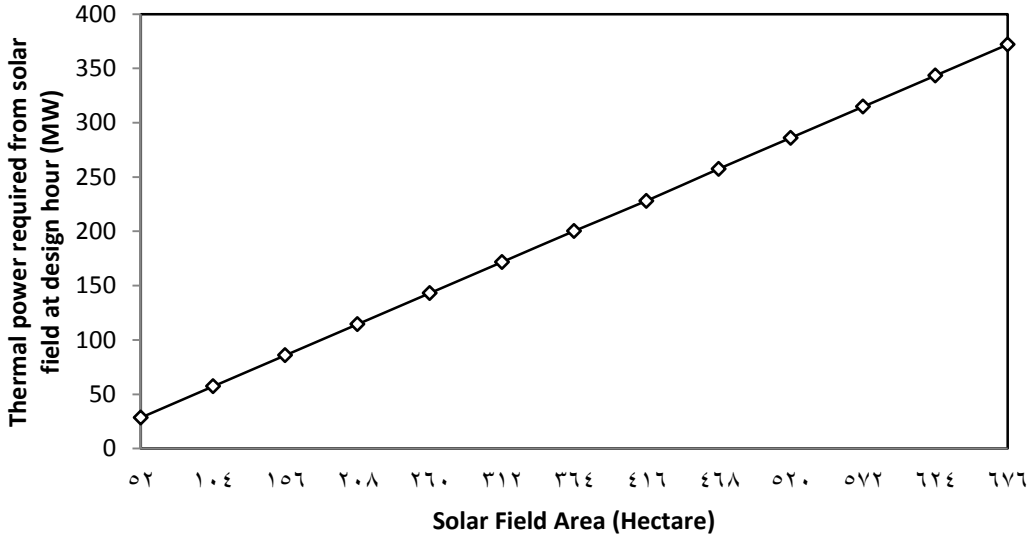

Figure 10.4: Thermal power required from a solar field of an ST at design hour

Table 10.2: Solar multiples for different gas turbine sizes integrated with different solar field areas

	Solar multiple										
Gas	**Solar field area of ST (hectare)**										
Turbine	**52**	**104**	**156**	**208**	**260**	**312**	**364**	**416**	**468**	**520**	**572**
30	0.08	0.16	0.25	0.33	0.41	0.49	0.58	0.66	0.74	0.82	0.91
50	0.08	0.16	0.24	0.32	0.40	0.48	0.56	0.64	0.73	0.81	0.89
70	0.07	0.14	0.22	0.29	0.36	0.43	0.51	0.58	0.65	0.72	0.79
90	0.06	0.12	0.18	0.24	0.30	0.35	0.41	0.47	0.53	0.59	0.65
110	0.05	0.10	0.16	0.21	0.26	0.31	0.37	0.42	0.47	0.52	0.57
130	0.05	0.11	0.16	0.21	0.26	0.32	0.37	0.42	0.47	0.53	0.58
150	0.05	0.10	0.15	0.20	0.25	0.30	0.35	0.40	0.45	0.50	0.55

Figure 10.5 depicts the obtained thermal power from integrate different sizes of ST system with different gas turbine sizes.

As can be seen in Figure 10.5, thermal power obtained from solar field increases significantly when solar field size is increasing up to specific point for each gas turbine size. The maximum specific thermal power required from solar field occurs when fuel consumption by combustion chamber is very close to zero during a solar time. That means there is no room for solar energy integration after that point for each gas turbine; this is because the temperature and mass flow rate of hot gases entering each gas turbine size is constant at design hour. One can note that the optimal solar field area for each gas turbine is almost much close to that specified points as can be seen later on.

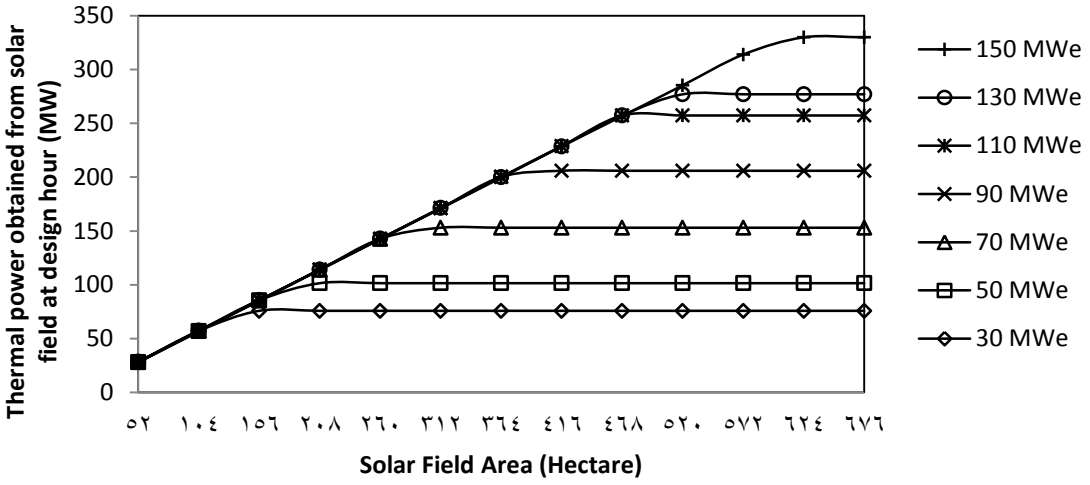

Figure 10.5: Thermal power obtained from solar field of LFR integrated with different gas turbine sizes.

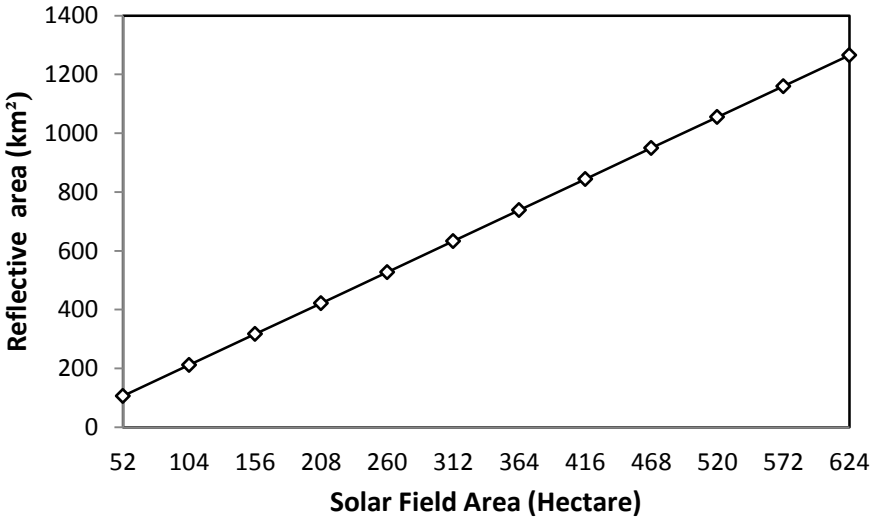

Figure 10.6: Reflective area of an ST system versus land areas.

Furthermore, Figure 10.5 shows that the small gas turbine of 30 MWe does not need much energy from the solar integration at design hour (about 85.2 MW). However, the large gas turbine of 150 MWe has a large amount of thermal power obtained from solar field (about 329.8MW). Figure 10.6 presents a total reflective area of a ST system for

different gas turbine sizes. These results are important for comparing integrations of different solar technologies for different configurations.

Figures of merit such as instantaneous solar share, annual solar share, annual CO_2 avoidance, LEC, and SLEC have been calculated for each gas turbine size at different solar field size in order to assess the performance of integrated ST with gas turbine cogeneration system.

First of all, instantaneous solar share is a ratio of an energy generated from the ST system to a total energy generated from both of the solar and fuel energy input to the plant at the design hour. Figure 10.7 depicts instantaneous solar share for integrating different solar field sizes of ST system with different gas turbine sizes. According to the Figure, an instantaneous solar share is increasing while solar field size is increasing up to specific point for each gas turbine size. Beyond that specified points, the instantaneous solar shares are remaining constants. The reason behind that behavior, is the over sizing of solar field area, which is not usable after that specified point as stated above. Furthermore, the plant with small gas turbine of 30 MWe does not require much energy from the solar integration at design hour. However, the plant with large gas turbine of 150 MWe has a large amount of instantaneous solar share from the solar integration at design hour.

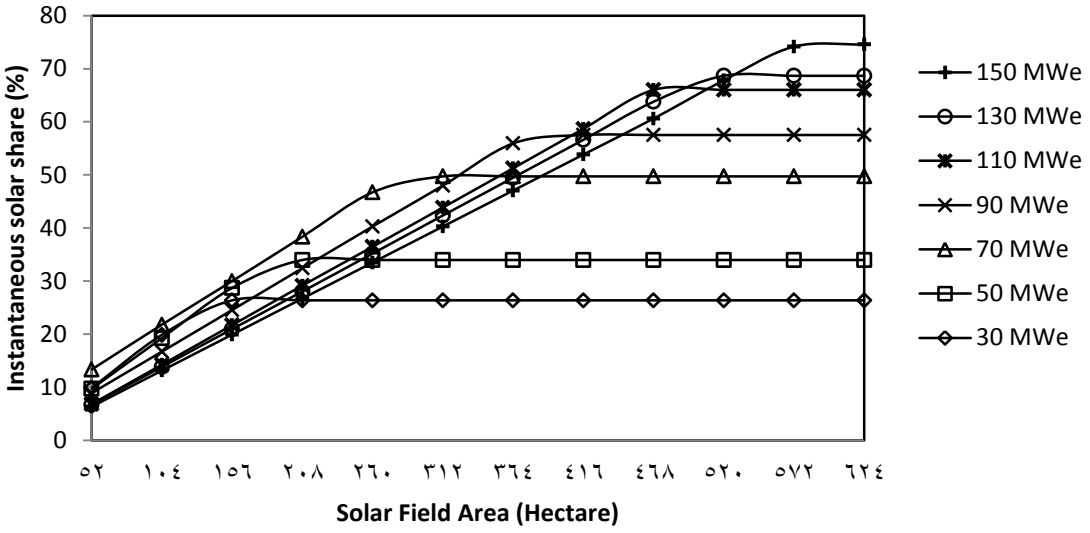

Figure 10.7: Instantaneous solar share for integrating different field sizes of an ST system with different gas turbine sizes.

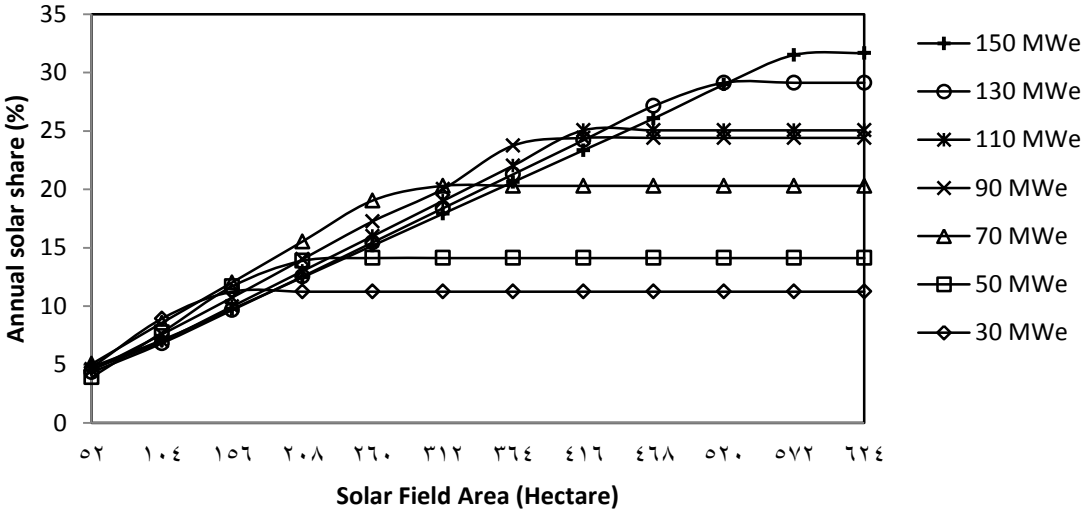

Figure 10.8: Annual solar share for integrating different field sizes of an ST system with different gas turbine sizes.

To calculate how much percent of the energy produced per year from the integrated solar gas turbine cogeneration power plant is due to the solar energy, one needs to calculate the

annual solar share. Figure 10.8 shows how an annual solar share increases in response to increase the solar field size which integrated with different gas turbine size. According to the Figure, the annual solar share rose significantly up to specific solar field size for each gas turbine size. Beyond that specific point, annual solar share remained a constant. The reason behind that behavior is that there is no room for solar energy integration to the plant after that specified points as stated above. Furthermore, Plant with small gas turbine of 130 MWe does not require much annual energy from the solar integration (about 11.2%). However, the small gas turbine of 150 MWe has a large amount of annual solar share (about 31.5%).

Economic analysis has been performed in terms of levelized energy cost (LEC) and solar levelized energy cost (SLEC). The LEC and SLEC are very important thermo-economic figures of merits that are used to estimate the cost of energy production from a given power plant design. Figure 10.9 illustrates the LEC in US¢/kWh for different solar field sizes integrated with different gas turbine sizes. Whereas Figure 10.9 shows how the SLEC varies in response to rise in a solar field area for different gas turbine sizes.

According to simulation results in Figure 10.9, LEC increased slightly by increasing solar field area for gas turbine size greater than 90 MWe. But the incremental is high when the solar field is integrating with gas turbine size less than 90 MWe. This is because the over size of the solar filed is higher for small gas turbine. The LEC couldn't give the optimal solar field size, but SLEC has minimal point, which is corresponding to the optimal solar field size for each gas turbine size.

As shown in Figure 10.10, SLEC declined significantly by increasing solar field size up to specific point for each gas turbine size. Beyond that specific point, SLEC increased dramatically by increasing solar field area. The reason behind that behavior, is the over sizing of solar collector size, which is not fully utilized after that solar filed area. In other words, the optimal specific field area occurs when fuel consumption by combustion chamber is much closed to zero during a solar time. That means there is no room for solar energy integration to the plant after those points. Furthermore, the simulation results seem to show what the optimal solar field area can be integrated with each gas turbine size, this areas was determined at the minimum values of SLEC. The optimal solar field areas are 104, 156, 260, 364, 468, 520, and 572 for gas turbine size 30, 50, 70, 90, 110, 130, and 150 MWe respectively.

Integrating solar tower system with gas turbine cogeneration has an environmental effect since increasing of solar share result in reduction of total fuel consumption, which is required for conventional cogeneration cycle to cover specific load, as a result CO_2 emissions have been reduced as shown in Figure 10.11. In this Figure, the annual CO_2 emissions for a reference gas turbine cogeneration plant were presented at zero solar field area.

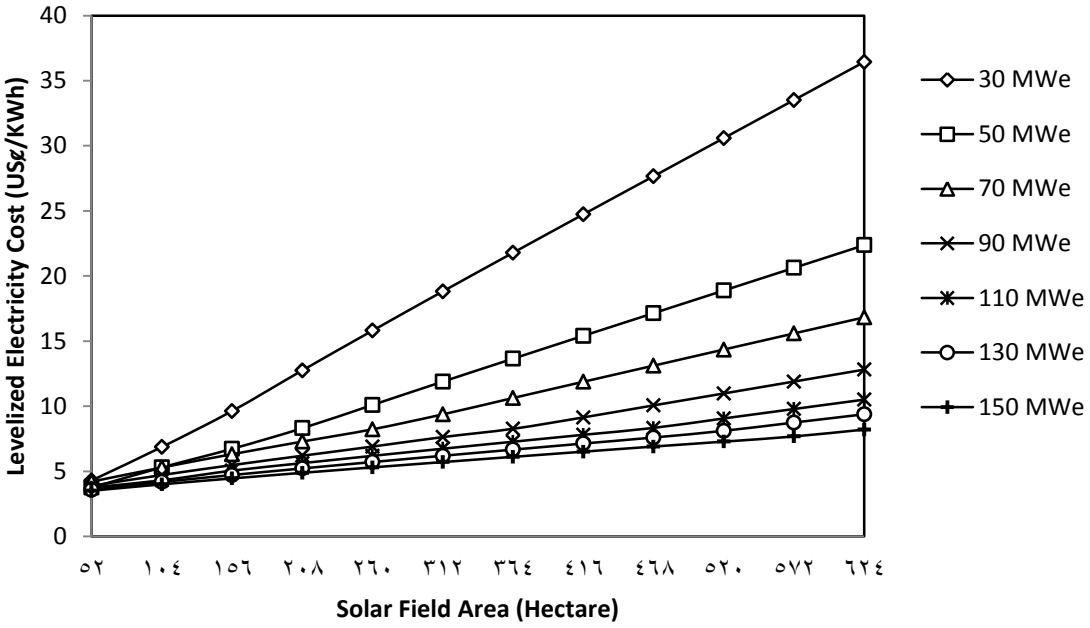

Figure 10.9: Levilized electricity cost for integrating different field sizes of an ST with different gas turbine sizes.

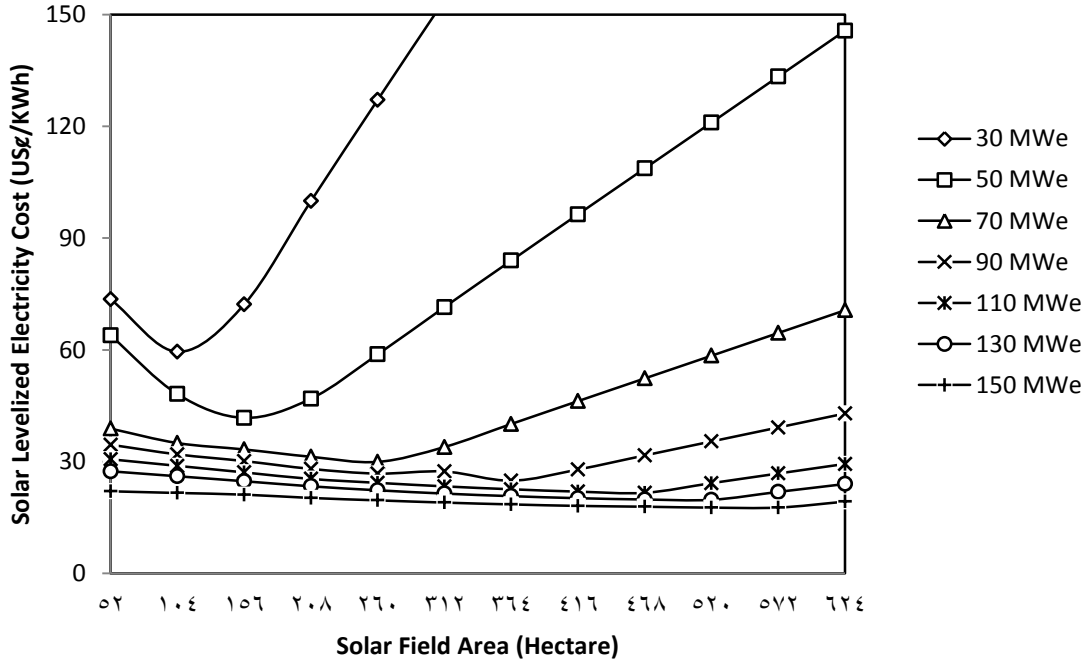

Figure 10.10: Solar levilized electricity cost for integrating different field sizes of an ST with different gas turbine sizes.

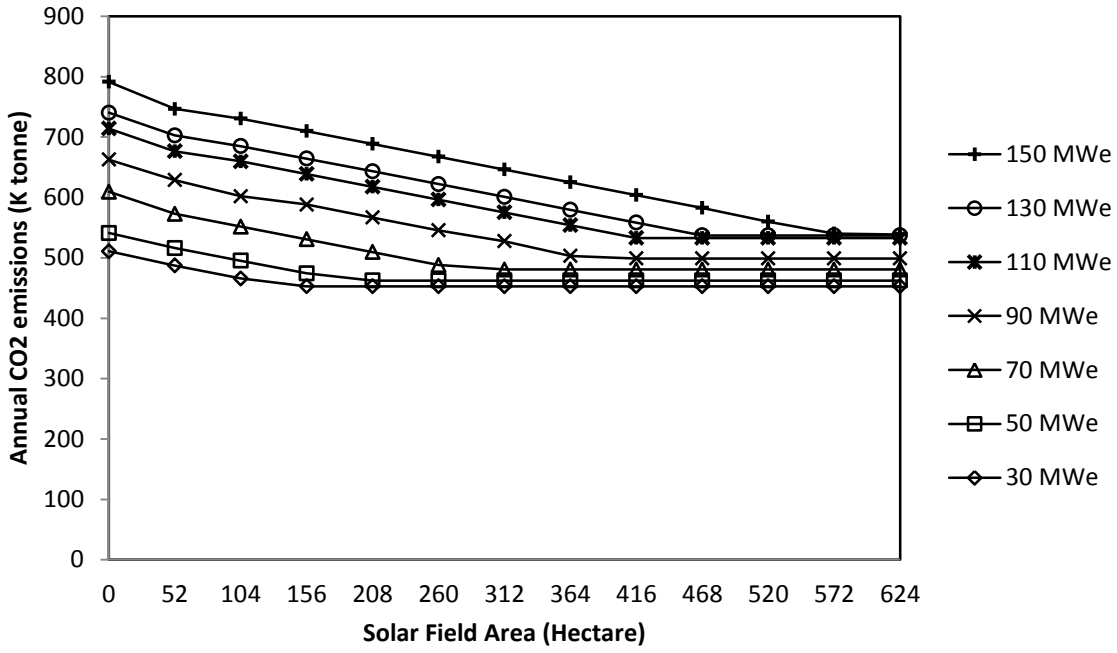

Figure 10.11: Annual CO_2 emissions from different gas turbine plants integrated with different solar field sizes of ST

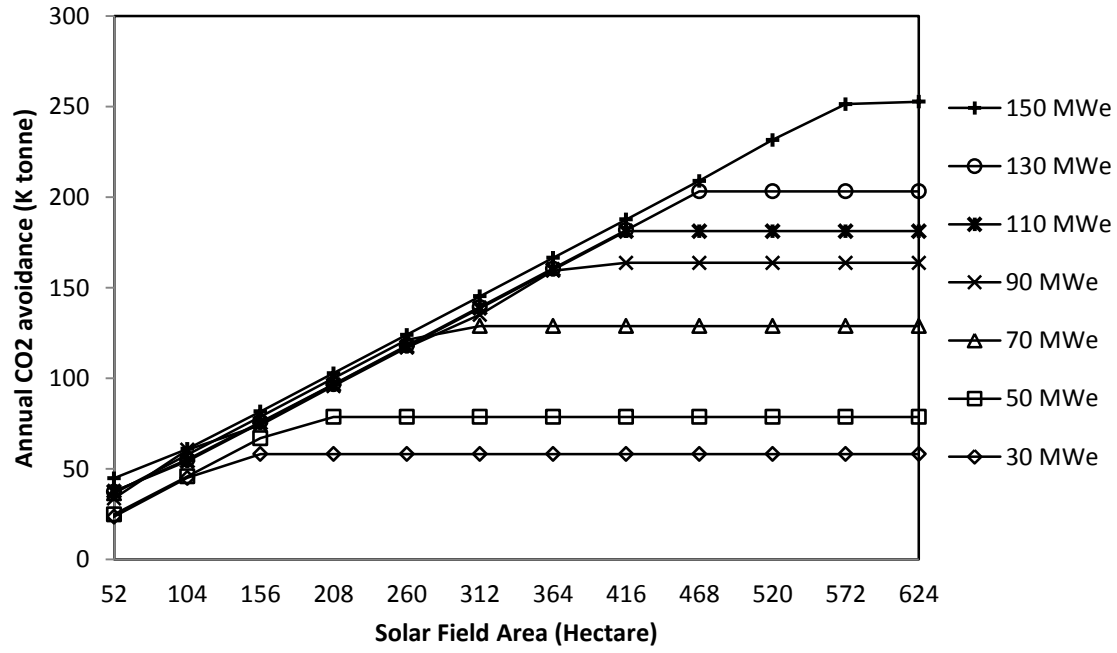

Figure 10.12: Annual CO_2 avoidance for integrating different field sizes of ST with different gas turbine sizes.

An annual CO_2 avoidance is defined as the annual reduction of CO_2 emission due to the solar energy utilization. As can be seen in Figure 10.12, the annual CO_2 avoidance increased significantly by increasing solar field area until reach specific point for each gas turbine size. After that specified points the annual CO_2 avoidance was remaining constants. The best avoidance was achieved by integrating ST system with large gas turbine size of 150 MWe.

the optimal solar field size for integrated ST with different gas turbine size have been determined, which are 104, 156, 260, 364, 468, 520, and 572 hectares for gas turbine size 30, 50, 70, 90, 110, 130, and 150 MWe respectively. One can select the optimal gas turbine size that can be integrated with solar collector by comparing all parameters corresponding to the optimal solar field area for each gas turbine size. Figure 10.13 shows the optimal area of solar field for different gas turbine size. As shown, the optimal field size of ST was increased by increasing gas turbine size. The large gas turbine size has a large solar field area that can be integrated with. This is because; the large gas turbine has a big room in a gas side for solar integration.

The optimal instantaneous solar share can be achieved by integrating ST system with different gas turbine size has been identified. Figure 10.14 shows that the optimal instantaneous solar shares have increased behavior with increasing gas turbine size.

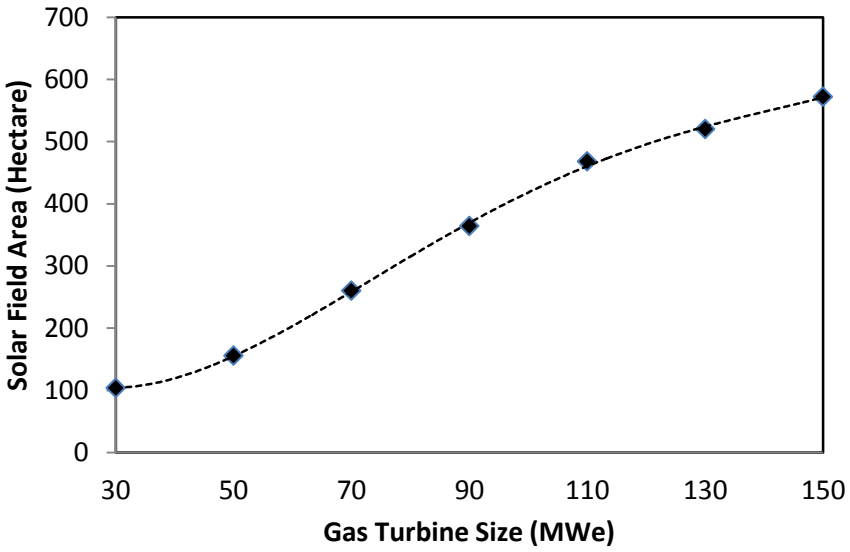

Figure 10.13: Solar field area of ST system at the optimal solar integration for different gas turbine sizes.

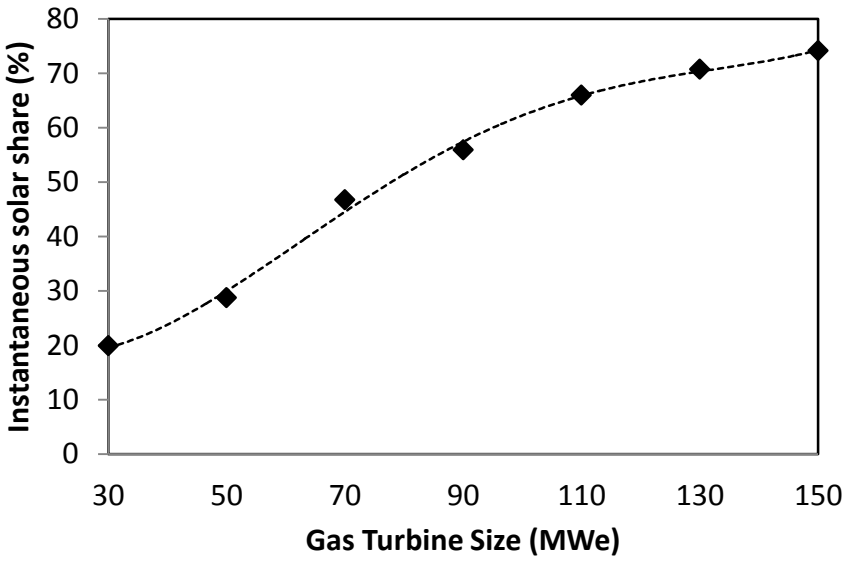

Figure 10.14: Instantaneous solar share at the optimal solar integration of ST for different gas turbine sizes.

To find out what percent of the energy produced per year from the proposed plant is from solar energy, one needs to calculate an annual solar shares. The annual solar share at the optimal solar integration is presented in Figure 10.15 for different gas turbine sizes. As

expected, the optimal solar share is higher when the ST integrated with a large gas turbine size. For example, the optimal annual solar share is 31.5% for integrating ST system with 150 MWe gas turbine size, whereas it is 8.9%, for integrating ST system with 30 MWe gas turbine size.

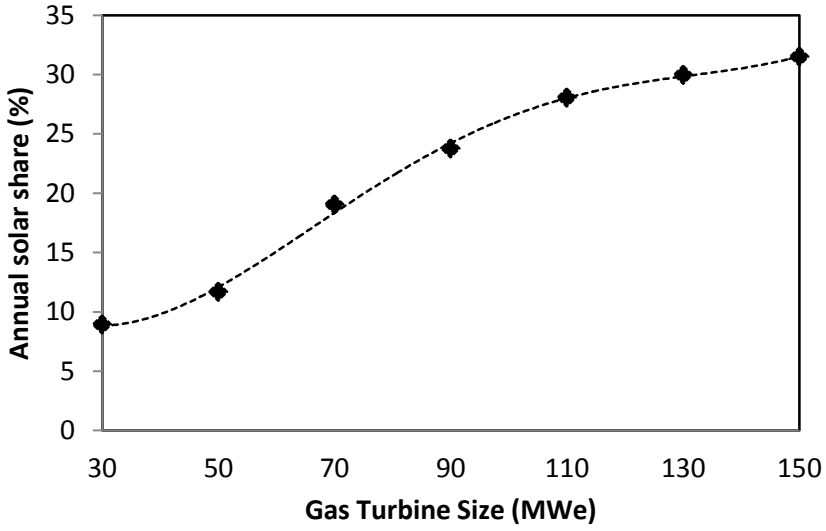

Figure 10.15: Annual solar share at the optimal solar integration of ST for different gas turbine sizes

A LEC was evaluated for both, the conventional gas turbine cogeneration and the integrated optimal size if ST system with gas turbine cogeneration plant (Figure 10.16). The results in this Figure indicate that integrating ST with the conventional gas turbine cogeneration plant will result in a major increase in the LEC compared to the conventional cogeneration power plant. LEC couldn't give the optimal gas turbine size, but SLEC has minimal points, which are corresponding to the optimal gas turbine size. The SLEC for the optimal solar integration with different gas turbine size was presented in Figure 10.17. As shown, the hybrid solar gas turbine cogeneration systems with the gas

turbine greater than 90 MWe have the lowest SLEC to convert solar energy into thermal energy.

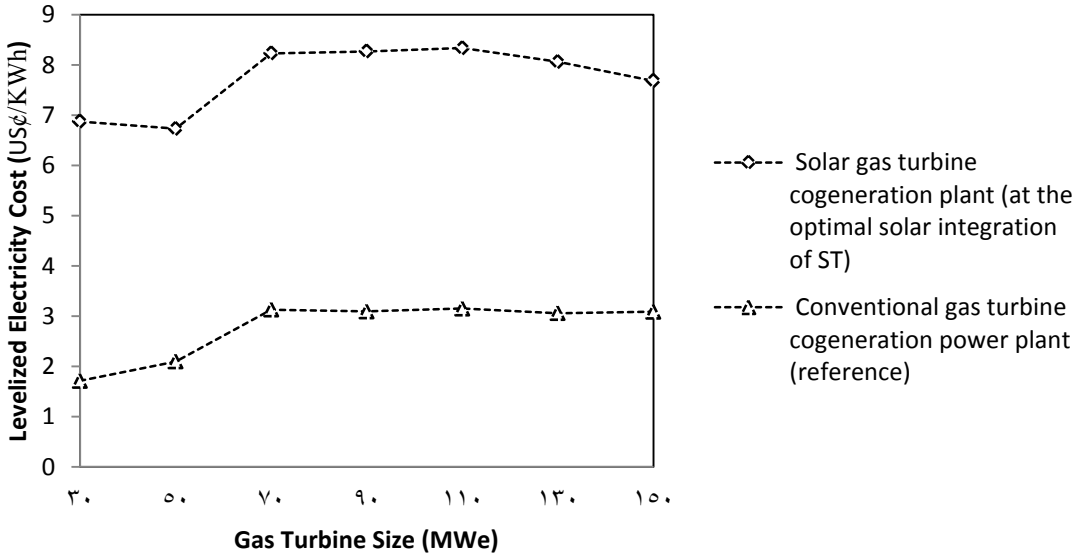

Figure 10.16: LEC for both the conventional gas turbine cogeneration plant and solar gas turbine cogeneration plant (at the optimal ST integration).

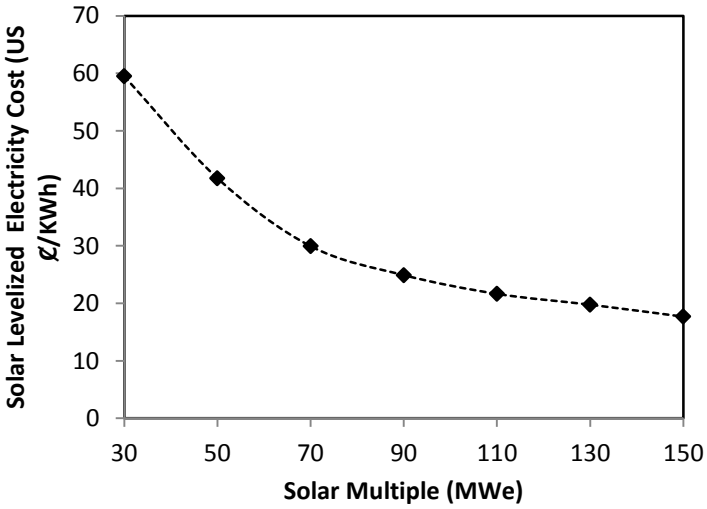

Figure 10.17: SLEC at the optimal solar integration of ST for different gas turbine sizes.

Since the integrated ST with gas side in a gas turbine cogeneration system leads to a major incremental in the levelized energy cost compared to the conventional gas turbine cogeneration power plant, the integration leads to a considerable reduction in CO_2 emission. Figure 10.18 depicts the annual CO_2 emission for both, the integrated optmail size of ST with gas turbine cogeneration system and the conventional gas turbine cogeneration system.

Annual CO_2 avoidance is defined as the annual reduction of CO_2 emission due to the solar energy utilization. Figure 10.19 shows the annual CO_2 avoidance, which is the difference between the amount of CO_2 emissions from both, the conventional gas turbine cogeneration power plant and the integrated ST system with gas turbine cogeneration plant.

As shown in Figure 10.19, the minimum CO_2 avoidance was for integrated ST with 30 MWe gas turbine size (45 K tonne of CO_2), and this avoidance increases with increasing gas turbine size, which leaves with 251 K tonne of CO_2 for 150 MWe. These results suggest that the cost of integrating solar energy with the conventional gas turbine cogeneration plant might be comparable to the integration of carbon dioxide elimination (avoidance) device to the conventional plant.

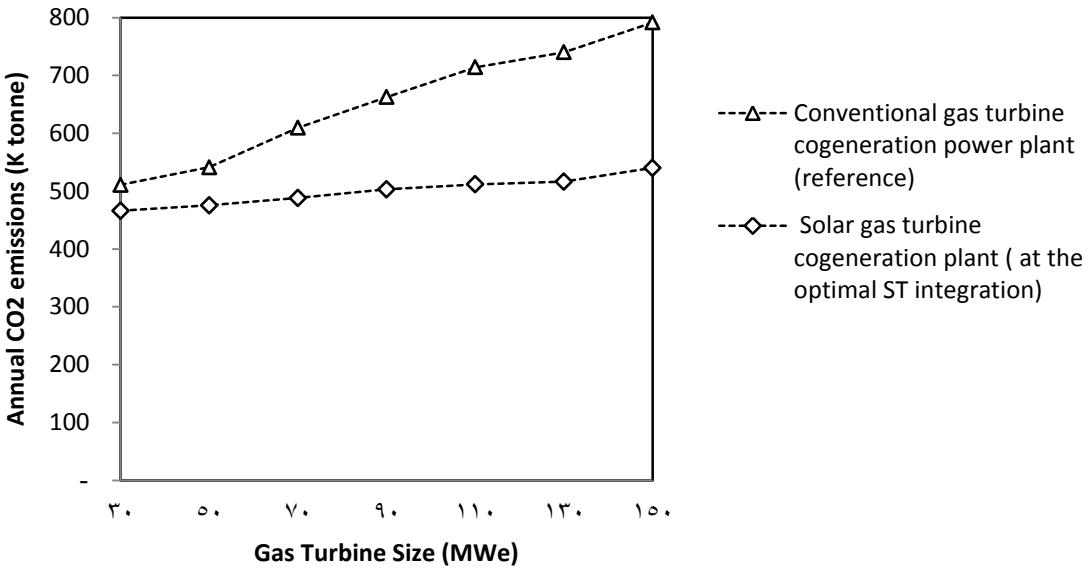

Figure 10.18: Annual CO_2 emissions from both conventional gas turbine cogeneration and solar gas turbine cogeneration plant (at the optimal ST integration).

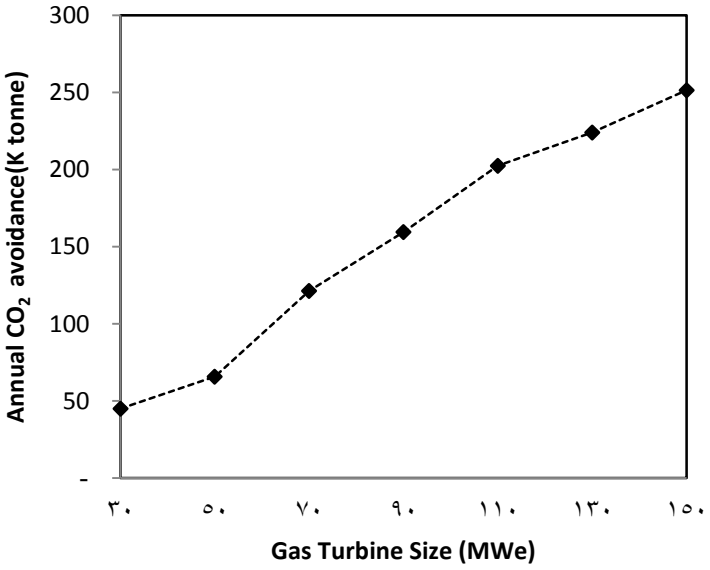

Figure 10.19: Annual CO_2 avoidance at the optimal solar integration of ST for different gas turbine sizes.

In reality, CO_2 capture technology is used to avoid CO_2 emissions from conventional power plants. One of the main importance reasons to integrate solar energy with cogeneration power plant is to avoid CO_2 emissions from power plants. So economical comparing of these two different technologies for CO_2 avoidance is very importance to assess wither integrated solar energy with cogeneration power plant is economical feasible or not. One can use a capture technologies with conventional power plant to avoid the same CO_2 emissions, which avoided by integrating solar energy. It is worth to note the capturing one tonne of CO_2 required 160 US$ [77].

Figure 10.20 presents a comparison between LEC by using different CO_2 avoiding technologies. As shown, integrated ST with gas turbine cogeneration system has proved the economical feasibility less than CO_2 capture technology.

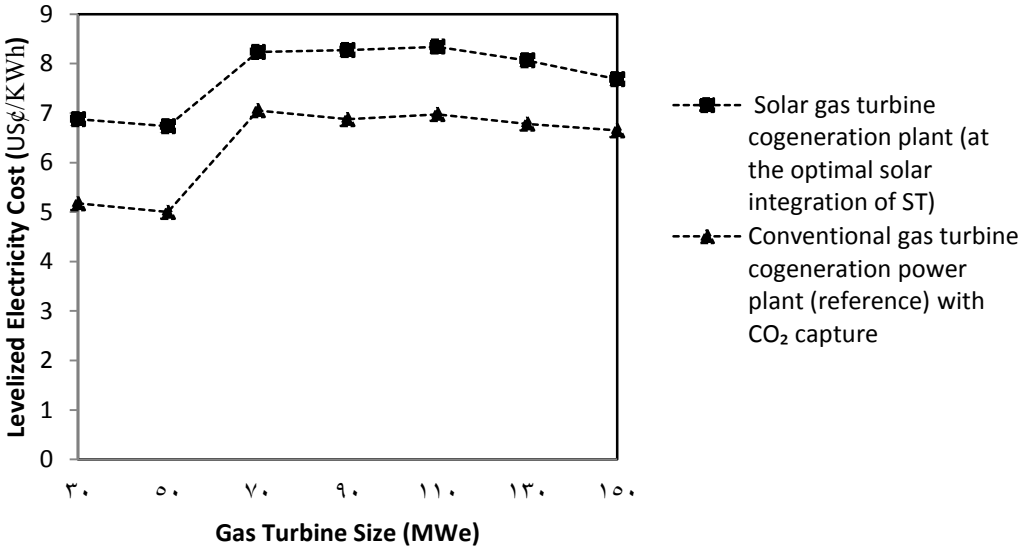

Figure 10.20: Comparing LEC for different CO_2 avoiding technologies

The solar collector size at the optimal solar integration has been determined for all gas turbine size integrated with ST technology. Also levelized electricity cost (LEC) and annual CO_2 emissions have been determined for all gas turbine size. The International Renewable Energy Agency reported in 2012 that the LEC of solar tower power plants were in the range 17 to 26 US¢/ kWh [78]. So one can compare the LEC of the present study with the minimum value of LEC reported by International Renewable Energy Agency, which is 17 US¢/ kWh.

Figure 10.21 depicts the LEC versus annual CO_2 emission for different solar gas turbine plants at optimal design. Point one presents the LEC and annual CO_2 emission of reference cycle with 150 MWe. Where point three presents the minimum LEC and annual CO_2 emission (equal to zero) of solar tower power plant [78]. Point two presents the LEC and annual CO_2 emission of the present design where annual CO_2 emission is lower. Since gas turbine size of 30 MWe integrated with ST has the lower CO_2 emission, one can define point two at this design.

The line linked between point one and point three represents the literature reference lines. By comparing present designs with this line, one can note that the LEC is reduced by integrating ST technology with gas turbine cogeneration system and some present designs are under these lines. The line linked between point one and point two represents the lowest values for the best designs in the present study. The best designs can be considered as the design when it's representing point located below or on the line.

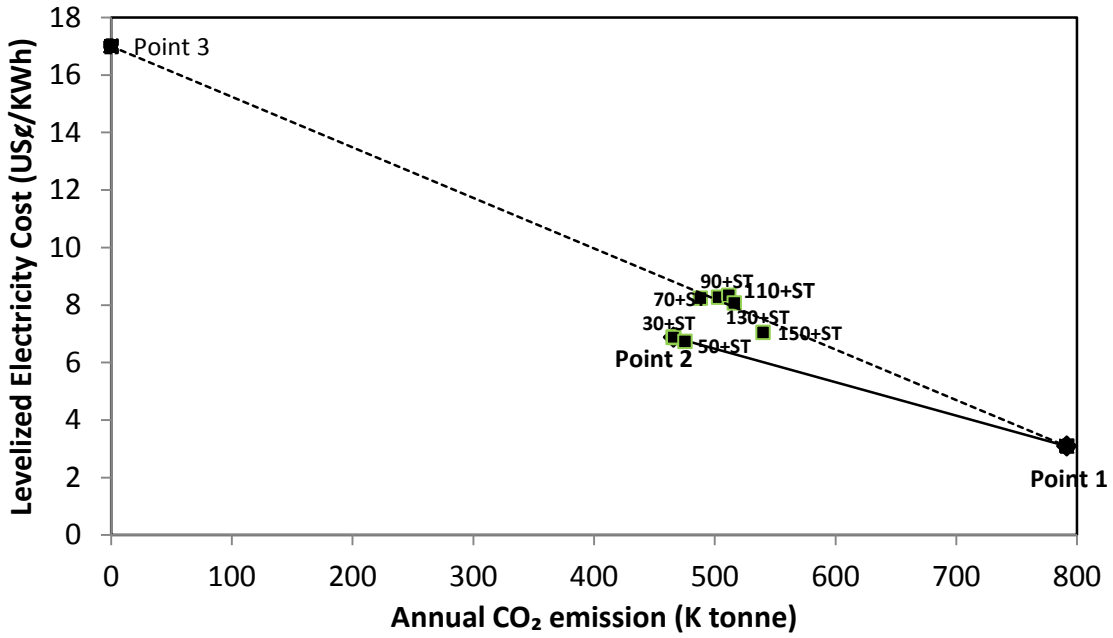

Figure 10.21: Levelized electricity cost versus annual CO_2 emission for different gas turbine sizes integrated with optimal solar integration of ST.

According to the results presented in the Figure 10.21, the annual CO_2 avoidance is higher when the ST is integrated with small gas turbine size, and the LEC is higher when the ST is integrated with small gas turbine size. So one can conclude that the integration of the optimal solar filed size of ST with gas turbine size range between 30 to 50 MWe have a sufficient ability for solar energy utilization.

Figure 10.22 depicts the total plant efficiency versus annual CO_2 emission for different solar gas turbine plants at optimal design. Point one presents the total plant efficiency and annual CO_2 emission of reference cycle with 150 MWe. Where Point two presents the total plant efficiency and annual CO_2 emission of the present design where annual CO_2 emission is lower. Since gas turbine size of 30 MWe integrated with ST has the lower

CO_2 emission, one can define point two at this design. The line linked between point one and point two represents the higher values for the best designs in the present study. The best designs can be considered as the design when it's representing point located on or close the line.

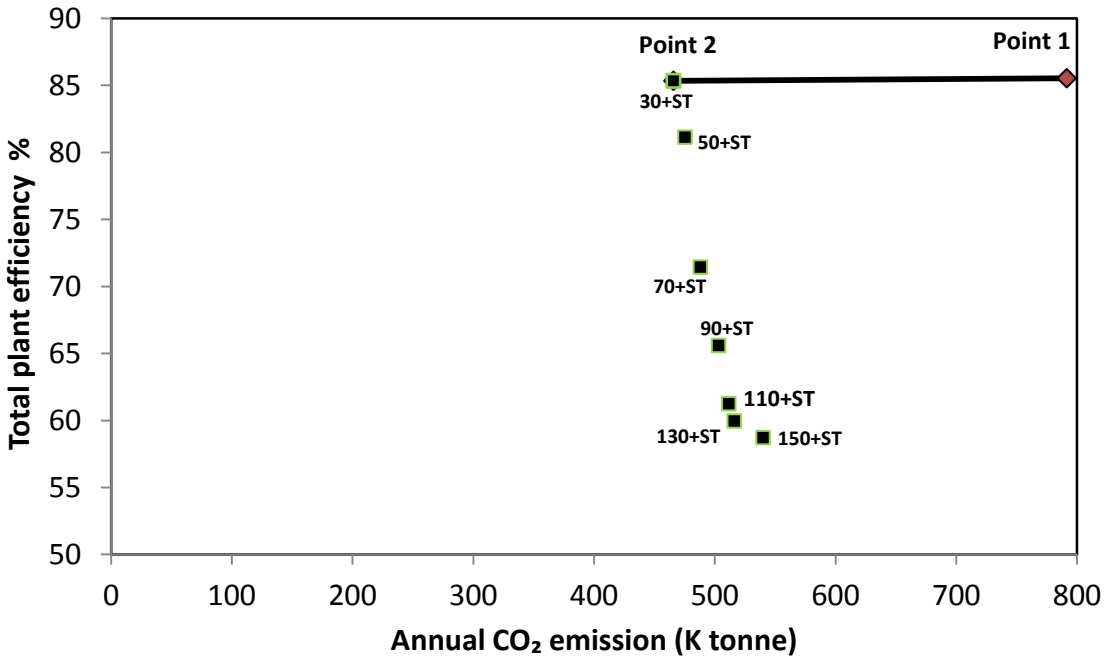

Figure 10.22: Total plant efficiency versus annual CO_2 emission for different gas turbine sizes integrated with optimal solar multiple of ST.

According to the results presented in the Figure 8.23, the annual CO_2 avoidance and total plant efficiency are higher when the 104 hectare of ST system is integrated with 30 MWe gas turbine size. According to Figure 10.21, the integration of the optimal solar filed size of ST with gas turbine size range between 30 and 50 MWe have a sufficient ability for solar energy utilization. One can conclude that the 30 MWe gas turbine size integrated with optimal solar field area (104 hectare) of solar tower has a sufficient ability for solar energy utilization.

10.3 Concluding Remarks

An integrated solar gas turbine cogeneration system that generates steam at a constant flow rate of 81.44 kg/s at P = 45.88 (bar) and temperature of T = 394°C throughout the year in addition to the generation of electricity have been simulated and assessed for different the gas turbine sizes. THERMOFLEX with PEACE simulation software was used to assess the performance of each proposed integration designs. The Thermo-economical analysis was conducted for a site in Dhahran city at the eastern province of Saudi Arabia. From this study, one can draw the following conclusions:

- Solar energy is a promising technology and introducing integrated ST with gas turbine cogeneration system offers much potential for large-scale application with stable power supply.
- The optimal solar field areas have been determined for integrating ST with different gas turbine size, which are 104, 156, 260, 364, 468, 520, and 572 hectare for gas turbine size 30, 50, 70, 90, 110, 130, and 150 MWe respectively.
- The results have proved that the annual solar share was higher when the ST is integrated with a large gas turbine size; also the annual CO_2 avoidance is higher when the ST integrated with a large gas turbine size.
- The LEC of electricity from gas turbine cogeneration integrated with ST system is ranged between 6.9 US¢ to 8.4 US¢/ kWh in the present study. Where the

International Renewable Energy Agency reported in 2012 that the LEC of solar tower power plants was in the range 17 US¢ to 29 US¢/ kWh [78].

- The results indicate that an integrating the ST with a conventional gas turbine cogeneration plant will result in a major increase in the LEC compared to the conventional cogeneration power plant.

- The results have proved that the integrated ST with gas turbine cogeneration system has less economical feasibility than CO_2 capture technology.

- The results have proved that the 30 MWe gas turbine size integrated with optimal solar field area (104 hectare) of solar tower has a sufficient ability for solar energy utilization.

CHAPTER 11

COMPARISON OF THE THREE MAIN CONCENTRATING SOLAR POWER TECHNOLOGIES

Till now there are no reliable data for Fresnel power plants because up to now there is no large Fresnel power plant in operation, except the first large plant, Novatec Solar's PE2 with 30MW which has been completed and it is in operation since August 2012 [79]. After the construction of the Solarmundo collector in Liege/Belgium, Haberle with his team claimed that the total cost of Solarmundo collector was reduced by nearly 50% compared to the parabolic trough solar collector (measured in €/m^2 of aperture area)

In the year 2012, Morin et al. made a comparative study between a 50 MW linear Fresnel power plant and a 50 MW parabolic trough power plant [81]. In their study; a direct steam generating systems have been considered; The Euro trough has been used as a type parabolic trough collector and the PSA have been used as a type Fresnel linear Fresnel reflector; both plants was considered without thermal storage. Their results have proven that the solar field of a linear Fresnel power plant must achieve installation costs of about 55% of the specific installation costs of a parabolic trough field (measured in €/m^2 of aperture area) in order to enable a Fresnel power plant to reach the same LEC like a parabolic trough power plant and, hence, to be cost-competitive with it.

In the present study, comparison was carried out in terms of Thermo-economic performance. In order to outline some advantages and drawbacks of three Concentrating Solar Power (CSP) technologies, three different configurations was investigated: the first based on integrate a PTC with steam generation side in a gas turbine cogeneration power plant, the second based on integrate a LFR with steam generation side in a gas turbine cogeneration power plant, and the third one based on integrate ST with gas side in a gas turbine cogeneration power plant. Thermo-economic assessment was carried out with a commercial code named THERMOFLEX with PEACE. This code, originally developed to assess performances at nominal and off-design conditions, has recently included also solar field component.

In order to make a consistent comparison, all solar plants are designed at the same designing conditions in Dhahran city at the eastern province of Saudi Arabia; all the plants are considered to generate steam at a constant flow rate of 81.44 kg/s at P = 45.88 (bar) and temperature of T = 394°C around the year; all the plants are considered with same gas turbine size which ranged between 30 to 150 MWe.

11.1 How to Calculate Levelized Energy Cost, and Solar Levelized Energy Cost

It is well known; in the cogeneration system there are two main products, which are steam and electric energy. According to literature [44, 45, 46, 47, and 48] one can calculate the Levelized Energy Cost (LEC) of cogeneration system by fixing the cost of one of the products (usually steam) at its local market price, and calculate the net cost of the other (usually electricity). The first definition was used to calculate LEC in the earlier chapters. To make a consistent comparison we used the other two definitions this chapter.

1) When the electricity is the primary product and the steam is the byproduct, one can used Eq. 11.1 to calculate LEC. In the present study, a steam price was assumed higher than the respective fuel price by 20% [44, and 45]. Levelized Electricity Cost (LEC_1) could be defined as follows;

$$LEC_1 = \frac{I_{tot} * fcr + OM_{ann} + F_{ann} - steam\ energy\ cost}{E_{electrical,ann}} \quad (11.1)$$

2) When the steam is the primary product and the electricity is the byproduct, one can used Eq. 11.1 to calculate LEC In the present study; the electricity price was assumed 5 US¢/kWh [46]. Levelized Thermal Energy Cost (LEC_2) could be defined as follows;

$$LEC_2 = \frac{I_{tot} * fcr + OM_{ann} + F_{ann} - electrical\ energy\ cost}{E_{thermal,ann}} \quad (11.2)$$

3) When the steam and electricity are the primary products, Levelized Energy Cost (LEC_3) could be defined as follows;

$$LEC_3 = \frac{I_{tot} * fcr + OM_{ann} + F_{ann}}{E_{thermal,ann} + E_{electrical,ann}} \quad (11.3)$$

Where

I_{tot} : Total investment cost.

fcr : Annuity factor.

OM_{ann} : Annual operation and maintenance costs.

F_{ann} : Annual cost of fuel consumption

E_{ann} : Annual total electrical energy (kWh)

According to Dersch at el. [34] the calculation of solar levelized energy cost can be considered when the annual solar share is based on input and output data (fuel consumption/kWh) as shown in the following formula.

$$SLEC = \frac{LEC_{ISGC} - \left[(1 - SS) * LEC_{GCP,Ref}\right]}{SS} \quad (11.4)$$

LEC_{ISGC} : levelized energy cost for integrated gas turbine solar cogeneration power

$LEC_{GCP,Ref}$: levelized energy cost for gas turbine cogeneration power (reference cycle)

SS : Annual solar share

Since SLEC is a function in LEC definition, and three definition of LEC one can get three definition of SLEC as follows:

$$SLEC_1 = \frac{LEC_{ISGC,1} - \left[(1 - SS) * LEC_{Ref,1}\right]}{SS} \quad (11.5)$$

$$SLEC_2 = \frac{LEC_{ISGC,2} - \left[(1 - SS) * LEC_{Ref,2}\right]}{SS} \quad (11.6)$$

$$SLEC_3 = \frac{LEC_{ISGC,3} - \left[(1 - SS) * LEC_{Ref,3}\right]}{SS} \quad (11.7)$$

11.2 Comparing Results of all Configurations

For comparison purpose between the three linear technologies, Parabolic Trough Collector (PTC), Linear Fresnel Reflector (LFR), and Solar Tower (ST) system, we have taken some important thermo-economic parameters. Table11.1 gives some of the important parameters of integrating different CSP technologies with different gas turbine sizes.

As stated above, the PTC and LFR were integrated to a steam side, where the ST system was integrated to a gas side of gas turbine cogeneration power plant. Since there is a big room for solar energy in the steam side of small gas turbine size, the instantaneous and annual solar shares are higher for those plants when they integrated with PTC or LFR. On the other hand, there is a big room for solar energy in gas side of a large gas turbine size. As results, the instantaneous and annual solar shares are higher for those plants when they integrated with ST system.

According to the Table, the instantaneous solar shares are almost the same for all configurations at 70 MWe gas turbine size; this is because the plants have the same room for solar integration, weather this integration in steam side or in gas side. Although the instantaneous solar shares are very close for all configurations at 70 MWe gas turbine size, the configuration with the ST has a higher annual solar share compared to configurations with PTC and LFR. This is because the solar radiation was collected by mirrors with a dual axis tracking system in ST system, whereas the PTC and LFR system have one axis tracing system that controlled to rotate the collector in North-South tracing axis, so that means ST system has more sufficient ability to collect solar radiation throughout a year.

For all gas turbine size, annual share value of Linear Fresnel Reflector is not too far compared to that of parabolic trough; this is due particularly to the utilization those technologies in steam generation side.

Furthermore, the results presented in Table 11.1 indicate that the Fresnel collector has about 79% of the thermal performance of a parabolic trough per aperture area. However, this lower performance is overcompensated by significantly lower investment and lower operation and maintenance costs of the collector field. Also according to the Table, the solar tower system has about 50% of the thermal performance of the PTC per aperture area. This is because the concentration radio of PTC is very high compared to the others two technologies, that leads to obtained solar thermal energy with less aperture area.

Table 11.1: Comparison between three different configurations operated by different gas turbine sizes.

Gas Turbine Size		30	50	70	90	110	130	150
Optimal solar multiple	PTC*	0.80	0.80	0.60	0.50	0.40	0.30	0.30
	LFR*	0.80	0.80	0.60	0.50	0.40	0.30	0.30
	ST**	0.16	0.24	0.40	0.41	0.47	0.53	0.55
Total active aperture	PTC	381,140	381,140	285,855	238,213	190,570	142,928	142,928
	LFR	489,234	489,234	366,926	303,112	244,617	180,804	180,804
area (m^2)	ST	211,704	316,886	527,034	738,214	949,667	1,054,527	1,159,726
Total reflective area	PTC	422,038	422,038	316,529	263,774	211,019	158,264	158,264
	LFR	489,234	489,234	366,926	303,112	244,617	180,804	180,804
(m^2)	ST	211,704	316,886	527,034	738,214	949,667	1,054,527	1,159,726
	PTC	104	104	78	65	52	39	39
Field area (hectare)	LFR	93	93	70	58	47	35	35
	ST	104	156	260	364	468	520	572
Solar thermal power	PTC	205,616	205,711	154,391	128,659	95,507	77,318	63,837
	LFR	207,372	207,372	155,528	128,488	98,959	76,641	63,866
(kW) at design hour	ST	57,197	85,617	142,725	200,311	257,258	285,223	313,829
Usable thermal power	PTC	539.5	539.7	540.1	540.1	501.2	541.0	446.6
	LFR	423.9	423.9	423.9	423.9	404.6	423.9	353.2
(W/m^2 of aperture area)	ST	270.2	270.2	270.8	271.3	270.9	270.5	270.6
Instantaneous solar	PTC	69.6	66.8	47.8	36.5	24.5	19.2	13.5
	LFR	70.7	67.3	47.3	36.5	25.1	19.2	13.1
share (%)	ST	19.9	28.7	46.7	55.9	66.0	70.7	74.2
Annual solar share (%)	PTC	24.7	22.6	15.9	12.4	8.8	6.7	5.2
	LFR	23.9	22.4	15.4	12.4	8.5	6.4	5.7
	ST	8.9	11.7	19.0	23.8	28.1	30.0	31.5
Annual CO_2 emission	PTC	386.0	419.5	513.2	581.1	651.8	691.3	748.9
	LFR	389.7	422.2	516.1	584.3	653.4	692.8	750.7
(hybrid) (K tonne)	ST	465.9	475.5	488.2	503.2	511.7	516.3	540.2
Annual CO_2 avoidance	PTC	125.7	121.6	96.2	81.5	62.2	48.9	42.6
	LFR	122.1	119.0	93.4	78.4	60.6	47.4	40.8
(K tonne)	ST	45.8	65.7	121.3	159.4	202.4	223.9	251.4

* Definition of solar multiple $\left(SM = \frac{P_{th,solar}}{P_{th,total}}\right)$

** Definition of solar multiple $\left(SM_{st} = \frac{P_{th,solar}}{P_{th,Gas\ Turbine} + P_{th,duct\ burner}}\right)$

With the cost figures of LFR, PTS, and STS; and the performance figures as presented in the Tables 11.2 and 11.3, the resulting energy costs of the Fresnel type collector are below the energy costs of the PTC system for all gas turbine size. Of course the trough system has the big advantage of being experimentally and commercially validated whereas the figures of the Fresnel collector are only theoretical.

Also according to tables 11.2 and 11.3, the resulting energy cost of the solar tower type is higher than the other technologies at all gas turbine sizes. This is because the obtained temperature from ST system is almost 1000 ºC, which is very higher compared to the others two technologies. Consequently, the ST system required a large area as can be shown in table 11.1.

Table 11.2: Comparison between three different configurations in terms of Levilized Energy Cost (LEC).

Gas Turbine Size		30	50	70	90	110	130	150
Parabolic Trough	Electrical (LEC_1)	9.14	6.51	5.65	4.76	4.34	3.92	3.87
Collector (PST)	Steam (LEC_2)	2.28	2.14	2.14	1.83	1.65	1.44	1.34
System	Total (LEC_3)	2.51	2.53	2.57	2.55	2.56	2.5	2.55
Linear Fresnel	Electrical (LEC_1)	6.77	5.09	4.85	4.23	3.98	3.62	3.64
Reflector (LFR)	Steam (LEC_2)	2.06	1.91	1.87	1.67	1.52	1.32	1.22
System	Total (LEC_3)	2.31	2.34	2.43	2.43	2.46	2.41	2.48
Solar Tower (ST)	Electrical (LEC_1)	6.88	6.73	8.23	8.27	8.34	8.06	7.68
	Steam (LEC_2)	2.32	2.17	2.6	2.84	3.14	3.17	3.21
System	Total (LEC_3)	2.07	2.54	3.02	3.33	3.64	3.7	3.79

Table 11.3: Comparison between three different configurations in terms of Solar Levilized Energy Cost (SLEC).

Gas Turbine Size		30	50	70	90	110	130	150
Parabolic Trough Collector (PST) System	Electrical ($SLEC_1$)	31.85	21.64	19.00	16.51	16.63	15.96	18.20
	Steam ($SLEC_2$)	4.41	4.61	4.97	5.31	6.23	6.53	8.40
	Total ($SLEC_3$)	4.36	4.55	4.95	5.24	5.90	6.08	7.30
Linear Fresnel Reflector (LFR) System	Electrical ($SLEC_1$)	22.82	15.47	14.24	12.62	12.82	11.83	12.78
	Steam ($SLEC_2$)	3.50	3.77	4.11	4.35	4.86	4.85	5.69
	Total ($SLEC_3$)	3.65	3.57	3.91	4.16	4.81	4.79	5.55
Solar Tower (ST) System	Electrical ($SLEC_1$)	59.50	41.76	29.94	24.90	21.64	19.76	17.68
	Steam ($SLEC_2$)	6.87	7.66	7.28	7.69	7.98	8.00	8.10
	Total ($SLEC_3$)	6.70	7.18	6.85	7.03	7.14	7.10	7.05

11.3 Comparison between Different CO_2 Avoiding Technologies

In real life, there is a technology for CO_2 avoiding which called CO_2 capture technology. Also in the present study, one of the important reasons of integrating CSP technologies with conventional cogeneration system is global warming which is a related to CO_2 emissions. So comparison between these different technologies is very important to assess whether this integration is economical feasible or not. Figures 10.1-a, and 10.1-b present a comparison between LEC by using different CO_2 avoiding technologies.

According to Figures 10.1-a and 10.1-b, one can conclude that the integrating PTC with gas turbine cogeneration system has proved the economical feasibility more than CO_2 capture technology for gas turbine size less than 110 MWe. However, the integrating LFR with gas turbine cogeneration system has proved economical feasibility more than

CO_2 capture technology for all gas turbine size. But the integrating ST with gas turbine cogeneration system has proved the economical feasibility less than CO_2 capture technology.

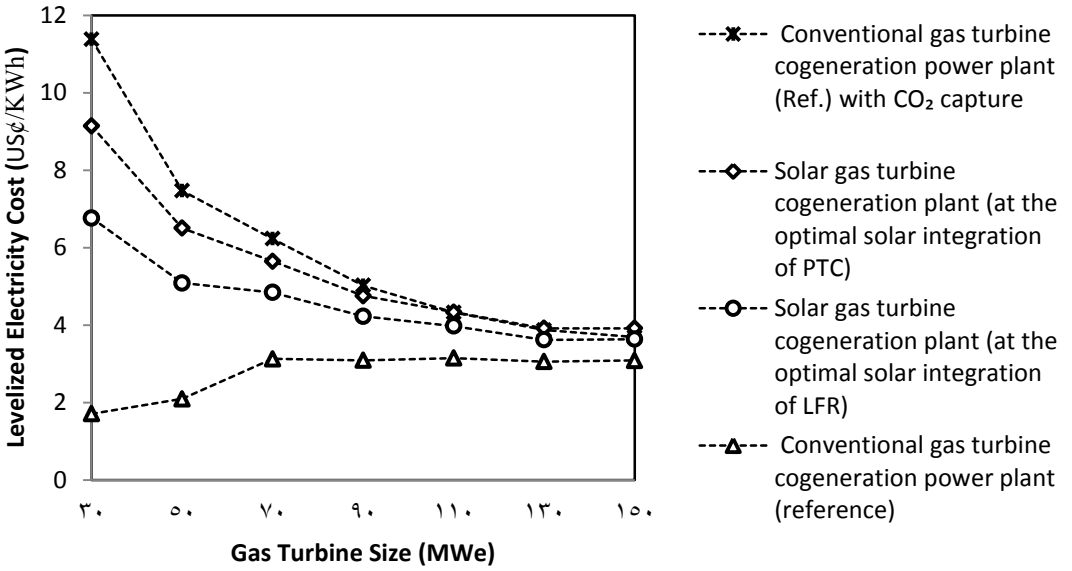

Figure 11.1-a: Levelized electricity cost for different CO_2 avoiding technologies (Ref., PTC, and LFR)

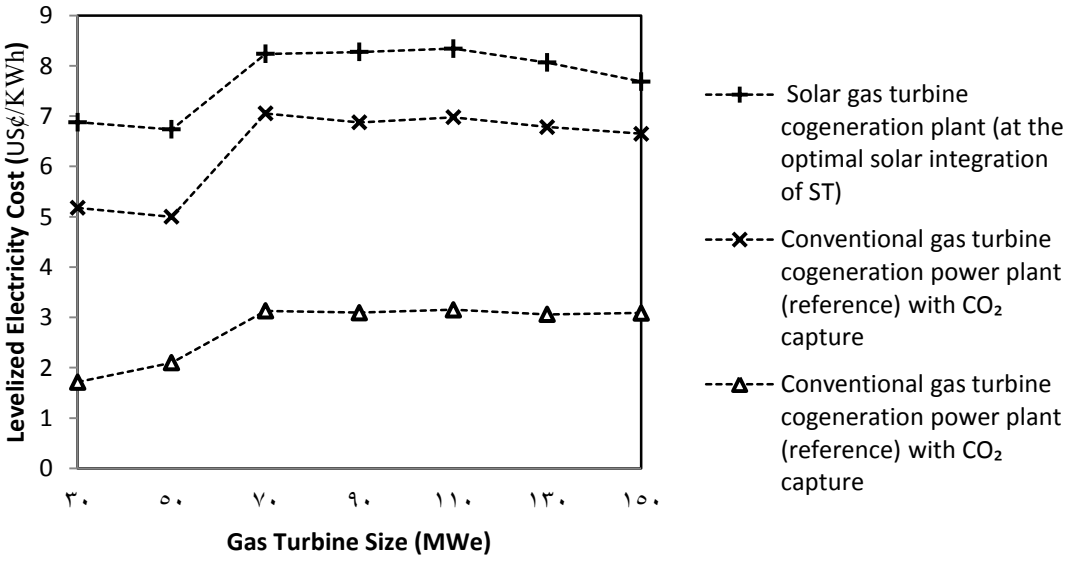

Figure11.1-b: Levelized electricity cost for different CO_2 avoiding technologies (Ref., ST)

11.4 Comparison between Different Plant in Terms of LEC and Annual CO_2 Emissions

The optimal solar collector size has been determined for all gas turbine size integrated with different solar technologies. Also levelized electricity cost and annual CO_2 emissions have been determined for all gas turbine size integrated with different solar technologies.

International Renewable Energy Agency reported in 2012 that the LEC_1 of parabolic trough power plants were in the range 20 to 36 US¢/ kWh, and for solar tower power plants were in the range 17 to 29 US¢/ kWh [78]. One can compare the LEC of the present plants with the minimum LEC of both PTC and ST power plant, which are 20US¢/ kWh, and 17 US¢/ kWh.

Figure 11.2 depicts the LEC_1 versus annual CO_2 emission for different solar gas turbine plants at the optimal integration. Point one presents the LEC_1 and annual CO_2 emission of reference cycle with 150 MWe. Where point three presents the minimum LEC and annual CO_2 emission (equal to zero) of parabolic solar power plant [78]. Point four presents the minimum LEC and annual CO_2 emission (equal to zero) of solar tower power plant [78].

Point two presents the LEC_1 and annual CO_2 emission of design where annual CO_2 emission is lower. Actually, there are two designs give lower value of annual CO_2

emission, one of them accrues at the integration of LFR system with 30 MWe gas turbine cogeneration plant, the other one accrues at integration of PTC system with 30 MWe gas turbine cogeneration plant. Point two in Figure 11.2 presents the LEC and annual CO_2 emission of design where LFR integrated with 30 MWe gas turbine cogeneration plant, because the LEC_1 for this point is lower.

In the Figure 11.2, the lines linked between point one with points three and four represent the literature reference lines. By comparing present designs with these lines, one can note that the levelized electricity cost (LEC_1) is reduced by integrating CSP technologies with gas turbine cogeneration system and most present designs are under these lines. This is because two main reasons, first one the industrial simulation land was located in the high insolation region, where the solar energy conversion system can produce the greatest amount of energy from specific solar collector field size; the second one, the output thermal energy in the present design is greater than output electrical energy for all gas turbine size, which doesn't cost a lot.

Also in the Figure 11.2, the line linked between point one and point five represents the default design to reduce CO_2 emissions by CO_2 capture technology with conventional gas turbine cogenerations power plant. By comparing present designs with this line, one can note that the most present designs are under these lines. The line linked between point one and point two represents the default design to reduce CO_2 emissions by integrating CSP technologies with gas turbine cogenerations power plant. The best designs can be considered as the design when it's representing point located below the line.

Figure 11.3 depicts the total plant efficiency versus annual CO_2 emission for different solar gas turbine plants at optimal solar integration. Point one presents the total plant efficiency and annual CO_2 emission of reference cycle with 150 MWe. Where Point two presents the total plant efficiency and annual CO_2 emission of the present design where annual CO_2 emission is lower. Since gas turbine size of 30 MWe integrated with LFR has the lower CO_2 emission with low value of LEC, one can define point two at this design. The line linked between point one and point two represents the higher values for the best designs in the present study. The best designs can be considered as the design when it's representing point located on or above the line.

According to the Figure 11.2, one can conclude that the optimal integration configuration is found to be solarization steam side in conventional gas turbine cogeneration plant integrated with LFR system for gas turbine size ranged between 50 to 90 MWe. But according to the Figure 11.3, the total plant efficiency of 50 MWe integrated with LFR is better than 70 and 90 MWe. So one can conclude that the integration of the optimal solar multiple (0.8) of LFR with 50 MWe gas turbine size has a sufficient ability for solar energy utilization.

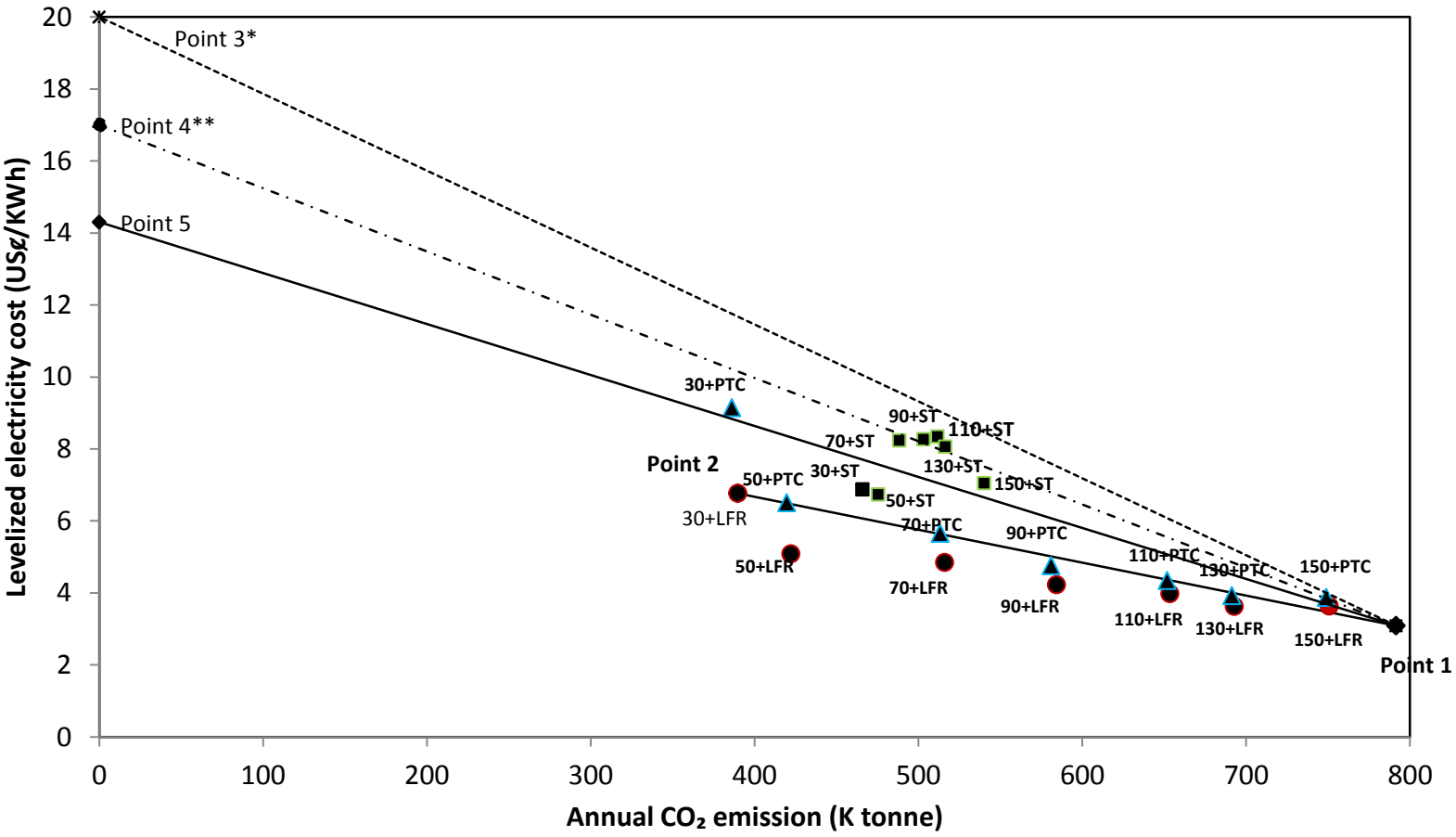

Figure 11.2: Levelized Electricity cost (LEC) versus annual CO_2 emission for different solar gas turbine designs

* LEC1 of parabolic trough power plants [78]. ** LEC_1 of solar tower power plants [78].

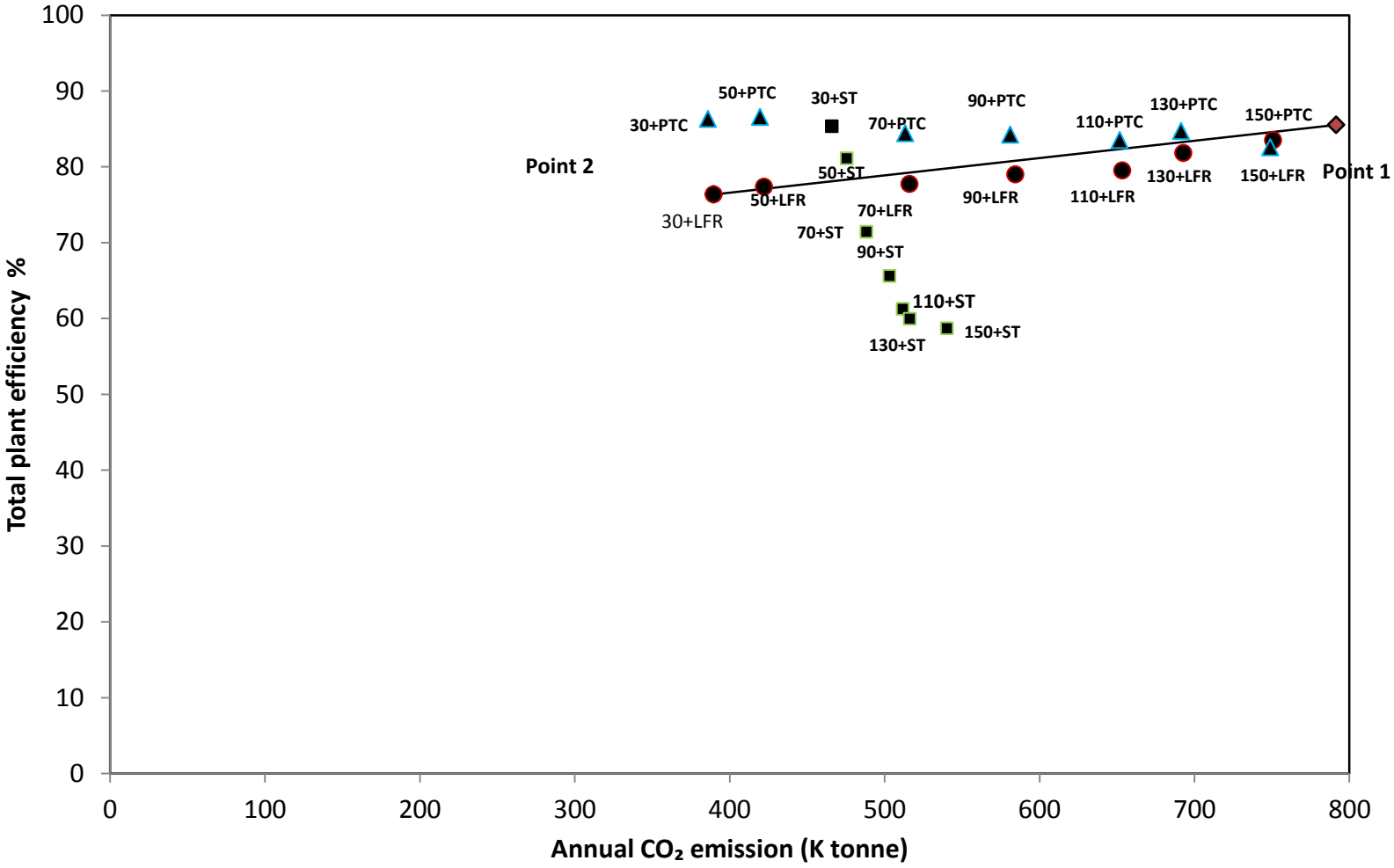

Figure 11.3: Total plant efficiency versus annual CO_2 emission for different solar gas turbine designs.

11.5 Applying the Optimal Integration Configuration for Different Locations in Saudi Arabia

After achieving the optimal integration configuration under Dhahran weather conditions, which is solarization steam side in the conventional gas turbine cogeneration plant integrated with LFR with 50 MWe gas turbine size. This plant was considered in this section, and it has been applied in different cities in Saudi Arabia, which are Jeddah, Jizan, Riyadh, and Tabuk.

In order to make a consistent comparison between plants performance in a different sites; The same solar power plant was considered, which is the optimal LFR size (93 hectare) integrated with steam side of 50 MWe gas turbine cogeneration plant; the plant was operated at the same designing hour, which is solar noon at average day in a month ; the plant was operated at location's monthly average ambient temperature and relative humidity; the plant was considered to generate a steam at a constant flow rate of 81.44 kg/s at P = 45.88 (bar) and temperature of T = 394°C throughout the year at different locations.

In order to evaluate the performance of the solar power plant at different cities, it is necessary to determine solar radiation intensity, an average ambient temperature, and an average relative humidity. Figure 11.4 presents the solar radiation at noon solar time for different cities in Saudi Arabia, and Figures 11.5 and 11.6 present the average monthly temperatures and relative humidity respectively for different cities in Saudi Arabia.

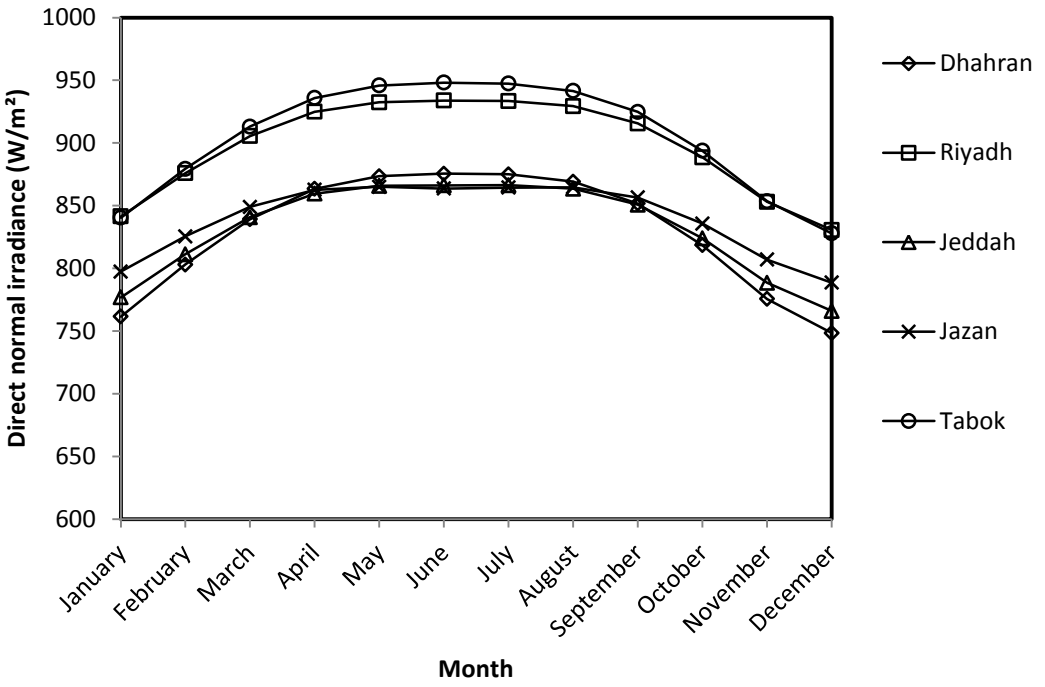

Figure 11.4: Solar radiation at noon time for different cities in Saudi Arabia

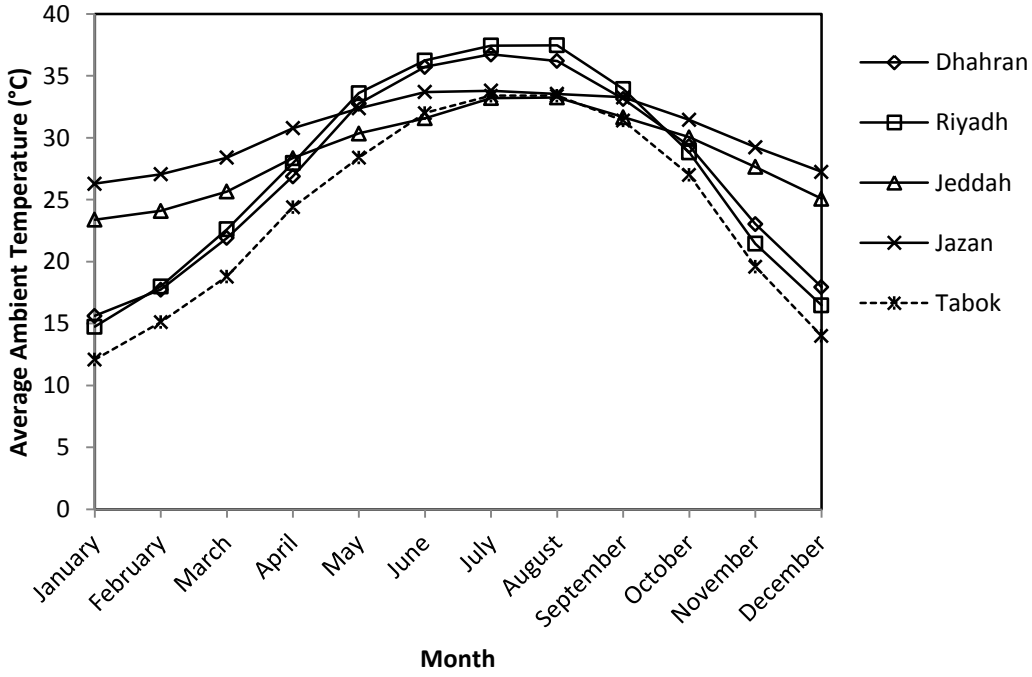

Figure 11.5: Average ambient temperature for different cities in Saudi Arabia

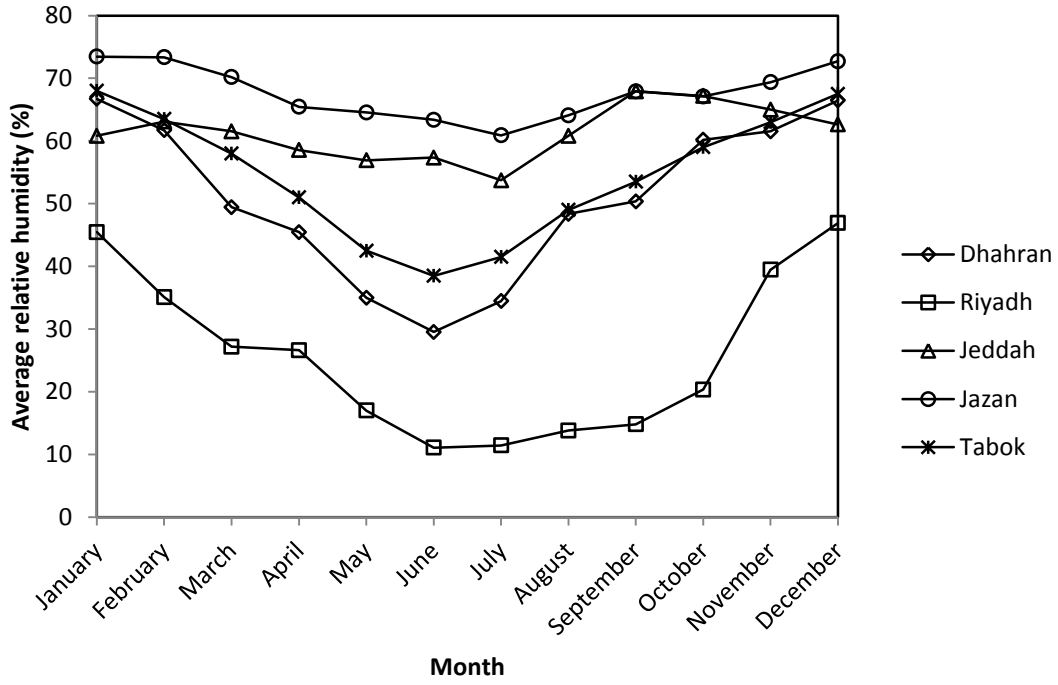

Figure 11.6: Average relative humidity for different cities in Saudi Arabia

Temperature and relative humidity are the most important weather parameters affecting electric load generated by power utilities in many parts of the world. The results of this simulation show that, the annual total efficiency for conventional gas turbine cogeneration power plant at different cities (Figure 11.7). As can be seen, Riyadh and Tabuk have higher total plant efficiency (about 96.9 %). Whereas the small total efficiency was for plant operated in Jeddah (about 95.42 %). Figure 11.7 shows that the annual CO_2 emissions for both, the conventional power plant and solar integration power plant.

After studying the performance of considered solar power plant under different locations, annual solar share has a different profile trend among different locations as shown in

Figure 11.9. That is due to difference of solar radiation for those different locations also due to difference weather conditions.

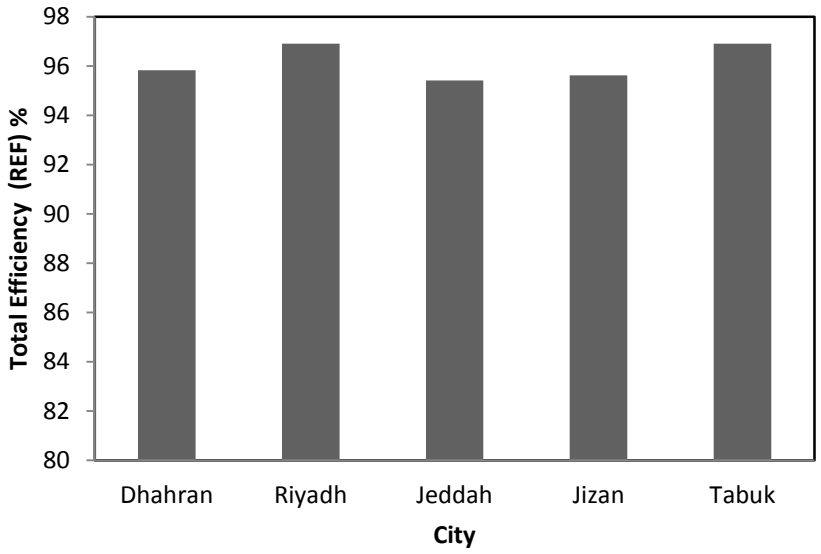

Figure 11.7: Total plant efficiency for the conventional power plant operated in different cities in Saudi Arabia.

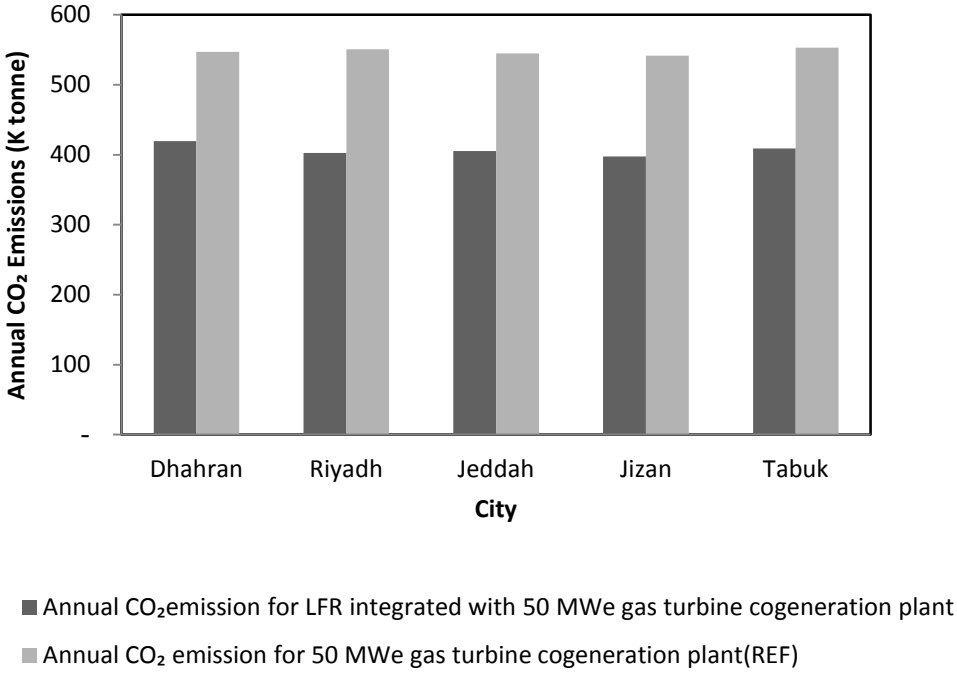

Figure 11.8: Annual CO_2 emissions from the plants operated in different cities in Saudi Arabia.

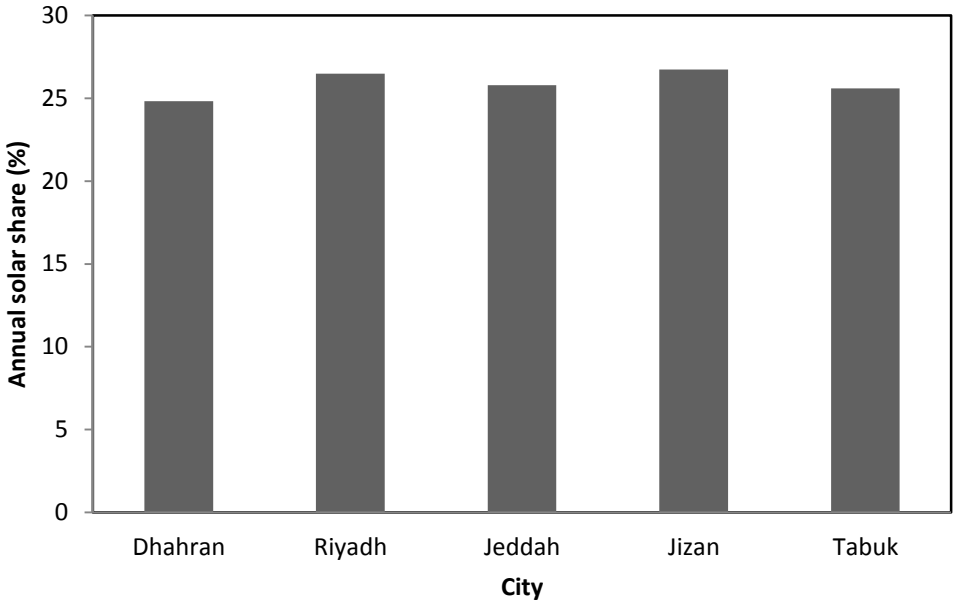

Figure 11.9: Annual solar share for the solar power plant operated in different cities in Saudi Arabia.

Due to accumulation way of solar power plant performance over the year; annual solar share has a room to give variation among different locations which will affect the economic performance parameters (LEC and SLEC) as shown in Figures (11.10 and 11.11); and the LEC of conventional power plant also has a room to give variation among different locations which will affect the economic performance parameters (LEC and SLEC) as shown in Figures (11.10 and 11.11). As shown in Figure11.10, the LEC for conventional power plant was changed reverse trends of total plant efficiency. In other words, the plant operated in a city with high efficiency has low LEC. For example, plant operated in Jeddah has lower efficiency but this plant has higher LEC.

From previous economic figures, Jizan city has the lowest LEC which is 4.74 US¢/MWh and SLEC which is 11.62 US¢/MWh. That means the proper location to apply considered

integration configuration is Jizan city. The considered configuration is the optimal LFR size (93 hectare) integrated with steam side of 50 MWe gas turbine cogeneration plant.

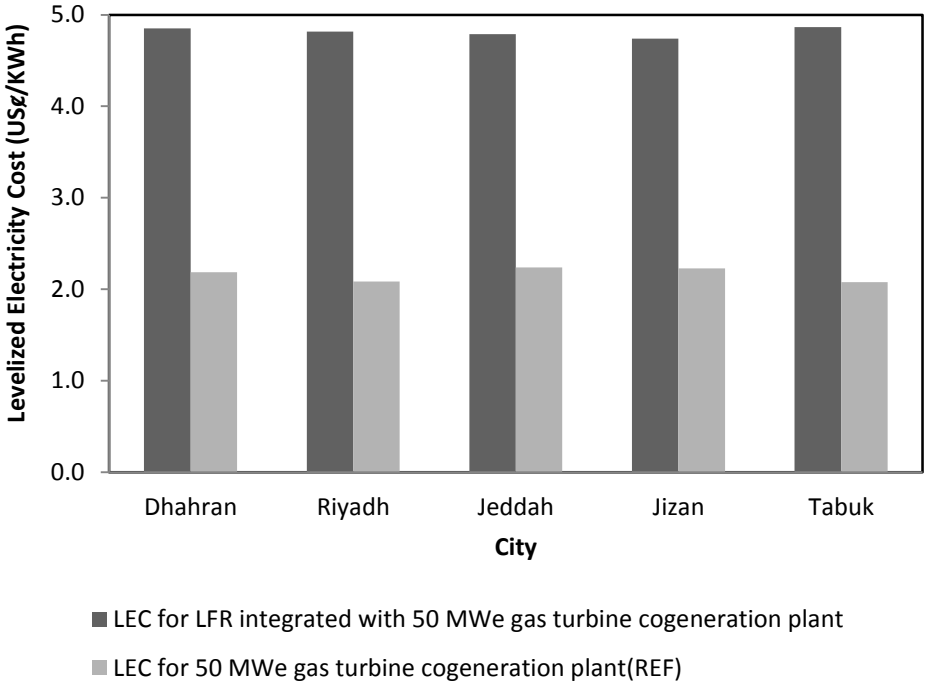

Figure 11.10: Levelized electricity cost for the plants operated in different cities in Saudi Arabia.

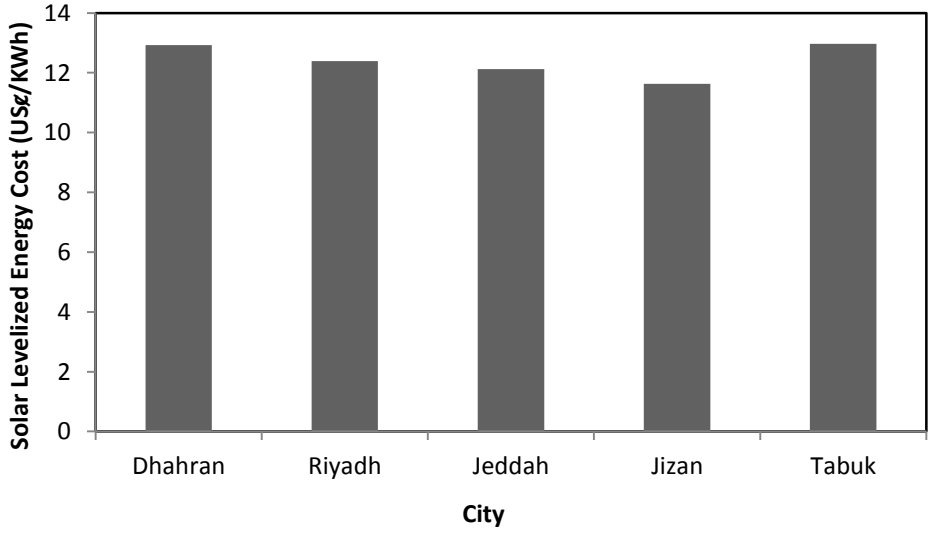

Figure 11.11: Solar levelized electricity cost for the plant operated in different cities in Saudi Arabia.

11.6 Concluding Remarks

For comparison purpose between the three Concentrating Solar Power (CSP) technologies, the Parabolic Trough Collector (PTC), the Linear Fresnel Reflector (LFR), and the Solar Tower (ST) system, three different configurations was investigated: the first based on integrate PTC with steam generation side in gas turbine cogeneration power plant, the second based on integrate LFR with steam generation side in gas turbine cogeneration power plant, and the third one based on integrate ST with gas side in gas turbine cogeneration power plant. The comparison was carried out in terms of Thermo-economic performance. Thermo-economic assessment was carried out with a commercial code named THERMOFLEX with PEACE.

According to the result, the advantages of LFR has considerable lower solar levelized energy costs for the solar thermal energy (at the same solar multiple) and, hence, of the whole power plant (at the same nominal power), the higher land use efficiency. The disadvantage is that the thermal performance per aperture area is still lower than PTC.

The result of annual solar share gives, annual solar share value of LFR was not too far compared to that of PTC; that was due particularly to the utilization those technologies in steam generation side. PTC and LFR both show a higher solar share for gas turbine smallar than 70 MWe. In contrast, ST system has a higher solar share for gas turbine greater than 70 MWe.

The result presented above indicates that; the LFR has about 79% of the thermal performance of PTC per aperture area. However, this lower performance is overcompensated by significantly lower investment and lower operation and maintenance costs of the collector field; the ST system has about 50% of the thermal performance of the parabolic trough per aperture area.

With the cost figures of LFR, and PTS; and the performance figures as presented above, the resulting energy costs of the Fresnel type collector below the energy costs of the PTC system. Of course the PTC system has the big advantage of being experimentally and commercially validated whereas the figures of the LFR are only theoretical. This is why the LFR must be a pilot plant under real operation conditions including commercial aspects.

With the cost figures of ST system; and the performance figures as presented above, the resulting energy costs of the solar tower type was higher than other technologies at all gas turbine sizes. This is because the solar tower system has about 50% of the thermal performance of the parabolic trough per aperture area.

According to the above, one can conclude that the optimal integration configuration is found to be solarization steam side in conventional gas turbine cogeneration plant integrated with LFR system for 50 MWe gas turbine size. The levelized electricity cost for this plant is 5.1 US₵/ kWh. The proper location to apply optimal integration configuration is Jizan city.

CHAPTER 12

CONCLUSIONS

An integrated solar gas turbine cogeneration system that generates steam at a constant flow rate of 81.44 kg/s at P = 45.88 (bar) and temperature of T = 394°C around the year in addition to the generation of electricity have been simulated and assessed for different CSP technologies and different sizes of the gas turbine. Three different configurations was investigated: the first based on integrate PTC with steam generation side in gas turbine cogeneration power plant, the second based on integrate LFR with steam generation side in gas turbine cogeneration power plant, and the third one based on integrate ST with gas side in gas turbine cogeneration power plant.

THERMOFLEX with PEACE simulation software was used to assess the performance of each proposed integration design. Thermo-economical analysis was conducted for different designs to reach at the optimal operating design under Dhahran weather conditions. From the present study, one can draw the following conclusions:

- Solar energy is a promising technology and introducing integrated PTC, LFR, and ST with gas turbine cogeneration system offers much potential for large-scale application with stable power supply.

- The optimal solar field areas have been determined for each integration configuration with different gas turbine size.

- The results show that, annual solar share value and annual CO_2 avoidance of LFR were not too far compared to that of PTC; that was due particularly to the utilization those technologies in steam generation side.

- The results have proved that the integrated PTC with gas turbine cogeneration system has more economical feasibility than CO_2 capture technology for gas turbine size smaller than 110 MWe.

- The results have proved that the integrated LFR to gas turbine cogeneration system has more economical feasibility than CO_2 capture technology for all gas turbine size.

- The results have proved that the integrated ST with gas turbine cogeneration system has less economical feasibility than CO_2 capture technology.

- The result proved that LFR has about 80% of the thermal performance of a PTC per aperture area. However, this lower performance is overcompensated by significantly lower investment and lower operation and maintenance costs of the collector field.

- The result proved that the ST system has about 50% of the thermal performance of the PTC per aperture area.

- The results indicate that integrating the CSP technologies with the conventional gas turbine cogeneration plant will result in a logical increase in the levelized energy cost compared to the conventional cogeneration power plant.

- The resulting energy cost of the Fresnel type collector is below the energy costs of the parabolic trough collector.

- The resulting energy cost of the solar tower type is higher than other technologies at all gas turbine size.

- Among of different gas turbine sizes integrated with the optimal solar multiple of PTC, the optimal design is found to be the 50 MWe gas turbine size integrated with 0.8 solar multiple of PTC (104 hectare of solar filed).

- Among of different gas turbine sizes integrated with the optimal solar multiple of LFR, the optimal design is found to be the 50 MWe gas turbine size integrated with 0.8 solar multiple of LFR (93 hectare of solar filed).

- Among of different gas turbine sizes integrated with the optimal solar multiple of ST system, the optimal design is found to be the 30 MWe gas turbine size integrated with 0.16 solar multiple of ST (104 hectare of solar filed).

- The optimal integration configuration is found to be solarization steam side in 50 MWe gas turbine cogeneration plant integrated with 93 hectare of LFR.

- The results indicate that the proper location to apply optimal integration configuration is Jizan city.

APPENDICES

Building a Conventional Gas Turbine Cogeneration Model by Using THERMOFLEX: Step-by-Step

THERMOFLEX lets you connect components in a flexible fashion to build a graphic model. You then edit the inputs describing each component, calculate your cycle, and then view the outputs. The following detailed step-by-step description assumes all THERMOFLEX program settings and behaviors are left at their default values. If not, some of the steps will require slightly different actions on your part.

1. Draw System Stage

1.1. Gas Turbine & Ambient Air Supply

To construct this conventional cogeneration from scratch, first click on the Gas / Air Icon Group on the Icon Selector. Click the Gas Turbine (GT PRO) icon from the Icon List and move the mouse to locate it near the middle of the empty flowsheet. Click the mouse again to drop it in place. By default, THERMOFLEX will attach the icon to the invisible grid so it may shift slightly when dropped. The icon is highlighted (drawn with a yellow background) to indicate it is the **currently selected** item on the flowsheet. The current item is subject to certain additional commands as described below. It will remain highlighted in this way until another icon is added, some other component is clicked, or some other action is taken.

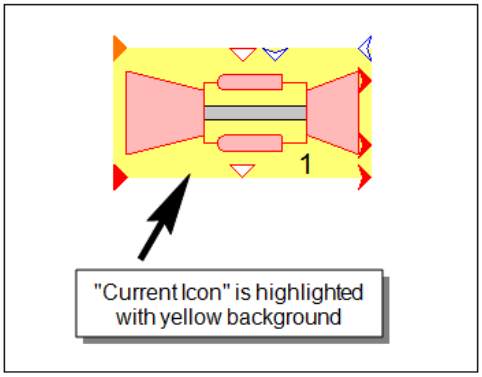

Next move the pointer over the Icon Selector strip at the bottom of the screen to summon the Gas / Air Icon List. Whenever the mouse moves over the Icon Selector while an Icon Group button is toggled down, the Icon List for the selected group will reappear. Click the Gas / Air Source icon (top - leftmost choice) from the Icon List to add it to the model. Drag the source near the compressor inlet node on the lower left corner of the gas turbine icon. As the Source's outlet node nears the Gas Turbine's air inlet node, the node triangles disappear and a dashed line is drawn between the icons to indicate these nodes will be connected and a stream will be defined if the Source is dropped here. When this happens, drop the source so it automatically snaps to the gas turbine forming the connection.

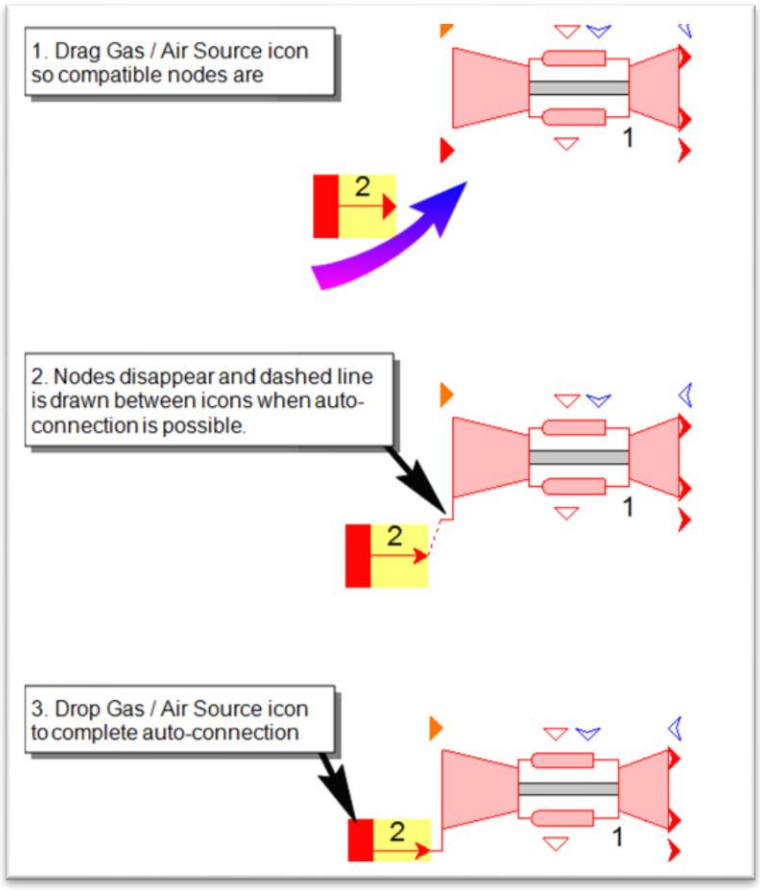

Now that these icons have been connected, drag the newly added Gas / Air Source to the left. THERMOFLEX will automatically draw a rectilinear connection line between the two nodes and show a stream display with the stream number and placeholders for state data.

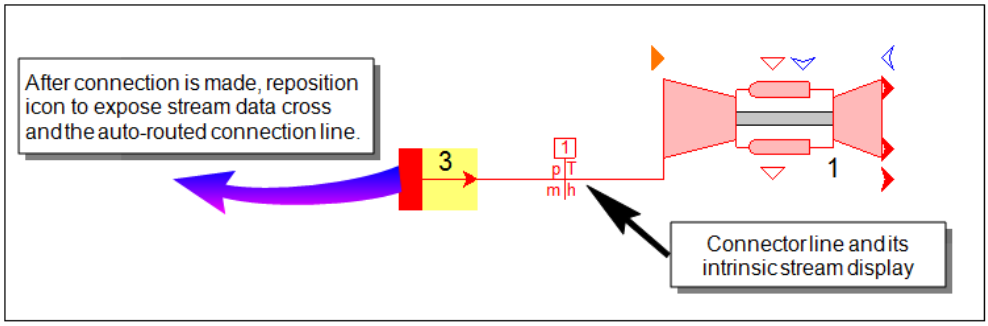

Next, click the Other Fluids Icon Group and select the Fuel Source icon (top - leftmost) from the Icon List. Drag it near the Gas Turbine's Fuel Supply node at the top left corner of the gas turbine icon. Once the auto-connection dashed line is drawn, drop the fuel source to complete the connection. Reposition the Fuel Source Icon to the left of the gas turbine, just above the Gas / Air Source. Icon indices are assigned as icons are added to the model, and by default, indices are shown on each icon. These indices are used to identify icons in messages and output displays. Stream numbers are also assigned automatically as streams are created.

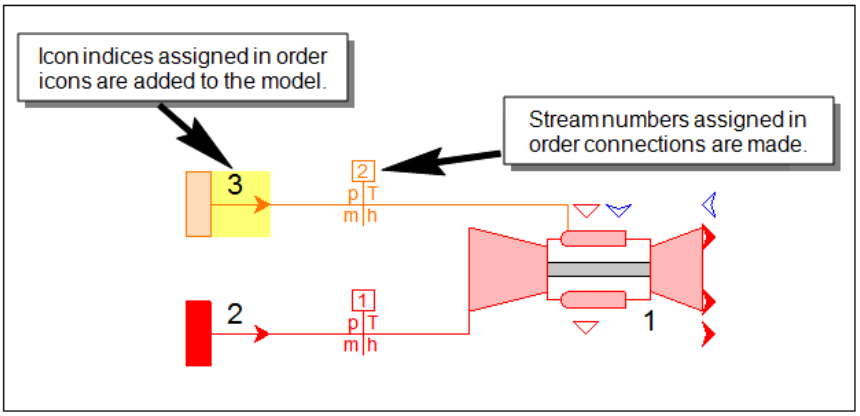

1.2. Heat Recovery Steam Generation with Duct Burner

Now we'll draw a simple heat recovery steam generation (HRSG), and connect it to the gas turbine exhaust to make process steam.

Click Boilers / HRSGs group on the Icon Selector button strip. Select the Superheater (PEC) icon and place it above and to the right of the gas turbine icon. then you have to rotate the Supercenter to get the correct gas flow rate direction , you can do that by right

clicking on mouse and select transpose +(or pressing F9) . Next, add an Evaporator (PEC) icon to the model and rotate it, then drag it to the right side of the Superheater and. As the Evaporator nears the Superheater, the flue gas nodes and water/steam nodes will auto-connect as shown below. Drop the Evaporator and THERMOFLEX will connect it to the superheater, and attach the icons to each other. Next, drag the evaporator to the right to expose the stream displays and connector lines.

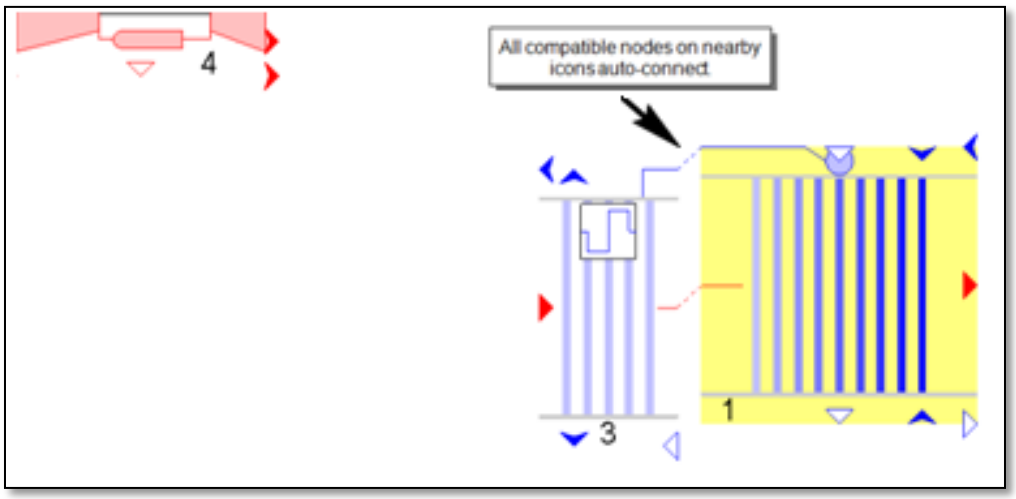

Now, add an Economizer icon to the model, and attach it to the right face of the evaporator using the same techniques. Once connected, move the Economiser to the right to expose the connections and stream displays.

Next, click the Flue Gases group on the Icon Selector. Click the Duct Burner Classic to add it to the model. Connect the Duct Burner to the Superheater gas inlet node. Drag the Duct Burner left to expose the gas display. Next, click the Other Fluids Icon Group and select the Fuel Source icon (top - leftmost) from the Icon List. Drag it near the Duct

Burner's Fuel Supply node at the bottom of the Duct Burner icon. Once the auto-connection dashed line is drawn, drop the fuel source to complete the connection.

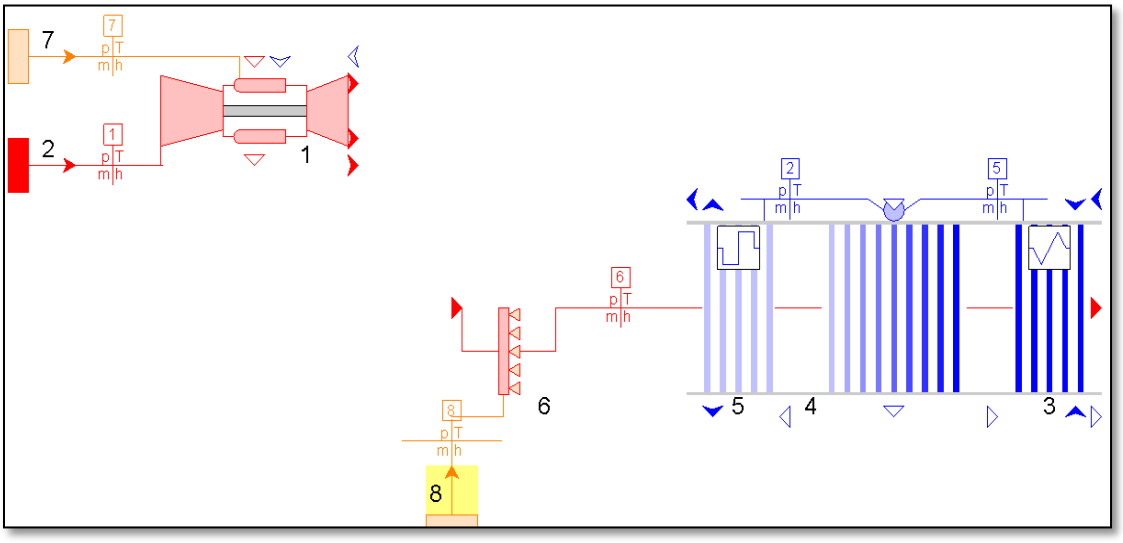

Now, connect gas turbine outlet with duct burner gas inlet.

Next, click the Flue Gases group on the Icon Selector. Click the Concrete Stack to add it to the model. Connect the Concrete Stack to the Economiser gas outlet node. Drag the Stack right to expose the gas display.

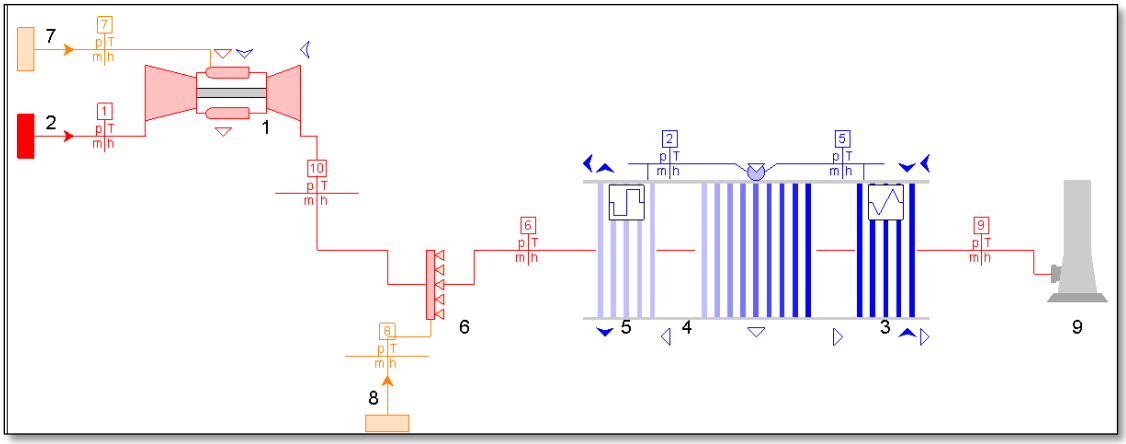

1.3. Pump with Water Sours

Now, click the General group on the Icon Selector. Click the General Pump, to add it to the model at the above and to the right of the HRSG. Next move the pointer over the Icon Selector strip to summon the Water / Steam Icon List. Whenever the mouse moves over the Icon Selector while an Icon Group button is toggled down, the Icon List for the selected group will reappear. Click the Water Source icon (top - leftmost choice) from the Icon List to add it to the model, and then transpose the icon to get the right direction of water flow rate. Drag the source near the General Pump inlet node on the right of the General Pump icon. As the Source's outlet node nears the General Pump's water inlet node, the node triangles disappear and a dashed line is drawn between the icons to indicate these nodes will be connected and a stream will be defined if the Source is dropped here. When this happens, drop the source so it automatically snaps to the General Pump forming the connection.

1.4. Output Process

Now, click the Legacy group on the Icon Selector. Click the Process, to add it to the model at the above and to the left corner of the HRSG. Then connect the General Pump, Economiser, and Process icon.

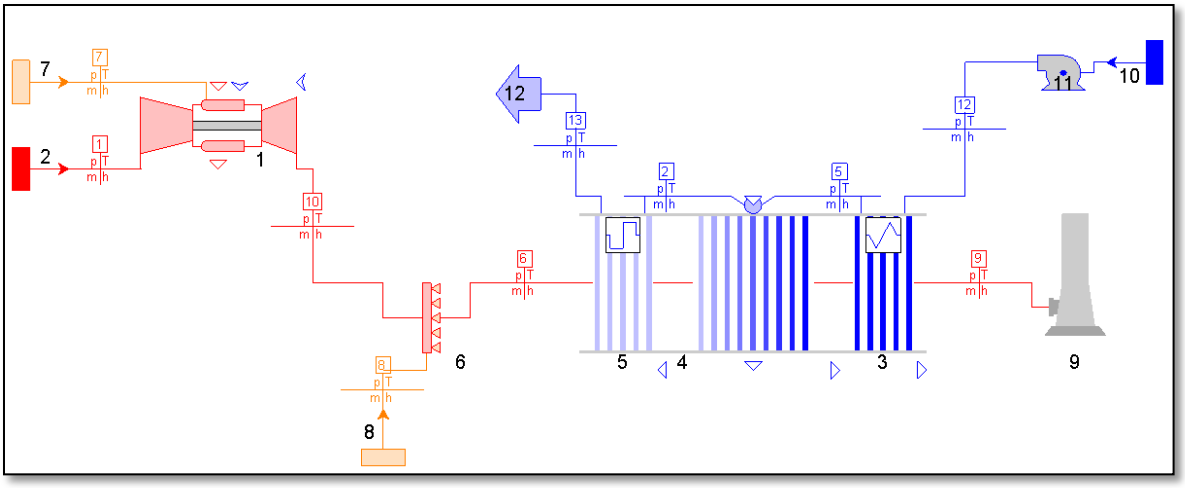

2. Check Drawing Transition

The Check Drawing transition (F3) is where THERMOFLEX reviews the drawing to verify it is complete and properly-defined, before moving to the Edit Inputs stage. THERMOFLEX performs a number of tests on the drawing, such as verifying all mandatory nodes are connected to other components, and testing that each stream has been assigned a fluid type. All valid THERMOFLEX models will pass these tests. However, passing these drawing tests does not absolutely guarantee the model drawing is logically configured and 100% error free.

3. Edit Inputs Stage

If the Check Drawing transition tests pass, the program moves to the Edit Inputs stage. The Check Drawing transition button will then be disabled and the Check Inputs transition will be enabled. The Edit Drawing button is always enabled since the model can be put back into Edit Drawing stage at any time.

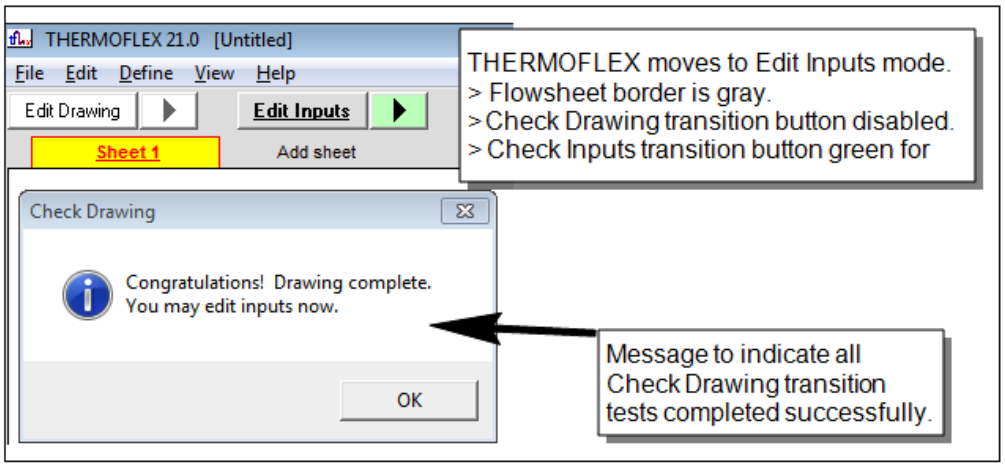

Double-click any component's icon from the flowsheet to open its input menu. Alternatively, click to highlight an icon and press F2 to summon the icon's input menu. Press the Edit Inputs button on the Navigator bar to open the Site Conditions input menu

In our cycle, for water source component, all the default values were used, for example, we was choose 25 °C and 1.014 bars for water temperature and pressure respectively. Also the fuel component, all the default values were used, which are 25 °C and 20.68 bars for fuel temperature and pressure respectively. When you are done editing a component's inputs, click the OK button to save changes and return to the flowsheet view. Click Cancel to ignore changes and revert to the previously set inputs

An Air Source is used to specify the conditions of a flow of air into a gas turbine. In our works we was choose the Ambient air method (specify conditions in Site Menu) to satisfy an Air Source conditions.

Duct Burner component is intended for use in models of heat recovery boilers with supplementary firing. It heats the incoming flue gases to Superheater by burning an

appropriate amount of the connected fuel. Alternatively, it burns a user-defined amount of fuel, specified by its mass flow rate or by its LHV or HHV energy content. In the proposed work we specify all the default values except control mode was changed to LHV.

Process component simply sends steam, or hot water, to an external use. In the proposed work we specify AS available in the Phase; 45.88 bar for the pressure; 81.44 kg/s for the steam temperature, and strong in flow priority.

Process[12]		0 - As available
1. Phase		0 - As available
2. Pressure	bar	45.88
3. Temperature	C	
4. Quality		
5. Flow	kg/s	81.44
6. Flow priority		Strong
7. Temperature of desuperheating water	C	

The superheater heats steam by cooling flue gases. The mass flow rate and the inlet state of both streams are dictated by the network, in both design and off-design modes. In design mode, the exit steam temperature is an input, and the program computes the corresponding heat transfer rate, exit state of the flue gas stream, and heat transfer ability. In the proposed work we specify all the default values except exit temperature was changed to 394°C.

HRSG Assembly

An HRSG assembly is built to define a unit comprised of THERMOFLEX/PEACE building blocks. Except for ducts, all components forming an assembly must include PEACE calculations to find their sizes, weights and costs.

Components which defined as parts of an HRSG Assembly:

- PEACE Economiser
- PEACE Evaporator
- PEACE Integral Deaerator
- PEACE Superheater
- PEACE OTB Element
- Duct Burner
- HRSG Stacks
- Catalyst
- Duct

To create or edit a HRSG assembly, choose the HRSG Assembly item from the Define menu. This item is only be available if the current model includes HRSG assembly components from the list above

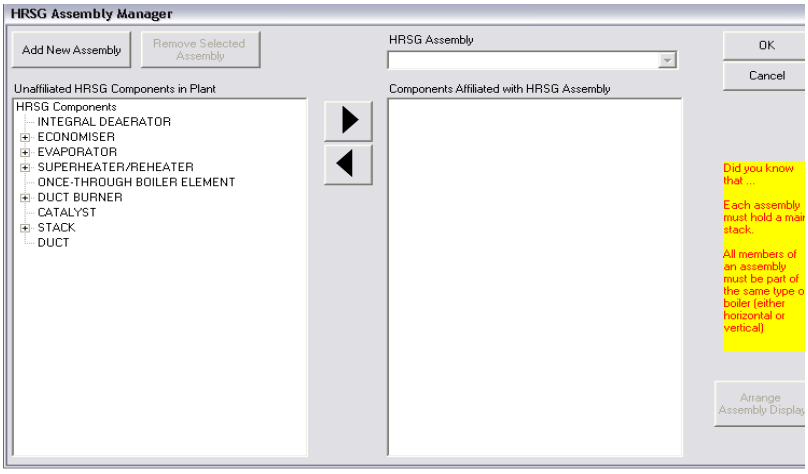

The left hand side window Unaffiliated HRSG Components in Plant holds all components available for an HRSG assembly. The right hand side window shows Components Affiliated with HRSG Assembly, i.e. all components selected as members of

the current assembly. In the screen image shown above, no assembly has yet been defined, thus the empty right window.

To create a new assembly, click on the Add New Assembly button. The new assembly will be given a default name, shown in the pull down list HRSG Assembly. If you desire a specific name for the assembly, then simply edit the name within the pull-down list.

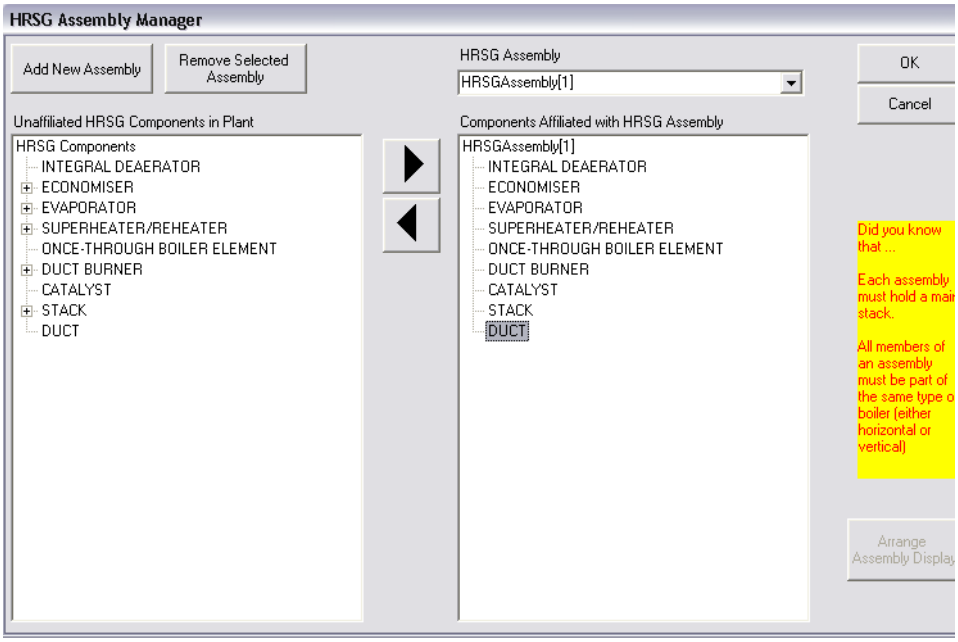

When the assemblies have been defined, you can save the assemblies by pushing OK. This will instruct the program to do preliminary checks, and if no errors are found, to save the assemblies.

Gas Turbine Main Inputs – Engine Selection

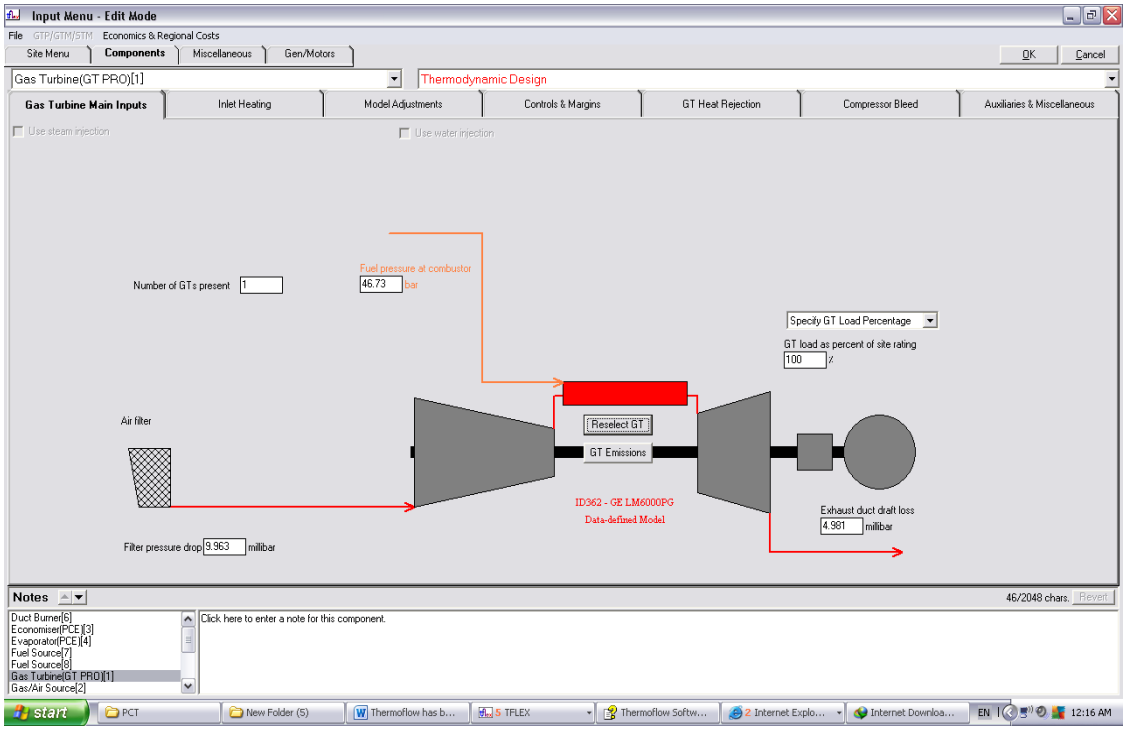

When the Gas Turbine (GT PRO) component is selected from the **Icon Selector** and placed on the drawing, it is initialized with the characteristics of a GE 6541B gas turbine. When the user reaches the Gas Turbine Main Inputs tab shown above, an alternate selection may be made by clicking the button labeled Reselect GT.

Because the GT PRO database contains over four hundred GT models, various selections at the top of the screen allow the user to restrict the display to the categories or power output range of interest. The button Display Entire GT Library can be used to make sure all are displayed. The Engine Selection Filter panel allows restricting the display to a range of nominal power outputs. Checking **Show new specs** only further restricts the list to machines which are currently available new, and the checkboxes below it enable the

display of either, or both, 50 Hz and 60 Hz machines. The list may also be sorted in ascending or descending order of power output, or alphabetically by manufacturer name.

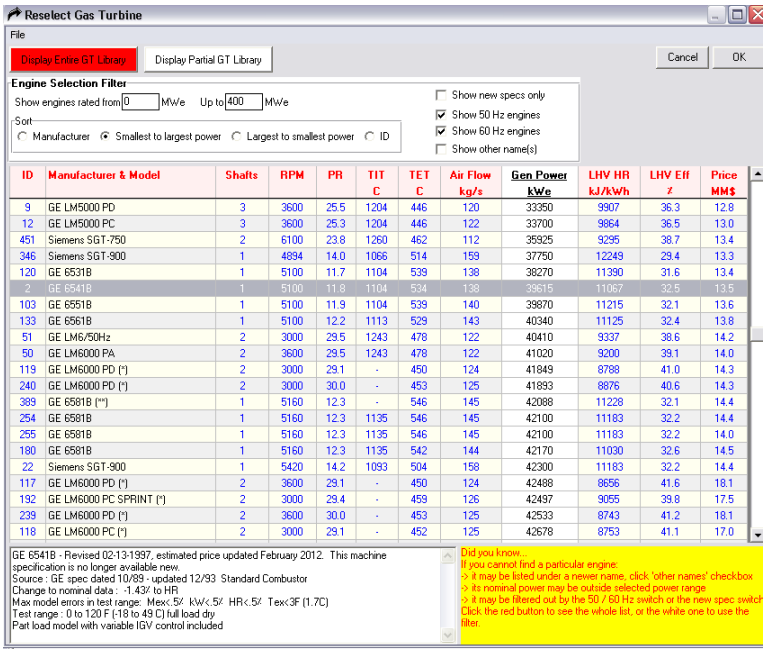

You can move the highlight bar to any machine. Performance data shown for each engine is (a) at ISO conditions: 59 °F (15 °C), 60% relative humidity, and sea level, (b) using methane as a fuel, and (c) with no inlet or exhaust pressure losses. To select a machine, move the highlight bar to the machine you want, and then click on the OK button. This will take you back to the Gas Turbine Main Inputs menu, where the newly-selected gas turbine's name and ID number will be visible. In the proposed simple i select the GE6101FA type.

Site Menu

The Site Menu tab is accessed in Edit Inputs mode by pressing F2 or by opening the Edit Inputs menu of a component. It allows a single specification to be made that propagates to all Gas/Air Sources that are declared to be “Ambient Air”.

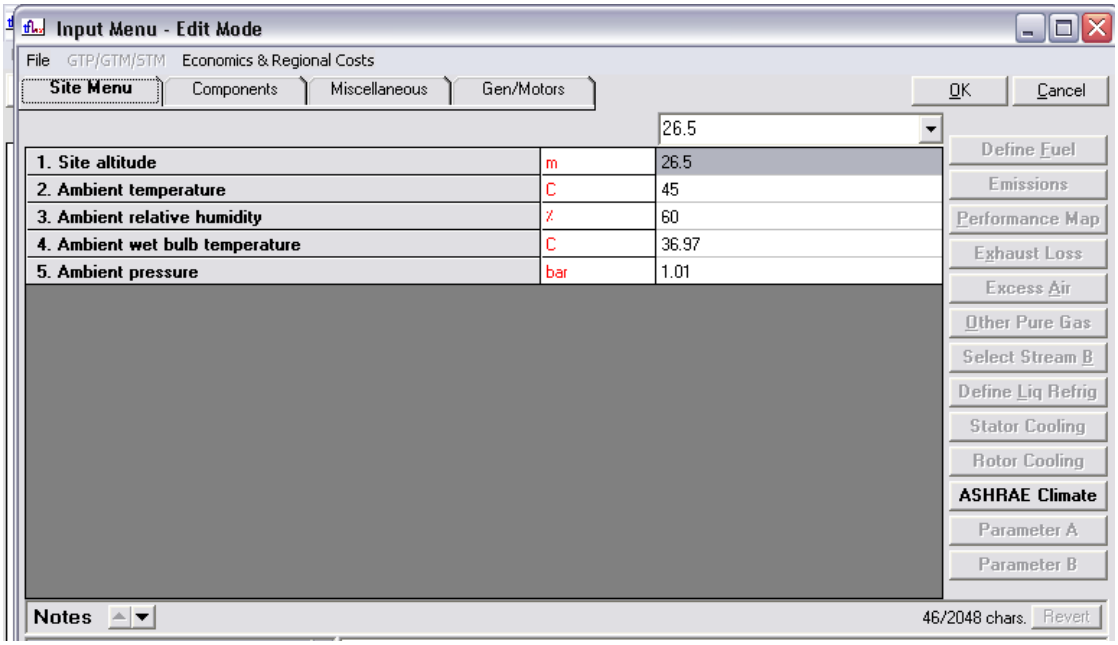

Control Loop

The Control Loop instructs THERMOFLEX to adjust certain Control Variables in order to cause another Set Point Variable to attain a desired value. It may also be set to cause a pair of variables to attain equality to one another. The latter is termed Parameter Matching Control. We will consider the system given

From the Define menu on the main menu bar, select Control Loops, and the following dialog is displayed:

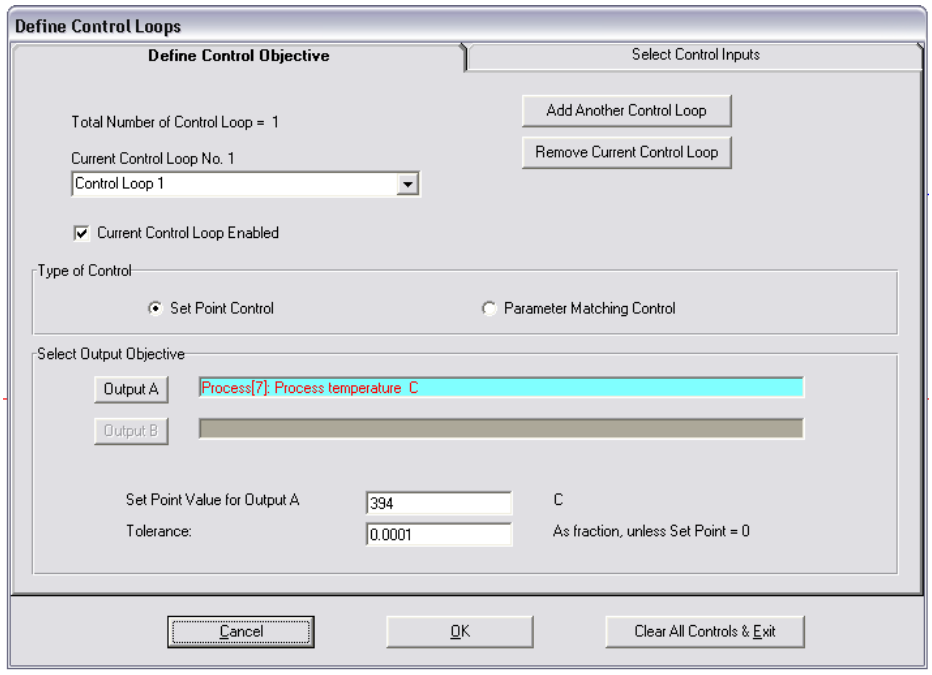

We want to achieve a certain value of thermal power of the process, so we choose the Set point Control option.

Next, we go to the Select Output Objective panel and click the Output A button. This invokes a list of model output parameters, organized in four categories:

1. Plant Parameters, (e.g. power, efficiency, etc.);
2. Gen/Motor Powers, (e.g. generator output, motor input, other auxiliary powers)
3. Component Parameters, (e.g. power output of a GT PRO Gas Turbine, power input to a Gas/Air Compressor, etc.)
4. Stream Parameters, (e.g. pressure, temperature, or flow of any stream

For this example, open the Plant Parameters category to see a list of choices provided. Select Component Parameters then select process- delivery temperature and return to the

screen shown above. Next, enter the desired temperature, 394 in the box labeled Set point Value for Output A.

After you have set the output objective to net power output, you need to specify the inputs that THERMOFLEX will use to achieve that objective. Click on the Select Control Inputs tab, invoking the screen shown below with Primary Control Input panels. THERMOFLEX will vary this first, to try to attain the objective. If the objective cannot be achieved, it will vary the upper and lower control inputs.

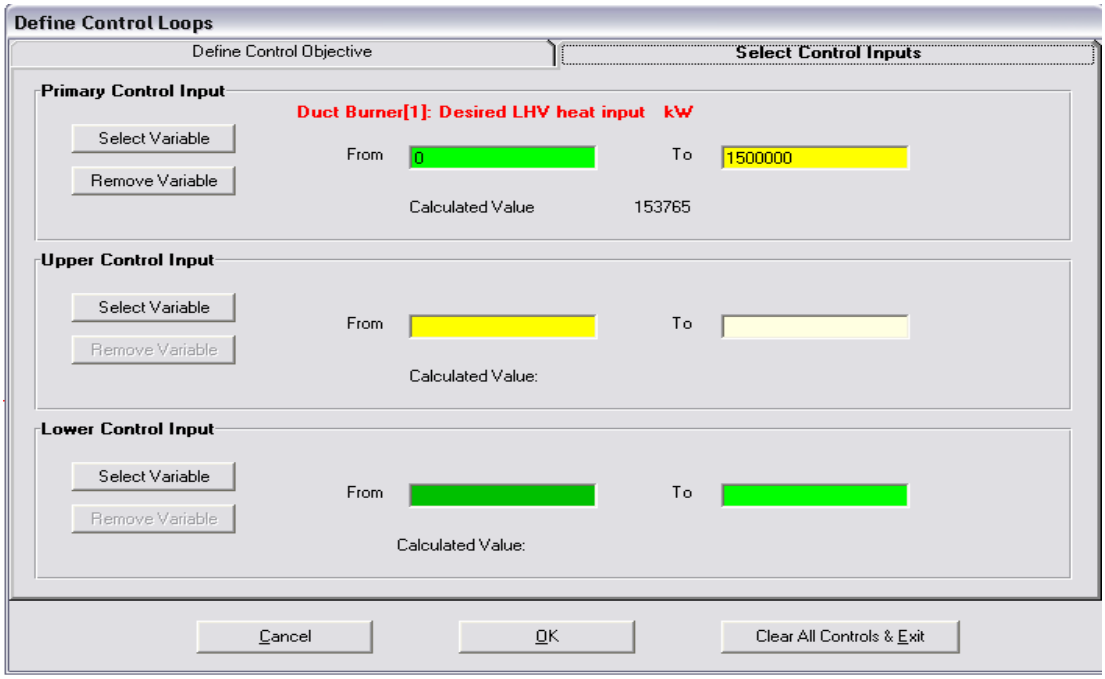

In the Primary Control Input panel, click on Select Variable to get the following input parameter list:

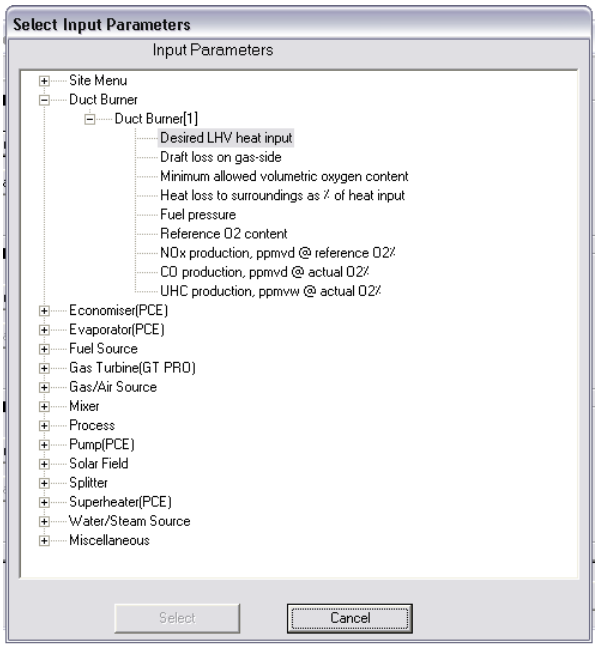

Select the Desired LHV heat for of Duct Burned [1] from the list box, either by double-clicking it, or by highlighting it and pressing Select. For this example, we would like to vary the LHV of the duct burner between 0 and 1500000, so enter the minimum value, 0 into the From box; and the maximum value, 1500000, into the To box. When done, click the OK button to dismiss the Control Loop definition window and return the Flowsheet view. Now, press F5 to check inputs and launch the computation

Check Inputs Transition

When you have completed your inputs, you need to Check Inputs to move on to Compute. Check Inputs is invoked by pressing the ▶ button beside the Edit Inputs button on the Navigator bar. Alternatively, the F4 and F5 keys do the same.

The Check Inputs transition will identify missing definitions or inconsistent data, especially conflicts in pressure definitions in *design* mode.

4. Calculation Stage

After successfully dealing with any messages that arose at the Check Inputs transition, THERMOFLEX has done what it can to check the inputs, and has eliminated any obvious inconsistencies

When the computation is finished a dialog box with file saving options and summary message information is displayed. The dialog box shown here is an example, and it indicates no messages of any sort have been generated. The happy face is a reflection of yours.

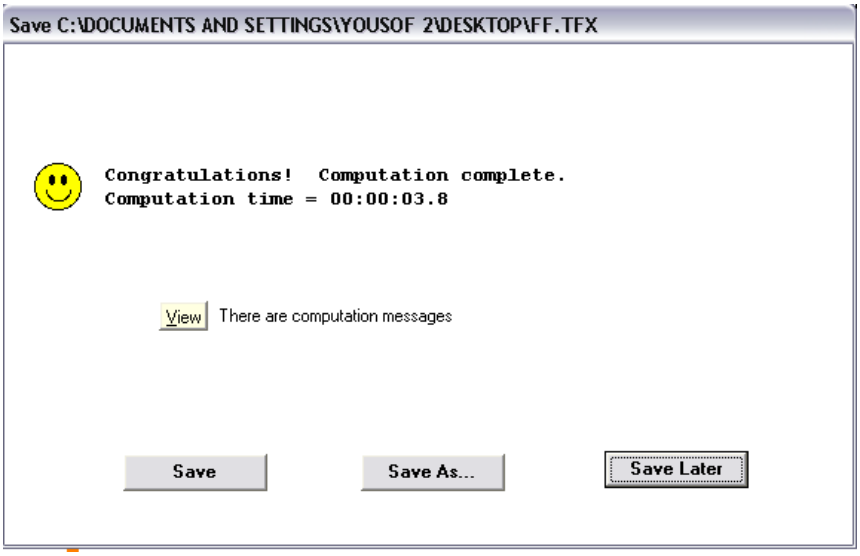

Click the Save button to store the result in a file with the current TFX filename, quietly overwriting a previous one with the same name. Click the Save As button if you want to choose a different TFX file to store the result. Click the default Save Later button if you do not wish to save the results yet.

5. View Output Stage

Once the calculation has been completed, the flowsheet border changes to light yellow and the yellow Output View buttons are enabled on the Navigator bar to indicate THERMOFLEX is in the View Outputs stage.

By default, THERMOFLEX chooses the Flowsheet output view following calculation. Therefore, the display will change only in that the border color changes, and the numerical data displayed on the various graphic elements is updated with the results from the most recent calculation.

Double-click any component to automatically switch to the Component view for that component. From there, select the Flowsheet button to redisplay the flowsheet and sheet selector strip

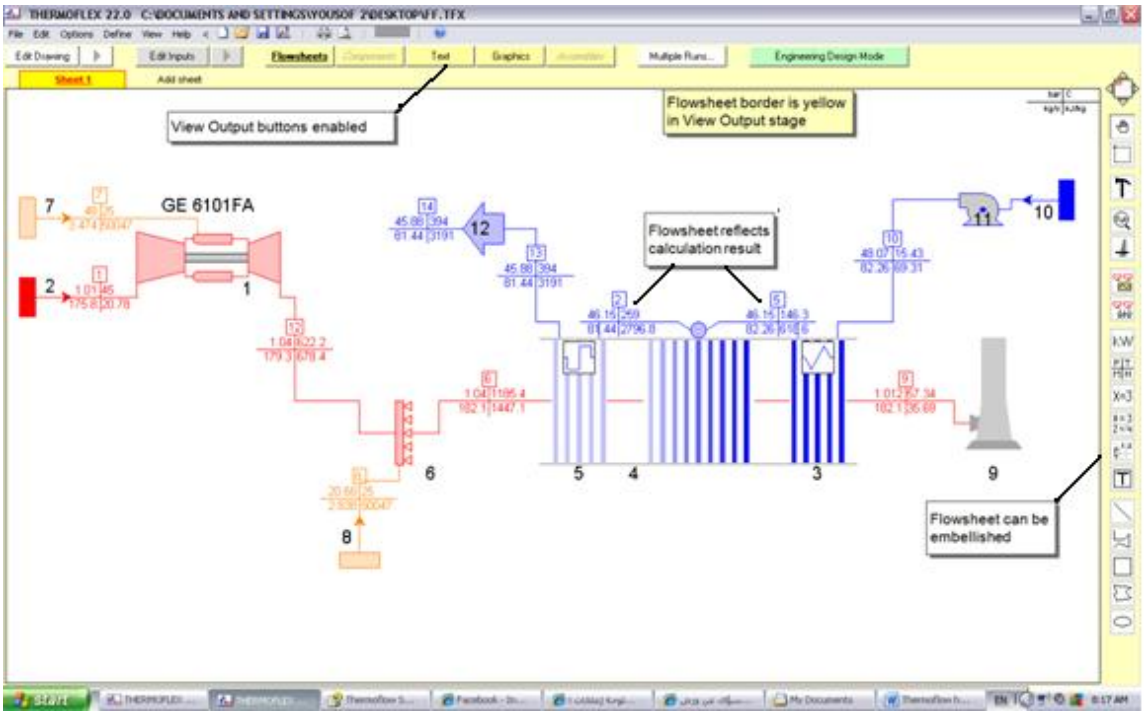

REFERENCES

[1] EDUCOGEN, the European educational tool on cogeneration, second edition, December 2001.

[2] David Flin, Cogeneration A user's guide, The Institution of Engineering and Technology, London, United Kingdom (2010).

[3] Boyce, M.P., Handbook for cogeneration and combined cycle power plants, ASME Press, New York, 2002.

[4] Williams, Hessami, M. Akbar, Two Case Studies of Cogeneration Systems Design and Economic Feasability. Heat Recovery Systems and CHP, Volume 13, Issue 2, March 1993, Pages 167‑186

[5] Onovwiona, H.I., and Ugursal V.I., Residential cogeneration systems: review of the current technology Renewable and Sustainable Energy Reviews, Volume 10, Issue 5, October 2006, Pages 389‑43.

[6] Renewables 2009, Solar Thermal Power Plant Industry, Renewables-made in Germany. http://www.renewables-made-in-germany.com/index.php?id=229&L=1 (Date of access: 27.4.2012).

[7] Martin Kaltschmitt, Wolfgang Streicher, Andreas Wiese, Renewable Energy - Technology, Economics and Environment (2007).

[8] SS 2006, Schott Solar, Schott Memorandum on Solar Thermal Power Plant Technology,http://www.schott.com/solar/english/download/schott_memorandum_e.pdf . (Date of access: 27.4.2012).

[9] Greenpacks 2008, California's First Solar Thermal Plant in 20 Years http://www.greenpacks.org/2008/10/31/california's-first-solar-thermal-plant-in-20-years/ (Date of access: 27.4.2012).

[10] John D Pye, Graham L Morrison, Masud Behnia , Transient Modelling of Cavity Receiver Heat Transfer for the Compact Linear Fresnel Reflector, Department of Mechanical and Manufacturing Engineering ,University of New South Wales (2003).

[11] Thomas R. Mancini, Catalog of Solar Heliostats, IEA-Solar Power and Chemical Energy Systems, Task III: Solar Technology and Applications, 2000. http://www.fika.org/jb/resources/Heliostat%20Catalog.pdf

(Date of access: 29.5.2012).

[12] William W. Bathie, Fundamentals of Gas Turbines Second Edition, Iowa State Univ. of Science and Technology. New York. January 1996.

[13] Ganapathy V., Waste Heat Boiler Deskbook. Fairmont Press,Distributed by Prentice-Hall in Lilburn, GA, Englewood Cliffs, NJ , 1991.

[14] Ganapathy, V., Simulation Aids Cogeneration System Analysis, Chemical Engineering Progress, Pp.27–31, 1993.

[15] Ganapathy, V., Heat-Recovery Steam Generators: Understand the Basics, Chemical Engineering Progress. Pp.32–45, 1996.

[16] Karthikeyan R., Hussain M. A., Reddy B. V., and Nag P. K , Performance Simulation of Heat Recovery Steam Generators in a Cogeneration System, International Journal of Energy Research. International Journal of Energy Research, Vol.22, Issue 5, Pp.399–410, April 1998.

[17] Kim T.S., Oh, C.H., Ro, S.T., Comparative Analysis of the Off Design Performance for Gas Turbine Cogeneration Systems, Heat Recovery Systems and CHP. Vol. 14. Issue 2, Pp.153–163, 1994.

[18] Rosen M.A., Reductions in energy use and environmental emissions achievable with utility-based cogeneration: Simplified illustrations for Ontario ,Vol.61, (1998)163-174.

[19] Faqeeh، E.A.M. Khalifa and A.M. Radhwan، "A Case Study of Cogeneration for Jeddah and Yanbu Petromin Refineries in Saudi Arabia"، J. Heat Recovery Systems & CHP، Vol.9، No.5، pp.485-491,1989.

[20] Kanoglu Mehmet., Dincer Ibrahim, Performance assessment of cogeneration plants, Energy Conversion and Management, Vol. 50 (2009) 76–81.

[21] Hamed O A., Al-Washmi H A.,& Al-Otaibi H A, Thermoeconomic analysis of a power/water cogeneration plant, Energy, Vol. 31, (2006) 2699.

[22] M. Habib, S. Said, J. Al-Bagawi, Thermodynamic performance analysis of the Ghazlan power plant, Energy ,Volume 20, Issue 11, 1995, Pages 1121‑1130.

[23] Chicco G, Mancarella P. Assessment of the greenhouse gas emission from cogeneration and trigeneration systems. Part I: models and indicators. Energy 2008; 33(3):410–7.

[24] Kutscher C.F., Davenport R. L., Dougherty D. A., Gee R. C., Masterson P. M., May E. K., Design approaches for solar industrial process heat system. SERI/TR-253-1356, Solar Energy Research Institute, Golden, Colo. (1982).

[25] Kalogirou S., Parabolic trough collector system for low temperature steam generation: design and performance characteristics, Applied Energy, vol. 55, pp. 1-19, (1996).

[26] Ibrahim S. M. A. ,The forced circulation performance of a sun tracking parabolic concentrator collector, Proceedings of the World Renewable Energy Congress, pp. 568-571, (1996).

[27] Almanza R., Lentz A. and Jiménez G. Receiver behavior in direct steam generation with parabolic troughs, Solar Energy, vol. 61, no. 4, pp. 275-278, (1997).

[28] Bakos G. C., Adamopoulos D., Soursos M. and Tsagas N. F. Design and constructionof a line-focus parabolic trough solar concentrator for electricity generation, Proceedings of ISES Solar World Congress, Jerusalem, p. 16, (1999).

[29] Forristall, Russell. , Heat Transfer Analysis and Modeling of a Parabolic Trough Solar Receiver Implemented in Engineering Equation Solver, National Renewable Energy Laboratory, NREL/TP-550-34169. October 2003.

[30] Cohen G. and Kearney D., Improved Parabolic Trough Solar Electric System Based on the SEGS Experience, In Proceeding of the ASES Annual Conference. SOLAR 94, 147-150. , 1994.

[31] Dagan E., Müller M. and Lippke F., Direct Steam Generation in the Parabolic Trough Collector, Report of Platafoma Solar de Almeria, Madrid, 1992.

[32] Lippke F., Direct Steam Generation in the Parabolic Trough Solar Power Plants - Numerical Investigation of the Transient and the Control of a Once-Through System, J of Solar Energy Eng. 118, 9-14, 1996.

[33] Alrobaei H., Novel integrated gas turbine solar cogeneration power plant, Desalination, vol. 220, pp. 574-587, 2008.

[34] Dersch J., M. Geyer, U. Herrmann, S. Jones, B. Kelly, R. Kistner, W. Ortmanns, R. Pitz-Paal, and H. Price, Trough integration into power plants--a study on the

performance and economy of integrated solar combined cycle systems, Energy, vol. 29, pp. 947-959, 2004.

[35] Behar O., A. Kellaf, K. Mohamedi, and M. Belhamel, Instantaneous performance of the first Integrated Solar Combined Cycle System in Algeria, Energy Procedia, vol.6 ,pp.185–193, 2011.

[36] Montes M.J., Rovira A., Munoz J.M. Martinez-Val, Performance analysis of an Integrated Solar Combined Cycle using Direct Steam Generation in parabolic trough collectors , Applied Energy 88 (2011) 3228–3238.

[37] Horn M., Fuhring H., Rheinlander J., Economic analysis of integrated solar combined cycle power plants A sample case: The economic feasibility of an ISCCS power plant in Egypt , Energy 29 (2004) 935–945.

[38] Gur Mittelman , Michael Epstein , A novel power block for CSP systems, Solar Energy 84 (2010) 1761–1771.

[39] Baghernejad A. , Yaghoubi M. ,Exergoeconomic analysis and optimization of an Integrated Solar Combined Cycle System (ISCCS) using genetic algorithm Energy Conversion and Management 52 (2011) 2193–2203.

[40] Ahmed Eter, Modeling and Optimization of a Hybrid Solar Combined Cycle (HYCS), MSc Thesis, M.E, KFUPM, 2011.

[41] Esmail M. A. Mokheimer, M. A. Habib and Ahmad Eter, Development of Solar Gas Turbine Cogeneration Systems in Saudi Arabia, Mechanical Engineering Department King Fahd University of Petroleum and Minerals, Dhahran. 2011.

[42] Casals, X. G., Modeling and optimizing the use of parabolic trough technology with Rankine cycles for electricity production, January 2000.

[43] Anon, (2011), http://www.power-technology.com/projects/saudi_aramco/ (Date of access: 28.4.2012).

[44] Loncar D., Bogdan Z, Duic N., An analysis of legal and market framework for the cogeneration sector in Croatia. Energy 34 (2009) 134–143.

[45] Loncar D., Ridjan I., Medium term development prospects of cogeneration district heating systems in transition country e Croatian case, Energy 48 (2012).

[46] Alaska Energy Authority, Analysis and Recommendations for Diesel Efficiency, Combined Heat and Power, Wind Power, and End Use Efficiency, Volume II, April 2004.

[47] Stefan j, Ljubljana, Methodology for Determining the Reference Costs for High Efficieny Cogeneration , Ministry of the economic Repuplic of Slovenia , No. 360-82 / 2009.

[48] Hongtao L., Francois M., Daniel F., Power and cogeneration technology environomic performance typification in the context of CO_2 abatement part II: Combined heat and power cogeneration, Energy 35 (2010) 3517e3523

[49] Hamada Boiler, comparison chart of cost of steam in various countries http://www.hamadaboiler.com/en/savingcalculation.html

(Date of access: 28.4.2012).

[50] U.S. Energy Information Administration, EIA, Natural Gas Futures Prices (NYMEX). http://tonto.eia.doe.gov./dnav/ng/ng_pri_fut_s1_d.htm ,

(Date of access: (13.3.2013).

[51] U.S. Energy Information Administration, Form EIA, Average Retail Price of Electricity to Ultimate Customers by End-use Sector, 2003 - December 2012. http://tonto.eia.doe.gov./electricity/monthly/epm_table_grapher.cfm?t=epmt_5_3 Date of access: (13.3.2013).

[52] Hamada boiler, Comparison chart of steam cost in various countries. http://www.hamadaboiler.com/en/savingcalculation.html , Date of access: (13.3.2013).

[53] Stuetzle, T. "Automatic control of the 30 MWe SEGS VI parabolic trough plant". Master's thesis, University of Wisconsin-Madison, College of Engineering, 2002.

[54] Fernandez-Garcıa A., Zarza E., Valenzuela L., Perez M. , Parabolic-trough solar collectors and their applications, Renewable and Sustainable Energy Reviews 14 (2010) 1695–1721.

[55] Geyer M, Lupfert E, Osuna R, Esteban A, Schiel W, Schweitzer A, et al. EUROTROUGH—Parabolic trough collector developed for cost efficient solar power generation. SolarPACES, 2002. In: 11th International Symposium on Concentrated Solar Power and Chemical Energy Technologies, Sept 4-6, 2002, Zurich, Switzerland.

[56] Osuna R; Esteban A.; Fuentes F.; Langenkamp, J ; Schiel, W.; Zarza, E.; Lüpfert, E.; Mandelberg, E. ; Final Report ,UROTROUGH II. Extension, Test and Qualification of EUROTROUGH from 4 to 6 Segments at Plataforma Solar de Almería, April 2003.

[57] Duffie, John A., Solar Engineering of Thermal Processes. 2006, John Wiley & Sons, 2006. New York.

[58] Mokheimer, KFUPM-MIT Report, CER-10-20

[59] Patnode, A. M. "Simulation and performance evaluation of parabolic trough solar power plants". Master's thesis, University of Wisconsin-Madison., College of ngineering, 2006.

[60] National Renewable Energy Laboratoty (NREL), Solar Advisor Model CSP Reference Manual for Version 3.0, 2009.

[61] Electricity & Cogeneration Regulatory Authority (ECRA) Saudi Arabia, Activities & Achievements of the Authority in 2011, June 2012.
http://www.ecra.gov.sa/Home.aspx
Date of access: (23.4.2013).

[62] Gaul, H., and Rabl, A., 1980. "Incidence-angle modifier and average optical efficiency of parabolic trough collectors". Journal of Solar Energy Engineering, 102, pp. 16–21.

[63] Dudley, V., Kolb, G., Sloan, M., and Kearney, D., Test results: SEGS LS-2 solar collector," Sandia National Labs., Albuquerque, NM (United States), 1994.

[64] Kalogirou, S., 2004. "Solar thermal collectors and applications". Progress in energy and combustion science, 30(3), pp. 231–295.

[65] Goswami, D., and Kreith, F., 2008. Energy conversion. CRC.

[66] Montes M., Abánades A., Martínez-Val J., and Valdés M., 2009. "Solar multiple optimization for a solar-only thermal power plant, using oil as heat transfer fluid in the parabolic trough collectors". Solar Energy, 83(12), pp. 2165 – 2176.

[67] Giostri A., Binotti M., Silva P., Macchi E., Manzolini1G. "Comparison of Two Linear Collectors in Solar Thermal Plants: Parabolic Trough vs Fresnel", ASME 2011 5th International Conference on Energy Sustainability, August, 2011, Washington.

[68] Stine W. B., and Harrigan R.W., 1985. Solar Energy Fundamentals and Design: With Computer Applications. Wiley-Interscience, Apr.

[69] Lippke F., 1995. Simulation of the part-load behavior of a 30MWe SEGS plant. Tech. rep., SAND–95-1293, Sandia National Labs., Albuquerque, NM (United States).

[70] Ricardo Vasquez Padilla Simplified Methodology for Designing Parabolic Trough Solar Power Plants, Thesis, University of South Florida.

[71] Hottel H.C., A Simple Model for Estimating the Transmittance of Direct Solar Radiation Through Clear Atmospheres, Solar Energy, Vol 18, pp. 129-134, Pergamon Press, 1976.

[72] Pilkington Solar International GmbH, Germany Bundesministerium für Bildung Wissenschaft Forschung und Technologie, Status report on solar thermal power plants: experience, prospects and recommendations to overcome market barriers of parabolic trough collector power plant technology, Pilkington Solar International, 1996, Report ISBN 3-9804901-0-6.

[73] Kistner R., Keitel T., Felten B. and Rzepczyk T. Analysis of the potential for cost decrease and competitiveness of parabolic trough plants. in SolarPACES 2009.

[74] The World Bank, MENA Assessment of the Local Manufacturing Potential for Concentrated Solar Power (CSP) Projects, Final Report - December 2010.

[75] NietoJ.M., Levelised Cost of Thermosolar Energy, Short and Medium-term Reduction Opportunities. Solar Power Generation Summit Barcelona. February 23-24, 2009.

[76] NREL report, Renewable Energy Technology Characterizations, Topical Report, December 1997.

[77] IEA Energy Technology Essentials, Report, December 2006

[78] International Renewable Energy Agency, Renewable Energy Technologies: Cost Analysis Series, Concentrating Solar Power, volume 1: Power Sector, June 2012

[79] NOVATEC SOLAR, http://www.novatecsolar.com/56-1-PE-2.html

[80] Häberle A. et al. (2002): The Solarmundo line focussing Fresnel collector. Optical and thermal performance and cost calculations. http://solarpaces-csp.org/CSP_Technology/docs/solarpaces_fresnel_9_2002.pdf.
Date of access: (17.4.2013).

[81] Morin G., Dersch J., Platzer W., Eck M., Haberle A.,Comparison of Linear Fresnel and Parabolic Trough Collector power plants, Solar Energy 86 (2012) 1–12

[82] Gnielinski V., "New equations for heat and mass transfer in turbulent pipe and channel flow," International Chemical Engineering, vol. (16:2), pp. 359–363., 1976.

[83] CleanEnergy , ACTION PROJECT, Puerto Errado 2 Thermosolar Power Plant (PE2), Case Study, Linear Fresnel Concentrating Solar Power (LFR CSP). http://www.cleanenergyactionproject.com/CleanEnergyActionProject/CS.Puerto_Errado_2_Thermosolar_Power_Plant___Concentrating_Solar_Power_Case_Study.html. Date of access: (20.4.2013).

Vitae

Name	: Yousef Naji Dabwan Ahmed
Nationality	: Yemen
Date of Birth	:3/5/1979
Email	: eng_yousof@hotmail.com
Address	: Sana'a Yemen (00967711006698)
Academic Background	: M.S (Mechanical Engineering)

May 2013

King Fahd University of Petroleum and Minerals

Dhahran, Saudi Arabia.

BS. (Mechanical Engineering)

June 2004 Sana'a University

Sana'a, Yemen.